Process intensification and integration for the production of vaccines and viral vectors

Dissertation

zur Erlangung des akademischen Grades

Doktoringenieur

(Dr.-Ing.)

von

Gwendal Gränicher, M.Sc. EPFL

geboren am

31. Oktober 1994 in Palo Alto, USA

genehmigt durch die Fakultät für Verfahrens- und Systemtechnik der Otto-von-Guericke Universität Magdeburg

Promotionskommission:

Prof. Dr.-Ing. Andreas SEIDEL-MORGENSTERN	(Vorsitz)
Dr. Jose CASTILLO	(Gutachter)
Prof. Dr. Manuel J.T. CARRONDO	(Gutachter)
Prof. Dr.-Ing. Udo REICHL	(Gutachter)

eingereicht am: 02. Juli 2021.

Promotionskolloquium am: 16. Dezember 2021

“Any sufficiently advanced technology is indistinguishable from magic.”

- Arthur C. Clarke

To my parents and Aldina.

Abstract

The use of eukaryotic cell cultures has led to successful production and commercialization of many complex biopharmaceuticals and viral-based vaccines. Since 1940s, this allowed the development of many vaccines against e.g., poliomyelitis and measles. Later in 1986, the first biopharmaceutical was commercialized using Chinese Hamster Ovary (CHO) cells. Especially for biopharmaceuticals production, huge progress in the field of cell culture engineering has been achieved through media and process optimization, and lately process intensification and integration, allowing drastic yield increase. However, few innovations have been implemented for viral-based vaccine production because of relatively low profit margins.

Viruses can be used as vaccines, which are among the most cost-effective medical interventions and indispensable for control of pandemic threats, saving annually millions of lives. Viruses can also be used as viral vectors for gene therapy, which is currently revolutionizing medicine in treatments against e.g., cancer, infectious or cardiac diseases. A rising demand for fast and high-yield production processes for viral-based therapeutics has been observed over the past decade. For vaccination, an efficient production process allows to rapidly produce in high amount cost-effective doses for seasonal epidemics and pandemics, such as the COVID-19 pandemic. For viral-based gene therapies, fast and high-yield production processes would allow to decrease production cost (e.g., 2.1 million $ pricing for viral-based Zolgensma® gene therapy treatment) and to accelerate the supply of viral vectors for commercialization and clinical trials.

Process intensification and integration in suspension cell culture using chemically-defined medium could be one answer to an ever increasing pressure on manufacturing costs and capacities in virus manufacturing. The process intensification approach consists in increasing host cell concentration by using a cell retention device. The process integration approach consists in directly linking the cell culture with purification.

This thesis presents methods for process intensification and integration for influenza A virus (IAV) production, with a possible use as an inactivated virus vaccine against seasonal and pandemic influenza, and for Modified Vaccinia virus Ankara (MVA) production, with a possible use as a viral vector for vaccination against various challenging pathogens or the treatment of some types of cancers.

For IAV production, PBG.PK2.1, a new mammalian suspension cell line is first presented. Evaluation of optimized IAV propagation in high cell density culture using a membrane-based cell retention system demonstrated promising performance: A maximum HA titer of 3.93 log_{10}(HA units/100 µL) was obtained. The glycosylation of the antigen HA was also studied.

Second, different cell retention devices for IAV production in perfusion mode were compared and optimized, in order to provide platform knowledge for process intensification of virus production. IAV was produced using AGE1.CR.pIX cells at concentrations up to 50 x 10^6 cells/mL at similar infection conditions using either a membrane-based system, an acoustic settler or an inclined settler. The virus was successfully harvested through the acoustic settler and the inclined settler cell retention devices. For concentrations of about 25 x 10^6 cells/mL, perfusion cell cultures using the acoustic settler and the inclined settler showed a 2.0-fold and 3.2-fold increase in the total number of virions produced, compared to the membrane-based system. In addition, a lower amount of large-sized aggregates in the harvest was observed when using the acoustic settler. Overall, a clear advantage was observed for continuous virus harvesting after the acoustic settler or the inclined settler operation mode were optimized.

This platform approach was equally applied to MVA production using AGE1.CR.pIX cells: first, different options for cell retention devices in perfusion mode were compared as before. Hollow-fiber bioreactors and an orbital-shaken bioreactor in perfusion mode, both available for single-use, were evaluated as well. Productivity for the virus strain MVA-CR19 was compared to results obtained from batch and continuous production reported in literature. Using a stirred-tank bioreactor, a perfusion strategy with working volume expansion after virus infection resulted in the highest yields. Overall, infectious MVA titers of 2.1–16.5 x 10^9 $TCID_{50}$/mL were achieved in these intensified processes. Taken together, this part shows a novel perspective on high-yield MVA production and addresses options for process intensification, also in full single-use.

Third, a scalable suspension cell culture-based perfusion process, integrating MVA harvesting through an acoustic settler with semi-continuous purification was developed. A capacitance probe was used to control the perfusion flow rate and to evaluate the optimal time of harvesting. A MVA space-time yield of 1.05 x 10^{11} $TCID_{50}/L_{bioreactor}$/day was obtained for an integrated perfusion process, which is 6-fold higher than for batch cultures. Without further optimization, purification by steric exclusion chromatography resulted in an overall product

recovery of 50%. To decrease the level of host cell DNA prior to chromatography, a novel inline continuous DNA digestion step was integrated into the process. A detailed cost analysis comparing integrated production in batch mode versus production in perfusion mode showed that the cost per dose for MVA can be reduced by a factor of 2.8 for this intensified small-scale process.

By collecting different process intensification strategies for IAV and MVA, together with process integration and cost analysis approaches for MVA, a sound basis for a better understanding on how to proceed for next generation virus production processes for vaccination or gene therapies is given.

Zusammenfassung

Die Verwendung von eukaryotischen Zellkulturen hat zur erfolgreichen Produktion und Kommerzialisierung vieler komplexer Biopharmazeutika und viraler Impfstoffe geführt. Seit den 1940er-Jahren ermöglichte dies die Entwicklung vieler Impfstoffe gegen z. B. Poliomyelitis und Masern. Später, 1986, wurde das erste Biopharmazeutikum unter Verwendung von *Chinese Hamster Ovary* (CHO)-Zellen kommerzialisiert. Speziell für die Produktion von Biopharmazeutika wurden enorme Fortschritte auf dem Gebiet der Zellkulturtechnik durch Medien- und Prozessoptimierung und in letzter Zeit auch durch Prozessintensivierung und -integration erzielt. Dies ermöglichte eine drastische Steigerung des Ertrags. Für die Impfstoffproduktion auf Virusbasis wurden jedoch aufgrund der relativ geringen Gewinnmargen nur wenige Innovationen umgesetzt.

Viren können als Impfstoffe verwendet werden und zählen zu den kosteneffektivsten medizinischen Interventionen. Für die Kontrolle einer Pandemie ist eine kostengünstige Lösung unverzichtbar und kann jährlich Millionen von Leben retten. Zudem können Viren auch als virale Vektoren für die Gentherapie eingesetzt werden. Sie revolutionieren derzeit die Medizin bei der Behandlung von z. B. Krebs, Infektions- oder Herzkrankheiten. In den letzten zehn Jahren ist ein steigender Bedarf an schnellen und ertragreichen Produktionsprozessen für virusbasierte Therapeutika zu beobachten. Für Impfungen ermöglicht ein effizienter Produktionsprozess die schnelle Herstellung von kostengünstigen Dosen in hohen Mengen für saisonale Epidemien und Pandemien, wie z. B. die COVID-19-Pandemie. Für virusbasierte Gentherapien würden schnelle und ertragreiche Produktionsprozesse es ermöglichen, die Produktionskosten zu senken (z.B. kostet die virusbasierte Gentherapie Zolgensma® momentan 2,1 Mio. $) und die Bereitstellung von viralen Vektoren für die Kommerzialisierung und klinische Studien zu beschleunigen.

Die Prozessintensivierung und -integration in der Suspensionszellkultur unter Verwendung eines chemisch definierten Mediums könnte eine Antwort auf den immer stärker werdenden Druck auf die Herstellungskosten und Kapazitäten in der Virusherstellung sein. Der Ansatz der Prozessintensivierung besteht in der Erhöhung der Wirtszellkonzentration durch den Einsatz einer Zellhaltevorrichtung. Der Ansatz der Prozessintegration besteht in der direkten Verknüpfung der Zellkultur mit der Aufreinigung.

In dieser Arbeit werden Methoden zur Prozessintensivierung und -integration für die Produktion von Influenza-A-Viren (IAV) und Modifizierten Vaccinia-Viren Ankara (MVA) vorgestellt. IAV können als inaktivierter Virusimpfstoff gegen saisonale und pandemische Grippe verwendet werden. MVA können als viraler Vektor für die Impfung gegen verschiedene Krankheitserreger oder die Behandlung einiger Arten von Krebserkrankungen dienen.

Für die IAV-Produktion wird zuerst PBG.PK2.1, eine neue Säugetier-Suspensionszelllinie, vorgestellt. Die Evaluierung der optimierten IAV-Vermehrung in Hochzelldichtekultur unter Verwendung eines membranbasierten Zellrückhaltesystems zeigte vielversprechende Ergebnisse: Es wurde ein maximaler HA-Titer von 3,93 $\log_{10}$(HA-Einheiten/100 µL) erreicht. Die Glykosylierung des Antigens HA wurde ebenfalls untersucht.

Zweitens wurden verschiedene Zellrückhaltevorrichtungen für die IAV-Produktion im Perfusionsmodus verglichen und optimiert, um eine Plattform für die Prozessintensivierung der Virusproduktion zu schaffen. IAV wurde unter Verwendung von AGE1.CR.pIX-Zellen in Konzentrationen von bis zu 50 x 10^6 Zellen/mL bei ähnlichen Infektionsbedingungen entweder mit einem membranbasierten System, einem *acoustic settler* oder einem *inclined settler* produziert. Das Virus konnte erfolgreich durch den *acoustic settler* und den *inclined settler* geerntet werden. Im Vergleich zum membranbasierten System zeigten Perfusionszellkulturen mit dem *acoustic settler* und dem *inclined settler* bei Konzentrationen von ca. 25 x 10^6 Zellen/mL eine 2,0- bzw. 3,2-fache Steigerung der Gesamtzahl der produzierten Virionen. Darüber hinaus wurde bei Verwendung des *acoustic settler* eine geringere Menge an großformatigen Aggregaten in der Ernte beobachtet. Insgesamt wurde ein klarer Vorteil für die kontinuierliche Virusernte beobachtet, nachdem der *acoustic settler* oder die Betriebsart des *inclined settler* optimiert wurden.

Dieser Plattformansatz wurde auch auf die MVA-Produktion mit AGE1.CR.pIX-Zellen angewandt: Zunächst wurden wie zuvor verschiedene Optionen für Zellhaltevorrichtungen im Perfusionsmodus verglichen. Zusätzlich wurden *hollow-fiber bioreactors* und ein *orbital-shaken bioreactor* im Perfusionsmodus, welche beide für den Einmalgebrauch verfügbar sind, evaluiert. Die Produktivität für den Virusstamm MVA-CR19 wurde mit den in der Literatur berichteten Ergebnissen aus der Batch- und kontinuierlichen Produktion verglichen. Bei Verwendung eines Rührkessel-Bioreaktors führte eine Perfusionsstrategie mit Arbeitsvolumenerweiterung nach der Virusinfektion zu den höchsten Erträgen. Insgesamt

wurden in diesen intensivierten Prozessen infektiöse MVA-Titer von 2,1–16,5 x 10^9 $TCID_{50}$/mL erreicht. Insgesamt zeigt dieser Teil eine neuartige Perspektive auf die Hochertrags-MVA-Produktion und adressiert Optionen zur Prozessintensivierung auch für *full single-use*.

Drittens wurde ein skalierbarer, auf Suspensionszellkulturen basierender Perfusionsprozess entwickelt, der die MVA-Ernte durch einen *acoustic settler* mit einer halbkontinuierlichen Aufreinigung integriert. Eine Kapazitätssonde wurde verwendet, um die Perfusionsflussrate zu regeln und den optimalen Erntezeitpunkt zu ermitteln. Eine MVA-Raum-Zeit-Ausbeute von 1,05 x 10^{11} $TCID_{50}/L_{Bioreaktor}$/Tag wurde für einen integrierten Perfusionsprozess erzielt, was 6-mal höher ist als bei Batch-Kulturen. Ohne weitere Optimierung führte die Aufreinigung durch *steric exclusion chromatography* zu einem Gesamtproduktertrag von 50 %. Um den Gehalt an Wirtszell-DNA vor der Chromatographie zu verringern, wurde ein neuartiger kontinuierlicher *inline*-DNA-Verdauungsschritt in den Prozess integriert. Eine detaillierte Kostenanalyse, in der die integrierte Produktion im Batch-Modus mit der Produktion im Perfusions-Modus verglichen wurde, zeigte, dass die Kosten pro Dosis für MVA bei diesem intensivierten Prozess im kleinen Maßstab um den Faktor 2,8 reduziert werden können.

Durch die Zusammenstellung verschiedener Prozessintensivierungsstrategien für die Produktion von IAV und MVA sowie die Prozessintegrations- und Kostenanalyseansätzen für die Produktion von MVA, wurde eine solide Grundlage für ein besseres Verständnis für die Vorgehensweise bei Virusproduktionsprozessen der nächsten Generation für Impfungen oder Gentherapien geschaffen.

Acknowledgements

The Acknowledgements section is empty in the electronic PDF version of this dissertation according to paragraph 4.1.1. of the Regulations for the submission of depositary copies to the library of the Otto von Guericke University Magdeburg within the framework of doctoral and habilitation procedures as of 5th November 2019, which partially states that "[. . .]. The document does not include a CV, acknowledgments or further personal data. [. . .]".

More information:

https://www.ub.ovgu.de/ub_media/Service/Formulare/Pflichtexemplarrichtlinie_englisch-p-934.PDF.

Table of contents

Abbreviations

Abbreviation	Description
AAV	Adeno-associated virus
AS	Acoustic settler
ATF	Alternating tangential flow
AV	Active volume
C	Carrier (glass)
CA	Cell aggregates
CAP	CEVEC's amniocyte production
CAR	Chimeric antigen receptor
CD19	Cluster of Differentiation 19
CEF	Chicken embryo fibroblast
cGMP	Current Good Manufacturing Practice
CHO	Chinese hamster ovary
CRISPR	Clustered regularly interspaced palindromic repeats
CS	Cell suspension
ct	Threshold cycle
DF	Diafiltration
DNA	Deoxyribonucleic acid
DO	Dissolved oxygen
DoE	Design of experiment
dsDNA	Double-stranded DNA
DSP	Downstream processing
EMA	European Medicine Agency
EV	Enveloped virion
F	Polysulfone foil
FDA	US Food and Drug Administration
H	Harvest (clarified fluid)
HA	Hemagglutinin
HCD	High cell density
HEK	Human embryonic kidney
Hex	Hexose
HexNAc	*N*-acetylhexosamine
HFBR	Hollow-fiber bioreactor
HIV	Human Immunodeficiency Virus
hpi	Hours post infection
HPLC	High performance liquid chromatography
HSV	Herpes simplex virus
IAV	Influenza A virus
IBV	Influenza B virus
Ig	Immunoglobulin

IS	Inclined settler
kbp	Kilo base pairs
LMH	Liter of filtrate per m^2 surface of filter per hour
M1	Influenza virus matrix protein 1
M2	Matrix protein 2 ion channel
mAb	Monoclonal antibody
Man	Mannose
MDCK	Madin-Darby canine kidney
MOI	Multiplicity of infection
MV	Mature virion
MVA	Modified Vaccinia virus Ankara
MW	Molecular weight
N-1 perfusion	Intensified cell culture prior to bioreactor inoculation
NA	Neuraminidase
NEP	Nuclear export protein
NP	Nucleoprotein
OSB	Orbital-shaken bioreactor
OSB-ATF	Orbital-shaken bioreactor coupled to an ATF
P	Piezoceramic and transducer
PA	Influenza virus polymerase complex
PAT	Process analytical technology
PB1	Influenza virus polymerase complex
PB2	Influenza virus polymerase complex
PBS	Phosphate-buffered saline
PCV1	Porcine circovirus 1
PEG	Polyethylene glycol
PERV	Porcine endogenous retrovirus
PES	Polyethersulfone
pfu	Plaque forming units
PLS	Partial least square
PS	Polysulfone
psi	Pounds per square inch
qPCR	Quantitative Polymerase Chain Reaction
R	Reflector
Re	Reynolds number
RNA	Ribonucleic acid
rpm	Rotation per minute
RSV	Respiratory Syncytial Virus
SE	Cell separation efficiency
SF	Shake flask
Sf9	*Spodoptera frugiperda* 9
SOP	Standard operating procedure
SRID	Single radial immune-diffusion

STR	Stirred-tank bioreactor
STR-AS	Stirred-tank bioreactor coupled to an acoustic settler
STR-ATF	Stirred-tank bioreactor coupled to an ATF
STR-IS	Stirred-tank bioreactor coupled to an inclined settler
SXC	Steric exclusion chromatography
T	Temperature
TFF	Tangential flow filtration
TMP	Trans-membrane pressure
TOI	Time of infection
U	Unit
UF	Ultrafiltration
USP	Upstream processing
VCC	Viable cell concentration
vg	Viral genome
VLP	Virus-like particle
WHO	World Health Organization
ZKBS	*Zentrale Kommision für die Biologische Sicherheit*

Symbols

Symbol	Description	Unit
$AC_{DNA,h}$	Average DNA concentration in the harvest between t_{n-1} and t_n	g/L
$AC_{glc,h}$	Average glucose concentration in the harvest between t_{n-1} and t_n	mol/L
$AC_{lac,h}$	Average lactate concentration in the harvest between t_{n-1} and t_n	mol/L
$AC_{tProt,h}$	Average total protein concentration in the harvest between t_{n-1} and t_n	g/L
$AC_{vir,h}$	Average virus particle concentration in the harvest between t_{n-1} and t_n	virions/mL or $TCID_{50}$/mL
A_e	The electric field area between the two electrodes (determined by the manufacturer)	m^2
A_{min}	Minimum settling area	m^2
B_v	Volume fraction of cells (biomass) in the culture medium	-
C	Capacitance signal	F
$C_{DNA,b}$	DNA concentration in the bioreactor	g/L
$C_{glc,0}$	Glucose concentration in the fresh medium	mol/L
$c_{glc,b}$	Target glucose concentration in the bioreactor	mol/L
$c_{glc,m}$	Glucose concentration in the medium	mol/L
$C_{glc,n}$	Glucose concentration at time n (t_n)	mol/L
$C_{lac,n}$	Lactate concentration at time n (t_n)	mol/L
C_m	Cell membrane capacitance	F/m^2
c_s	Cell culture compound (such as glucose) concentration	mol/L
CSPR	Cell-specific perfusion rate	L/cell/day
CSVY	Cell-specific virus yield	virions/cell or $TCID_{50}$/cell
$C_{tProt,b}$	Total protein concentration in the bioreactor	g/L
C_{vir}	i) Influenza virus particle concentration or ii) concentration of infectious MVA produced	i) virions/mL or ii) $TCID_{50}$/mL
$C_{vir,\ SXC\ in}$	Infectious MVA concentration in the SXC feed	$TCID_{50}$/mL
$C_{vir,\ SXC\ out}$	Infectious MVA concentration in the eluate	$TCID_{50}$/mL
$C_{vir,b}$	i) Influenza virus particle concentration in the bioreactor or ii) concentration of infectious MVA produced in the bioreactor	i) virions/mL or ii) $TCID_{50}$/mL
$C_{vir,tot}$	i) Concentration of influenza virus particles produced (in total) or ii) concentration of infectious MVA produced (in total)	i) virions/mL or ii) $TCID_{50}$/mL
D	Stirrer diameter	m
d_e	Electric field length (between two electrodes, determined by the manufacturer)	m
F_A	Acoustic radiation force	$kg \times m/s^2$
F_B	Buoyancy or gravity force	$kg \times m/s^2$
f_c	Critical frequency	Hz
F_D	Viscous drag force	$kg \times m/s^2$
g	Gravitational force	m/s^2

J	Permeate flux	m/s
L	Characteristic length	m
n	Sampling time	-
N	Stirring speed	rpm
n_f	Number of fibers (for an ATF membrane)	-
p_h	Perfusion ratio between t_{n-1} and t_n	-
P_v	Volumetric virus productivity	virions/L/day or $TCID_{50}$/L/day
Q	Perfusion flow rate	m^3/s or L/h
q_{glc}	Cell-specific glucose consumption rate	mol/cell/h
q_{gln}	Cell-specific glutamine consumption rate	mol/cell/h
q_{lac}	Cell-specific lactate production rate	mol/cell/h
q_{NH4+}	Cell-specific ammonium production rate	mol/cell/h
Q_r	Recirculation flow rate	m^3/s or L/h
q_s	Cell-specific substrate consumption rate and by-product production rate	mol/cell/h
r	Mean radius of the cell	m
R	Internal radius of the recirculation tube	m
STY	Space-time yield	$TCID_{50}/L_{bioreactor}$/day
t	Cultivation time	h
$TCID_{50}$	Median Tissue Culture Infectious Doses	$TCID_{50}$/mL
t_d	Cell population doubling time	h
t_n	Time n	h
t_{tot}	Time from bioreactor inoculation until maximum Vir_{tot}	h
v	Velocity of the fluid	m/s
v_c	Settling velocity of the cells in the gravitational field	m/s
V_e	Partial medium exchange volume	m^3 or L
V_h	Harvested volume between t_{n-1} and t_n	m^3 or L
Vir_{tot}	i) Total number of influenza virus particles produced in the harvest vessel and in the bioreactor or ii) total number of infectious MVA produced in the harvest vessel and in the bioreactor	i) virions or ii) $TCID_{50}$
$V_{SXC\ in}$	Volume of the SXC feed	m^3 or L
$V_{SXC\ out}$	Volume of the SXC eluate	m^3 or L
V_{tot}	Total volume of medium spent including cell growth phase until time point of maximum Vir_{tot}	m^3 or L
V_w	Working volume	m^3 or L
x	Viable cell concentration	cells/mL
x_b	Viable or dead cell concentration in the bioreactor	cells/mL
x_h	Viable or dead cell concentration in the harvest	cells/mL
$x_{v,b,max}$	Maximum concentration of viable cells in the bioreactor obtained until time point of maximum Vir_{tot}	cells/mL
$Y_{lac/glc}$	Lactate yield based on glucose consumption	-
β-dispersion	Loss of polarization over a range of the frequencies (for a capacitance probe).	-

γ	Shear rate	1/s
ΔC	Difference of the background capacitance at high frequency to the measured capacitance signal.	F
Δt	Time interval between two medium replacements	h
$\Delta\varepsilon_{max}$	Maximum permittivity signal which is the difference between the permittivity signal at low frequency and the permittivity signal at high frequency	F/m
ε	Permittivity signal.	F/m
η	Dynamic viscosity of the liquid	kg/m/s
μ	Cell-specific growth rate	1/h
ρ_c	Volumetric density of the cell	kg/m^3
ρ_l	Volumetric density of the liquid	kg/m^3
σ_i	Intracellular conductivity	S/m
σ_m	Cell culture medium conductivity	S/m
τ	Mean residence time	h

List of figures

List of tables

Chapter 1

Introduction

This chapter is partially based on the following publication:

Gränicher G, Tapia F, Behrendt I, Jordan I, Genzel Y, Reichl U. Production of Modified Vaccinia Ankara Virus by Intensified Cell Cultures: A Comparison of Platform Technologies for Viral Vector Production. *Biotechnology Journal*, 2020.

Vaccination is among the most cost-effective of medical interventions [1] and is indispensable for control of pandemic threats [2, 3] caused by highly pathogenic viruses such as SARS-CoV-2, Ebola or some strains of influenza virus. One way to produce vaccines is by using inactivated viruses or life-attenuated viruses in order to trigger the immune system. However, viral-based vaccine design is complex and challenging, and viruses are often difficult to produce.

In the last decades, the field of gene therapies emerged, showing great potential to cure several diseases, e.g. in oncology. According to the US Food and Drug Administration (FDA), gene therapies consist in the genetic material delivery, allowing to modify its expression or to alter the biological properties of living cells for therapeutic use [4]. Since the first clinical study for a gene therapy was initiated in the 1990s, over 2500 clinical trials have been conducted [5], leading to the current commercialization of six gene therapies (see section 2.2). Over 1140 clinical trials are currently employing viral vectors for gene therapies [6]. For efficient treatment, it has been found that a high dose of the gene vector would be needed. The dose depends on the targeted tissue/organ, and the delivery strategy (e.g. local versus systemic delivery). For example, up to 10^{14} adeno-associated virus (AAV) viral genome (vg) per kg of patient bodyweight is needed for the treatment of muscular dystrophy [7]. Which such a high dose, it has been estimated that one patients could be treated [7] with one batch of a bioreactor >100 L [8]. With a payment model of 425'000 $/year for a duration of 5 years, totalizing a final price of 2.1 million $ (www.novartis.com), the viral-based gene therapy Zolgensma® is the world's most expensive drug [6]. Other authorized viral-based gene therapy products are also often above 300'000 $ per treatment [9]. Although there is a need for higher transparency regarding the final gene therapy pricing, one reason justifying the high pricing is the high cost of R&D and manufacturing [10-13].

With the constant pandemic threats, such as the current COVID-19 pandemic due to the coronavirus SARS-CoV-2, it is clear that not only for gene therapy approaches, but equally for vaccine development, the capacity to quickly produce high amounts of virus particles is urgently needed to answer ever increasing demands for inactivated viruses, life-attenuated viruses and viral vectors. Cell culture-based cost-effective vaccines to replace traditional time-consuming and laborious vaccines (using for example chicken embryo) is also needed. In the current COVID-19 pandemic, new technologies such as mRNA vaccine seem to surpass viral-based vaccines regarding development and manufacturing speed, and vaccination efficacy.

Still, viral-based vaccines are crucial to allow large vaccination campaigns, either using adenoviral vectors (e.g. AstraZeneca), inactivated coronavirus (e.g. Sinovac Biotech) or others (such as Modified Vaccinia virus Ankara-based vector or life-attenuated / replication-defective coronaviruses).

By consequence, the need to develop efficient and large-scale cell culture-based virus manufacturing processes has raised [7, 14]. Compared to traditional recombinant protein production, the production of whole virus particles has additional constraints such as risk of mutations, loss of infectivity and rapid access to proper biological safety facilities. Although pharmaceutical production of viruses dates back to the early 1940s, other challenges that are of biological nature are still as valid today as they were almost 100 years ago: viruses are obligate parasites and require a second biological entity, the host, for replication. As one consequence, a host cell during the seed train and an infected or transfected host cell during the production interval need to be amenable for biotechnological manipulation. In addition, some viruses have an extremely narrow host range and require a special or even unique substrate. This property calls for further development of carefully adjusted or novel upstream and downstream processes. More specifically, intensified suspension cell cultures directly integrated to a purification process could contribute to reduce manufacturing costs and to increase the supply of high-quality viral-based vaccines and viral vectors for clinical trials and commercialization.

1.1 Scope of the thesis

A high demand for viral-based vaccines and gene therapies increases the pressure to find innovative solutions to intensify the production of inactivated or live virions. To address this, the scope of the presented work is to evaluate different alternatives regarding an integrated production of virions, in perfusion mode and using suspension cells. Two different virus types, namely influenza A virus (IAV; for vaccination) and Modified Vaccinia virus Ankara (MVA; for gene therapy) were produced. On the upstream processing (USP) side, two different suspension cell lines (PBG.PK2.1 and AGE1.CR.pIX) were tested with different perfusion strategies. Cell culture platforms using e.g., the alternating tangential flow (ATF) filtration, the acoustic settler (AS), the inclined settler (IS) or the hollow-fiber bioreactor (HFBR) system were

evaluated. For MVA only, the perfusion process was then integrated to a semi-continuous downstream processing (DSP) strategy, economically evaluated and compared with current state-of-art virus production in batch.

To allow for such a comprehensive comparison of different virus production platforms, part of the data was not generated by the author himself or was only partially generated by the author. In order to avoid any confusion, a detailed list of individual contributions are available at the end of each results & discussion chapter (chapters 4–8).

Chapter 2

Theoretical background

This chapter is partially based on the following publications:

Gränicher G, Coronel J, Pralow A, Marichal-Gallardo P, Wolff M, Rapp E, et al. Efficient influenza A virus production in high cell density using the novel porcine suspension cell line PBG.PK2.1. *Vaccine*, 2019.

Gränicher G, Coronel J, Trampler F, Jordan I, Genzel Y, Reichl U. Performance of an acoustic settler versus a hollow fiber-based ATF technology for influenza virus production in perfusion. *Appl Microbiol Biotechnol*, 2020.

Gränicher G, Tapia F, Behrendt I, Jordan I, Genzel Y, Reichl U. Production of Modified Vaccinia Ankara Virus by Intensified Cell Cultures: A Comparison of Platform Technologies for Viral Vector Production. *Biotechnology Journal*, 2020.

Gränicher G, Babakhani M, Göbel S, Jordan I, Marichal-Gallardo P, Y. G, et al. A high cell density perfusion process for Modified Vaccinia virus Ankara production: Process integration with inline DNA digestion and cost analysis. *Biotechnol Bioeng*, 2021.

2.1 Vaccines

The concept of vaccination is to help our immune system to develop protection from a disease. This concept seemed to be started in 430 BC where people were reported to survive a deadly contagious disease when contracted once [15]. The production of safer vaccines, meaning the use of an attenuated or inactivated form of the pathogen for vaccination, was later reported for the first time by Edward Jenner in the eighteenth century. Infection with cowpox led to vaccination against the deadly smallpox [16], opening the way to the generation of live, attenuated vaccines. More than 80 years later, Louis Pasteur found a technique in order to attenuate organisms in the laboratory leading to vaccination against for example cholera, leading later to the first generation of inactivated vaccines [16]. Several techniques for the inactivation or attenuation of pathogenic agents have since then been developed which are: heat, desiccation, exposure to oxygen, use of chemicals (such as formalin) and passaging in atypical host species [16]. In the 1940s the discovery that viruses could be grown in *in vitro* cultures using animal cells allowed the development of vaccines (mainly whole inactivated vaccines) against e.g., poliomyelitis, measles, mumps, rubella, varicella, hepatitis A and, more recently, rotavirus and influenza [15]. Live attenuated vaccines have been among the most powerful vaccination forms, however it has been associated with genetic instability and residual virulence [17]. In order to avoid the mentioned downsides, several strategies such as reassortment, reverse genetics, recombination, deletion mutants, codon deoptimization and control of replication fidelity have been developed [17]. Next to inactivated and live attenuated viral-based vaccines, different strategies have been later developed such as viral vectors or virus-like particles (VLPs) [17]. According to the World Health Organization (WHO), vaccines annually save the life of more than 2.5 million people [18]. A list of approved vaccines is listed below (Table 1).

Table 1: List of human vaccines, including their form of vaccination and their approximate time of availability [19] [16].

Approximate time of availability	Vaccine or target	Comment on form of vaccination
1798	Smallpox	Related animal virus
1885	Rabies	Live attenuated by chemical attenuation
1885	Anthrax	Live attenuated by chemical attenuation
1896	Typhoid	Inactivated whole organism
1896	Cholera	Inactivated whole organism
1897	Plague	Inactivated whole organism
1923	Diphtheria	Toxoids
1926	Whole-cell pertussis	Inactivated whole organism
1927	Tuberculosis	Live attenuated by passage *in vitro*
1927	Tetanus	Toxoids
1935	Yellow fever	Live attenuated by passage *in vitro*
1938	Influenza	Inactivated whole virus
1944	Japanese Encephalitis	Use of extracts and subunits
1955	Poliovirus	Inactivated whole organism
1960	Anthrax	Extracts and subunits
1962	Poliovirus	Live attenuated by cell culture passage
1963	Measles	Live attenuated by cell culture passage
1969	Rubella	Live attenuated by cold adaptation
1970s	Influenza	Extracts and subunits
1971	Adenoviruses	Live attenuated by cell culture passage
1974	Meningococcal	Polysaccharides
1976	Rabies	Extracts and subunits
1977	Pneumococcal	Polysaccharides
1986	Hepatitis B	Recombinant proteins
1987	Human influenza type B	Protein-conjugated capsular
1989	Ty21a typhoid	Live attenuated by auxotrophy
1995	Varicella	Live attenuated by cell culture passage
1995	Hepatitis A	Inactivated whole organism
1995	Tyhpoid	Polysaccharides
1996	Acellular pertussis	Recombinant proteins
1998	Lyme disease	Recombinant proteins
2002	Pneumococcal	Polysaccharide
2003	Live influenza	Live attenuated by cold adaptation
2003	Live influenza	Live attenuated with use of reassortants
2005	Rotavirus bovine-human	Live attenuated with use of reassortants
2005	Rotavirus 89-12	Live attenuated by cell culture passage
2006	Zoster	Live attenuated by cell culture passage
2006	Human papillomavirus	Virus-like particle
2020	COVID-19	mRNA encoding spike protein in prefusion form
2020	COVID-19	Adenovirus, viral vector encoding spike protein
2020	COVID-19	Inactivated virus, extracted spike protein subunit

2.1.1 Influenza virus

Influenza virus belongs to the *Orthomyxoviridae* family, which is divided into four types, namely A, B, C and D. It is an enveloped virus. The virus possesses eight negative-sense, single-stranded RNA segments as its genome. It measures 80-120 nm in diameter. The influenza virus types A and B are dangerous for humans, and responsible for seasonal epidemics and pandemics. The IAV is present in many animal reservoirs such as birds, pigs, dogs and horses, and can be transmitted to humans through zoonosis [20]. The two major antigenic surface proteins are hemagglutinin (HA) and neuraminidase (NA). The structure of an influenza virus particle is illustrated below (Figure 1).

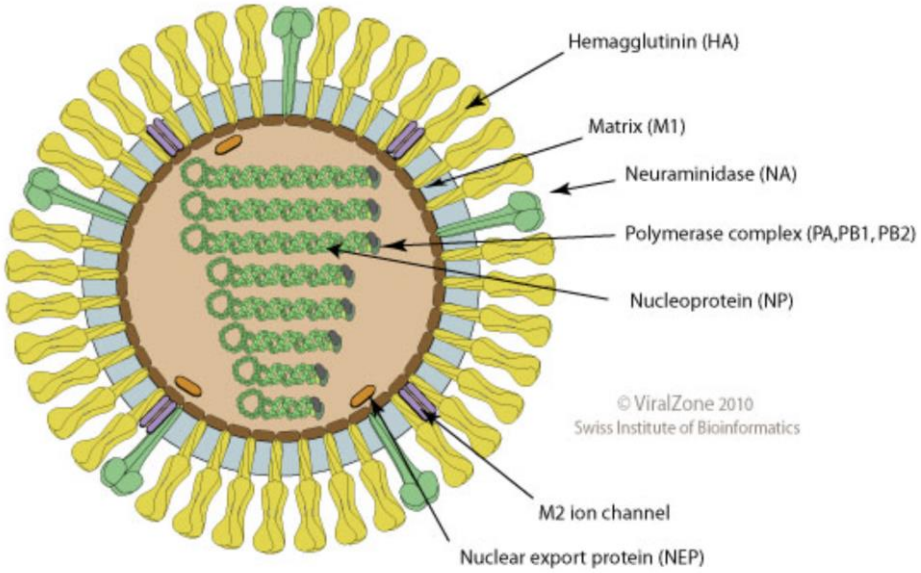

Figure 1: Illustration of an influenza A virus particle (source: https://viralzone.expasy.org/6?outline=all_by_species, Swiss Institute of Bioinformatics).

Seasonal influenza virus epidemics are estimated to cause 2–5 million cases of severe illness and up to 500'000 deaths per year worldwide. Through "antigenic drifts", IAV is responsible for seasonal epidemics as influenza viruses escape from human herd immunity. Antigenic drifts are caused by selective immunological pressure from mutated influenza viruses (obtained through viral RNA replication errors), giving each year new reassortants of HA and NA [21]. Another mechanism generating seasonally new influenza virus strains permits two different virus strains to reassort genetic material with one another upon coinfection, leading to "antigenic shifts" [22].

In addition to seasonal epidemics, IAV can cause as well pandemics at irregular intervals. As an example, the influenza pandemics of 1918 caused approximately 40 million deaths [21]. Influenza virus pandemics typically originate from animal reservoirs [20].

To reduce the burden attributed to seasonal and pandemic influenza, multiple approaches, including vaccines and antiviral drugs, have been developed [20]. Vaccination is the major measure to prevent and control influenza virus infections [23]. Each year, a new influenza vaccine has to be generated. Vaccine antigenic mismatch through for example alteration in antigen glycosylation can reduce the efficiency of the vaccine [20, 22] There are several ways to produce influenza viral vaccines, as illustrated in Figure 2 (from Harding et al. (2018) [22]).

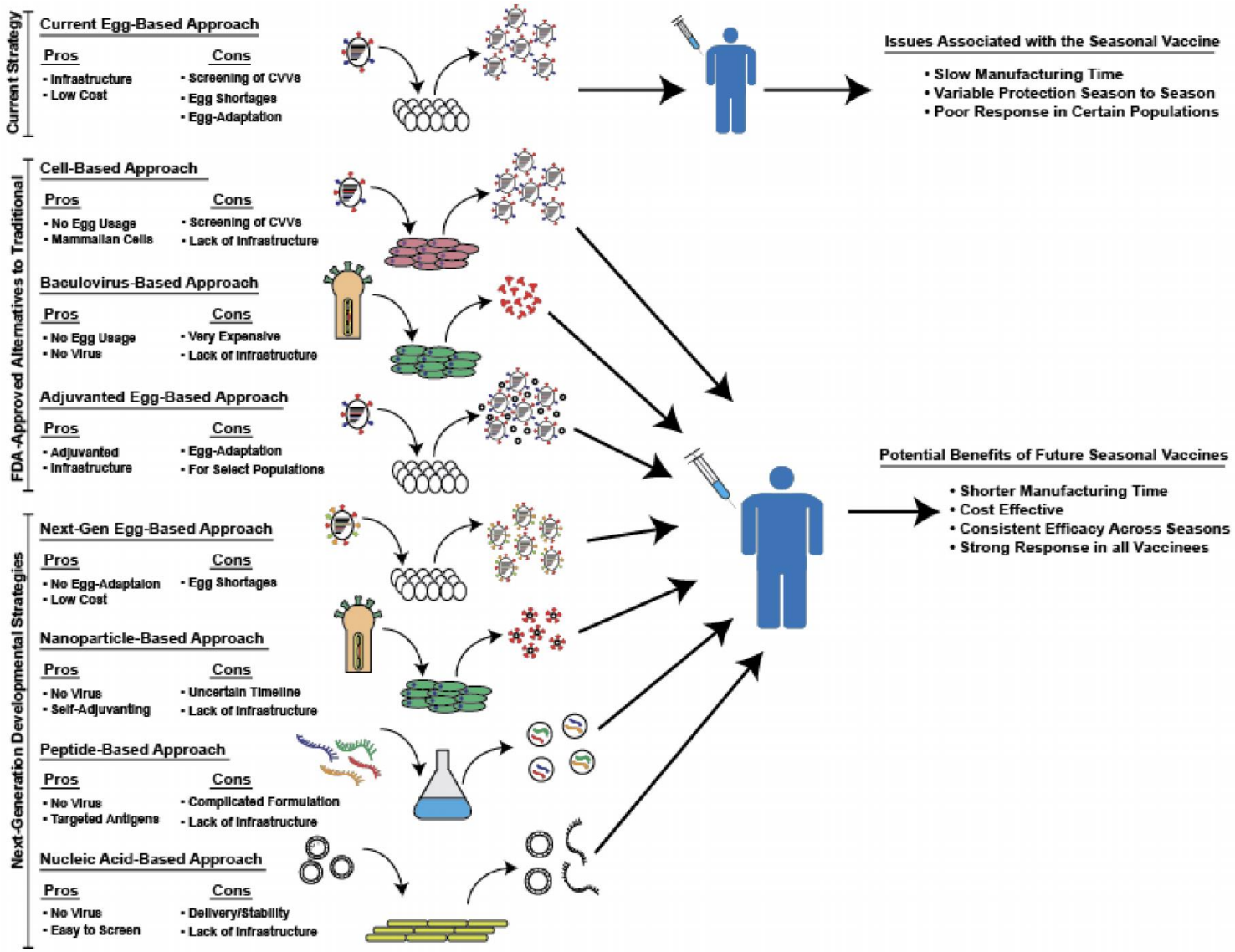

Figure 2: Illustration of the current available influenza vaccines, listed with the different pros and cons (Source: Figure 1 in Harding et al. (2018) [22]).

First vaccination strategies were developed in the 1940s, which consisted of producing inactivated whole-virions, using chicken egg embryos for virus propagation [24]. To date, the manufacture of egg-based inactivated vaccines is still the major production technique and starts by identifying the circulating influenza virus strains, and generates then trivalent or quadrivalent vaccines based on two IAV strains and one or two IBV strains. Every egg-based vaccine genome is based on a 6-segment influenza virus backbone (e.g. H1N1/A/PR/8/34 strain), giving high titers in chicken embryos. The backbone is not encoding for the new two major glycoproteins reassortants, HA and NA. After influenza virus propagation in chicken eggs, the produced virus is purified. The egg-based inactivated standard influenza vaccine is split using ether and/or detergent. HA and NA are, in the case of subunit vaccines, purified and enriched. Influenza vaccines are standardized based on the HA content, measured through the single radial immune-diffusion (SRID) assay. The vaccine has to contain 15 µg of HA protein per virus strain and should be stable for one year. Live-attenuated influenza vaccine can be as well produced in eggs by propagating cold-adapted influenza virus strains in chicken embryos. The manufacturing technique of egg-based inactivated or live-attenuated influenza vaccine remained similar over the years, and its low cost per dose allows protection from influenza disease in both developed and developing countries. Vast infrastructure for producing egg-based influenza vaccines currently exists and is required to meet the annual demand of new seasonal vaccines for the global population. It is estimated that the current egg-based manufacturing industry is capable of producing 1.5 billion doses annually. Currently, this number is difficult to reach using other vaccine manufacturing techniques [21, 22, 24].

However, egg-based influenza vaccine production presents many disadvantages. In case of pandemics, the influenza vaccine production capacity using this technology would be limited by a lack of manufacturing infrastructure and egg availability [25]. It would be necessary to increase the production by a factor of 1.5 in order to ensure world's population protection within one year. In addition, the presence of egg components can induce allergic reactions [24]. In order to produce high-yield egg-based influenza vaccines, the seed virus has to be adapted to the host cells, which extends the production time and reduces flexibility regarding influenza vaccine manufacturing. In addition, some virus strains such as the A/Fujian/411/2002 strain can still present very low yields even after adaption. Finally, it has

been shown that the virus adaptation process in the chicken embryo host can decrease the vaccine efficiency through alteration of the major antigen glycosylation [22].

To avoid egg-based influenza vaccine production, many alternatives have been developed as illustrated in Figure 2. Only two other egg-free production techniques have been approved by the authorities such as the FDA, which are both cell culture-based (Table 2). The first technique allows the propagation and the production of influenza virus using different cell culture systems as described into more details in section 2.3. The second technique consists in producing recombinant HA subunits with insect cell cultures and the baculovirus expression system. Both techniques allow for a higher production flexibility and present less glycosylation attenuation compared to egg-based influenza vaccine production [22, 24]. Manufacturing costs of cell-based vaccines tend to be higher than for egg-based products. However, it has been argued that costs can be decreased significantly using highly optimized cell culture processes [26]. Many other research studies aiming to improve influenza vaccines through for example a universal vaccine are currently being conducted [20, 22, 24].

Table 2: List of the currently FDA approved human influenza vaccines (https://www.fda.gov/vaccines-blood-biologics/vaccines/vaccines-licensed-use-united-states, 05.10.2020).

Product name	Trade name	Manufacturer	Vaccine type	Production host / system
IAV Vaccine, H1N1 2009	-	CSL Limited	Inactivated viral-based	Egg-based
IAV Vaccine, H1N1 2009	-	MedImmune	Live attenuated viral-based	Egg-based
IAV Vaccine, H1N1 2009	-	ID Biomedical Corporation of Quebec	Inactivated viral-based	Egg-based
IAV Vaccine, H1N1 2009	-	Novartis Vaccines and Diagnostics	Inactivated viral-based	Egg-based
IAV Vaccine, H1N1 2009	-	Sanofi Pasteur, Inc.	Inactivated viral-based	Egg-based
IAV Vaccine, H5N1	-	Sanofi Pasteur, Inc	Inactivated viral-based	Egg-based
IAV Vaccine, H5N1	-	ID Biomedical Corporation of Quebec	Inactivated viral-based	Egg-based
IAV Vaccine, H5N1	Audenz	Seqirus Inc.	Inactivated viral-based	MDCK cell culture-based
Influenza Vaccine	Fluad [a)] , Afluria [a)], Fluvirin, Agriflu	Seqirus Inc.	Inactivated viral-based	Egg-based
Influenza Vaccine	Flucelvax [a)]	Seqirus, Inc.	Inactivated viral-based	MDCK cell culture-based
Influenza Vaccine	FluLaval [a)]	ID Biomedical Corporation of Quebec	Inactivated viral-based	Egg-based
Influenza Vaccine	FluMist [a)]	Medimmune	Live attenuated viral-based	Egg-based
Influenza Vaccine	Fluarix [a)]	GlaxoSmithKline Biologicals	Inactivated viral-based	Egg-based
Influenza Vaccine	Fluzone [a)]	Sanofi Pasteur, Inc	Inactivated viral-based	Egg-based
Influenza Vaccine	Flublok [a)]	Protein Sciences Corporation, now Sanofi Pasteur	Recombinant HA	Insect sf9 cells, baculovirus expression system

IAV, Influenza A vaccine; HA, Hemagglutinin.

[a)] Includes as well the quadrivalent form.

2.2 Gene therapies

According to the FDA, gene therapy is a technique that modifies a person's genes to treat or cure disease. Gene therapies can work by several mechanisms: i) Replacing a disease-causing gene with a healthy copy of the gene, ii) inactivating a disease-causing gene that is not functioning properly., or iii) introducing a new or modified gene into the body to help treat a disease. This class of therapy is being investigated in order to treat many diseases such as cancer, genetic disease, and infectious diseases (Figure 3) [27].

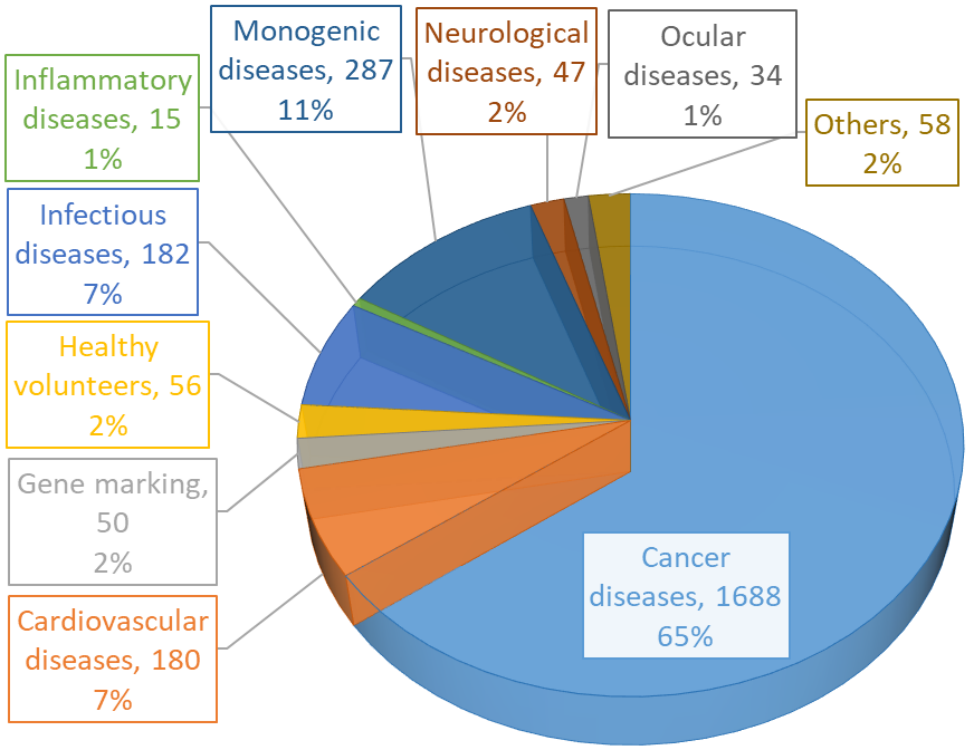

Figure 3: Human conditions addressed in gene therapy clinical trials, with their corresponding number of clinical trials and percentage numbers until 2017 (adapted from *The Journal of Gene Medicine, Gene Therapy Clinical Trials Worldwide*. Available at http://www.abedia.com/wiley/).

The first concept of gene therapy was reported in the 1970s by the first virus-mediated gene transfer and the creation of the first recombinant DNA molecule. It was then proposed that some human genetic conditions could be treated by the administration of exogenous DNA. The first challenge was the development of a delivery system for gene transfer, which was for the first time approved for human clinical trials using a murine retrovirus vector in 1990. Several clinical trials were halted in 1999 after the death of Jesse Gelsinger for the treatment of ornithine transcarbamylase deficiency. His death was linked to a severe immune reaction

to the recombinant adenoviral vector. Another major halt of gene therapy clinical trials occurred in 2003. It was observed that the insertion of a therapeutic gene treating a type of immunodeficiency led to leukemia of 4/10 of the treated patients. Enormous technological advances have been since then achieved, especially regarding the improvement of safety of delivery vectors and the development of better assays for risk assessment. This led to the first gene therapy approval in 2012 in Europe (Glybera®), which is based on an AAV vector [28]. To date, six gene therapies are approved by the FDA, as listed in Table 3.

Table 3: List of currently FDA approved gene therapies (https://www.fda.gov/vaccines-blood-biologics/cellular-gene-therapy-products/approved-cellular-and-gene-therapy-products, 05.10.2020).

Trade name	Manufacturer	Product description	Targeted disease
Imlygic	Amgen Inc.	Live, attenuated HSV-1 genetically modified to express huGM-CSF tumor growth inhibitor.	Melanoma
Kymriah	Novartis Pharmaceuticals Corporation	CD19-directed genetically modified autologous T cell immunotherapy comprised of autologous T cells that are genetically modified using a lentiviral vector to encode an anti-CD19 CAR. [a)]	B-cell lymphoblastic leukemia and diffuse large B-Cell lymphoma.
Luxuturna	Spark Therapeutics, Inc.	Adeno-associated virus vector-based gene therapy	Bi-allelic RPE65 mutation-associated retinal dystrophy.
Tecartus	Kite Pharma, Inc.	CD19-directed genetically modified autologous T cell immunotherapy. T cells are harvested and genetically modified ex vivo by retroviral transduction to express an anti-CD19 CAR. [a)]	Mantle cell lymphoma
Yescarta	Kite Pharma, Inc.	CD19-directed genetically modified autologous T cell immunotherapy. T cells are harvested and genetically modified ex vivo by retroviral transduction to express an anti-CD19 CAR. [a)]	Large B-cell lymphoma
Zolgensma	AveXis, Inc., now Novartis Gene Therapies	Adeno-associated virus vector-based gene therapy	Bi-allelic survival motor neuron 1 gene mutation-associated spinal muscular atrophy

HSV, Herpes simplex virus; CD19, cluster of differentiation 19; CAR, chimeric antigen receptor.

[a)] The therapy is a so-called cell therapy, however, the therapeutic cells are genetically modified.

Several vectors for gene therapy are currently being tested in clinical trials as shown in Figure 4. The ideal delivery system should meet several criteria, including (i) a good safety profile; (ii) easy production; (iii) good stability in target cells, and (iv) a high transgene capacity [29]. The most used delivery system is viral-based (Figure 4). Viruses are ideal vehicles for delivery of

genetic information, both for vaccine purposes and gene therapy. Issues that may affect synthetic DNA or RNA such as packaging and delivery of the payload [30, 31], amplification at the target site, and expression of foreign genetic information in the face of cellular defenses [32, 33] are already inherent properties of the infectious cycle. To date, all FDA approved gene therapies are using viral vectors for gene delivery (Table 3).

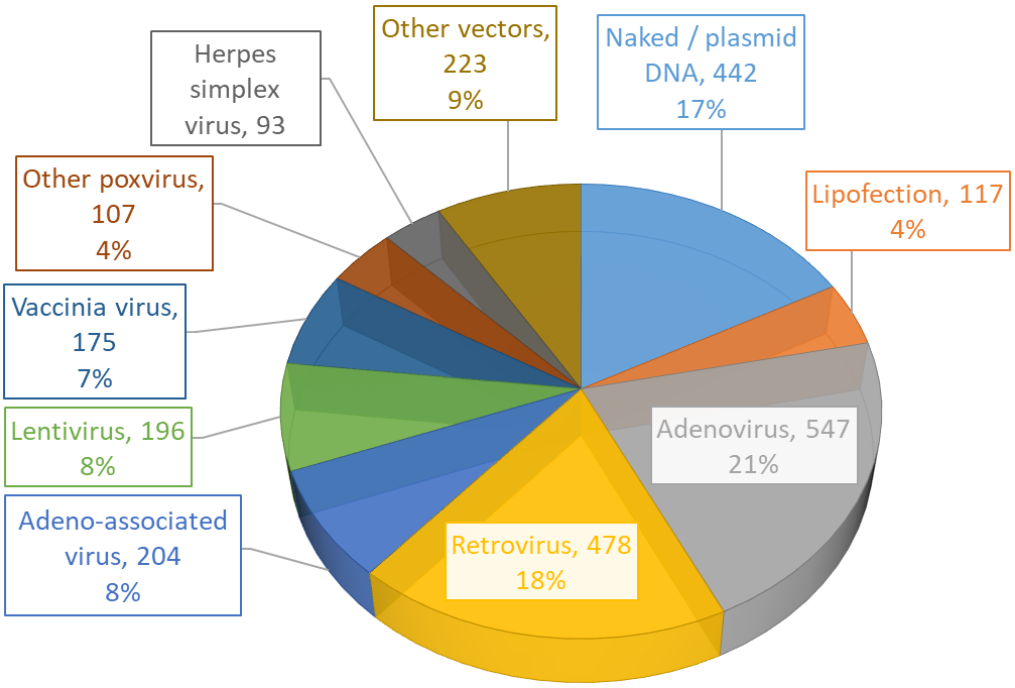

Figure 4: Different vectors used in gene therapy clinical trials, with their corresponding number of clinical trials and percentage numbers until 2017 (adapted from *The Journal of Gene Medicine, Gene Therapy Clinical Trials Worldwide*. Available at http://www.abedia.com/wiley/)

Some safety issues are still of a major concern when using viral vectors for gene therapy, as listed below (Table 4). To enhance safety, different strategies have been adopted, such as: avoiding viral vector replication, promoting their inactivation and attenuating their natural toxicity [29].

Table 4: Advantages and disadvantages of viral vectors used in gene therapy (adapted from Nóbrega et al. (2020) [29]).

Advantages	Disadvantages
High efficiency in gene transfer both *in vitro* and *in vivo*	Potential for immune and/or inflammatory response triggering
Long-term persistence in some cases	Limited cloning capacity
Broad cell targets	Complex production
Broad range of viruses to use	Limited tropism to certain types of cells in some cases
Natural tropism towards infection	Possibility of insertional mutagenesis
Evolved mechanism of endosomal escape	Molecular infection mechanism not fully understood

More recently, new techniques based on nucleases such as the clustered regularly interspaced palindromic repeats (CRISPR) systems can precisely edit the human genome. The high efficiency of CRISPR technology led to an enormous boost in its use and the first approved clinical trial started in 2016 in China [28].

2.2.1 Modified Vaccinia virus Ankara

MVA is a DNA virus strain, which was derived from the Vaccinia virus. Vaccinia virus belongs to the *Poxviridae* family, being widely used as the first vaccine for smallpox. It is double enveloped and has a size of about 250-350 nm diameter, being one of the largest viruses described [29, 34, 35]. The structure of the vaccinia virus is illustrated below (Figure 5).

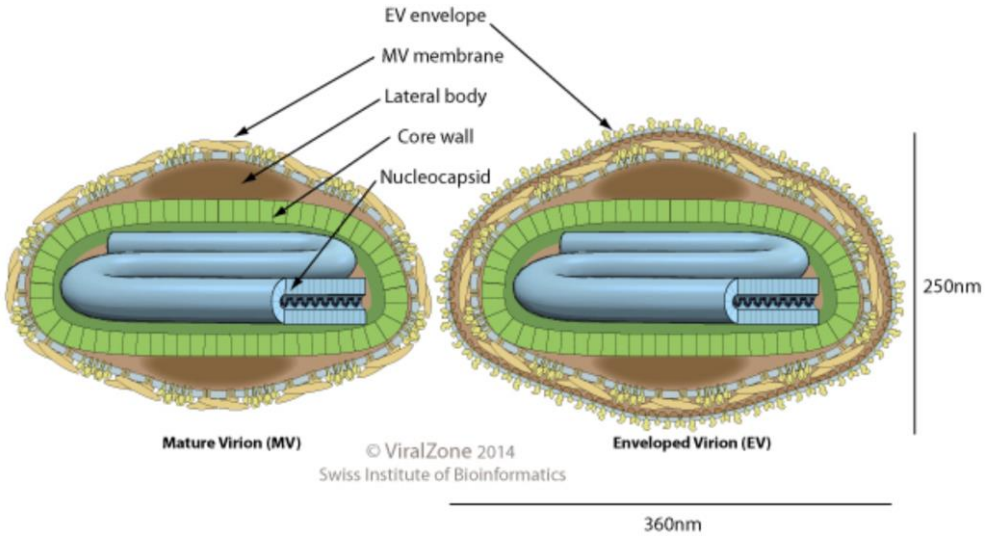

Figure 5: Illustration of a vaccinia virus (source: https://viralzone.expasy.org/149?outline=all_by_species, Swiss Institute of Bioinformatics).

MVA is replication-deficient in cells of mammalian origin, but can replicate in avian cells as it was adapted over many passages to this host. MVA can enter any target cell and activate its own molecular life cycle to express viral as well as recombinant genes. For this reason, recombinant MVA containing heterologous genes with therapeutic use have been developed, and are extremely safe for use. MVA was obtained by Mayr and Munz at the University of Munich in 1968 through 516 passages of a Vaccinia virus Ankara (originally propagated at the Turkish vaccine institute in Ankara for smallpox production) in chicken embryo fibroblast (CEF) tissue cultures. Major phenotypic changes of the new MVA strain were observed compared to the initial Vaccinia virus Ankara. MVA has lost the ability to cause cytopathic effect in e.g., human, porcine or bovine cells. It has been observed that it cannot form plaques in tissue cultures such as CEF, primary bovine, porcine kidney cells or HeLa cells. Loss of MVA virulence was also observed after its inoculation in rabbits, mice, macaques or humans. However, MVA maintained immunogenicity as a smallpox vaccine [34].

After MVA vg sequencing, it has been observed that it had been shortened from 208 to 178 kbp, with six major deletions sites, affecting many genes with functions in virus-host cell interaction, for example important immunomodulatory genes. The large deletion allows for large genes (> 5 kb) to be inserted compared to other viral vectors.

Generation of the first recombinant MVA has been reported in 1992. Surprisingly, only the recombinant genes were expressed, showing the viral vector to be exceptionally safe. Recombinant MVA was also shown to be immunogenic and to elicit strong cytotoxic T cell response towards the produced recombinant antigen [34].

A smallpox vaccine using MVA has been granted marketing authorization by the European Medicine Agency (EMA) and the Canada Health in 2013 [34] and by the FDA in 2019 (https://www.fda.gov/vaccines-blood-biologics/development-approval-process-cber/2019-biological-license-application-approvals), showing the potential of the viral vector to be used against other diseases.

For the reasons mentioned above, MVA can be considered as one viral vector of choice for gene therapy [34]. It is a promising viral vector for use against various infectious pathogens such as coronavirus [36], and for immunotherapy and the treatment of some types of cancers, as listed in Table 5.

Table 5: List of active or completed clinical trials, phase II and III, using Modified Vaccinia virus Ankara as a viral vector (https://clinicaltrials.gov, 06.10.2020).

Name	Sponsor	Product description	Targeted disease	Clinical phase trial
Ad26.ZEBOV + MVA-BN-Filo	1 MRC/UVRI Uganda Research Unit on Aids 2-10. Janssen Vaccines & Prevention B.V. 11. University Antwerp 12. Crucell Holland BV	Use of an adenoviral vector + MVA vector as a boost for vaccination	Ebola virus disease	II and III
Ad26.ZEBOV + MVA-BN-Filo + MenACWY	Janssen Vaccines & Prevention B.V.	Use of an adenoviral vector + MVA vector as a boost + MenACWY [a)] drug for vaccination	Ebola virus disease	III
MVA-BN-RSV	Bavarian Nordic	MVA viral vector for vaccination	RSV Infection	II
MVA-BN-Brachyury + atezolizumab PROSTAC	University of Utah	MVA viral vector for immunotherapy	Prostate adenocarcinoma	II
Multi-peptide CMV-MVA Vaccine	City of Hope Medical Center	MVA viral vector for vaccination	Cytomegalovirus complications	II
Ad26.HPV16 and/or Ad26.HPV18 + MVA.HPV16/18	Janssen Vaccines & Prevention B.V.	Use of an adenoviral vector + MVA vector as a boost for vaccination	Human papillomavirus types 16 and 18	II
Ad26.Mos.HIV + MVA-Mosaic	Janssen Vaccines & Prevention B.V.	Use of an adenoviral vector + MVA vector as a boost for vaccination	HIV	II
MVA-nef	National Institute of Health	MVA viral vector for vaccination	HIV	II
Ad26.Mos.HIV + MVA-Mosaic + gp140 DP	National Institute of Health	Use of an adenoviral vector + MVA vector as a boost + the go140 DP [a)] drug for vaccination	HIV	II
mFOLFOX6 + MVA-BN-CV301 + FPV-CV301 + Nivolumab	Hoosier Cancer Research Network	Use of a fowpox viral vector and MVA viral vector plus mFOLFOX6 [a)] and Nivolumab [a)] drugs for immunotherapy	Metastatic colorectal cancer	II

RSV, Respiratory Syncytial Virus; HIV, Human Immunodeficiency Virus

[a)] Drug name.

The MVA viral vectors from the list of clinical trials described in Table 5 have been generated by adaptation to CEF [37] and cannot replicate in human recipients. Because of this strong

attenuation, it is currently estimated that about 10^8 plaque forming units (pfu; virus infectivity) per dose are required for efficient vaccination [38].

2.3 Cell culture-based virus production

The first generation of cell culture-based viral vaccines led to the production of polio vaccine in 1955 using adherent Vero cells, followed by the development of many other vaccines such as measles, rubella, influenza, smallpox or hepatitis A [16, 19]. The use of cell cultures for vaccine generation allows a shorter process time and higher flexibility compared to other alternatives such as egg-based production. As mentioned in section 2.2, gene therapies also use cell culture technology for viral vectors generation since the 1970s, such as retrovirus, adenovirus or AAV.

Cell culture-based virus production processes are generally separated in two phases: USP and DSP. The USP part includes the cell culture and the DSP part comprises the purification (DSP is tackled extensively in section 2.4). Different cell culture platforms have been developed to support cell culture-based virus production as reviewed by Gallo-Ramirez et al. 2015 [39]. Cell culture media can contain animal components. The use of chemically-defined medium (not using animal components) allows a risk reduction of adventitious agent contamination such as prions or viruses. Its composition is known, increasing reproducibility and safety.

Adherent cells are cultivated using static systems such as roller bottles or multilayers systems, using a stirred-tank bioreactor (STR) together with micro-carriers or using a packed-bed bioreactor with macrocarriers. The first cell culture-based vaccines and viral-based gene therapies, were generated using static systems. Performing suspension cell culture is more straightforward and typically needs a STR. In addition, cell culture in suspension allows an easier scale-up. Suspension cell cultures can be eventually intensified through perfusion mode, as described in section 2.6. Different options for cell substrates are described in section 2.3.1. Cell culture-based virus production processes are typically run in batch or in fed-batch mode. For adherent cell culture systems, equally intensified processes are available. Here, one simple option for process intensification is a multiple harvests strategy. This can increase product stability and reduce effects of interference of released enzymes or defective virus particles.

Most sophisticated virus production systems (reported in the literature) are using immortalized Good Manufacturing Practice (GMP)-compliant cells, in perfusion, using chemically-defined medium. However, this is only applied in academy [40]. In the industry, an example of sophisticated vaccine production is the company Seqirus producing a cell culture-based influenza vaccine using suspension Madin-Darby canine kidney (MDCK) cells (Table 2). Cell culture based vaccine production has been proved to be safe using chemically-defined media with suspension cells. However, in the case of seasonal influenza vaccine, this technology is minimally used for global supply [22].

Once a cultivation system is chosen, the cell culture is usually started free of any virus until a certain cell concentration is reached. The USP step is divided in two phases: the cell growth phase and the virus production phase. In order to then start the virus production, several ways can be performed such as transient transfection (e.g., AAV, lentivirus), induction of virus expression (e.g. AAV, lentivirus) or simply by the infection with a seed virus at a certain multiplicity of infection (MOI; e.g., IAV, MVA, adenovirus). The addition of other compounds may be needed to increase the virus production, such as trypsin for IAV production. At time of infection (TOI), the cell culture medium might be changed through medium exchange with fresh medium, bioreactor volume dilution or through perfusion. After an incubation time, typically between 1 to 5 days, the cell culture is harvested. Especially for adherent cells, multiple harvest strategies are often pursued. As the virus production is usually lytic, the harvest usually contains cell debris and optimal harvest time is very critical to avoid virus degradation. In case the virus remains intracellular, the cells are lysed. The product is then cell clarified typically through depth filtration or centrifugation [7, 41-43]. Virus purification is extensively described in section 2.4.

2.3.1 Cell substrates for virus production

Some viruses have an extremely narrow host range and require a special or even unique cell substrate. Ideally, a host cell line should have a doubling time of 20–30 h with high viability, allow easy scale-up, and enable fast virus production to high titers with low protein and DNA concentration in the virus harvest to facilitate purification [44]. Moreover, safety aspects should be assessed. In particular, the cell line should be free of any adventitious agents and have low tumorigenic and oncogenic potential [45].

Cell substrates for influenza virus production

Influenza vaccines, are typically manufactured using MDCK cells (suspension or adherent cells) or Vero cells (adherent cells), namely Influvac® (Solvay Pharmaceuticals Inc.), Influjject® (Baxter Vaccines) [44] and Flucelvax® (Seqirus) [22]. Other suspension cell lines, such as AGE1.CR®, PER.C6® [44], EB66® [24] or DuckCelt®-T17 [46], have also been evaluated for influenza vaccine production. Highest reported influenza virus yields were obtained in MDCK suspension cells with titers of 3.9 $\log_{10}$(HA units/100 µL) for influenza A/PR/8/34 virus [47]. Although several cell lines have been tested, there are still significant efforts to develop more potent cell lines. As influenza pandemics can arise from different animal reservoirs, having a larger choice of cell substrates from different species for production is beneficial [44]. Also, differences in productivity can be observed depending on influenza virus strain and cell line origin.

Although several cell substrates have been proposed for influenza virus production only two cell lines (Vero and MDCK cells) are recommended by the WHO [48]. Preference for MDCK cells has been observed as use of Vero cells for influenza vaccine production has been discontinued in 2012 (Preflucel®). MDCK cells seem to be preferred over Vero cells as they allow for a fast and robust cells growth, with high influenza virus productivity [44]. In addition, they are highly permissive to a wide range of influenza virus strains, sometimes without needing adaption [48, 49]. Influenza virus titers have been observed to be higher for MDCK cells than for processes using Vero cells [50, 51]. Another strong advantage is that it has been made possible for MDCK cells to grow in suspension since 1997 [52], and commercialize human influenza vaccine using MDCK suspension cells already in 2007 [53]. Successful adaption of Vero cells growing in suspension has been reported in academic research only since 2009. Up to now, suspension Vero cells still present long doubling time over 40 h and frequently form aggregates [54].

Cell substrates for MVA production

For large vaccine programs or gene therapies, the necessary yields are difficult to obtain with the conventional CEF production substrate that was also used for stepwise MVA attenuation. CEF cultures are anchorage-dependent primary cells with a limited lifespan and require animal-derived components in the culture medium for growth. These animal-derived components involve, however, the risk of contamination with adventitious agents and should be avoided for use in GMP production.

To circumvent this concern for production of MVA, an avian suspension cell line (AGE1.CR.pIX) was developed by ProBioGen AG together with IDT Biologika [55]. From the beginning it was aimed for cell growth in chemically-defined medium [56]. The subsequent virus production phase involved the addition of a (also chemically-defined) medium to induce suspended cell aggregates to facilitate MVA spreading, as a large fraction of the infectious poxviruses are disseminated by direct cell-to-cell contact. Induction of aggregates improved virus yields and recently cost-efficient production of some vaccine candidates was described [57, 58]. To facilitate process intensification and enable continuous virus harvesting, an MVA strain with reduced dependency on direct cell-to-cell contacts would be beneficial. Such a strain, MVA-CR19, was obtained from avian suspension cells [59, 60] that are used in this thesis. The AGE1.CR.pIX cell line was shown to efficiently produce current GMP (cGMP)-grade MVA-based human vaccine and to be as efficient and safe as MVA-based human vaccine produced with CEF [57]. The MVA production process using MVA-CR19 seed virus with suspension AGE1.CR.pIX cells in chemically-defined medium is considered here to be the most sophisticated.

Alternatively, other avian immortalized suspension cell line called EB66 developed by Valneva also allows the production of MVA [61]. The cell line was derived from duck embryonic stem cells and was immortalized without genetic, viral or chemical modification, becoming suitable for vaccine and therapeutic protein production [62]. However, the production of MVA using this cell line requires cell aggregation and the virus remains intracellular [61], which are disadvantages for process intensification. To avoid the use of CEF for static cultures, IDT Biologika developed an immortalized chicken cell line called DF-1.

2.4 Virus purification

Once a cell-free harvest is obtained, the DSP is initiated. For inactivated cell culture-based vaccine production (influenza vaccine), the virus is inactivated by adding for example Triton or formaldehyde. To decrease host cell DNA impurities, endonucleases such as Benzonase® or Denarase® might be used. Other impurities such as host cell proteins, empty capsids or production reagents are then later removed through several steps of filtration, ultrafiltration

/ diafiltration (UF/DF), ultracentrifugation (such as the iodixanol gradient technique) and chromatography steps (such as ion-exchange chromatography) [7, 41-43].

The use of filtration or chromatography technologies for virus purification are extensively reviewed [63-65]. In particular for the polishing step, anion exchange chromatography or affinity chromatography, both using beads, are part of the standard procedure for purification. If needed and in order to concentrate the product before purification, an UF/DF is typically performed. Unlike for monoclonal antibodies (mAbs) production, the downstream purification drastically differs following the type of the produced virus. Virus can differ in size, in being either enveloped or non-enveloped, in the place of virus replication within the cells, in virus budding or in the composition of membrane. It depends if an inactivated whole virus vaccine, a subunit vaccine or a live-attenuated vaccine is envisioned. Then particularly, buffer and temperature choice need to foresee possible virus degradation or inactivation. As such, some processes request cell lysis, and others require only to harvest the supernatant. This has a major impact on DSP design. Early harvest time points are preferred as with ongoing cell lysis proteases and other degrading enzymes are released. The virus stability following incubation time, pH condition, buffer composition, product aggregation especially influences the DSP design.

Total recoveries (from the bioreactor harvest to the purified virus particle) of 61–63% for adenovirus [66, 67], 41% for MVA [61], 52% for influenza virus [68] or 20–60% for AAV [67, 69] were reported. A typical downstream process scheme from the bioreactor harvest to the purified virus particle is shown below (Figure 6).

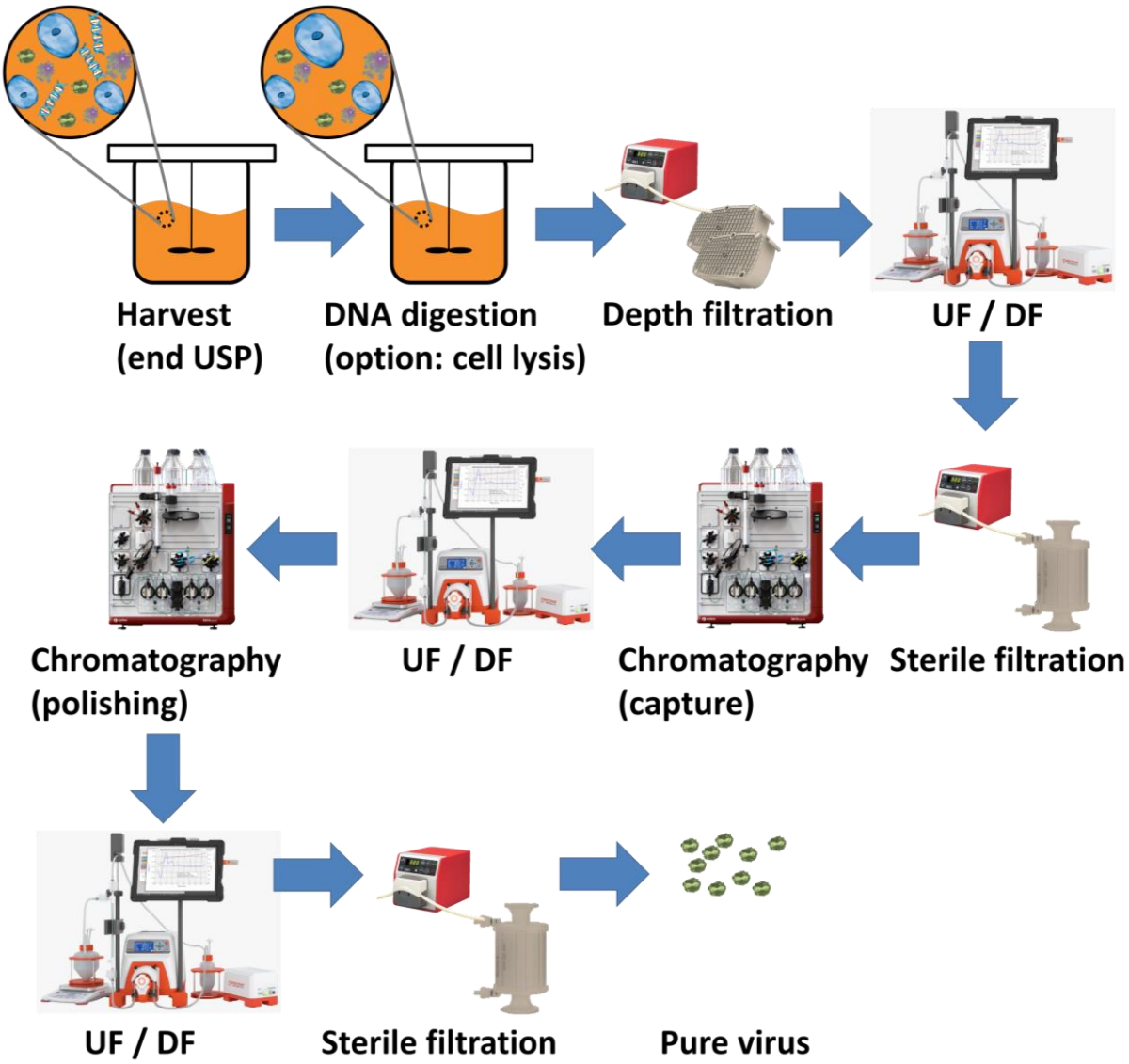

Figure 6: Illustration of a typical large-scale purification process of a viral vector**.** The virus is produced in cell cultures, in a bioreactor. At the end of the upstream processing (USP), the bioreactor is harvested. The host cell DNA impurity can be digested by an enzyme, and the cells can be eventually lysed. To remove the cells and cell debris, a depth filtration is performed (in general, using two different depth filters: Primary and secondary depth filtration). The material can be concentrated and/or buffer exchanged with an ultrafiltration / diafiltration step (UF/DF). A filtration step is performed prior to chromatography to protect the chromatography column. A first chromatography is performed to capture the viral vector (capture step). A UF/DF can be performed, mainly to change the buffer composition prior the second chromatography (polishing step). After the second chromatography, the material can be again buffer exchanged (in the formulation buffer) or concentrated (UF/DF) and sterile filtered.

2.4.1 Membrane filtration

Membrane-based virus filtration is a technology of choice for traditional vaccine or gene therapy manufacturing, due to its robustness and scalability. It can be used as a cell clarification step through depth filtration, microfiltration, TFF (tangential flow filtration) and for membrane-based perfusion (section 2.6.1). Different filter materials can be used such as

regenerated cellulose, polysulfone (PS), or regenerated polyethersulfone (PES). In addition, diatomaceous earth can be used in depth filters [63-65]. The pore size of the filter is in the range of 0.1 to 75 µm. The general goal is to obtain virus in cell culture medium, free of cell debris or entire cells. The membrane cut-off should be smaller than the cell diameter or the cell debris, while allowing the virus to pass through the membrane.

Alternatively, the product of interest (here: the virus) can be retained by the filter. The product can be concentrated (UF) and/or the buffer can be exchanged, washing away small molecules and undesired salts (DF). The general molecular weight cut-off of the membrane for UF/DF is 100–750 kDa.

A major challenge when filtering virus and retaining only the impurities is filter fouling. Filter fouling is a phenomenon by which elements are deposited at the surface of the filter, causing a decrease of the filtration performance. The filtration performance is defined here by the filtration flux (flow rate), the trans-membrane pressure (TMP) and the product sieving. The product sieving (often calculated in percentage) is the efficiency to separate the product from the retentate (impurities retained by the filter).

The causes of filter fouling during virus manufacturing are multiple. It is not only due to the relatively large size of some viruses (> 80 nm for influenza virus) and possible virus aggregate formation, but also depends on virus-induced apoptosis and cell lysis, and the release of host cell DNA and proteins. Chemicals such as antifoam can also contribute to filter fouling. Wang et al. (2017) have shown that cell debris in the 100 nm size range actively contributes to lower product sieving [70].This potentially results in cake formation, narrows pores or blocks completely the membranes and thus prevents the recovery of virus through such membranes.

Filter fouling is a complex process and many models have been developed for membrane-based cell culture clarification and perfusion [71-76]. There are two types of filter fouling: the reversible filter fouling and the irreversible filter fouling. i) The reversible filter fouling is when a concentration polarization is formed in the liquid phase near the membrane and reversed when the pressure from the permeate flow is released. ii) The irreversible filter fouling is formed through deposit formation.

The mechanisms for membrane fouling are: pore blocking, intermediate pore blocking, pore constriction, and cake formation. Pore blocking is the main factor for irreversible membrane

fouling [72, 74]. Product sieving [75] and filter fouling can be correlated to the increase in permeate flux or TMP (in Pa) [71], which can be modeled through Darcy's law:

$$\mathbf{J} = \frac{\mathbf{\Delta P}}{\boldsymbol{\eta} \times \mathbf{R_t}} \quad (1)$$

With J, the permeate flux (m/s);
ΔP, the trans-membrane pressure (TMP; Pa);
η, the dynamic viscosity of the liquid (kg/s/m) and
R_t, the total membrane resistance (1/m).

The total membrane resistance is mainly driven by filter fouling. In order to avoid a TMP increase over time, the main parameter to consider is the permeate flux [71, 76, 77]. In order to decrease membrane fouling, a tangential flow filtration can be operated, instead of a dead-end orthogonal filtration.

Another way to decrease filter fouling is by using an adapted membrane material (a screening is needed) or through the use of larger pore sizes [73, 78, 79]. Moreover, if the pores are uniform or changing in pore size over the length of the pores or if the structure is smooth or rough, this will impact on the product sieving. Finally, the membrane material, surface charge, pore size distribution, surface roughness and salt concentration / composition in the raw material are also important parameters to consider regarding the decrease of product sieving [80].

2.4.2 Steric exclusion chromatography

The use of steric exclusion chromatography (SXC) was first reported by Lee et al. (2012) [81]. The authors reported the purification of immunoglobulin (Ig) G, IgM and bacteriophages by using hydroxyl-substituted polymethacrylate monoliths as the stationary phase and polyethylene glycol (PEG) to retain the product of interest in the stationary phase, before decreasing PEG concentration for elution. The selectivity pf SXC is mainly a function of the molecular size of the targeted molecule to purify. SXC is on several points similar to precipitation provoked by molecular crowding. Investigation of the phenomenon was already reported in 1958, showing that physical interactions between chemically non-reactive solutes should result in the steric exclusion of the solutes from each other. This should create a zone

around a given solute molecule, such as a protein, in which the concentration of other solutes is deficient compared to their concentration in the bulk solution [81]. The creation of such a discontinuous zone, which is unfavorable, creates an increase in free energy, which drives redistribution of elements in order to reach a lower energy state (thermodynamic destabilization) [81, 82]. Several parameters can influence the steric exclusion phenomenon which are: (i) the increase of the solute concentration, (ii) the solute size, (iii) the chemical properties of the solutes which influence and modify steric effects through repulsive or attractive forces among solute, (iv) pH and conductivity, which influence electrostatic interactions between solutes and (v) the alteration of the water by salt or other small molecules addition [81].

The use of SXC was further developed in our group by Marichal-Gallardo et al., showing in 2017 that IAV could be successfully purified using a regenerated cellulose membrane and PEG [82]. PEG is an inert, non-ionic, soluble and weakly hydrophobic organic polymer. The polymer does not interact with most hydrophilic surfaces [81]. Due to its properties, PEG size is variable. When PEG is added to a solution containing non-purified virus, a thermodynamic destabilization is created as described in the previous paragraph. To reduce the free energy state, the surface between the virus particle components / the membrane and the solute will be reduced. By consequence, the virus particles associate between each other and with the membrane, without any direct chemical interaction [82]. The hydrophilic property of the regenerated cellulose membrane is furthermore beneficial as PEG is sterically excluded from hydrophilic surfaces and the association between a virus and a hydrophilic surface is even more favoured [83]. The rest of the impurities present in the solution (entities smaller than the virus particles) aren't affected by the PEG solution and will be simply washed away [82, 83]. The purified product will then be eluted by decreasing the PEG concentration. To increase the thermodynamic destabilization, one can increase the PEG concentration, the PEG size, the protein concentration and the protein size [81]. The thickness of the PEG-deficient zone is proportional to the hydrodynamic radius (related to its molecular mass) of the PEG [82]. The SXC mechanism is illustrated below (Figure 7):

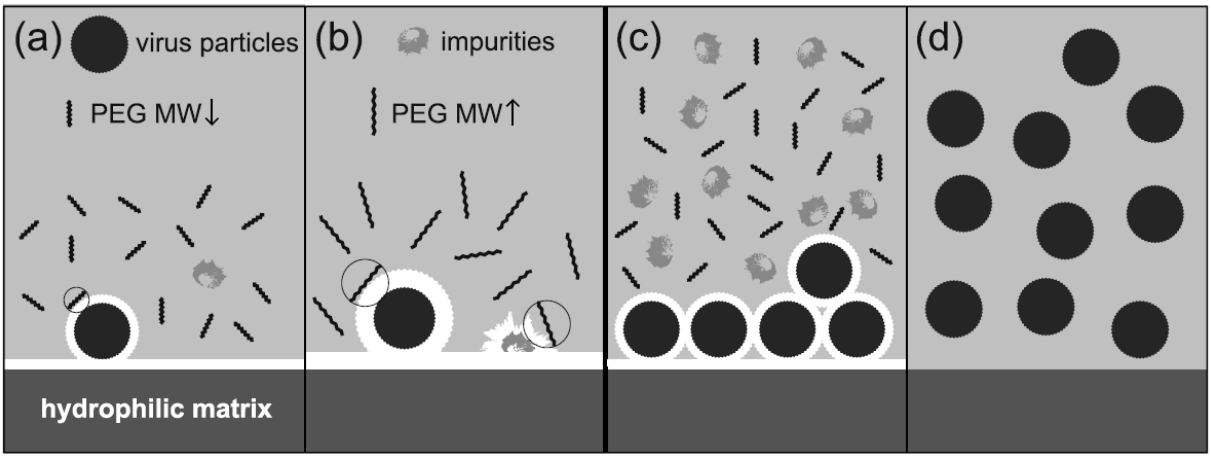

Figure 7: Illustration of the mode of action for steric exclusion chromatography. (a) Creation of a polyethylene glycol (PEG)-deficient zone (white zone), which can be increased by increasing the PEG molecular weight (MW) (b), allowing smaller impurities to be excluded from the bulk solvent like the virus particles. By increasing the PEG concentration, several large-sized particles will associate with each other plus the hydrophilic membrane in order to decrease the contact area with the bulk solvent (c). For the purified virus particles elution, the PEG concentration is decreased (d), disrupting the steric exclusion (source: Figure 1 from Marichal-Gallardo et al. (2018) [82]).

The use of SXC for virus particle purification presents many advantages compared to other DSP techniques. First, as mentioned in section 2.4, most of the chromatography techniques are based on beads, which limits the surface interactions between very large particles (such as viruses) and the beads. In the case of SXC, the size of the entity to be purified does not affect separation performance as the small pore size of the regenerated cellulose membrane (stationary phase) allows for convective mass transport (not influenced by diffusive transport). In addition, the absence of diffusive transport decreases in this case the peak broadening (for elution) and increases the maximum product capacity of the membrane [82, 83]. Finally, no column bead packing is needed, and the material used for SXC (regenerated cellulose and PEG) is cheaper than the beads.

2.5 Process analytical technology

One option to avoid process failure and to achieve desired quality attributes of a product is the use of process analytical technology (PAT), as introduced by the FDA in 2004 [84]. PAT allows through real-time monitoring with in-line, on-line and at-line measurements the analysis, the control and the improvement of a production process, giving more confidence in meeting quality requirements [85]. PAT is also needed for process control and automation

[86]. Options allowing real-time monitoring to control a bioreactor are listed in Table 6 (non-exhaustive list).

Table 6: Options allowing real-time monitoring of a mammalian cell culture (non-exhaustive list; adapted from Yee et al. (2018) [87]).

Measured parameter(s)	Monitoring instrument	Technology description
Glucose and lactate	BioPAT Trace	Measures online the glucose and lactate concentration through enzymatic reaction and amperometric detection.
Glucose [a)]	Raman spectrometer	Measures online the glucose concentration through the collection of a set of spectra and corresponding accurate offline measurements. Multivariate statistical techniques, such as PLS regression, are used to link spectral data with model-predicted outputs.
Glucose, glutamate, glutamine, ammonium and lactate	Auto-sampler connected to a metabolite measurer (NovaFlex or Bioprofile Flex)	Measures at-line metabolites through a sensor using enzymatic reaction and amperometric detection.
Glucose and glutamine [b)]	Auto-sampler connected to a HPLC	Different chromatography technique such as a silica stationary phase with propyl amine functionality, and detection by measuring a refractive index.
Oxygen concentration and oxygen consumption rate	Mass spectrometry	Off-gas analysis by mass spectrometry.
pH	pH probe	Potentiometric or optical pH meter
Oxygen concentration and oxygen consumption rate	DO probe and gassing mass flow controllers	Amperometric or optical DO sensor with mass flow controllers
Cell concentration or biomass	Optical sensor	Measures the turbidity of the cell culture to determine the biomass concentration.
Viable cell concentration or biomass [c)]	Capacitance sensor	Measures the electric capacitance of the cell culture to determine the viable biomass concentration.

PLS, Partial least square; HPLC, High performance liquid chromatography; DO, dissolved oxygen.

[a)] Raman spectroscopy was also reported to be able to monitor: Glutamine concentration, glutamate concentration, lactate concentration, ammonium concentration, viable cell concentration, total cell concentration, osmolality, antibody titer, antibody glycosylation and amino acid concentration [87].

[b)] An HPLC system can be also implemented to measure other entities such as antibody, virus capsid or amino acids.

[c)] The capacitance sensor can also deduct the cell size variation or changes of cell metabolism through variation of cell membrane capacitance or intracellular conductivity (section 2.5.1).

Among several options depicted in Table 6 for PAT, the online probe measuring the electric capacitance signal has already been shown to efficiently monitor cell growth, cell size, metabolic state, apoptosis and viral infection [88-91]. One key process parameter, the optimal time of virus harvest, could be determined using the electric capacitance signal for some virus strains such as measles or AAV [92, 93]. By determining for each different batch the optimal time of harvest, the material might become more homogenous and simplify DSP.

2.5.1 Capacitance probe

The use of a capacitance probe (or dielectric spectroscopy) for cell culture online biomass monitoring has been first introduced by Harris et al. in 1987 [94]. Since then, it has been widely used for monitoring plant cell cultures, microbial fermentations or animal cell cultures such as Chinese hamster ovary (CHO) cells [95], in a setup as illustrated below (Figure 8). Lately, capacitance probes were also used to monitor other aspects such as the cell cycle, the oxygen uptake rate or different virus production steps [88, 89].

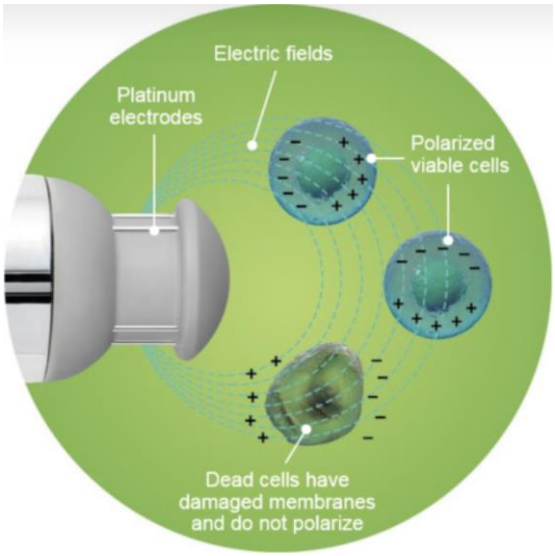

Figure 8: Illustration of a capacitance probe in cell culture, monitoring biomass formation from viable cells (source: https://www.hamiltoncompany.com/process-analytics/viable-cell-density-incyte).

A capacitance probe generates an electric field alternating between 0.1 and 10 MHz (suitable range for animal cell culture). Due to the alternating electric field, a charge separation will operate at the poles of the cells, as their cytoplasm is surrounded by a non-conducting cellular membrane. The cells act by consequence as mini-capacitors. At a very low frequency of the signal generated by the probe, the cells are polarized, increasing the capacitance signal within the solution of the cell culture broth. At high frequency, the cells cannot polarize and the capacitance signal is thus low. By consequence, the cells do not contribute to the capacitance signal, and this is then often taken as the cell culture medium capacitance signal or background capacitance. Entities without an intact non-conductive membrane such as dead cells cannot be polarized. A distribution is obtained when measuring the capacitance signal over a wide range of frequencies, as illustrated in Figure 9A. The loss of polarization over a

range of frequencies is referred as the β-dispersion (Figure 9A). By subtracting the background capacitance at high frequency to the measured capacitance signal (called ΔC, in F), there is a proportionality between the biovolume and ΔC as illustrated in Figure 9B. As long as the cell size remains constant, the biovolume can be correlated to the viable cell concentration (VCC) by linear regression. However, typically the cell size might change over time. The variation in the cell size can be observed with the critical frequency variation (f_c, in Hz; Figure 9C). F_c is the frequency at which the cell polarization is half complete (Figure 9C). For the same biovolume (and the same ΔC), in the case the cell diameter decreases, the f_c will increase as the cells are depolarized faster (due to their smaller size; see Figure 9C) [95].

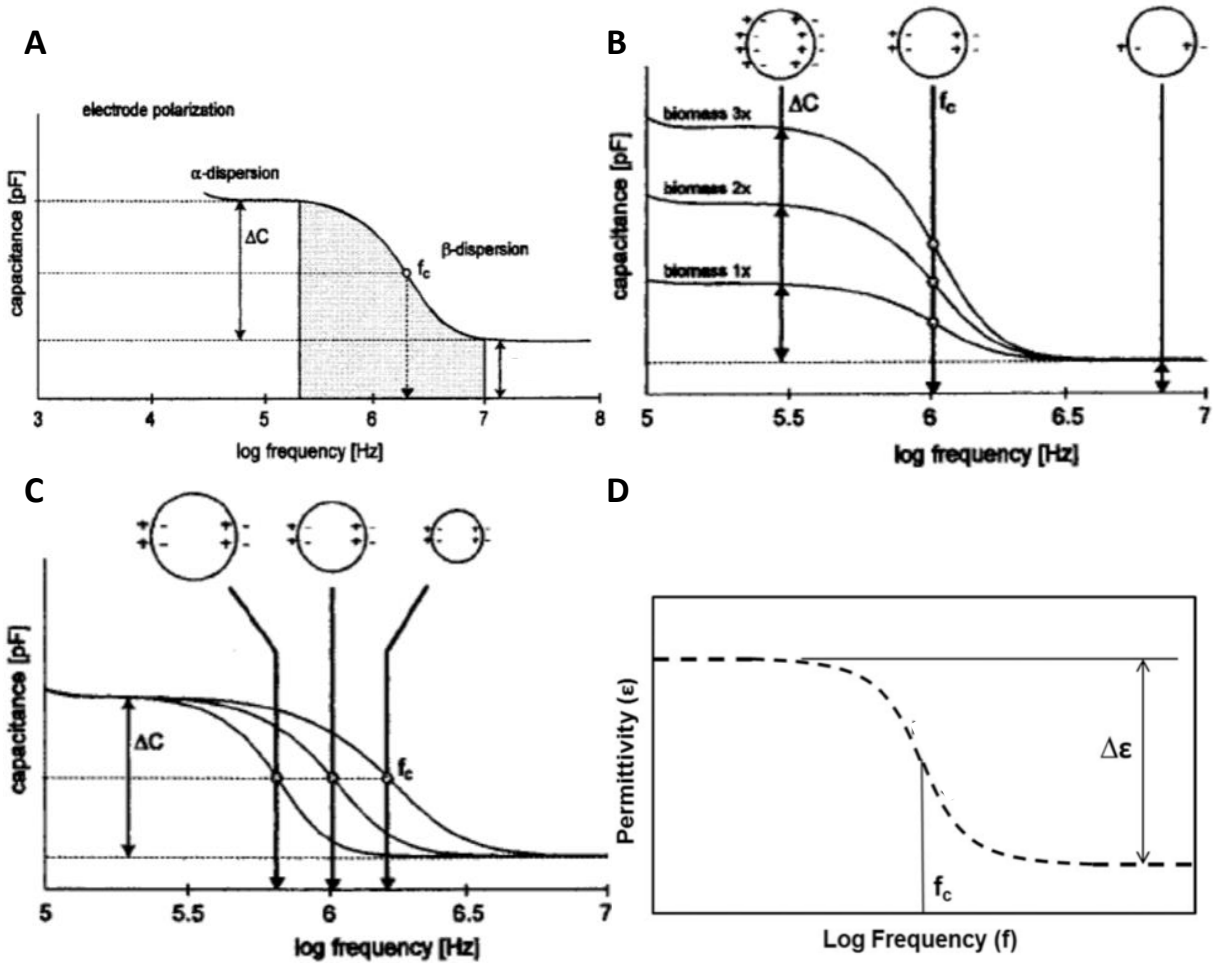

Figure 9: Different illustrations of the β-dispersion from a capacitance probe, plotting the capacitance signal or the permittivity signal in function of the frequency of the alternating electric field. (A) A typical illustration of the capacitance signal versus the frequency. (B) Modification of the capacitance signal in function of the biomass or biovolume increase. (C) Modification of the critical frequency (f_c) in function of the cell diameter decrease. (D) Typical β-dispersion reported by the capacitance probes nowadays (the permittivity ε, in pF/m and the logarithmic frequency, in log([Hz])), (source: Figure 1A from Cannizzaro et al. (2003) [95]; Figure 2B and 2C from Cannizzaro et al. (2003) [95]; Figure 1D from Downey et al. (2014) [96]).

The permittivity signal (ε, in F/m) is sometimes reported instead of the capacitance signal (C, in F) (Figure 9D). The most important value of the permittivity signal is the maximum permittivity signal ($\Delta\varepsilon_{max}$, in F/m), which is the difference between the permittivity signal at low frequency and the permittivity signal at high frequency (illustrated in Figure 9D). The capacitance signal (C, in F) can be converted into the permittivity signal (ε, in F/m) as follow [88]:

$$\mathbf{C} = \boldsymbol{\varepsilon} \times \frac{\mathbf{A_e}}{\mathbf{d_e}} \quad (2)$$

With A_e, the electric field area, between the two electrodes (determined by the manufacturer; m^2) and
d_e, the electric field length, between the two electrodes (determined the manufacturer; m).

There are several ways to directly correlate β-dispersion with the VCC. Two examples are a simple linear regression between the $\Delta\varepsilon_{max}$ and the VCC or a principal component analysis followed by the establishment of a partial least square (PLS) model prediction [95].

According to the theory of Schwann established in 1957, the cells can be considered as spherical mini-capacitors, and different information specific to the cell such as the intracellular conductivity (σ_i, in S/m, which is F/s/m) and the cell membrane capacitance (C_m, in F/m^2) can be calculated [88, 89]. The volume fraction of cells in the cell culture medium and the cell radius is calculated following the cell radius size distribution (from raw data from an automated cell counter such as a ViCell XR).

$$\Delta\boldsymbol{\varepsilon}_{\mathbf{max}} = \mathbf{3\pi} \times \mathbf{r^4} \times \mathbf{x} \times \mathbf{C_m} \quad (3)$$

$$\mathbf{f_c} = \frac{\mathbf{1}}{\mathbf{2} \times \boldsymbol{\pi} \times \mathbf{r} \times \mathbf{C_m} \times \left(\frac{\mathbf{1}}{\boldsymbol{\sigma}_\mathbf{i}} + \frac{\mathbf{1}}{\mathbf{2} \times \boldsymbol{\sigma}_\mathbf{m}}\right)} \quad (4)$$

$$\boldsymbol{\sigma}_\mathbf{i} = \frac{\mathbf{8} \times \boldsymbol{\pi} \times \mathbf{f_c} \times \Delta\boldsymbol{\varepsilon}_{\mathbf{max}} \times \boldsymbol{\sigma}_\mathbf{m}}{\mathbf{9} \times \mathbf{B_v} \times \boldsymbol{\sigma}_\mathbf{m} - \mathbf{4} \times \boldsymbol{\pi} \times \mathbf{f_c} \times \Delta\boldsymbol{\varepsilon}_{\mathbf{max}}} \quad (5)$$

$$\mathbf{C_m} = \frac{\mathbf{4} \times \Delta\boldsymbol{\varepsilon}_{\mathbf{max}}}{\mathbf{9} \times \mathbf{r} \times \mathbf{B_v}} \quad (6)$$

With r, the cell radius (m);
B_v, the volume fraction of cells in the culture medium (-) and
σ_m, the cell culture medium conductivity (S/m).

2.6 Process intensification through suspension cell culture in perfusion mode

Process intensification allows to increase productivity while decreasing other factors such as costs and time. Process intensification is highly needed to supply an increasing demand for viral vectors as the gene therapy field is currently a highly growing field needing high amounts of material at high concentration for R&D, clinical trials and commercialization [7, 97]. One option for intensified biological manufacturing is high cell density (HCD) perfusion cultures [98, 99]. Indeed, by having a higher VCC in the bioreactor, more virus could be potentially produced while the bioreactor working volume is not increased. The definition of a perfusion process is the continuous addition of fresh medium and removal of supernatant from a bioreactor. By performing so, the cell culture does not reach limiting substrate or toxic metabolite levels allowing higher VCCs. Operation in perfusion mode is generally more efficient and more flexible (by decreasing bioreactor volume) than other cultivation strategies such as batch processes allowing high VCCs (10^7–10^8 cells/mL) and high volumetric productivities [98-100]. In case of influenza pandemics, intensified cell culture-based perfusion cultures allowing a rapid and small foot-print production of viruses could be of particular interest [101]. In addition, product quality attributes can be improved in perfusion cultures, for example, by preventing the accumulation of growth inhibitors and metabolic waste products [102].

Perfusion cell cultures can be performed using adherent or suspension cells. For adherent cells, the bioreactor supernatant can be simply continuously removed and replaced with fresh medium, except for bioreactors using micro-carriers. For suspension cells, a retention device has to be coupled to the bioreactor in order to separate the cells from the supernatant [103-105].

As for cell culture-based virus production in batch mode (section 2.3), USP virus production in perfusion mode is typically divided in two phases, cell growth and virus production. The difference compared to batch is that a higher VCC is reached, when running in perfusion mode at the TOI. For recombinant protein production, VCC is kept constant at a high value of $> 40 \times 10^6$ cells/mL via cell bleeding during production in perfusion mode (Figure 10A). For virus production, the VCC is not kept constant and decreases after virus infection, due to the cytotoxicity of viral replication (Figure 10B).

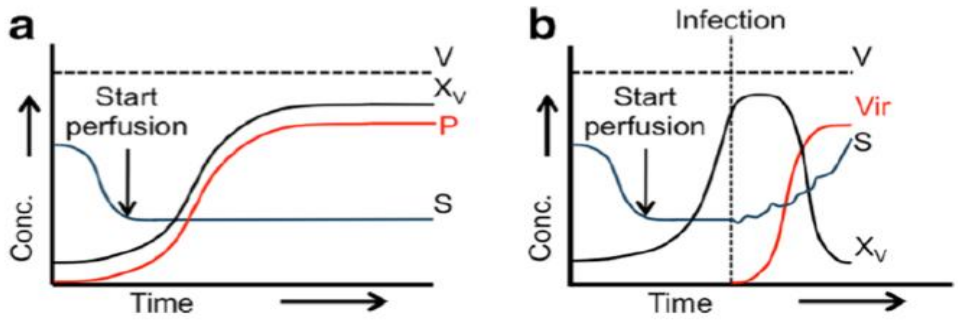

Figure 10: Illustration of cell culture-based recombinant protein production (a) and virus production (b), both in perfusion mode. The red line corresponds to the recombinant protein concentration for graph a and to the virus concentration for graph b. The blue line corresponds to the substrate concentration and the black line corresponds to the viable cell concentration. Source: Figure 1 from Tapia et al. (2016) [104]. The horizontal dashed line shows the constant volume for both cultivations and the vertical dashed line in b) indicates time point of infection.

While recombinant protein production in perfusion mode has been established in the industry for many years [106], virus production in perfusion mode is mainly pursued in academic research [40, 104]. Viruses such as influenza virus [103, 107] attenuated yellow fever virus [91], adenovirus [108], lentivirus [109] and MVA [90, 110] have already been investigated for intensified production in perfusion culture.

To reach a HCD, a device allowing the cell retention inside of the bioreactor is needed. Ideally, a cell retention device should be robust, have a high cell retention efficiency while not damaging cells, allow high-yield production, be scalable to a perfusion flow rate of at least 1000 L/day, enable low running costs, be commercially available (eventually in single-use) and, depending on process requirements, allow continuous harvesting [111]. The continuous harvesting of recombinant proteins has been shown to improve cell-specific productivity and product quality due to a shorter residence time inside the bioreactor [112]. Additionally, total process time (and costs) could be further reduced if scaling-up is done already from frozen HCD cryo-bags and if perfusion cultures are integrated with continuous DSP [98, 100].

Most perfusion studies in laboratory-scale bioreactors for virus vaccine or viral vector production were carried out using filtration systems, such as spin-filters [113], ASs [107-109], and membrane-based TFF [91, 114] or ATF devices [103, 110, 115]. Examples of cell retention devices that potentially enable continuous virus harvesting are: AS [107], centrifuge, hydrocyclone [116] and IS [105, 117]. Membrane-based cell retention devices such as the ATF system usually retains the virus inside of the bioreactor, although new membranes are being

currently developed to avoid product retention, as addressed in section 2.4.1 and 2.6.1, and shown in chapter 8. First insights regarding the potential advantages of continuous virus harvesting have been already shown [107, 109]. Petiot et al. (2011) showed, for example, that degradation of virus particles in the bioreactor was reduced when production was carried out under mild hypothermia (35°C) and the supernatant was immediately stored at 2–8°C [107]. Three promising cell retention devices for virus production in perfusion mode are described in more details in sections 2.6.1 to 2.6.3 as they were used throughout the work of this thesis.

It is important to mention that perfusion processes might be used as well to generate high density cell banks, or for intensified HCD fed-batch processes through an intensified cell culture prior to fed-batch bioreactor inoculation (N-1 perfusion). In addition, hybrid processes combining fed-batch and perfusion modes during one bioreactor run can also increase productivity [98].

2.6.1 Alternating tangential flow filtration

Membrane-based ATF is to date the most commonly used cell retention technology in recombinant protein production allowing continuous harvesting and manufacturing, such as for mAbs [98]. However, when it comes to virus production in perfusion mode, there is no cell retention technology showing clear advantages over the other. Potential issues regarding membrane filtration of virus raw material are described in section 2.4.1.

The tangential flow reduces the filter fouling (section 2.4.1). This led in a first time to the development of TFF technology, used as a cell clarification step for a batch or a fed-batch cultivation, and then used for perfusion cultures. Briefly, the cells are continuously recirculated in a loop using a pump, passing through a hollow-fiber membrane, and turned back to the bioreactor. Later, the ATF technology, with its alternating tangential flow, was developed and patented by Refine Technology in 2000. In this system, a diaphragm pump pushes and pulls the cell suspension in the intracapillary space of the fibers in an alternated way with a cycle of around 1 min, as illustrated in Figure 11. The term to quantify this exchange flow rate is called the ATF exchange flow rate.

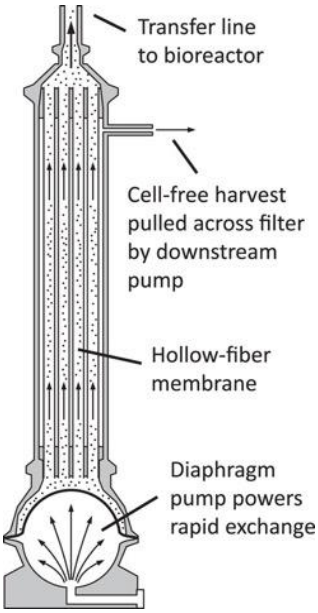

Figure 11: Illustration of an ATF system for suspension cell culture (source: Figure 1 from Walther et al. (2019) [71]) shown here is the flow out of the cell culture back into the bioreactor.

When using an ATF device, there is no need for a recirculation pump and only one connection to the bioreactor is needed instead of two [118]. It was shown for CHO cell cultures in perfusion mode in recombinant protein production that the use of an ATF device reduced the shear stress on the cells and eventually reduced product retention inside of the bioreactor, compared to TFF systems. When using a cut-off of the membrane of > 0.2 µm typically recombinant proteins can pass the membranes, however membrane blocking can still occur [74, 102, 119]. However, it has been shown later that the negative impact of shear stress on cell culture could be reduced for TFF devices by using a low shear recirculation pump such as the one produced by Levitronix [70]. In this case, product sieving (described in section 2.4.1) was found to be similar. The general advantages of ATF over TFF are: i) The presence of alternating flow allowing back flushing and reducing membrane fouling (called the Starling recirculation phenomena), ii) the presence of the diaphragm reducing shear stress which increases cell viability and product sieving, and iii) the need of only one port for connection to the bioreactor. The advantages of TFF over ATF are i) the simplicity of the system and ii) higher robustness.

The ATF system is as well suited for larger scales allowing perfusion flow rates > 1000 L/day [111] and is used as well for biopharmaceuticals manufacturing with 1000 L bioreactors [120] or at N-1 stage for intensified mAb manufacturing in fed-batch mode for 3000 L bioreactors

[77]. The scale-up and scale-down procedure is relatively simple to perform (see Appendix, section 10.1 for scale-up considerations), as TFF is already a well-established process cell clarification procedure (section 2.4.1). To date, CHO VCCs up to 214 x 10^6 cells/mL were reached using membrane-based perfusion systems [98]. Various ATF and TFF systems (and lately, new Tangential Flow Depth Filtration) and single-use membranes available from small to large scale are commercially available by Repligen.

Perfusion cultures with hollow-fiber membranes did support cell growth up to 160 x 10^6 cells/mL and subsequent virus production to very high virus titers. However, efficient direct virus harvesting through the membrane in a continuous mode was not well supported by the available membranes. Virus retention inside the bioreactor was observed using various setups, including different membrane materials and larger pore sizes (0.2–0.65 µm in PES or in PS), for different viruses, such as IAV [103], MVA [110] and flaviviruses [91]. In addition, high cell concentration increased host cell derived impurity levels in the supernatant. Other reasons, as already described in section 2.4.1, can increase product retention and filter fouling, such as the large size of viruses (e.g., 80 nm for influenza virus), host cell DNA release in the supernatant due to cell death and the release of small debris in the 100 nm size range.

The total membrane resistance is mainly driven by filter fouling, which is observed through a TMP increase. In order to avoid a TMP increase over time, the main parameter to consider is the permeate flux [71, 76, 77] (section 2.4.1). In the case of the perfusion cultivation, the permeate flux (which is defined by the perfusion rate and the filtration surface) is recommended not to exceed 48–60 L/m^2/day [71, 121]. The ATF exchange flow rate might be important only if this leads to higher cell death, which results in more cell debris formation, higher viscosity and by consequence membrane fouling [70]. Using larger filter pore size is a way to decrease filter fouling [73, 78, 79]. Clearly, the geometry of the membrane also has to be taken into account, as a longer hollow-fiber lead to increased TMP [121].

The effect of the ATF system on the cell viability and cell metabolism should be considered as well when trying to reduce filter fouling. The main parameters to take into account are: i) The residence time of the cells in the ATF system (dead volume), and ii) the shear stress caused by the ATF exchange flow rate [70, 71].

2.6.2 Acoustic settler

ASs use the density difference between the cells and culture media for separation. The settling velocity of the cells in the gravitational field (v_c, in m/s) is described as follows (based on the Stokes Law) [122]:

$$\mathbf{v_c} = \frac{(\boldsymbol{\rho_c} - \boldsymbol{\rho_l}) \times \mathbf{g} \times \mathbf{r^2}}{\mathbf{18} \times \boldsymbol{\eta}} \quad (7)$$

With ρ_c, the volumetric density of the cell (kg/m^3);
ρ_l, the volumetric density of the liquid (kg/m^3);
g, the gravitational force (m/s^2);
r, the mean radius of the cells (m) and
η, the dynamic viscosity of the liquid (kg/s/m).

The AS chamber is illustrated in Figure 12A. Briefly, an acoustic wave is emitted within the chamber through the piezoceramic and transducer, and is reflected back with the reflector. This builds up a resonance field with characteristic areas of pressure nodes (illustrated in Figure 12A). The frequency used needs to be between 1 and 3 MHz. A frequency below 1 MHz could disrupt the cells [123]. The pressure nodes are separated from each other by a half wavelength distance. The ultrasonic forces drive the cells towards the pressure nodes of the resonance field. Once the cells are in the nodes, they will start to clump and settle down [122]. Figure 12B illustrates the forces applied on the cells for settling. The radiation force F_A is a function of the compressibility difference between cells and the medium, driving the cells towards the pressure nodes of the resonance field [111, 122]. By forming cell clumps, v_c is increased as the radius is increased (Equation 7).

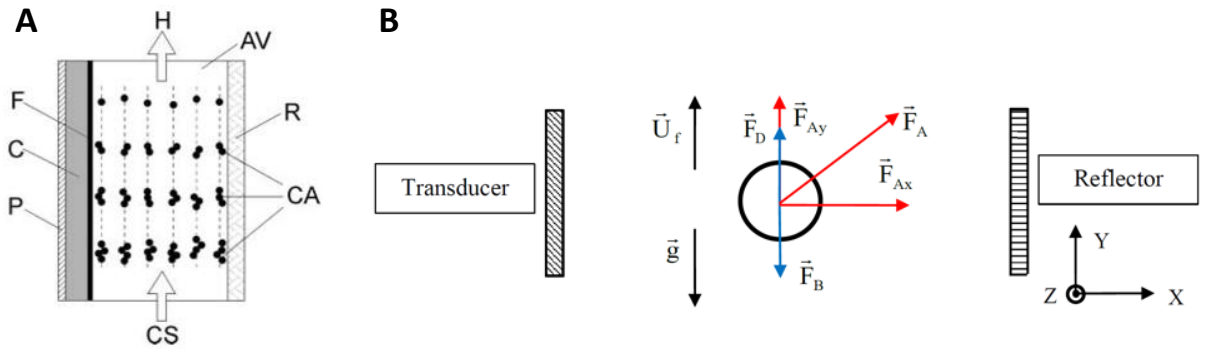

Figure 12: Schematic view of an acoustic settler chamber. (A) P: piezoceramic and transducer, C: carrier (glass), F: polysulfone foil, AV: active volume, R: reflector, CA: cell aggregates, CS: cell suspension, H: harvest (clarified fluid). The pressure nodes of the standing acoustic field are schematically indicated by dashed lines (source: legend and figure of Fig. 7 from Castilho et al. (2002) [122]). (B) Forces applied on the cells in an acoustic chamber. F_A is the acoustic radiation force, F_D is the viscous drag force and F_B is the buoyancy or gravity force (source: Figure 5 from Chitale et al. (2015) [124]).

Ultrasonic separators are robust, without moving parts, easily cleaned and sterilized in-place and do not require any physical barrier for cell retention [123]. Trampler et al. reported in 1994 for the first time the use of an AS for mammalian cell culture in perfusion mode [125]. High cell retention efficiency (above 90%) was reported for several perfusion cultivations using an AS, as reviewed in detail by Shirgaonkar et al. (2004) [123]. Notably, it has been shown for cell cultures coupled to an AS that: (i) the perfusion process can last at least 110 days [126], (ii) VCCs up to 42 x 10^6 hybridoma cells could be reached [127] and (iii) a perfusion flow rate up to 200 L/day with a cell retention efficiency of 96% is feasible [128]. Applikon Biotechnology is able to supply ASs proven under cGMP conditions with a perfusion flow rate up to 1000 L/day (https://www.applikon-biotechnology.com/en/products/perfusion/biosep/). Larger manufacturing devices are available and capable of handling 2000 L/day, but no experience is reported in the literature [112]. Interestingly, the preferential removal of dead cells over viable cells is possible, based on the cell size variation [123]. The standard setup of an AS connected to a bioreactor is illustrated below (Figure 13).

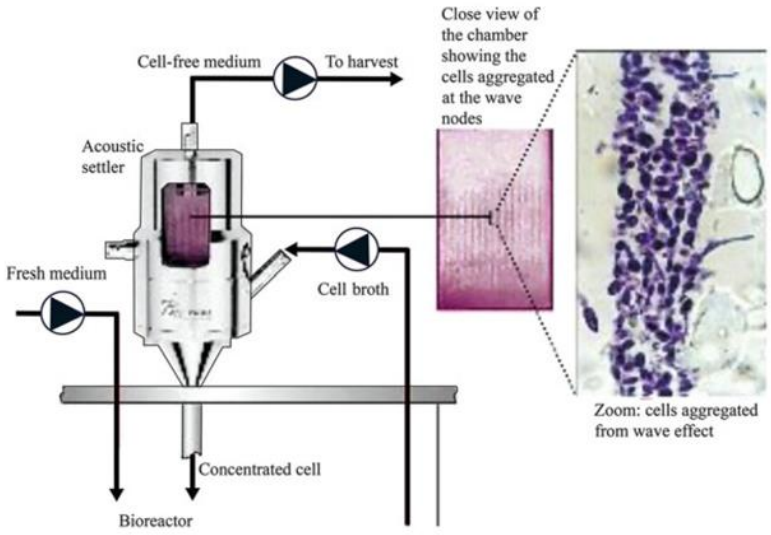

Figure 13: Typical configuration of an acoustic settler for perfusion cell culture. The cell broth is inserted in the acoustic settler through a recirculation pump and sent back to the bioreactor as concentrated cells. At the top of the acoustic chamber, cell-free medium is harvested. (source: https://www.applikon-biotechnology.com/en/products/perfusion/biosep/, Applikon Biotechnology).

Issues regarding the use of an AS are the lack of scale-up experience, and the possibility of the AS to heat up following its perfusion parameters, especially as the residence time of the cells within the acoustic chamber is longer as compared to the membrane-based ATF system. To overcome the heating issue, a cooling system was developed by passing water through one chamber located next to the chamber containing the acoustic waves. Alternatively, an air stream applied on the chamber can efficiently cool the system. The increased heat in the acoustic chamber has been shown to have a negative impact on the cell culture, productivity and cell retention efficiency [123].

Actions to increase the cell retention efficiency are reviewed by Shirgaonkar et al. (2004) [123]. Most efficient is probably the modification of the recirculation flow rate, in function of the harvesting flow rate. In function of the acoustic chamber size, the harvesting flow rate should be optimized. In addition, the backflush frequency can be changed as well. The backflush occurs when the harvesting pump is pumping back the cells to the bioreactor, while the acoustic waves are turned off. This parameter thus has an influence on the residence time of the cells within the chamber. Finally, the power level in the acoustic chamber (generating the acoustic waves) can be increased. Higher power results in higher force applied on the cell in the pressure nodes, but also a higher temperature elevation the acoustic chamber. A power

level in the chamber up to 220 W/L has been reported without influence on the cell viability or product formation [122].

2.6.3 Inclined settler

The use of an IS as a cell retention was first reported in 1920 by separating blood corpuscles from untreated blood [129]. ISs allow cell separation through sedimentation due to the gravitational field [117]. They include several inclined plates or lamellae on which the cell sedimentation occurs more rapidly than in free cell broth due to a convection phenomenon [118]. The recommended settling area should be in practice 3-times higher than the minimum settling area (A_{min}, in m^2), described as follow [122]:

$$\mathbf{A_{min}} = \frac{\mathbf{Q}}{\mathbf{v_c}} \tag{8}$$

With Q, the perfusion flow rate (m^3/s) and
v_c, the settling velocity of the cells, described in Equation 7 (m/s).

As illustrated in Figure 14, the cells are pumped into the lower part of the IS, and sedimented cells are directly sent back to the bioreactor. At the top of the IS, the cell-free medium is harvested. The cells are continuously circulated through the IS and pumped back into the bioreactor (Figure 14). Intermittent vibrations applied on the IS avoid cell attachment on the inclined plates and help to support a faster sedimentation of cells at the lower part of the IS [130].

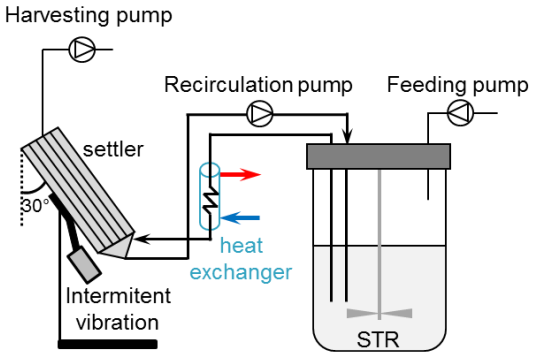

Figure 14: Perfusion cell culture set-up using an inclined settler. Cells are recirculated in a loop using a peristaltic pump. At the top of the inclined settler, another peristaltic pump harvests cell-free medium. The addition of fresh medium through the feeding pump allows maintaining the working volume at steady state. Blue and red arrows indicate the flow direction (water recirculation) in the heat exchanger.

One important advantage of these devices (as for the AS) is the preferential removal of non-viable cells and debris due to the size difference compared to viable cells. This results in the retention of predominantly viable cells [131]. In addition, ISs are simple and robust devices, which are successfully used for the manufacturing of several biopharmaceuticals, such as recombinant blood factors [120, 132]. Furthermore, they are applied in the seed train of fed-batch processes [133] at scales up to 3000 L/day [134]. Perfusion operation for the production of biologicals using these devices can last up to 3–5 months [135]. Lately, compact gravitational settlers employing another geometry, in single-use, with higher cell retention efficiency are commercially available from Sudin Biopharma [136].

ISs also have disadvantages. The maximum VCCs in perfusion cannot exceed 20–30 x 10^6 cells/mL as the cell retention efficiency drops at higher VCCs. Another disadvantage of the IS is the complex and time-consuming optimization of process parameters such as the cooling temperature, the recirculation flow rate, the settler geometry and size, and the intermittent vibration frequency. In addition, ISs have relatively large footprints [111]. Finally, there is a relatively long residence time of cells in the IS (non-controlled environment), which can be up to 1.5 h [111, 130]. To minimize side effects, cells that exit the bioreactor are cooled in a heat exchanger to avoid heat convections in the settler and thus increase cell retention efficiency, to keep a low shear stress environment and to slow down cell metabolism [111, 118, 130, 137]. Cooling temperatures as low as 4°C for CHO cell cultures have been reported [118].

2.7 Process integration of perfusion cell cultures

The process integration approach aims to seamless link all the different bioprocess steps from production (typically cell culture in USP, described in section 2.3) to final purification (DSP, described in section 2.4).

The implementation of an integrated perfusion process is an option to decrease manufacturing costs and to potentially increase the quality of a product [98, 100, 138, 139]. Integrated bioprocesses can decrease costs as it avoids the use and need of holdup tanks between the different bioprocess steps. By having an integrated bioprocess, the production time is also reduced as dead times between difference bioprocess steps are reduced or

removed. As dead times are reduced, the product is faster purified and stabilized, avoiding product loss and degradation, increasing thus its quality.

While a considerable amount of research has been conducted on integrated perfusion for recombinant protein production (such as mAb) [78, 86, 106, 140-142], there are to the knowledge of the author no results presenting the possibility for an integrated virus production in perfusion mode. Although the mentioned advantages for process integration were observed only for cell culture-based recombinant protein production, the same benefits are expected to be observed for cell culture-based virus production

To fully exploit the potential of integrated bioprocesses, the cell culture and biopharmaceutical production should be operated in perfusion mode. Biopharmaceutical production in perfusion mode allows for continuous harvesting. For an integrated perfusion system, this allows to directly purify the continuously harvested product, in continuous or in semi-continuous mode. The DSP footprint is reduced for (semi-)continuous DSP (linked to a cell culture in perfusion mode) as a smaller amount of product has to be purified at the same time. The product is purified as soon as it is harvested (for continuous USP). There is no need to purify large pools of harvest from continuous USP, kept in tanks.

Although not studied for virus production, but only for cell culture-based recombinant protein production, the continuous harvesting directly followed by (semi-)continuous DSP also decreases product degradation, which increases productivity and product quality [98, 100, 138, 139]. In the case of virus production, product degradation specifically includes: Virus inactivation (loss of infectivity), virus aggregation and potential attenuated glycosylation leading to changes in immunogenicity.

The recombinant protein produced in integrated perfusion processes tends to present a more homogeneous quality as every produced protein in the cell culture supernatant has the same residence time in the bioreactor, unlike for batch or fed-batch processes. This allows to have a more controlled environment. As an example, Walther et al. (2019) made a head-to-head comparison for an antibody production process in fed-batch or in perfusion mode, and showed that antibodies produced in perfusion mode showed less charge variants and less half-antibodies (defect). However the glycosylation was in this case similar for fed-batch and perfusion [138]. Continuous product harvesting, is expected from regulatory authorities for biopharmaceutical production [143].

As already mentioned in section 2.6, it is very important to differentiate integrated perfusion processes for recombinant protein production or for virus production. In the case of recombinant protein production, the production process can be kept in continuous mode over a long period of time (> 1 month). During this whole time, the product is continuously harvested and purified. In the case of integrated perfusion for virus production, the virus production phase timeframe is limited (up to 3 days for MVA production), due to the lytic nature of virus replication. In this case, the product (here the virus) is continuously harvested only for a few days, and during this timeframe the product can be (semi-)continuously purified.

Figure 15 illustrates the stepwise integration of a perfusion bioprocess. In the first step (Figure 15A), only the USP is performed in continuous (continuous harvesting). To perform this, a harvest tank is still needed, in order to later purify the product with different chromatography and filtration steps. It is important to notice that the column sizes for chromatography are large in order to purify the drug substance in non-continuous mode. In the second step (Figure 15B), the first drug substance capture is operated in continuous mode, allowing the chromatography column to be smaller, reducing the footprint. However, following the chromatography technique (typically bead-based chromatography, section 2.4), the purification cycle time might be long (e.g. 180 min), requiring then the use of multiple columns for continuous DSP. Finally, the third step (Figure 15C) illustrates a fully continuous system, avoiding the need of a container for the harvest and using for each chromatography step a multi-column approach.

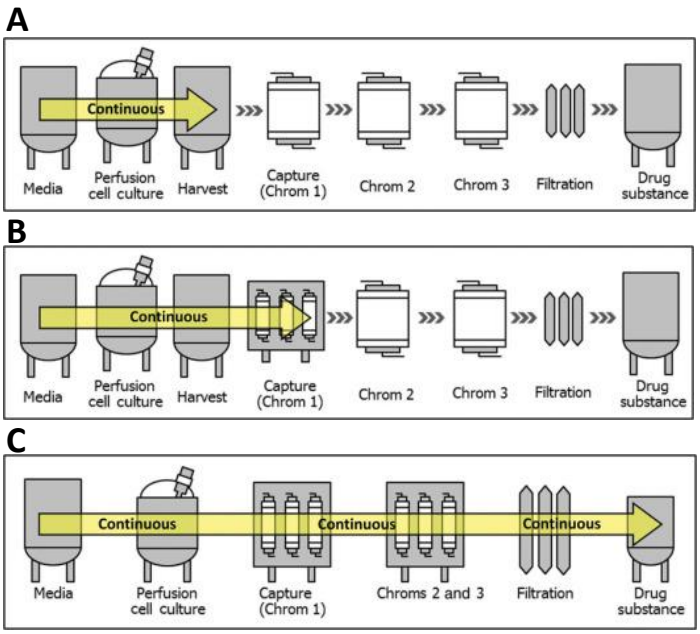

Figure 15: Illustrations of a partial-integrated continuous system (A and B) or a fully integrated continuous system (C) for recombinant protein production, in perfusion mode (source: Figures 1, 2 and 4 from Konstantinov et al. 2015 [106]).

Chapter 3

Materials and Methods

This chapter was partially based on the following book chapter and publications:

*Nikolay, A., *Bissinger, T., **Gränicher, G.**, Wu, Y., et al., Perfusion control for high cell density cultivation and viral vaccine production, in: Pörtner, R. (Ed.), *Animal cell biotechnology, Humana Press*, New York, 2020.

*Both authors contributed equally

The used standard operating procedures (SOPs) are listed in the Appendix, Table A.1. For a better visualization, Figure 16 illustrates which methods, described in the present chapter, were used for which experiments.

3.1 Cell lines for virus production

In the following, the cell lines used for virus production are listed and described. The cells used for virus titration assays are mentioned in sections 3.12.3–3.12.4 and the SOP list, Table A.1.

3.1.1 PBG.PK2.1® cell line

The novel suspension cell line PBG.PK2.1® was developed at ProBioGen AG (Berlin, Germany). The cell line was derived from immortal porcine kidney adherent cells. The cells were first adapted to grow in chemically-defined medium (CD-U5; ProBioGen AG, Berlin, Germany) and in suspension. The cell line was up to now not suitable for vaccine manufacturing due to a chronic infection with porcine circovirus 1 (PCV1) that is often found in porcine cells. Through single cell cloning, PBG.PK2.1 was cured from PCV1 after siRNA mediated suppression of the contaminating virus. The adherent as well as the suspension cell line are currently classified as biosafety level 2 as they contain copies of a porcine endogeneous retrovirus gene (reverse transcriptase; discussed in section 4.3.4).

The master cell bank was generated at the Bioprocess Engineering group after 2 passages (date: 21.08.2017) and the working cell bank was established after 9 passages (date: 14.09.2017). Cell banks storage, cell banking and thawing SOPs are listed in the Appendix, Table A.1. From the working cell bank, the cells were passaged every three days, until passage 40, if the cells were not used for virus production in shake flask (SF) or bioreactor cell seeding. The details for standard cell culture in SFs are in section 3.3.

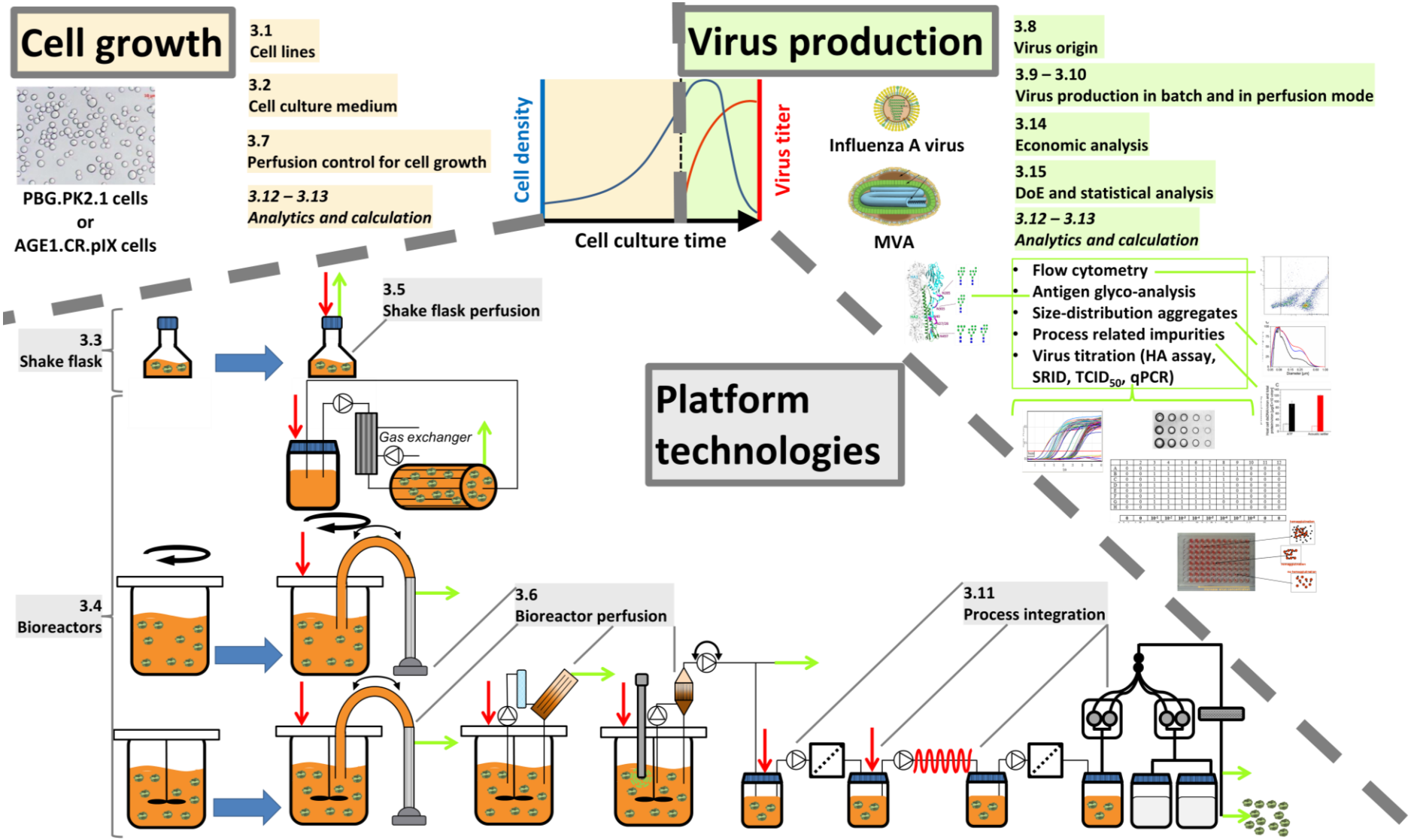

Figure 16: Scheme of the working processes described in chapter 3, including the section title, used in order to perform experiments as described in the results, chapters 4–8. The blue arrows indicate the process intensification step through perfusion cell culture.

3.1.2 AGE1.CR.pIX® cell line

The AGE1.CR.pIX® suspension avian designer cell line was developed at ProBioGen AG (Berlin, Germany) and IDT Biologika (Dessau-Roßlau, Germany). The cell line was derived from the retina of muscovy duck (*Cairina moschata* ST4) embryos, growing in adherent mode. The cells were immortalized through the insertion of the adenovirus genes E1A (triggering cell cycle progression and apoptosis) and E1B (leading to the repression of p53 transcription factor inducing apoptosis) in the cell line genome through transfection. In addition, the adenovirus pIX gene (suppressing anti-viral mechanisms of the host cell for more efficient vaccine production) was inserted through transfection as well. The newly generated cell line was then adapted to grow in suspension, in a chemically-defined medium (CD-U5; ProBioGen AG, Berlin, Germany) [55]. The cell line is cGMP conform.

The master cell bank was generated at the Bioprocess Engineering group after 3 passages (date: 25.08.2017) and the working cell bank was established after 6 passages (date: 04.09.2017). Cell bank storage, cell banking and thawing SOPs are listed in the Appendix, Table A.1. From the working cell bank, the cells were passaged every three days, until passage 40, if the cells were not used for virus production in SFs or bioreactor cell seeding. The details for standard cell culture in SFs are in section 3.3.

3.2 Cell culture medium for virus production

Chemically-defined CD-U5 (ProBioGen AG, Berlin, Germany) basal medium was supplemented with 2 mM L-glutamine (Sigma-Aldrich, St-Louis, MO, USA) and recombinant insulin-like growth factor (LONG-R^3 IGF, 50 ng/mL and 10 ng/mL final concentration for the PBG.PK2.1 cell line and the AGE1.CR.pIX cell line, respectively; Sigma-Aldrich, St-Louis, MO, USA). In chapters 5–7, chemically-defined CD-U3 (Biochrom-Merck KGaA, Darmstadt, Germany) basal medium was used instead of the CD-U5. The numbers indicate the stage of continued improvement of the medium composition.

3.3 Shake flask cell cultures

Cells were incubated in orbital shaker incubators (Multitron Pro, Infors HT, Basel, Switzerland) at 7.5% and 5.0% CO_2 with a shaking speed of 150 and 180 rpm with 50 mm shaking diameter for PBG.PK2.1 and AGE1.CR.pIX cells, respectively. Baffled 125 mL SFs with 50 mL working volume (V_w; Thermo Fisher Scientific, Waltham, MA, USA) were used. Cells were inoculated at a VCC of 0.8–1.0 x 10^6 cells/mL.

3.4 Bioreactors

3.4.1 DASGIP stirred-tank bioreactor

For PBG.PK2.1 cell culture in STR (chapter 4) or AGE1.CR.pIX cell culture in STR (cell culture in batch mode; chapter 8), a 1 L DASGIP bioreactor system (Eppendorf AG, Hamburg, Germany) was used with 450–1000 mL V_w. The bioreactor was inoculated from SF pre-cultures at a VCC of 0.8–1.0 x 10^6 cells/mL. The system was agitated with a pitched blade impeller (50 mm diameter) at 110 rpm (for PBG.PK2.1 cells) or 140 rpm (for AGE1.CR.pIX cells), upflow, with aeration by a L-sparger (1 mm pore size). The temperature was maintained at 37°C. The pH value was set at 7.2 by sparging CO_2. In chapter 8, 0.55 M NaOH was eventually added as well for pH control. For aeration at a dissolved oxygen (DO) level at 40%, air, O_2 and N_2 flow rates were controlled between 1 L/h and 9 L/h. During the virus production phase, pH was increased from 7.2 to 7.4 to mimic virus production condition in SFs (pH not controlled in SFs, only monitored).

3.4.2 BIOSTAT stirred-tank bioreactor

For AGE1.CR.pIX cell culture in STR and in perfusion mode (chapters 5–8), a 1 L Biostat B plus bioreactor (Sartorius AG, Göttingen, Germany) with a 600–1000 mL V_w was used. The bioreactor was inoculated at a VCC between 1 and 4 x 10^6 cells/mL. The system was agitated with a pitched-blade impeller (46 mm diameter) at 150–180 rpm, downflow. DO level was set to 40% and controlled through pure oxygen pulse sparging (no mass flow controller available) using an L-sparger (1 mm pore size). Carbon dioxide was used for pH control (pH 7.2). Temperature was controlled at 37°C.

3.4.3 Kühner orbital-shaken bioreactor

For scouting experiments regarding single-use perfusion bioprocesses for MVA production at laboratory scale, an orbital-shaken bioreactor (OSB) coupled to an ATF (OSB-ATF) system (chapter 7; max V_w: 10 L; Adolf Kühner AG, Basel, Switzerland) was operated as described previously for HCD IAV production [114]. Briefly, the bioreactor was shaken at 75–90 rpm. Gassing flow rates (air, O_2 and CO_2) were 300–500 mL/min. The percentage of O_2 in the gas mixture was set to 25–50% over the course of the cell growth phase to maintain the DO above 80%. Temperature was kept at 37°C, and the pH was monitored and manually controlled between 7.2 and 7.4 through CO_2 addition and 1 M NaOH addition.

3.4.4 PRIMER hollow-fiber bioreactor

A HFBR (PRIMER HF, 50 mL V_w, 0.5 m^2; Biovest International Inc., Tampa, FL, USA) was used and operated for MVA production with AGE1.CR.pIX cells (chapter 7), as described previously by Tapia et al. (2014) [144] for IAV production. Medium was recirculated constantly in the HFBR and multiple virus harvests of the extracapillary space of the HFBR were performed. Temperature was kept at 37°C, and the pH was monitored and manually controlled between 7.2 and 7.4.

3.5 Perfusion culture in shake flasks

Perfusion culture in SFs (pseudo-perfusion), as a scale-down model for HCD cultivation, is able to mimic “real” (scalable) perfusion systems. To maintain metabolite levels for extended cell growth (or virus propagation), medium exchanges are performed manually (see SOP list in Appendix, Table A.1). The partial medium exchange volumes (V_e; in mL) are calculated according to a fixed time schedule (generally < 24 h), however the V_e should not exceed 60% to avoid large cell culture condition variation [145]. Only the medium can be exchanged as the cell culture is centrifuged at 150 g for 10 min to settle down the cells.

$$\mathbf{V_e} = \frac{\mathbf{x} \times \left(\mathbf{e}^{\mu \times \Delta \mathbf{t}} - \mathbf{1}\right) \times \mathbf{V_w} \times \mathbf{CSPR}}{\mu} \quad (9)$$

With x, the viable cell concentration (cells/mL);
μ, the cell-specific growth rate (1/h);
Δt, the time interval between two medium replacements (h);
V_w, the bioreactor working volume (mL) and
CSPR, the cell-specific perfusion rate (mL/cell/h; see section 3.7).

3.6 Perfusion culture in bioreactors

DO, pH, aeration and temperature were set as described in section 3.2. The exception is for the perfusion bioreactor using the DASGIP bioreactor (chapter 4), where a micro-sparger (10 µm pore size) was used for aeration (gas flow rate varying from 0.3 to 4 L/h). Perfusion was started when either a glucose concentration of 18 mM was reached or the VCC exceeded 5–6 x 10^6 cells/mL. The bioreactor was inoculated at a VCC of 1 x 10^6 cells/mL from pre-cultures grown in SFs. In order to shorten the time to perfusion, the VCC at the time of inoculation was increased to 3 x 10^6 cells/mL (chapter 4; for PBG.PK2.1 cell culture in perfusion mode). Supplemented CD-U3 or CD-U5 (section 3.2) was used as perfusion medium. The perfusion rate was controlled as described in section 3.7. Depending on the used cell retention system for the perfusion, some cells were found in the harvest. The cell separation efficiency (SE, in %) was calculated as previously described [146]:

$$\mathbf{SE}\ (\%) = \left(\mathbf{1} - \frac{\mathbf{x_h}}{\mathbf{x_b}}\right) \times \mathbf{100} \quad (10)$$

With x_h, the viable or dead cell concentration in the harvest (cells/mL) and
x_b, the viable or dead cell concentration in the bioreactor (cells/mL).

3.6.1 Cell retention by alternating tangential flow filtration

An ATF2 cell retention system (Repligen, Waltham, MA, USA) coupled to a 1 L STR Biostat B Plus or 1 L STR DASGIP was used for perfusion culture, using a PES hollow-fiber membrane (0.2 µm pore size, 470 cm^2, 76 hollow-fibers with 0.9 mm diameter; Spectrum Laboratories-Repligen, Waltham, MA, USA; for chapters 4–8) or a novel hollow-fiber membrane (VHU2

membrane; < 10 µm pore size; estimated cutoff: Cells with a cell diameter ≤ 10 µm, measured with the ViCell XR, observed in the harvest by the author, data not shown; 527 cm^2, 9 hollow-fibers with 3.2 mm diameter; Artemis Biosystems, Cambridge, MA, USA; in the Appendix, section 10.5). The ATF system was connected to the bioreactor through a dip-tube with an inner diameter of 10 mm, delivered together with the ATF2 system. By using a diaphragm, the cell culture broth was pumped in and out through the membrane filter at an exchange flow rate of 0.9 L/min for chapter 4, and 0.8 L/min for chapters 5–8 and section 10.5.

For the testing of the new VHU2 membrane (section 10.5), the following was used only after the VCC started to decrease during the virus production phase. Before that, the PES hollow-fiber membrane was used.

For the OSB-ATF system with a 10 L V_w (chapter 7), an ATF2 controller together with a single-use PES membrane (0.2 µm pore size, 1300 cm^2 surface area, 76 hollow-fibers with 1 mm diameter; Repligen, Waltham, MA, USA) was used. An exchange flow rate of 1.5 L/min was adopted.

The membranes were used once. Before connecting the ATF system to the bioreactor, the ATF system was connected to a container filled with 1 L of demineralized water at 37°C. An exchange flow rate of 1.5 L/min and a perfusion flow rate of about 1 L/h (permeate re-directed to the container) were set for 90 min. The water container was replaced once with 1 L of fresh demineralized water after 45 min (during the water replacements, the ATF system was stopped). After 90 min, the ATF system was stopped, dismantled in order to remove the water while still keeping the membrane wet. The ATF system was then connected to the bioreactor and autoclaved (SOP for autoclaving listed in Table A.1).

3.6.2 Cell retention using an acoustic settler

An AS (10 L acoustic chamber version; SonoSep Technologies, Hinterbrühl, Austria; Figure 17A and B) with an acoustic power of 3 W and with a 2.1 MHz frequency applied for all runs was used in chapters 5–8, coupled to a 1 L STR Biostat B Plus. The acoustic chamber was cooled through a constant air flow (at room temperature) directly on the surface of the chamber. A cell culture volume of 10 mL was exposed to the acoustic waves. The connections to the acoustic chamber had an inner diameter of 3 mm. The dip-tubes connecting the acoustic chamber to the bioreactor had an inner diameter of 2 mm for the outlet (cells going out of the

bioreactor, in the acoustic chamber) and 4 mm for the inlet (cells returning to the bioreactor, leaving the acoustic chamber). The settler was operated in two different modes using a pump-based or a valve-based recirculation strategy (Figure 17).

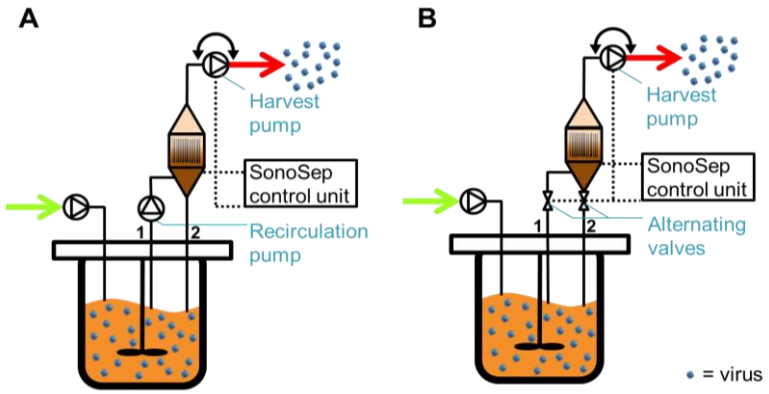

Figure 17: Scheme of pump-based and valve-based recirculation strategy for the use of an acoustic filter for cell retention for IAV production using AGE1.CR.pIX cells in perfusion mode. The cells were retained in the bioreactor using an acoustic settler (illustrated with brown color) with either a pump-based (A) or a valve-based recirculation strategy (B). The acoustic settler allowed continuous virus harvesting. Fresh medium was added continuously (green arrow) to feed the cells, while cell-free medium was removed (red arrow) to keep a constant bioreactor working volume. The pumps used for harvesting in both schemes are bi-directional in order to periodically backflush cells settled in the acoustic settler back into the bioreactor.

For the pump-based recirculation strategy (Figure 17A), cells entered the acoustic chamber through line 1 using a peristaltic pump (Watson-Marlow, Zollikon, Switzerland) with a constant recirculation rate between 3 and 8 reactor volumes per day (day^{-1}). It is important to note that in this case two pumps are used: one for the recirculation and one for the harvesting of the cell-free medium (harvest pump) (Figure 17A). When exposed to the periodic acoustic waves, the cells settled and were continuously returned to the bioreactor through line 2. The cell-free supernatant was collected cycle-wise through the harvest pump. The harvest pump operated for 3 min to remove cell-free supernatant before back-flushing part of the harvested material inside the acoustic chamber at the same flow rate for 30 sec. The back-flushing was done to enable high cell separation efficiencies. While back-flushing, the generation of acoustic waves was deactivated.

The valve-based recirculation strategy (Figure 17B) was first reported by Gorenflo et al. (2003) [126]. In a first step, the cells were pumped into the chamber through line 1 (either through the recirculation pump for the pump-based recirculation strategy (Figure 17A) or either through a combination of valves and the harvest pump for the valve-based recirculation

strategy (Figure 17B)). In a second step, the cells were kept in the chamber due to the acoustic field, while the cell-free medium was harvested for 3 min using the harvest pump. During this step, the valve from line 2 was kept closed for the valve-based system. In a third step, the generation of acoustic waves was deactivated and the harvest pump rotation was inverted to return the cells into the bioreactor through line 2, for 5–30 sec at flow rates varying from 10 to 55 mL/min. The valve from line 1 was closed during the back-flushing time (for the valve-based system). The volume of harvested medium per time determines the volumetric perfusion rate and the volume of cell culture returned into the bioreactor per time determines the volumetric recirculation rate.

In order to monitor the temperature in the AS, two sensors (80TK thermocouple module, FLUKE connected to a 73III multimeter, FLUKE, Everett, WA, USA) were used with the tip either on the top (outlet line) or at the bottom of the acoustic chamber (inlet/recirculation line). A culture with a VCC between 4 and 8 x 10^6 cells/mL was used for testing this set-up. In this experiment, the harvest line was redirected in the bioreactor instead of harvesting into flasks. To avoid contaminations due to the use of a sensor that cannot be autoclaved, the medium was supplemented with 0.1% (v/v) streptomycin (Sigma, Darmstadt, Germany) for the testing of the set-up but not for virus production (see temperature variation results, chapter 5, Table 14).

3.6.3 Cell retention using an inclined settler

A 1 L STR Biostat B Plus coupled to an IS CS10 (Biotechnology Solutions, San Francisco, CA, USA, kindly provided by T. Noll, Bielefeld) was used for perfusion cultivations for IAV or MVA production with AGE1.CR.pIX cells. The IS was operated at a recirculation flow rate of 35 mL/min, intermittent vibration (15 sec on, 10 min off) and with 30° angle, as described previously by Coronel et al. (2020a) [147], as illustrated in Figure 14. Water at different temperatures was recirculated in the heat exchanger (between 20°C and 27°C (chapter 6) or at 27°C (chapter 7)). When the perfusion was started, the bioreactor V_w was decreased to 650 mL due to sampling and the dead volume in the IS (about 275 mL). The IS was connected to the bioreactor through two dip-tubes (in and out) with a 4 mm inner diameter and with silicon tubes with a 5 mm inner diameter.

3.7 Perfusion control for cell growth

Different strategies were used to control the perfusion rate. At the bioreactor scale, the perfusion rate was changed by increasing the harvesting flow rate of the harvesting pump (for the ATF, acoustic settler, or IS). The V_w was automatically maintained by connecting a balance (Midrics 1; Sartorius Stedim Biotech, Göttingen, Germany) monitoring the bioreactor weight to a peristaltic pump controlling the perfusion feeding. When the weight was too low, the balance will activate the peristaltic pump, pumping then fresh medium inside the bioreactor (Figure 18). The perfusion rate was controlled by increasing the V_e (Equation 9) for cell cultures using SF (in semi-perfusion mode).

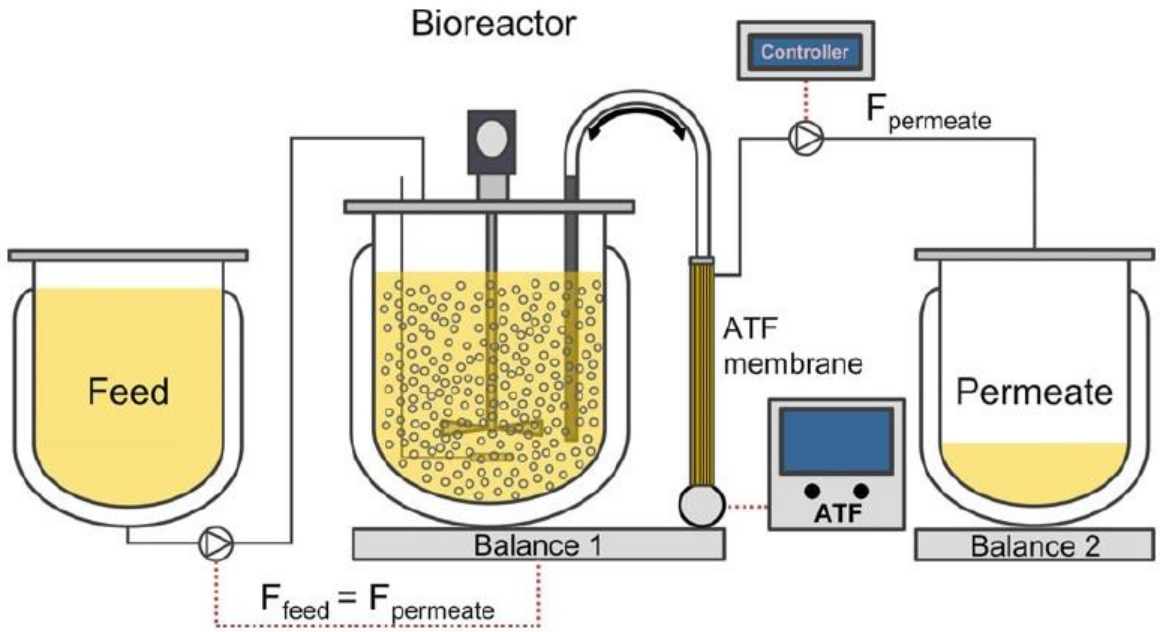

Figure 18: Illustration of a perfusion system allowing the control of the perfusion rate for suspension cell culture. In the present example, the stirred-tank bioreactor is coupled to an ATF system. The weight of the bioreactor is monitored by Balance 1, which sends signal to the feed pump in order to keep the bioreactor working volume constant. The perfusion flow rate (here, illustrated as $F_{permeate}$) is controlled either manually or automatically, during the cell growth phase (source: Figure 2 from Nikolay et al. 2020 [145]).

The amount of liquid perfused through the bioreactor can be expressed as a perfusion flow rate (in mL/day) or as a perfusion rate (in mL of perfused medium/V_w/day, resulting in day^{-1}). The recirculation flow rate (in mL/day) and the recirculation rate (in mL of recirculated medium/V_w/day, resulting in day^{-1}) are also important parameters for the AS and the IS (sections 3.6.2 and 3.6.3).

3.7.1 Manual perfusion control

With a constant CSPR of 70 and 50–60 pL/cell/day for PBG.PK2.1 and AGE1.CR.pIX cell line, calculated following cell-specific glucose consumption rate (q_{glc}, in mmol/cell/h), the perfusion flow rate (Q, in mL/day; only for perfusion bioreactor) was manually adjusted using the following equations [110]:

$$\mathbf{CSPR} = \frac{\mathbf{q_{glc}}}{\mathbf{c_{glc,m} - c_{g,b}}} \times \frac{\mathbf{10^{12}}}{\mathbf{24}} \quad (11)$$

$$\mathbf{Q} = \mathbf{x} \times \mathbf{e}^{\mu \cdot \mathbf{t}} \times \mathbf{V_w} \times \mathbf{CSPR} \times \mathbf{10^{-12}} \quad (12)$$

With $c_{glc,m}$, the glucose concentration in the medium (35 mM);
$c_{glc,b}$, the target glucose concentration in the bioreactor (6 mM);
μ, the cell-specific growth rate (1/h);
x, the viable cell concentration (cells/mL) and
V_w, the bioreactor working volume (mL).

3.7.2 Automated perfusion control

For bioreactor cultivations the perfusion rate can be controlled directly by the online measurement of the VCC through a capacitance probe (Incyte Arc, Hamilton, Bonaduz, Switzerland). The Incyte probe was operated in frequency scan mode as it measures the permittivity signal at 17 different frequencies (in 30 sec) in the range of 1–10 MHz. For the integrated perfusion process for MVA production (chapter 8), during the cell growth phase, a CSPR of 50 pL/cell/day was chosen. The online capacitance probe connected to a controller (ArcView Controller 265, Hamilton, Bonaduz, Switzerland) was used in order to control the Watson-Marlow harvest pump as previously described [145]. The signal from the capacitance probe was recorded every 12 min. The perfusion rate was therefore modified with the harvest pump following the VCC in the bioreactor given by the permittivity signal [145]. During the cell growth phase, the correlation between the VCC and the permittivity signal was determined through a linear regression (through the origin) by plotting the offline VCC (10^6 cells/mL) and the permittivity signal (pF/cm). The resulting slope of the regression was considered here as equal to the cell factor. This open-loop control system automatizes the perfusion process and runs with high precision based on the actual growth performance.

3.8 Viruses

3.8.1 Influenza virus

A MDCK cell-derived virus seed (human influenza virus A/PR/8/34 H1N1: Robert Koch Institute, Amp. 3138; 9.9×10^7 $TCID_{50}$/mL) was used for adaptation to the porcine cells. Additionally, porcine influenza virus A/Bakum/1832/00 H1N2 (IDT Biologika) and influenza virus B/Brisbane/60/2068 (National Institute for Biological Standards and Control, Amp. 09/168; infectious virus titer not available) were tested in SFs (chapter 4).

For efficient influenza A/PR/8/34 virus production using PBG.PK2.1 (chapter 4), this virus strain was adapted to this cell line by three passages in 50 mL V_w baffled SFs. To facilitate virus infection, trypsin (Gibco, # 27250-018) was prepared in PBS with 5000 trypsin units/mL according to the activity given by the manufacturer. For each passage, the VCC was set to 5×10^6 cells/mL at TOI with a trypsin activity of 10^{-6} trypsin units/cell. The cell culture supernatant was collected 36 hours post infection (hpi). For infection, 0.0004% v/v of the supernatant from the previous passage was transferred to the fresh cell culture medium. Before addition, cell cultures were centrifuged at 150 × g for 10 min to remove spent medium and were resuspended in fresh medium containing the virus to prevent any substrate limitation. After adaptation, a seed virus with an infectious virus titer of 2.02×10^9 $TCID_{50}$/mL was obtained.

3.8.2 Modified Vaccinia virus Ankara

The virus strains MVA-CR19 and MVA-CR19.GFP (which contains a green-fluorescent-protein insertion cassette) were provided by ProBioGen AG (Berlin, Germany). They were used, with a seed virus titer of 4.50×10^8 $TCID_{50}$/mL and 4.05×10^8 $TCID_{50}$/mL, respectively. For the integrated MVA production process (chapter 8), only the MVA-CR19.GFP virus seed was used.

To investigate the MVA-CR19.GFP virus stability, cell culture supernatant with an initial virus titer of 3.06×10^7 $TCID_{50}$/mL was incubated in 1.5 mL vials in an incubator at 37°C and kept at a pH over 7.2 (not shaken). The $TCID_{50}$ titer was measured after 6, 12 and 24 h, in triplicate.

3.9 Virus production in batch mode

All samples were centrifuged at 150 × g for 10 min and stored at -80°C.

3.9.1 Influenza virus

PBG.PK2.1 cells were grown up to a VCC of 6–7 x 10^6 cells/mL and diluted to a VCC of 5 x 10^6 cells/mL at TOI, in a SF or a bioreactor (chapter 4). Cell cultures were infected at a MOI of 10^{-5} infectious units/cell (based on $TCID_{50}$). Trypsin (porcine trypsin; from a stock solution of 5000 U/mL in PBS; Gibco, # 27250-018, Dublin, Ireland) was added at 0 and 16 hpi at 10^{-6} U/cell to facilitate infection. The use of such a low MOI was already shown in a previous study to be optimum for high-yield influenza virus production [43, 148]. In addition, it has to be taken into account that low MOI infections minimize the use of seed viruses required for each production run thus facilitating large scale virus manufacturing. Starting 24 hpi, the cell culture volume was increased with cell culture medium (as in section 3.2) from 550 mL to 710 mL to avoid substrate limitation, as the influenza virus replication was found to be slower than for AGE1.CR.pIX (> 36 hpi) [43].

3.9.2 Modified Vaccinia virus Ankara

The production of MVA was mainly done according to the production described previously by Lohr (2014) [43, 149]. Cell cultures were infected at an MOI of 0.05 infectious units/mL (based on $TCID_{50}$). The seed virus was previously sonicated in a water bath for 1 min at 45 kHz to avoid aggregate formation [145]. Once a VCC of 4–5 x 10^6 cells/mL was reached, the bioreactor was diluted to a VCC of 2.0 x 10^6 cells/mL and subsequently infected. The pH was kept at 7.4. The MVA in the supernatant was harvested when a cell viability of 70% was reached (chapter 8).

3.10 Virus production in perfusion mode

The samples were each time centrifuged at 150 × g for 10 min and stored at -80°C.

3.10.1 Influenza virus

When using PBG.PK2.1 cells (chapter 4), 0.8-0.9 bioreactor volume was replaced with fresh medium by applying a perfusion rate of 6–9 day^{-1} during the three hours before infection at a MOI of 10^{-5} infectious units/cell (based on $TCID_{50}$). The cell culture was infected at a VCC of 40–50 x 10^6 cells/mL. At 1 hpi, the bioreactor V_w was increased from 510 mL to 660 mL. At TOI, perfusion medium was supplemented with 22 trypsin units/mL and the pH increased from 7.2 to 7.4 (parameters defined based on previous optimization in SFs at HCD).

When using AGE1.CR.pIX cells (chapters 5 and 6), infection was at a MOI of 10^{-5} infectious units/cell (based on $TCID_{50}$) at a VCC of 25 x 10^6 or 50 x 10^6 cells/mL. The detailed process parameters regarding the strategy of trypsin addition are shown in Table 7. It was needed to add trypsin more than once in order to avoid trypsin out-dilution due to perfusion as described previously [115]. The molecular weight of trypsin is low enough (23 kDa) to allow easy passage through any cell retention device. To optimize virus production, one reactor volume was replaced with fresh medium 2–3 h before infection by increasing the perfusion rate to 8–12 day^{-1}. After infection, the perfusion was stopped for 1 h and then set to a constant perfusion rate between 1.5 and 2.0 day^{-1}. The bioreactor V_w was kept constant and controlled through a scale measuring the weight of the bioreactor connected to a feed pump as previously described [91].

Table 7: Strategy for trypsin addition during the infection phase of bioreactor cultivations of AGE1.CR.pIX cells for the production of influenza A/PR/8/34 virus in perfusion mode with either an acoustic settler, an inclined settler or an ATF system (control run).

Cell retention system	Run	Viable cell concentration at time of infection [x 10^6 cells/mL]	Trypsin [U/mL]		
			1st dose [a]	2nd dose [b]	Feed [c]
Acoustic settler	IAV_AS1	25	13	16	-
	IAV_AS2	25	13	15	-
	IAV_AS3	27	13	17	-
	IAV_AS4	25	13	18	-
	IAV_AS5	25	13	15	-
	IAV_AS6	25	13	25	-
	IAV_AS7	27	13	33	-
	IAV_AS8	49	13	25	-
	IAV_AS9	25	13	13	-
Inclined settler	IAV_IS3	24	38	38	-
	IAV_IS4	27	13	15	-
	IAV_IS5	52	25	15	-
	IAV_IS6	48	13	-	2
ATF	IAV_ATF1	25	13	20	-

IAV, influenza A virus; AS, acoustic settler; IS, inclined settler; ATF, alternating tangential flow (filtration).

[a] 1st dose addition at time of infection

[b] 2nd dose addition at 12–18 hours post infection

[c] Trypsin added in the feed medium (instead of adding a 2nd dose)

3.10.2 Modified Vaccinia virus Ankara

AGE1.CR.pIX cells were infected at a VCC of 25–50 × 10^6 cells/mL (chapters 7 and 8). One reactor volume was replaced with fresh medium 2–3 h before infection by increasing the perfusion rate to 8–12 day^{-1}. As for batch processes, a MOI of 0.05 was used with a sonicated seed virus, except for the large-scale OSB-ATF system (chapter 7). Due to seed virus limitation, a MOI of 0.01 was used in this case.

The perfusion runs used for MVA production between the STR-ATF, STR-AS and STR-IS were infected at a VCC of 20–30 × 10^6 cells/mL and after infection, the perfusion rate was kept constant at an average of 1.65 day^{-1} (chapter 7). For the scouting experiments regarding single-use perfusion bioprocesses at laboratory scale, the OSB-ATF system (maximum V_w: 10 L, Adolf Kühner AG) was operated using a hybrid perfusion mode approach, which was adapted from Vazquez et al. (2019) [90]. The V_w was increased from 5000 mL to 6300 mL during the infection phase while keeping the perfusion at steady-state, at a perfusion rate of 3.5 day^{-1}.

The HFBR system (PRIMER HF, 50 mL V_w, 0.5 m^2, Biovest International Inc., USA) was used and operated as described previously by Tapia et al. (2014) [144] for IAV production. Medium was recirculated constantly in the HFBR (in total 4.3–8.1 L medium was used) and multiple virus harvests of the extracapillary space were performed. Temperature was kept at 37°C, and the pH was monitored and manually controlled between 7.2 and 7.4.

For the integrated MVA production in perfusion mode (chapter 8), the cells were infected at a VCC of 50 x 10^6 cells/mL with MVA-CR19.GFP virus at a MOI of 0.05, with a STR-ATF or STR-AS system. After infection, the V_w was increased from 550 mL to 1000 mL at 12 hpi. From 0 to 12 hpi, the perfusion was stopped. After 12 hpi a constant perfusion rate of 1.75 day^{-1} was kept during the whole run. After 36 hpi, the V_w was decreased from 1000 mL to 800 mL in order to decrease the consumed amount of medium. In order to keep the perfusion rate, the harvest pump flow rate was decreased from 66.7 mL/h to 54 mL/h. For the ATF run, a VHU2 membrane was used only during virus harvesting (as described in section 3.6.1).

The virus infection dynamics was also monitored using the online capacitance probe (chapter 8). The MVA release in the cell culture supernatant was observed using the maximum permittivity signal $\Delta\varepsilon_{max}$ in pF/cm (see section 3.11 for process integration with DSP).

3.11 Process integration of MVA production

To perform an integrated virus production, in batch or in perfusion mode, the material was generated in a bioreactor (sections 3.9 and 3.10) in batch mode or in perfusion mode.

In batch mode, harvesting was initiated when the cell viability reached 70%. In perfusion mode, harvesting was initiated when MVA particles started to accumulate in the supernatant (about 40 hpi). Therefore, the harvest was directed to a harvest bottle (bottle B1 in Figure 19) kept at 4°C, and later purified. Harvesting of MVA particles released was initiated 10.6 h after the maximum permittivity signal was reached. This corresponded to the time when about 8 to 10% of the total number of infectious virions (Vir_{tot}, bioreactor and harvest vessel, section 3.13.3) was released from the infected cells. This definition was chosen to ensure high titers in the harvesting line (> 10^8 $TCID_{50}$/mL) and to avoid any product concentration step before chromatography. Samples during cell culture were taken every 8 to 14 h.

The raw material (MVA) was then purified as described in the present section. In the special case of the perfusion, the material was continuously harvested and semi-continuously purified as illustrated in Figure 19. For a better visualization, the real setup is shown in Figure 20.

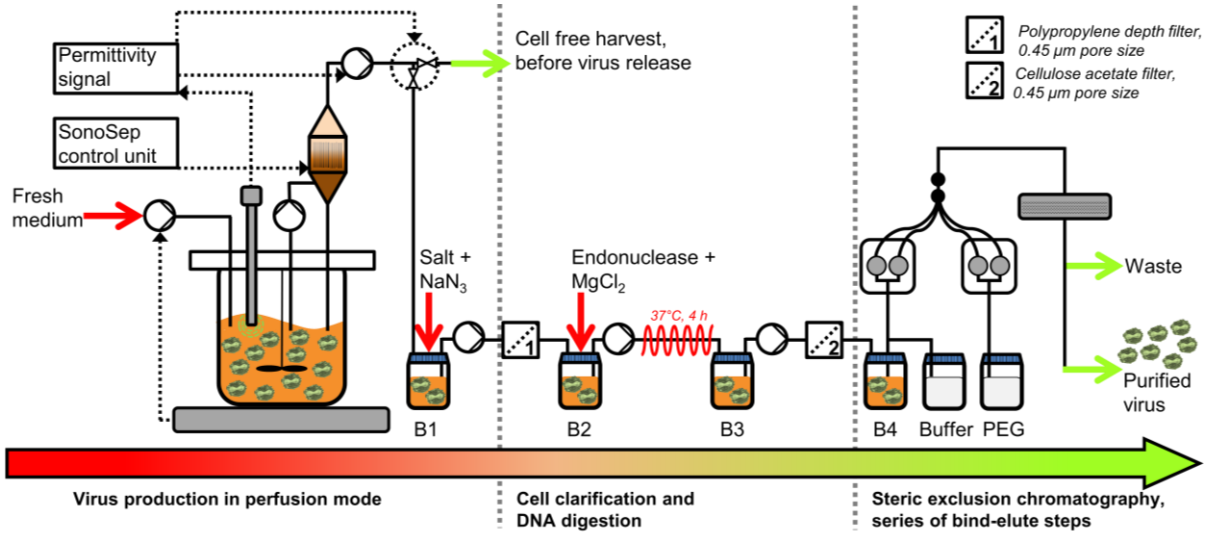

Figure 19: Scheme of an integrated process for cell culture-based virus production in perfusion mode. The integrated MVA production is separated in three main steps, separated by grey vertical dotted lines: 1) Virus production in perfusion mode using an acoustic filter, 2) cell clarification and DNA digestion, and 3) steric exclusion chromatography (SXC) as a series of bind-elute steps. MVA is produced using AGE1.CR.pIX cells grown in suspension in a stirred-tank bioreactor. To achieve high cell concentrations, the cells are retained in the bioreactor while cell-free medium is continuously harvested through the acoustic chamber controlled by the SonoSep control unit (acoustic filter as perfusion system). To allow a constant bioreactor working volume and weight, fresh medium is added into the bioreactor through a peristaltic pump controlled by a scale. During the cell growth phase, the harvest flow rate is controlled based on the estimation of the viable cell concentration using a capacitance sensor. After infection, a decrease in the permittivity signal indicates virus particle release, and initiates cell clarification and subsequent chromatography steps. The harvest containing MVA (which was first cell clarified through the acoustic settler) is collected into bottle B1. Salt and sodium azide (NaN_3) are added to bottle B1 as well. The virus harvest is then continuously filtered through a polypropylene depth filter with 0.45 µm pore size (Filter 1). For continuous endonuclease digestion (addition of endonuclease and magnesium chloride ($MgCl_2$) in bottle B2), the harvest is incubated into a plug-flow reactor (indicated with the coiled red tube) at 37°C with a residence time of 4 h. The endonuclease-digested product is continuously collected into bottle B3. After another filtration step using cellulose acetate depth filter with 0.45 µm pore size (Filter 2), the harvest is collected into bottle B4 at 4°C. An ÄKTA Pure 25 system is used to purify the virus harvest using membrane-based SXC operated in a semi-continuous bind-elute mode; the composition of buffer solutions (including buffer solution with PEG) used in purification are described in section 3.11.3. Finally, purified MVA is collected into 50 mL tubes (not illustrated). The color of the horizontal arrow going from red to green illustrates the stepwise purification of the MVA and the removal of contaminating host cell DNA.

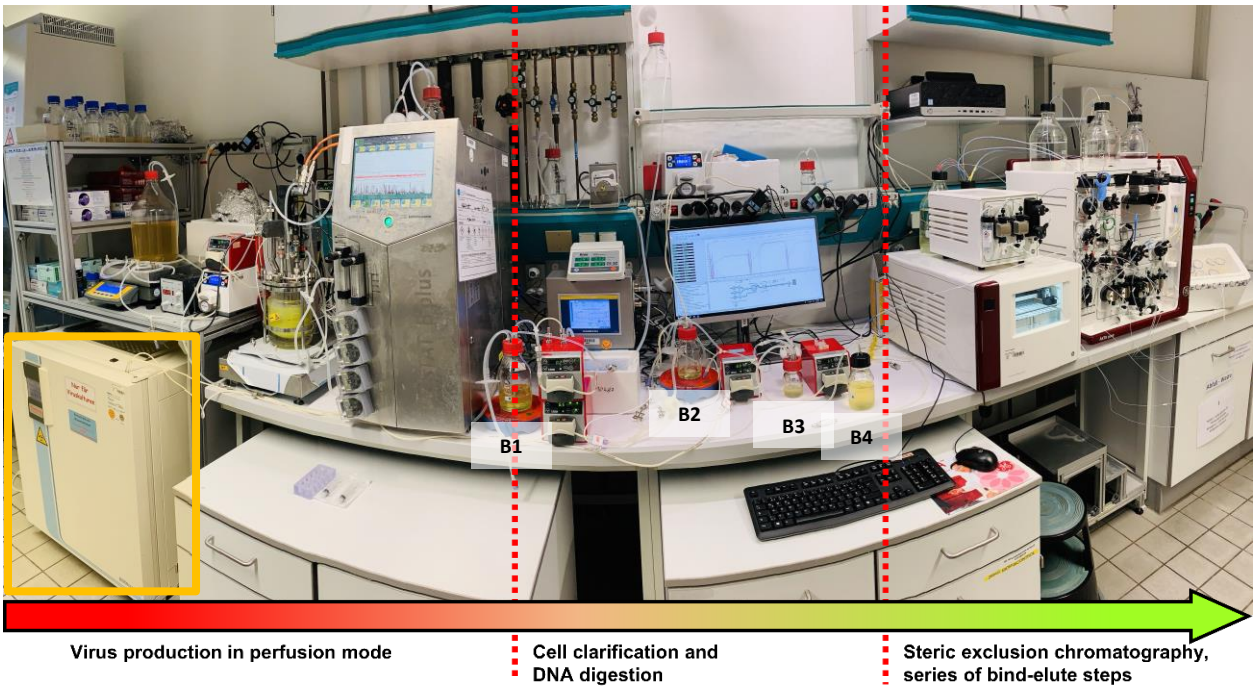

Figure 20: Picture of the process set-up, separated into three parts by red dashed vertical lines as shown in the scheme of Figure 19: 1) Virus production in the bioreactor (Biostat system coupled to an acoustic settler), 2) cell clarification and DNA digestion and 3) steric exclusion chromatography with an ÄKTA Pure 25 system operated in bind-elute mode. The plug flow reactor used for continuous DNA digestion at 37°C with a retention time of 4 h is located in the incubator, indicated by the orange square on the left side of the picture. The yellow color of the bioreactor and the bottles is due to the GFP protein expressed by the AGE1.CR.pIX cells after infection with the recombinant MVA.

3.11.1 Harvest and cell culture clarification

Batch

At the time of harvesting, 95.3% of the V_w was first clarified using the AS (10 L acoustic chamber version; SonoSep Technologies, Hinterbrühl, Austria) with an acoustic power of 3 W and a frequency of 2.1 MHz, at a flow rate of 252 mL/h. Sodium azide 0.05% v/v was added to the harvest to reduce contamination risk. Then 700 mM salt (NaCl, NaBr and KCl) was added and the supernatant was depth filtered using a polypropylene filter (PP3 Sartopure, 0.45 µm pore size, 120 cm^2 (5051306P4--OO--B) or 4.5 cm^2 (5055306PV--LX--C) filtration surface; Sartorius AG, Göttingen, Germany), at a constant flow rate of 0.45 mL/min/cm^2 and a filtration capacity of at least 126 L/m^2. The clarified cell culture supernatant was subsequently treated with endonuclease and further clarified as described in section 3.11.2. The choice of the depth filter and the salt level in the raw material was determined based on preliminary depth filtration testing (Appendix, section 10.5).

Perfusion

As described in section 3.11, the bioreactor was continuously harvested at 40 hpi onwards. The cell culture harvest from the AS was not suitable for direct purification using SXC as the contamination level of cells and cell debris passing through the cell retention device was too high. Therefore, the cell culture harvest was first collected in bottle B1 and salts were continuously added to reach 700 mM of NaCl, NaBr and KCl mixture, (as illustrated in Figure 19) to avoid virus interaction with the depth filter, to stabilize virus particles and to facilitate endonuclease treatment (Table 8). Sodium azide was also continuously added to bottle B1 (Table 8). The harvest was then clarified using a polypropylene depth filter with a pore size of 0.45 µm (filtration capacity of 240 L/m^2; Sartopure PP3, 120 cm^2 filtration area), transferred to bottle B2 (Figure 19) for DNA digestion and microfiltration as described in section 3.11.2.

Table 8: Process parameters used for continuous cell clarification and DNA digestion of cell culture harvest from the acoustic settler.

Parameter	Cell culture harvest	NaCl, NaBr and KCl salts	Sodium azide (NaN_3)	DENARASE®, diluted in PBS + 5% sucrose	Magnesium chloride ($MgCl_2$)
Initial concentration	-	6000 mM	6.2% v/v	1628 U/mL	176 mM
Final concentration	-	700 mM	0.08% v/v	37 U/mL	4 mM
Point of addition [a)]	B1	B1	B1	B2	B2
Flow rate$_{in}$ [mL/h]	54.0	7.5	0.8	1.5	1.5
Flow rate$_{out}$ [mL/h]	62.3	62.3	62.3	65.3	65.3

[a)] Bottle names according to the scheme shown in Figure 19.

3.11.2 DNA digestion and microfiltration

Batch

DNA in the supernatant was digested using endonuclease at a final activity of 35 U/mL (DENARASE®, enzyme activity > 250 U/µL determined by the manufacturer, 20804-100k; c-Lecta, Leipzig, Germany), mixed with 3 mM $MgCl_2$. The cell culture supernatant was incubated in a glass bottle for 4 h at 37°C and stirred at 100 rpm using a magnetic agitator. The endonuclease step was optimized by decreasing the amount of endonuclease needed to achieve DNA depletion up to 1000-fold within 4 h (Appendix, section 10.7). In a scouting experiment, the stability of infectious virions at 37°C was demonstrated for a period of at least 12 h (chapter 7). Finally, the treated cell culture supernatant was filtered using 0.45 µm cellulose acetate filters (Minisart NML Syringe Filter, 6.2 cm^2 total filtration area, 16555-K;

Sartorius AG, Göttingen, Germany) at a flow rate of 8 mL/min/cm^2 and a filtration capacity of 175 L/m^2. The treated cell culture supernatant was either stored at -80°C or directly purified through SXC, as described in section 3.11.3.

Perfusion

The clarified cell culture broth was continuously treated in bottle B2 with 37 U/mL endonuclease (DENARASE®) and with 4 mM $MgCl_2$ (Table 8). After bottle B2, the material was continuously transferred to a coiled silicone tube (3.2 mm inner diameter, 32.5 m length, GESSULTRA-C-125-2H; VWR, Radnor, USA) with a retention time of 4 h at 37°C in an incubator. The product was collected continuously into bottle B3. The harvest from bottle B3 was filtered using 0.45 µm cellulose acetate filters (filtration capacity of 290 L/m^2; Minisart NML Syringe Filter, 6 x 6.2 cm^2 total filtration area). The filtered product was then collected in bottle B4, and stored at 4°C before the chromatography step (described in section 3.11.3). As the process was operated continuously, the V_w of bottles B1, B2, B3 and B4 were kept constant at 180, 120, 60 and 120 mL, respectively.

3.11.3 Purification through steric exclusion chromatography

Membrane-based SXC was performed using an ÄKTA Pure 25 system (Cytiva, Uppsala, Sweden) as described previously [82], using PBS with NaCl, NaBr and KCl (700 mM final salt concentration) as elution buffer and polyethylene glycol (PEG, 81260-1KG; MW 6000, dissolved in PBS + 700 mM NaCl, NaBr and KCl; Sigma-Aldrich, St-Louis, USA) as equilibration buffer. A total surface of 70 cm^2 of regenerated cellulose (14 x 25 mm stacked membranes, 1 µm pore size, 10410014; GE, now Cytiva, Uppsala, Sweden) was used. Optimized purification settings (based on a design of experiment (DoE); Appendix, section 10.8) were determined as following: PEG concentration = 7.2% w/v, flow rate = 8.2 mL/min, with endonuclease treated raw material, containing 700 mM salts and using regenerated cellulose membranes.

UV was monitored at a wavelength of 280 nm and 360 nm. The column was operated at 27 to 75% breakthrough of the dynamic binding capacity of the column. This allowed purifying 45 mL sample per cycle, lasting 40 min in total, including column regeneration time. The column (XX3002500; EMD Millipore, Burlington, USA) was regenerated each time by flushing 25 mL of 2 M NaCl in 1 M NaOH. The membranes of the column were replaced every 4 cycles. Consecutive series of bind-elute steps allowed the purification of 67.5 mL/h of cell culture

supernatant. The SXC protocol used for purification was identical for both batch and perfusion cultures.

3.12 Analytics

3.12.1 Viable cell concentration and cell viability

VCC and viability were determined using a cell counter (Vi-CELL XR, Beckman-Coulter, Brea CA, USA) with trypan blue staining (see SOP list in Appendix, Table A.1). The detailed settings for the VCC and viability measurement with the Vi-CELL XR are listed in Table A.2. For the PBG.PK2.1 cell line, as the cells were forming aggregates (around 5 cells) when cultivated in a bioreactor, samples were first incubated for 5 min at 37°C with trypsin (60–80 U/mL; Gibco porcine trypsin #27250-018; trypsin activity according to the manufacturer; Thermo Fisher Scientific, Waltham, MA, USA) to disaggregate cells before using the cell counter. Viability was always measured without using trypsin as described in the SOP list (see Appendix, Table A.1). The coefficient of variation for mammalian VCC and viability quantifications was equal to 6% and 4%, respectively (measured for CHO cells, given by the manufacturer). The quantification range was 0.1–10.0 x 10^6 cells/mL (Validated range for MDCK cells, see SOP lists, Table A.1). For higher VCCs, the sample was diluted with fetal bovine serum (Gibco fetal bovine serum premium #A4766801).

3.12.2 Metabolites in the culture medium

Glucose, glutamine, lactate and ammonium concentrations were determined using a Bioprofile 100 plus (Nova biomedical, Waltham, MA, USA; see SOP list in the Appendix, Table A.1). Amino acid concentrations were measured using an Acquity H-Class UPLC instrument (Waters Corp, Milford, MA, USA; see SOP list Table A.1 in the Appendix). The validated metabolite measurement ranges and coefficient of variations of the assays are listed in Table A.3.

3.12.3 Influenza virus titration

Three different methods were used for virus particle titration. HA titer was determined as described earlier by Kalbfuss et al. [150] and quantified in $\log_{10}$(HA units/100 µL) with a discretization measurement error of ± 0.081 $\log_{10}$ units (see SOP list in Table A.1). The infectious virus titer was measured according to Genzel and Reichl with adherent MDCK cells [151] by median tissue culture infectious doses ($TCID_{50}$; see SOP list in Table A.1). The error of the assay is ± 0.3 $\log_{10}(TCID_{50}/mL)$. Pretreated primary antibody (40 µL per well of a 1:5 dilution in filtered PBS; equine influenza A anti-goat produced in goat; nanoTools, Teningen, Germany) and secondary antibody (40 µL per well of a 1:500 dilution in filtered PBS; Molecular Probes, # A-11015, Eugene, USA) were used for fluorescence staining. In addition, the HA content was quantified in µg/mL by a SRID assay as described previously [82] (see SOP list in Table A.1). A relative standard deviation of ≤ 17.3% was observed [82].

The virus particle concentration (C_{vir}; in virions/mL) obtained from the measured HA value was calculated using the following equation (based on Vazquez et al. 2018 [110]). Based on the discretization measurement error of the HA assay, the error of C_{vir} is equal to 20.5% for the upper value and 17.0% for the lower value.

$$\mathbf{C_{vir} = 2 \times 10^7 \times 10^{(\log_{10}(HA\ units/100\ \mu L))}} \quad (13)$$

3.12.4 MVA titration

For the result chapter comparing the production platforms for MVA production (chapter 7), only the infectious titer was quantified, through a $TCID_{50}$ assay, in $\log_{10}(TCID_{50}/mL)$, with 10-fold dilutions, and using half a 96-well plate per sample. For MVA-CR19 immunofluorescence, wells containing adherent Vero cells were incubated with polyclonal vaccinia virus antibodies (Quartett Immunodiagnostika, Berlin, Germany) at 1:1000 dilution in PBS containing 1% fetal calf serum, as described by Jordan et al. (2009) [55] (see SOP list in Table A.1). For MVA-CR19.GFP, wells containing adherent Vero cells with 10-fold sample serial dilutions were not incubated with antibodies as wells positive to this MVA strain were showing fluorescence, detectable under a fluorescence microscope (see SOP list in Table A.1). For virus titration of MVA-CR19, a standard deviation of ± 0.4 $\log_{10}(TCID_{50}/mL)$ was reported [90]. For virus titration

of the MVA-CR19.GFP virus strain, a standard deviation of ± 0.3 $log_{10}(TCID_{50}/mL)$ was reported [151]. On a linear scale and considering the error of the $TCID_{50}$ assay for the MVA-CR19.GFP virus strain, an error of 100% for the upper value and 50% for the lower value has to be taken into account for the total concentration of infectious MVA produced (C_{vir}).

For the integrated MVA production process result chapter (chapter 8), the infectious titer was quantified through a $TCID_{50}$ assay, in $log_{10}(TCID_{50}/mL)$, with 2-fold dilutions instead of 10-fold, and using half a 96-well plate per sample (4/8 rows; see SOP list in Table A.1). With the 2-fold dilution $TCID_{50}$ assay, a standard deviation of ± 0.077 $log_{10}(TCID_{50}/mL)$ was measured (standard deviation of a sample measured in triplicate, by three operators). On a linear scale, the $TCID_{50}$ assay contributes an error of + 19.4/-16.3% to C_{vir}.

The relative quantity of vg was measured as well for purification recovery calculations. In this case, a viral DNA sequence specific to MVA-CR19 and MVA-CR19.GFP was amplified through a qPCR assay (Rotor-Gene Q real-time PCR cycler; Qiagen, Hilden, Germany), and threshold cycle (ct) values were correlated to dilutions series of a standard sample (see SOP list in Table A.1).

For the infectious titration assay (through the $TCID_{50}$), all samples were sonicated in a water bath for 1 min at 45 kHz with an ultrasonic bath (USC600D; VWR, Radnor, PA, USA) to avoid aggregate formation [145] and underestimation of the virus titer. For samples purified with SXC, the samples were not sonicated with the water bath but with a VialTweeter for 1 min (UP200St, Power = 160 W, Amplitude = 100%, Pulse = 30%; Hielscher Ultrasound Technology, Teltow, Germany) in order to ensure virus disaggregation after SXC.

3.12.5 Flow cytometry

To quantify the percentage of infected and apoptotic cells over the whole cell population, samples from IAV infections with 2×10^6 cells were collected and fixed in 2% paraformaldehyde (Morphisto GmbH, Frankfurt am Main, Germany) for 30 min at 4 °C. After centrifugation (10 min, 300 × g, 4°C), the pellets were resuspended in 1 mL of cold PBS and transferred to 15 mL falcon tubes containing 4.5 mL of cold 70% ethanol (v/v). The samples were stored at -20°C until use. Antibody staining for viral nucleoprotein (NP) was done similarly to Frensing et al. [152] (see SOP list in Appendix, Table A.1). Briefly, the V_w for blocking and antibody incubations was reduced to 25 µL and the number of washing steps was

reduced to 1–2 times. Cells were then resuspended in the remaining 30–50 µL and DAPI was added (approx. 5 µg/mL). Using the ImageStream X mark II (Amnis, EMD Millipore, Burlington, MA, USA), 10'000 single cells per sample were collected. The IDEAS software (v. 6.2; Amnis/Merck KGaA, Darmstadt, Germany) was used to analyze the data. Cells positive for NP were determined as infected and apoptotic cells were measured using the DAPI signal and brightfield images [152].

3.12.6 Influenza A virus glycopeptide analysis

Influenza virus produced with PBG.PK2.1 cells (chapter 4) was harvested using g-force step-gradient centrifugation as described previously (see SOP list in the Appendix, Table A.1) [153, 154]. Site-specific glycopeptide analysis was performed according to Pralow et al. [155]. Briefly, influenza virus glycoproteins were sequentially digested using trypsin (Trypsin Sequencing Grade Modified, V5111; Promega, Madison, WIS, USA) and Flavastacin (AspN, P8104S; New England Biolabs, Ipswich, MA, USA) using a modified version of the filter-aided sample preparation method of Wisnievski et al. [155-157]. Glycopeptide enrichment was performed using hydrophilic interaction liquid chromatography solid phase extraction according to the modified workflow of Selman et al. [158], recently published by Hoffmann et al. [156]. Enriched glycopeptides were separated and measured on a reversed-phase liquid chromatography system coupled online to an LTQ Orbitrap Elite mass spectrometer (Thermo Fisher Scientific, Waltham, MA, USA). Data analysis was performed manually and semi-automated using glyXtool^{MS}, an in-house developed software for the analysis of glycopeptide mass spectrometry data, published by Pioch et al. [159].

3.12.7 Process-related impurities and aggregate

Total protein and DNA concentrations were assessed with a Bradford and a PicoGreen assay following methods described previously [82] (see SOP list in Table A.1). As the MVA is a DNA virus, the PicoGreen assay could not be performed for host cell DNA quantification. In this case (chapter 8), the relative concentration of contaminated host cell DNA was measured through a qPCR assay (Rotor-Gene Q real-time PCR cycler; Qiagen, Hilden, Germany), which was correlated with a standard host cell DNA concentration of lysed AGE1.CR.pIX cells measured through a PicoGreen assay as described earlier [82] (see SOP list in Table A.1). The host cell DNA concentration was then estimated in µg/mL.

The distribution of large-sized virus and other aggregates was measured using a disc centrifuge (CPS DC24000 UHR disc centrifuge; CPS Instruments Inc., LA, USA) following a method described earlier [160] (see SOP list in Table A.1).

3.13 Calculations

3.13.1 Growth and metabolism

For the batch cultivation mode, the cell-specific growth rate (μ, in 1/h), the cell-specific substrate consumption rate or the cell-specific by-product production rate (q_s, in mmol/cell/h) were determined using the following equations:

$$\mu = \frac{\ln(x(t_{n+1})/x(t_n))}{t_{n+1}-t_n} \quad (14)$$

$$Y_{x/s} = \frac{x(t_{n+1})-x(t_n)}{c_s(t_n)-c_s(t_{n+1})} \quad (15)$$

$$q_s = \frac{\mu}{Y_{x/s}} \quad (16)$$

With x, the viable cell concentration (cells/mL);
t, the cultivation time (h);
n, the sampling time point (-) and
c_s, the cell culture compound (such as glucose) concentration (mM).

To evaluate the metabolic state of cells in perfusion mode, the lactate yield based on glucose consumption ($Y_{lac/glc}$, no unit) was calculated as follows:

$$Y_{lac/glc} = \frac{(C_{lac,n}-C_{lac,n-1})+AC_{lac,h} \times p_h}{(C_{glc,n-1}-C_{glc,n})+(C_{glc,0}-AC_{glc,h}) \times p_h} \quad (17)$$

With $C_{lac,n}$, the lactate concentration at time n (t_n) (mM);
$AC_{lac,h}$, the average lactate concentration in the harvest between t_{n-1} and t_n (mM);
p_h, the perfusion ratio between t_{n-1} and t_n (mL perfused medium/mL working volume);
$C_{glc,n}$, the glucose concentration at time n (mM);
$C_{glc,0}$, the glucose concentration of the fresh medium (33 mM) (mM) and
$AC_{glc,h}$, the average glucose concentration in the harvest between t_{n-1} and t_n (mM).

3.13.2 Hydrodynamic stress and scale-up/scale-down

The ratio between the stirring power and the bioreactor volume was kept constant between the DASGIP and Biostat bioreactors, leading to the following formula [161]:

$$\frac{N_1^3 \times D_1^5}{V_{w1}} = \frac{N_2^3 \times D_2^5}{V_{w2}} \quad (18)$$

With N, the stirring speed of the bioreactor stirrer (rpm);
V_w, the working volume (mL) and
D, the diameter of the bioreactor stirrer (m).

To describe the different hydrodynamic stress conditions for the ATF system and the AS, the shear rate (γ, in s^{-1}) was estimated assuming laminar flow conditions in a cylinder based on the Reynolds number (Re) [119, 162, 163] (Re; laminar flow with Re < 2100).

$$\mathbf{Re} = \frac{\rho_l \times v \times L}{\eta} \quad (19)$$

$$\boldsymbol{\gamma} = \frac{4 \times Q_r}{n_f \times \pi \times R^3} \quad (20)$$

With ρ_l, the volumetric density of the liquid (kg/m^3);
v, the velocity of the fluid (m/s);
L, the characteristic length (m);
η, the dynamic viscosity of the liquid (kg/s/m);
Q_r, the recirculation flow rate (m^3/s);
n_f, the number of fibers (for an ATF membrane) (-) and
R, the internal radius of the recirculation tube (m).

The recirculation flow rate was determined following the exchange flow rate for the ATF system (between 0.8 and 1.0 L/min). For the AS, the maximum back-flushing flow rate was taken to calculate γ. To calculate γ (according to Equation 20) when comparing the AS with the ATF system for influenza production (chapter 5), the number of fibers for the ATF (n_f) was equal to 76, and the R was equal to 0.9 and 3.0 mm for the ATF and AS, respectively.

3.13.3 Virus productivity

The cell-specific virus yield (CSVY, in virions/cell for IAV and in $TCID_{50}$/cell for MVA) and the volumetric virus productivity (P_v, in virions/L/day for IAV and in $TCID_{50}$/L/day for MVA) were calculated using the equations below. The units are different for IAV and MVA as the CSVY and P_v are based on the HA assay (non-infectious virions, see section 3.12.3) for IAV and on the $TCID_{50}$ assay (infectivity assay, see section 3.12.4) for MVA.

$$\mathbf{Vir_{tot}} = \mathbf{C_{vir,b}} \times \mathbf{V_w} + \sum \mathbf{AC_{vir,h}} \times \mathbf{V_h} \quad (21)$$

$$\mathbf{C_{vir,tot}} = \frac{\sum \mathbf{Vir_{tot}}}{\mathbf{V_w}} \quad (22)$$

$$\mathbf{CSVY} = \frac{\mathbf{Vir_{tot,max}}}{\mathbf{X_{v,b,max}} \times \mathbf{V_w}} \quad (23)$$

$$\mathbf{P_v} = \frac{\mathbf{Vir_{tot,max}}}{\mathbf{V_{tot}} \times \mathbf{t_{tot}}} \quad (24)$$

With Vir_{tot}, the total number of virions produced (virions for IAV, and $TCID_{50}$ for MVA);
$C_{vir,b}$, the virus particle concentration in the bioreactor (virions/mL for IAV and $TCID_{50}$/mL for MVA);
V_w, the bioreactor working volume (mL);
$AC_{vir,h}$, the average virus particle concentration in the harvest between t_{n-1} and t_n (virions/mL for IAV and $TCID_{50}$/mL for MVA);
V_h, the harvested volume between t_{n-1} and t_n (mL);
$C_{vir,tot}$, the concentration of virions produced (in total) (virions/mL for IAV and $TCID_{50}$/mL for MVA);
$x_{v,b,max}$, the maximum concentration of viable cells in the bioreactor obtained until the time point of maximum Vir_{tot} (cells/mL);
V_{tot}, the total volume of medium spent including cell growth phase until the time point of maximum Vir_{tot} (mL) and
t_{tot}, the time from bioreactor inoculation until maximum Vir_{tot} (day).

To allow a comparison of Vir_{tot} calculated for cultivations with different V_ws, runs were normalized to 650 mL V_w. The error of Vir_{tot}, CSVY and P_v are based only on the virus titration of influenza virus or MVA. All the calculation for $C_{vir,tot}$, Vir_{tot}, CSVY and Pv were based on the HA titer (non-infectious titer) for IAV, and on the $TCID_{50}$ titer (infectious titer) for MVA.

For $C_{vir,tot}$, Vir_{tot} was cumulated over several consecutive runs using the same bioreactor to estimate process time over 30 days (chapter 7). For continuous processes, Vir_{tot} values were added over time, as shown in Equation 22.

The product recovery was calculated for integrated MVA production processes (chapter 8), as described for recombinant protein production in perfusion mode [70]. This is of interest to quantify eventual product retention during the different steps of the product purification. For perfusion, the recovery for each filtration or DNA digestion step was calculated as the average titer (between t_{n-1} and t_n) after and before the step as shown in Table 9.

Table 9: Parameters used to calculate the recovery for each filtration or DNA digestion step in perfusion mode.

Recovery [a]	Average infectious virus titer between t_{n-1} and t_n before the step	Average infectious virus titer between t_{n-1} and t_n after the step
Acoustic settler filtration [b]	Bioreactor supernatant	Bottle B1 [c]
Depth filtration	Bottle B1 [c]	Bottle B2 [c]
DNA digestion	Bottle B2 [c]	Bottle B3 [c]
Final filtration	Bottle B3 [c]	Bottle B4 [c]

[a] The recovery is calculated as the ratio of the average titer after and before the step.
[b] Ratio for the settler filtration recovery calculated similarly to the sieving coefficient calculated for recombinant protein perfusion cultures [70].
[c] Bottle names according to the scheme shown in Figure 19.

For batch cultures, the recovery was calculated stepwise as the ratio between the total amount of infectious virions after and before the filtration or DNA digestion step. The average was calculated as the average recovery of three integrated batch bioreactor runs.

For SXC, the percentage of recovered infectious virions in the elution (recovery, in %) was calculated after one purification cycle, as shown below.

$$\textbf{SXC recovery} = \mathbf{100} \times \frac{\mathbf{C_{vir,SXC\ out}} \times \mathbf{V_{SXC\ out}}}{\mathbf{C_{vir,SXC\ in}} \times \mathbf{V_{SXC\ in}}} \quad (25)$$

With $C_{vir,\ SXC\ out}$, the infectious virus concentration in the eluate ($TCID_{50}$/mL);
$V_{SXC\ out}$, the volume of the SXC eluate (mL);
$C_{vir,\ SXC\ in}$, the infectious virus concentration in the SXC feed ($TCID_{50}$/mL) and
$V_{SXC\ in}$, the volume of the SXC feed (mL).

The average SXC recovery of perfusion mode was the mean of all cycles performed for one integrated process. To reduce the consumption of spin tubes, buffers and regenerated

cellulose, the SXC was operated 23% of the period during the virus production phase, always with three to four consecutive cycles (intervals < 9 h). The average SXC recovery for the batch process was calculated based on the 4 x 3 purification cycles (the SXC column is replaced after four purification cycles).

For the integrated MVA production (chapter 8), the space-time yield (STY, in $TCID_{50}/L_{bioreactor}$/day) was calculated for batch and perfusion mode (integrated processes). This is of interest in order to assess the impact of process intensification on the bioreactor footprint. The bioreactor footprint is the main parameter changing in the presented integrated setup, when intensifying MVA production. The STY was calculated as follow:

$$\mathbf{STY} = \frac{\mathbf{Purified\ Vir_{tot}}}{\mathbf{V_w} \times \mathbf{t_{tot,integrated\ process}}} \quad (26)$$

3.13.4 Process-related impurity levels

The host cell DNA per total amount of virus (in µg/virions) and the total protein per total amount of virus (in µg/virions) were calculated using the following equations:

$$\mathbf{host\ cell\ DNA/virion} = \frac{\mathbf{C_{DNA,b} \times V_w} + \sum \mathbf{AC_{DNA,h} \times V_h}}{\mathbf{Vir_{tot}}} \quad (27)$$

$$\mathbf{total\ protein/virion} = \frac{\mathbf{C_{tProt,b} \times V_w} + \sum \mathbf{AC_{tProt,h} \times V_h}}{\mathbf{Vir_{tot}}} \quad (28)$$

With V_w, the bioreactor working volume (mL);
V_h, the harvested volume between t_{n-1} and t_n (mL);
$C_{DNA,b}$, the DNA concentration in the bioreactor (µg/mL);
$AC_{DNA,h}$, the average DNA concentration in the harvest between t_{n-1} and t_n (µg/mL);
$C_{tProt,b}$, the total protein concentration in the bioreactor (µg/mL) and
$AC_{tProt,h}$, the average total protein concentration in the harvest between t_{n-1} and t_n (µg/mL).

Contamination levels for host cell DNA/virion and total protein/virion for IAV production (chapters 5 and 6) were calculated to assess whether continuous virus harvesting has an advantage compared to ATF mode for subsequent DSP. The same calculation was performed for integrated MVA production (chapter 8), except that the host cell DNA and total protein were not divided per Vir_{tot} (Equations 27–28), but per the total number of MVA doses

produced. One dose was considered in the thesis as equal to 10^8 plaque forming units (PFU) [38], which is equivalent to 1.43 x 10^8 $TCID_{50}$ [164].

3.14 Economic analysis

To estimate the impact on cost per dose for an end-to-end MVA production for a batch or perfusion system, the process simulation software SuperPro Designer v10 (Intelligen Inc., Scotch Plains, USA) was used, based on data relevant to cost of good evaluation build and stored using Microsoft Excel (Microsoft Corporation, Redmond, USA). All the data from USP to DSP related to cost of good were collected at the Institute of Bioprocess Engineering, Max-Planck Institute, Magdeburg, Germany, at the 1 L bioreactor scale, in an R&D and academic environment.

Key assumptions used to compare batch and perfusion processes: i) Production runs over 47 weeks per year and the seed train process 65% of the time (31 weeks per year). ii) Fill & finish costs and duration are considered the same for batch and perfusion. iii) MVA preparations of both processes are assumed to have the same product quality. iv) All bioreactors are assumed to operate at maximum volume capacity. v) Indirect costs relevant for cost of goods evaluation such as waste disposal (similarly to other cost analysis publication for viral vector production [165]) and depreciation maintenance and plant depreciation were not considered for both systems. vi) Costs related to QA/QC, operation of the facility, and labor were taken from default values given by the SuperPro Designer software.

3.15 DoE and statistical analysis

To optimize the SXC (results in the Appendix, section 10.8.2), a DoE and contour plot analysis were generated using the MODDE® software (Sartorius AG, Göttingen, Germany).

For several yield calculation comparisons, the Student's t-test were performed using the Origin® software (OriginLab Corporation, Northampton, MA, USA), between for example two cell culture conditions (operated in duplicate/triplicate). The p-values < 0.05 were considered as statistically significant.

Chapter 4

Influenza A virus production in high cell density cultures using the novel porcine suspension cell line PBG.PK2.1

This chapter was based on the following publication:

Gränicher, G., Coronel, J., Pralow, A., Marichal-Gallardo, P., *et al.*, Efficient influenza A virus production in high cell density using the novel porcine suspension cell line PBG.PK2.1. *Vaccine*, 2019.

4.1 Introduction

In order to answer increasing demands in influenza vaccines, innovative cell culture bioprocesses have been developed. Volume-expanded fed-batch cultures [166], continuous bioprocesses [167] or HCD perfusion processes [103] have been evaluated for the production of various viral vaccines. IAV production using two-stage continuous bioreactors was already shown not to be suitable for continuous production, due to the presence of defective interfering particles [168]. Therefore, perfusion technology seems most promising. Up to now, and based on published literature, perfusion processes for IAV production were tested using the following suspension cell lines: AGE1.CR.pIX, AGE1.CR, CEVEC's amniocyte production (CAP), Vero and Human embryonic kidney (HEK) [90, 103, 107]. In addition, a semi-perfusion using SFs was also successful using MDCK suspension cell for influenza virus production [169]. It was believed that higher influenza virus titers could be reached in STR systems, in perfusion mode, especially for IAV strains from porcine origin. Swine population is one of the main reservoirs (together with avian population) regarding possible zoonosis, which occasionally is the origin of seasonal influenza or influenza pandemics [170].

Evaluating a HCD process with a new potential cell line producing higher influenza virus titers could make cell culture-based influenza vaccine manufacturing more attractive. In addition, as influenza pandemics can arise from different animal reservoirs, having a larger choice of cell substrates from different species for production is beneficial [44]. Also, differences in productivity can be observed depending on influenza virus strain and cell line origin. Finally, evaluating such a cell line is of high interest as well for the production of veterinary vaccines, especially to protect porcine population from influenza.

Here, PBG.PK2.1, a novel suspension cell line derived from immortal porcine kidney cells and growing in chemically-defined CD-U5 medium (ProBioGen AG) is presented. For the first time, influenza virus was propagated in a porcine suspension cell line. In order to assess the efficiency of the production process established, product quality, USP and DSP aspects were considered. The suitability of the cell line regarding its safety was also discussed.

4.2 Results

In order to efficiently evaluate a new cell line for the production of influenza vaccines, not only cell growth and virus propagation, but also key process parameters regarding USP and DSP should be assessed. In a first step, cell growth and metabolism of the PBG.PK2.1 cell line were evaluated without virus infection. Subsequently, influenza virus production was characterized and optimized in batch and perfusion mode in SFs and small scale bioreactors. Finally, viral hemagglutinin glycosylation of the produced IAV was analyzed, and protein and DNA impurity levels of crude harvests assessed.

4.2.1 Cell growth and metabolism

Cultivations in SFs (100 mL V_w) and in DASGIP bioreactors (550 mL V_w) were compared, both inoculated with about 1 x 10^6 cells/mL. PBG.PK2.1 cells showed similar viabilities above 97% (up to 144 h) with an exponential growth phase from 0–120 h for both scales (Figure 21A). VCCs and growth rates were slightly higher in SFs (Table 10). In bioreactors but not in SFs, small aggregates of about 5 cells were observed. The doubling population time of PBG.PK2.1 cell line was relatively high with 38 ± 11 h in CD-U5 medium. As shown in Table 10, the production and consumption rates of the main cell culture metabolites were similar in SFs and bioreactors.

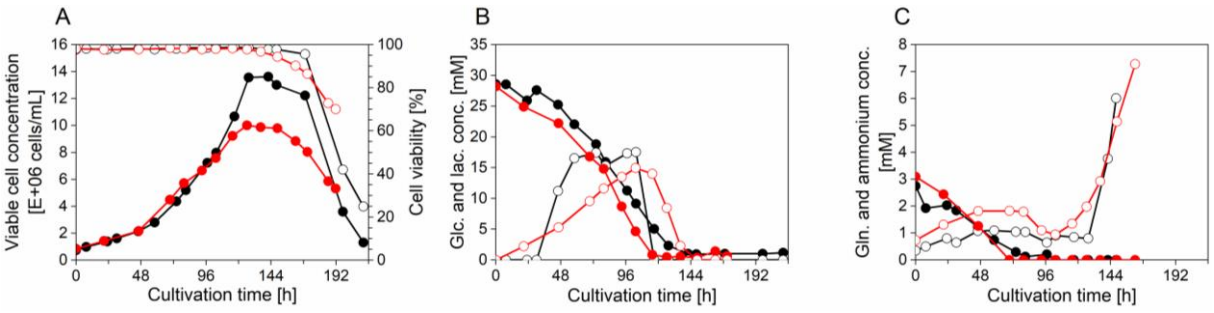

Figure 21: Growth of PBG.PK2.1 cells in CD-U5 medium in one representative run (of n=2) in a 100 mL V_w shake flask (black) and in one representative run (of n=3) in a 550 mL V_w stirred-tank bioreactor (red). (A) Viable cell concentration (●), cell viability (○) – (B) glucose (●) and lactate (○) concentrations – (C) glutamine (●) and ammonium (○) concentrations.

Table 10: Growth parameters of PBG.PK2.1 cells in chemically-defined CD-U5 medium in batch mode for shake flasks and bioreactors

	Cultivation time range [h]	Shake flask, n=2	Bioreactor, n=3
Cell-specific growth rate [h^{-1}]	20-120	0.021 ± 0.004 [a)]	0.020 ± 0.006
Doubling time [h]	20-120	34 ± 8	38 ± 11
Maximum cell concentration [10^6 cells/mL]		13.39 ± 0.04	9.86 ± 0.10
Cell diameter [µm]	20-120	15.19 ± 0.25	14.48 ± 0.46
q_{glc} [10^{-11} mmol/cell/h]	20-120	-6.64 ± 3.06	-6.64 ± 0.94
q_{gln} [10^{-11} mmol/cell/h]	20-70	-1.59 ± 0.37	-2.32 ± 0.65
q_{lac} [10^{-11} mmol/cell/h]	20-110	8.61 ± 3.19	3.79 ± 2.52
q_{NH4+} [10^{-11} mmol/cell/h]	20-70	1.04 ± 0.85	1.40 ± 0.06

q_{glc}, cell-specific glucose consumption rate; q_{gln}, cell-specific glutamine consumption rate; q_{lac}, cell-specific lactate production rate; q_{NH4+}, cell-specific ammonium production rate.

[a)] Mean and standard deviation

The main by-product concentrations were monitored, showing lactate concentration < 20 mM and ammonium concentration < 3 mM (Figure 21B and Figure21C). A decrease in lactate concentration was observed after 105 h cultivation time, once glucose level was less than 10 mM. Interestingly, porcine cells continued growth even after exhaustion of glutamine after about 80 h cultivation time (Figure 21A and Figure 21C). As data suggest that glutamine might not to be necessary for PBG.PK2.1 cell growth, glucose was used to determine the CSPR for process optimization and intensification.

4.2.2 Screening of virus propagation in shake flasks

As the influenza A/PR/8/34 seed virus was generated in MDCK host cells, the virus was first adapted to propagate more efficiently in PBG.PK.2.1 cells following the method described in section 3.8.1 (Figure 22A). Interestingly, neither higher $TCID_{50}$ nor HA titers were observed with increased number of passage. However, maximum titers were reached 12 hpi earlier for later passages compared with the first passage. For all further experiments of this study, the seed virus adapted after three passages in PBG.PK2.1 cells was used (HA value: 3.0 $\log_{10}$(HA units/100 µL); $TCID_{50}$ value: 1 x 10^7 $TCID_{50}$/mL). In a next step, MOIs between 10^{-2} and 10^{-5} and trypsin activities varying between 10^{-5} U/cell and 10^{-7} U/cell were tested to further improve influenza virus production. As shown in Figure 22D, optimum influenza A/PR/8/34 production was obtained using a MOI of 10^{-5} with a trypsin activity of 10^{-6} U/cell. The low MOI was in accordance with previous studies showing that MOIs equal or lower than 10^{-3} allowed higher titers for cell-based influenza A production [50, 171]. Under these optimized conditions, a

maximum titer of 3.38 log_{10}(HA units/100 µL) with a CSVY equal to 5375 virions/cells (Table 11) was obtained.

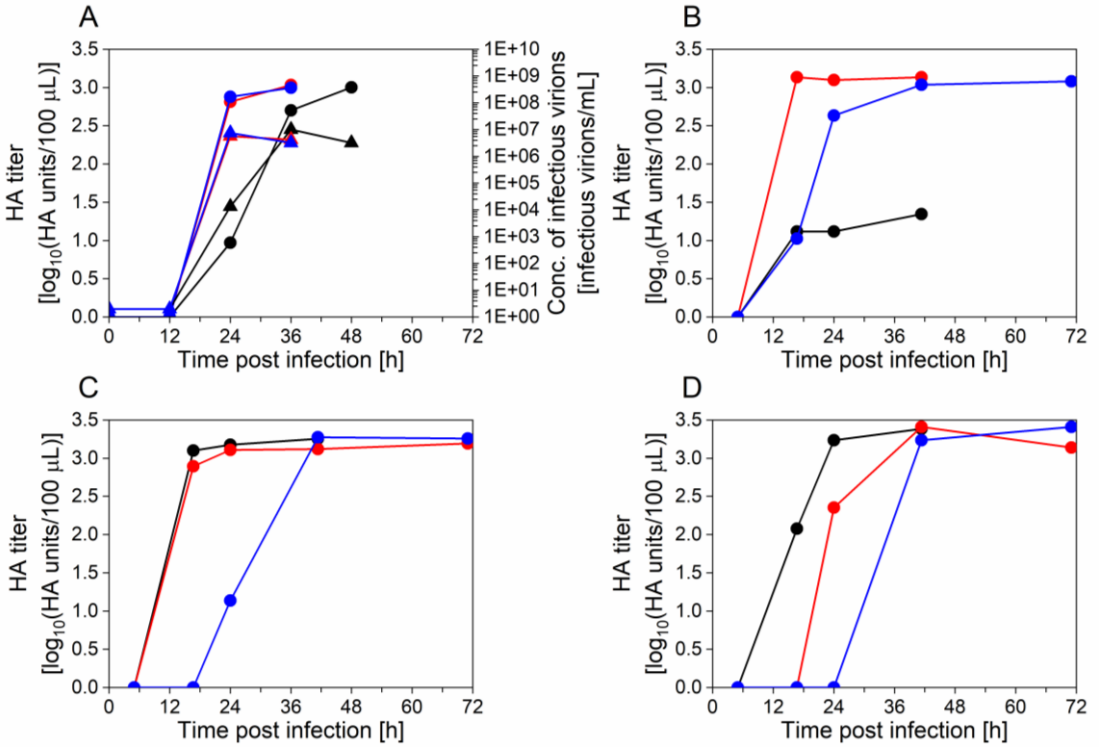

Figure 22: Optimization of influenza A/PR/8/34 virus production in PBG.PK2.1 cells cultivated in CD-U5 medium in shake flasks. (A) Virus adaptation: Influenza A/PR/8/34 virus passaged in PBG.PK2.1 cells. Passage 1 (black), passage 2 (red) and passage 3 (blue) are presented. HA titer (●) and $TCID_{50}$ titer (▲) are compared for each passage. (B) HA titer at MOI = 10^{-2} and trypsin activity of 10^{-5} U/cell (black), 10^{-6} U/cell (red) and 10^{-7} U/cell (blue) from adapted influenza A/PR/8/34 seed virus (third passage). (C) HA titer at MOI = 10^{-3} and trypsin activity of 10^{-5} U/cell (black), 10^{-6} U/cell (red) and 10^{-7} U/cell (blue). (D) HA titer at MOI = 10^{-5} and trypsin activity of 10^{-5} U/cell (black), 10^{-6} U/cell (red) and 10^{-7} U/cell (blue) from adapted influenza A/PR/8/34 seed virus (third passage).

Further screenings were also performed regarding porcine influenza A H1N2 (A/Bakum/1832/00) and influenza B (B/Brisbane/60/2068) virus production in SFs. Taking into account the optimized settings for influenza A/PR/8/34, maximum titers of 3.37 log_{10}(HA units/100 µL) and 2.89 log_{10}(HA units/100 µL) were obtained for porcine IAV and IAB, respectively (without prior virus adaptation and without optimized amount of seed virus).

Table 11: Influenza A/PR/8/34 virus production in PBG.PK2.1 cells considering key parameters for upstream and downstream processing.

	Optimized condition [a] Shake flask, n=5	**Batch mode** Bioreactor, n=3	**Perfusion mode** Bioreactor, n=2
Process time [b]	n.d.	144 ± 6 [c]	198 ± 7
Cell concentration at TOI [10^6 cells/mL]	5.0 ± 0.1	5.0 ± 0.1	46.0 ± 4.2
Maximum cell concentration [10^6 cells/mL]	9.0 ± 0.3	7.1 ± 0.3 [d]	44.4 ± 4.4 [d]
Maximum HA titer [$\log_{10}$(HA units/100 µL)]	3.38 ± 0.03	3.24 ± 0.04 [d]	3.93 ± 0.05 [d]
CSVY [virions/cell]	5375 ± 273	5006 ± 540	3929 ± 876
P_v [10^9 virions/L/day]	n.d.	5.88 ± 0.21	1.87 ± 0.29
Maximum infectious virus titer [10^8 $TCID_{50}$/mL]	n.d.	4.4 ± 1.2 [d]	32.0 ± 0.0 [d]
Max. HA content [µg/mL]	n.d.	5.62 ± 1.16 [d], [e]	20.21 ± 2.42 [d]
dsDNA impurity level per HA dose at optimal harvest time point [ng] [f]	n.d.	18170 ± 2460 [d], [e]	18960 ± 1860 [d]
Protein impurity level per HA dose at optimal harvest time point [µg] [f]	n.d.	520 ± 100 [d], [e]	379 ± 29 [d]

TOI, time of infection; HA, hemagglutinin; CSVY, cell-specific virus yield; P_v, volumetric virus productivity; dsDNA, double stranded DNA; n.d., not determined; hpi, hours post infection.

[a] Optimized conditions: MOI=10^{-5}, trypsin= 10^{-6} trypsin U/cell, total medium replacement at TOI (batch mode)

[b] Process time is from cell culture bioreactor inoculation until maximum reached HA titer

[c] Mean and standard deviation

[d] Bioreactor working volume increased by 30% after infection

[e] Values determined only for two bioreactors

[f] One HA dose = 15 µg, best harvest time point in batch mode = 48 hpi, best harvest time point in perfusion mode = 36 hpi.

4.2.3 Virus production in bioreactors

For larger scale influenza A/PR/8/34 virus production, cells were cultivated in DASGIP bioreactors with 550 mL V_w using the optimized MOI and trypsin activity (sections 3.4.1 and 3.9.1). The medium was not replaced at the TOI to simplify the process for larger scales. Consequently, higher host cell protein concentrations in the cell culture were expected. Trypsin was added again after 16 hpi at 10^{-6} U/cell to ensure complete virus infection. The cells were cultivated until a VCC of 6.8 x 10^6 cells/mL was achieved and diluted to 5 x 10^6 cells/mL before infection. The VCC before bioreactor dilution was selected following previous optimization studies performed in SFs (data not shown). To avoid glucose limitation, the bioreactor V_w was increased by 30% with supplemented CD-U5 medium at 24 hpi. A maximum HA titer of 3.24 $\log_{10}$(HA units/100 µL) was obtained between 36 and 48 hpi (Figure 23A). No limitation in glucose and glutamine was observed during the virus production phase (Figure 23C and Figure 23D). Moreover, no toxic levels were reached for lactate (20 mM) and ammonium (2–3 mM) during the first 48 hpi. Almost 100% of the cells were infected at the point of maximum titer (36–48 hpi) (Figure 23B).

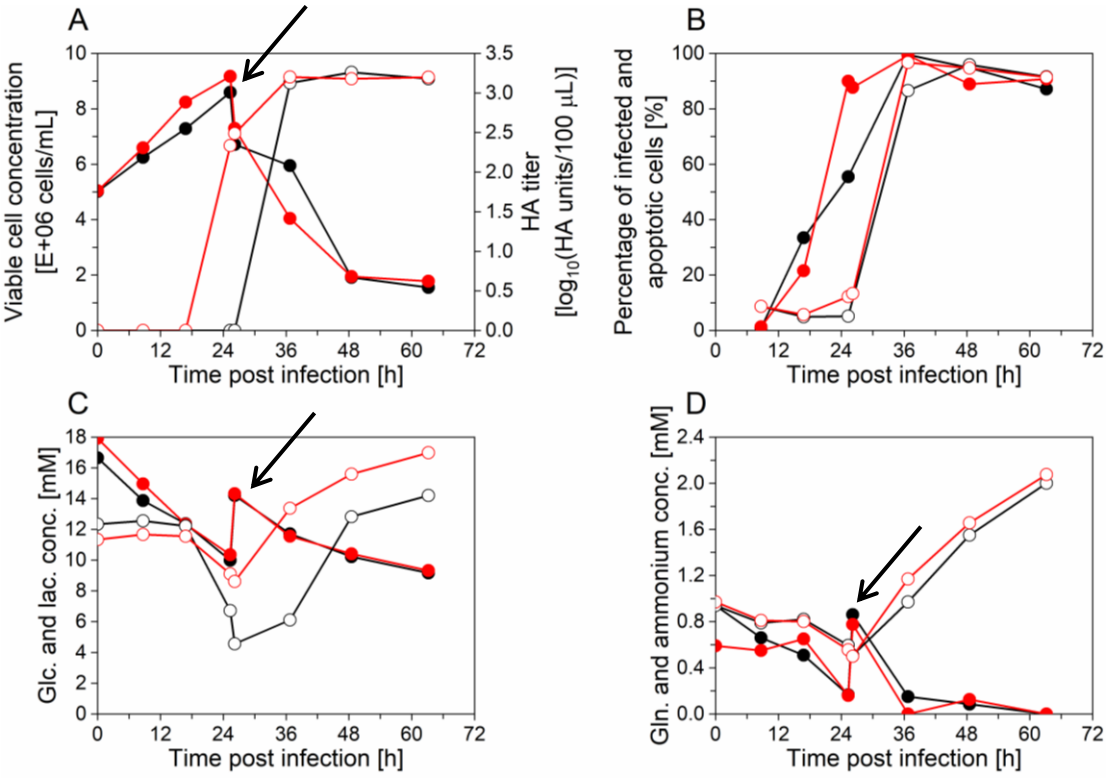

Figure 23: Influenza A/PR/8/34 virus production of run 1 (black) and run 2 (red) in bioreactors in batch mode using PBG.PK2.1 cell line growing in CD-U5 medium. Both cell cultures were from the same pre-culture. MOI of 10^{-5} with a trypsin activity of 10^{-6} U/cell were used at the time of infection. (A) Viable cell concentration (●), HA titer (○) – (B) percentage of infected cells (●), percentage of apoptotic cells (○) – (C) glucose (●) and lactate (○) concentrations – (D) glutamine (●) and ammonium (○) concentrations. Arrows indicate cell culture volume increase (from 550 to 710 mL) with fresh CD-U5 medium.

The maximum HA titer and CSVY value from the PBG.PK2.1 cell line was then compared to other cell lines (from data available in literature; Table 12). IAV produced in PBG.PK2.1 cells resulted in higher HA titers and CSVYs compared to adherent Vero cells, human or avian cells (Table 12). However, MDCK cells still outperform the porcine cells in terms of CSVY (40000 virions/cell) and maximum titer (3.9 $\log_{10}$(HA units/100 µL)) (Table 12). Nevertheless, very high infectious virus titers (4.4 x 10^8 $TCID_{50}$/mL) were obtained with PBG.PK2.1 cells.

Table 12: Comparison of maximum HA titer and cell-specific virus yields for different cell lines and bioprocess modes, either in shake flask or in stirred-tank bioreactors for batch processes, or in bioreactors for perfusion processes.

Cell line	Batch process		Perfusion process			Ref.
	Max. HA titer [log_{10}(HAU/100 µL)]	CSVY [virions/cell]	Max. HA titer [log_{10}(HAU/100 µL]	CSVY [virions/cell]	Cell conc. at TOI [10^6 cells/mL]	
Vero, adh.	2.6	4976	n.d.	n.d.	n.d.	[50]
MDCK, adh.	3.0	33255	3.9[a]	19000	16	[50, 144]
DuckCelt–T17, sus.	1.8	n.d.	n.d.	n.d.	n.d.	[46]
AGE1.CR, sus.	2.5	1292	3.5	1266	48	[103]
CAP, sus.	2.9	3883	3.7	4086	27	[103]
PER.C6, sus.	3.0	n.d.	n.d.	n.d.	n.d.	[172]
HEK293, sus.	3.0	4683	3.3[b]	3960	6	[103, 107, 171]
MDCK, sus.	3.9	40000	n.d.	n.d.	n.d.	[47]
PBG.PK2.1, sus.	3.2 -3.4	4466-5648	3.9 - 4.0	3053 - 4805	40 - 49	Pres. work

HA, hemagglutinin; U, units; CSVY, cell-specific virus yield; Max., maximum; conc., concentration; TOI, time of infection; adh., adherent; sus., suspension; n.d., not determined; Ref., reference; Pres., presented

[a] cell culture time = 72 h was taken as harvest point

[b] cell culture time =168 h was taken as harvest point

4.2.4 Process intensification

To further intensify influenza virus production, two cultivations were performed in perfusion mode using an ATF2 system and cells were infected at a concentration of around 46 x 10^6 cells/mL. Cell viability exceeding 97% and consistent growth during the exponential growth phase were observed before infection (Figure 24A). Using a cell-specific glucose consumption rate taking into account VCC avoided glucose limitations for both runs (Figure 24C). Glutamine levels were close or equal to zero for both runs (Figure 24D), but were not considered critical for this cell line (see section 4.2.1). Correspondingly, low ammonium concentrations below 1.5 mM were observed during the cell growth phase before infection. While at least 13 amino acids have been reported to be essential for mammalian cell growth [173] no limitations were observed for 12 of them during the whole cultivation period (data not shown). However, tryptophan levels close or equal to 0 mM were measured during the cell growth phase.

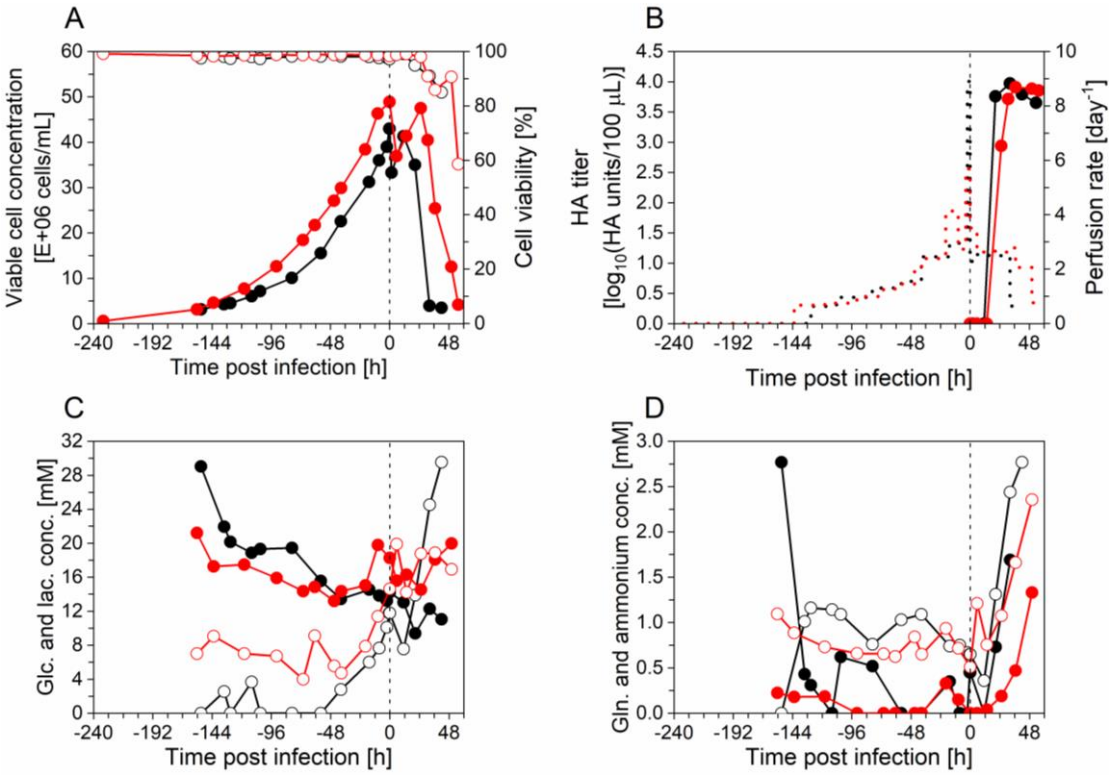

Figure 24: PBG.PK2.1 cell growth and influenza A/PR/8/34 virus production of run 1 (black) and run 2 (red) in bioreactor in perfusion mode. Cell cultures were from different pre-cultures. CD-U5 medium was used for the whole run. A DASGIP system coupled to an ATF2 system (0.2 µm membrane cut-off) was used for the perfusion runs. A trypsin activity of 22 U/mL in perfused medium and a MOI of 10^{-5} was applied at the time of infection. (A) Viable cell concentration (●), viability (○) – (B) HA titer (●), perfusion rate (dashed lines) – (C) glucose (●) and lactate (○) concentrations – (D) glutamine (●) and ammonium (○) concentrations. Dotted vertical lines correspond to the time of infection.

With higher VCCs, higher levels of non-quantified virus production inhibitors and limitation in other substrates can decrease the CSVY and titers [174, 175]. To avoid such limitations, fresh cell culture medium was added continuously by increasing the perfusion rate 3 h before infection. This resulted in an increase in the V_w by 30% after virus infection. Overall, a maximum titer of 3.93 $\log_{10}$(HA units/100 µL) (Figure 24B) was achieved in the bioreactor for both runs at 36 hpi. A CSVY of 3929 virions/cell was obtained in perfusion (Table 11), corresponding to a decrease of 30% compared to optimal virus infection conditions in batch mode (SF). Concerning the infectious virus titer, high titer of 3.2×10^9 $TCID_{50}$/mL were obtained in the perfusion cultures (Table 11).

The P_v in perfusion mode was equal to $1.9 \pm 0.3 \times 10^9$ virions/L/day, which was around three times lower compared to the batch processes performed at the same scale (Table 11).

4.2.5 Influenza A/PR/8/34 hemagglutinin glycosylation

Glycosylation of recombinant proteins (i.e. mAbs) is a critical quality attribute. For cell culture-based viral vaccines, yet no glyco-analysis of antigens is required by the authorities [176, 177]. Considering the use of different host cells for vaccine production with their significant impact on glycosylation it seems natural to equally consider this point. Different studies have shown the importance of IAV glycosylation in terms of immunogenicity [178, 179]. For the analysis of the multiple potential glycosylation sites located on HA and NA, state-of-the-art mass spectrometry-based site-specific glycopeptide analysis was necessary.

An overview on the data obtained for the site-specific glycopeptide analysis of IAV antigen HA propagated in the porcine cell line is given in Table 13. Surprisingly, exclusively high-mannose-type (Man) *N*-glycans were identified on the HA1 *N*-glycosylation sites N285 (Man7 and Man8) and N303 (Man8). Two potential *N*-glycosylation sites (N27/28 and N40) were found to be not glycosylated. *N*-glycosylation site N497, located at the HA2 domain, was also identified to carry high-mannose type *N*-glycans (Man6 and Man8), together with a potential hybrid-type *N*-glycan Hex7HexNAc3 (Hexose (Hex), *N*-acetylhexosamine (HexNAc)). All fragment ion spectra of the detected *N*-glycopeptides are shown in the Appendix. In contrast to the HA antigen, no glycopeptides were detected for NA. Furthermore, no *O*-glycopeptides of HA or NA were identified (Appendix, section 10.3).

Table 13: Overview on the site-specific glycopeptide analysis of the influenza A virus glycoprotein hemagglutinin produced in PBG.PK2.1 cells.

Site	Sequence	*N*-glycan composition	Enzyme protease [a)]	Fragment ion spectrum
N285	GFGSGIITS**N**	Man7	Trypsin + Flavastacin	Figure A.1
		Man8	Trypsin + Flavastacin	Figure A.2
N303	CQTPLGAI**N**	Man8	Trypsin + Flavastacin	Figure A.3
N497	**N**GTYDYPK	Man6	Trypsin	Figure A.4
		Man8	Trypsin	Figure A.5
		Hybrid Hex7HexNAc3	Trypsin	Figure A.6

ManX, high-mannose type *N*-glycan (X = number of mannoses); Hybrid, hybrid-type *N*-glycan [Hexose (Hex), *N*-acteylhexosamine (HexNAc)]. Red indicates the glycosylated asparagine.

[a)] Enzyme protease is used to hydrolyze peptide and generate suitable N-glycopeptides that can be detected and analyzed by mass spectrometry. Trypsin specifically cleaves peptide bonds when the carbonyl is followed by arginine or lysine, except if proline is on the carboxyl side or C-terminal of the residue. Flavastacin has a cleavage specificity towards the C-terminus of N-glycosylated asparagine residues.

4.2.6 Process-related impurities

Specifications for inactivated cell culture-derived whole-virion influenza vaccines are set by the European Pharmacopoeia Commission in terms of antigen content, protein levels, impurities such as DNA and endotoxins, residual infectivity, and others [63]. In order to determine the potential burden regarding DSP of the virus harvest produced, the impurities that are the most challenging in subsequent virus purification were measured: total protein and host cell DNA. According to the current European Pharmacopoeia Commission, cell culture-based influenza vaccines should have 15 µg of HA antigen per strain, < 10 ng DNA and the protein content should be < 6 × HA antigen content and < 100 µg per strain (final product).

HA contents up to 6.4 µg/mL and 21.9 µg/mL were obtained from bioreactor cultivations in batch and in perfusion mode, respectively. (Figure 25A). Following total protein (Figure 25B) and DNA (Figure 25C) levels over time, the best time of harvest (highest ratio of HA antigen per content of DNA (µg HA/ng DNA) and total protein (µg HA/µg total protein)) was determined to be 48 hpi for batch mode and 36 hpi for perfusion mode. At these time points, around 18500 ng dsDNA and up to 600 µg total protein were measured per HA dose for both modes (Table 11).

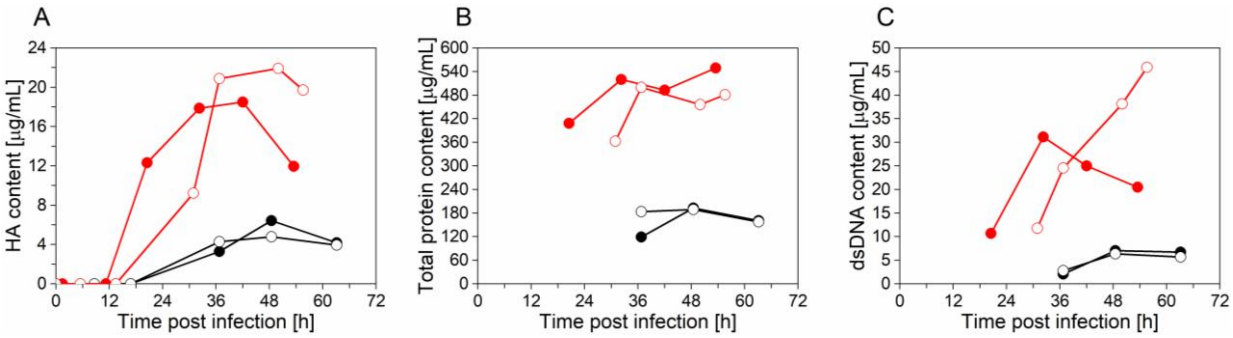

Figure 25: Influenza A/PR/8/34 virus production parameters, using the PBG.PK2.1 cell line, in batch mode for run 1 (●) and run 2 (○) and in perfusion mode for run 1 (●) and run 2 (○) to be considered for further downstream processing. (A) HA antigen content determined by SRID assay. (B) Total protein concentration in the cell culture broth determined by Bradford assay. (C) Host cell dsDNA concentration in the cell culture broth determined by PicoGreen assay.

4.3 Discussion

4.3.1 Growth and metabolism

When comparing lowest doubling time in batch mode with MDCK suspension cells (36 h [180]), HEK293 suspension cells (33 h [107]) and AGE1.CR cells (25 h [103]), PBG.PK2.1 cell line had a value of 38 ± 11 h in CD-U5 medium, which is in the average. A short doubling time allows a shorter production time leading to increased P_V. As the CD-U5 medium was developed initially for AGE1.CR cell culture, the composition of the medium might be further improved specifically for PBG.PK2.1 cells to even further reduce the doubling time.

As described in section 4.2.1, aggregates of about five cells were observed when cultivated in bioreactors. Most likely, this was due to a too low agitation speed, as aggregates were previously described for poorly agitated cell cultures [181, 182]. Such aggregates have been reported to create heterogeneity and to increase shear stress, which could affect maximum VCC and doubling time [181]. If the cell line would be considered for such processes, certainly more time needs to be invested into optimizing cultivation conditions. For this first characterization and evaluation of this cell line however, this was not in the focus of this study.

Lactate and ammonium are well-known by-products of animal cell culture. Lactate concentrations above 20 mM and ammonium levels as low as 2–3 mM have been shown not only to have adverse effects on growth for many mammalian cell lines [183-185], but also on virus vaccine production [186]. However, these limits were not exceeded during the exponential cell growth phase (Figure 21B and Figure 21C). The observed low lactate levels might result from the ability of the PBG.PK2.1 cells to use lactate as a carbon source after glucose depletion (section 4.2.1). Cell growth has been observed after glutamine depletion, suggesting that the cells might be able to synthesize themselves the needed amount of this amino acid. As glutamine has been reported to be the main source of ammonium accumulation [186], media without or a low glutamine content could be considered for PBG.PK2.1 cells for recombinant protein and virus manufacturing. This is similar to the avian cell line AGE1.CR growing in a comparable chemically-defined medium (CD-U2) without glutamine [187].

4.3.2 Virus production

Virus adaptation to the new cell line over several passages did not lead to higher virus titers. However, maximum titers were reached 12 hpi earlier for later passages compared with the first passage. This was similar to other mammalian cell lines such as Vero [50] or HEK293 cells [171], where an earlier onset of virus release has also been observed during virus adaptation.

As described in section 4.2.2, PBG.PK2.1 cells were permissive for at least three different influenza virus strains. A cell line permissive to many influenza virus strains is an advantage as it increases its versatility. Moreover, the high titers achieved for porcine influenza A H1N2 (A/Bakum/1832/00) could be of interest for the porcine vaccine market. The same strain was tested before in CAP cells, but resulted in a lower titer of 3.0 $\log_{10}$(HA units/100 µL) [188].

When scaling-up the process from SFs to bioreactors, a similar CSVY of 5006 virions/cell was observed in bioreactors, compared to the optimized process in SFs (Table 11), suggesting that this process is scalable to higher bioreactor volumes. As reported in section 4.2.3, the virus efficiently infected all cells of the cultures with current infection parameters. Eventually, trypsin addition could be reduced to a single addition at the TOI with an activity higher than 10^{-6} U/cell.

While comparing HA titers from different research groups is difficult, due to assay limitations and differences in cultivation platforms, it seems that the use of PBG.PK2.1 cells can result in higher influenza virus titers compared to, for example, PER.C6 or HEK293 cells (Table 12). Furthermore, as also reported in literature, the production of influenza B virus strains can result in lower titers compared to high-producer IAV strains [46, 188]. Nevertheless, more influenza virus strains from different animal origin should be tested in PBG.PK2.1 cells, to fully evaluate its permissiveness. It is important to mention the high $TCID_{50}$ titer obtained with the porcine cell line in batch mode (Table 11), which is of high interest regarding the production of life-attenuated influenza vaccines. This was also true for $TCID_{50}$ values reported for other high-producer cell lines such as HEK293 [107] or AGE1.CR [103] cells.

Regarding virus production in perfusion mode, the fact that similar doubling times were obtained as for batch cultivations in bioreactors (Table 10) suggests that cell growth was not impaired by the ATF system (and the high VCCs). The low levels of tryptophan reported in section 4.2.4 probably did not have an impact on the cell culture as a very low tryptophan

concentration of 0.05 mM is often recommended for mammalian cell culture [173]. In addition, the limit of quantification of the HPLC method used here was 0.25 mM.

Virus accumulation was observed when producing the virus with the ATF membrane. As previously reported [103, 110], the virus particles generally accumulate in the bioreactor when an ATF system is used for cell retention even with membrane pore sizes as large as 0.5 µm. Unspecific virus binding to the membrane and membrane fouling due to cell debris and DNA accumulation could explain this effect.

With the continuous supply of fresh medium, no limitation in glucose, and ammonium as well as lactate below critical values during the virus production phase were observed for perfusion cultures. Therefore, the reduction in CSVY when cultivating the cells in perfusion mode could be due to the presence of other, non-quantified inhibitors of virus production. Nevertheless, results are still very promising for HCD influenza virus production compared to other HCD processes using STRs coupled to an ATF system, using either CAP cells [103] (CSVY = 1883 virions/cell) or AGE1.CR cells [90] (CSVY = 1266 virions/cell) at concentrations above 30 x 10^6 cells/mL. A similar CSVY (3960 virions/cell) was also reported for influenza production in perfusion mode using HEK cells: however, the cell culture was infected at lower cell densities (6 x 10^6 cells/mL) [107]. The obtained titers have the potential to be further increased through a DoE approach. The maximum HA titer could for example be increased with medium optimization (based on a detailed metabolic characterization) [187, 189] as the CD-U5 medium was first designed for avian cell culture.

Similar to recombinant protein production in perfusion mode, one strategy to increase economic competitiveness and the P_v of perfusion processes is to reduce their perfusion rates. An iterative stepwise decrease of the perfusion rate as a medium development strategy has been shown to efficiently increase productivity for mammalian cell culture using an ATF system [190]. However, such a strategy should not compromise CSVY and cell growth by potentially increasing the concentration of inhibiting components in the cell culture medium. Another way to decrease the amount of spent medium is the better control of the perfusion rate. Manual adjustments of the perfusion rate did not always fit cell growth and led to temporary overfeeding during the cell growth phase (Figure 24B). For example in Figure 24C, the glucose concentration clearly exceeded 6 mM (section 3.6). One way to control the perfusion rate is to use an on-line capacitance probe for determination of VCC taking into

account cell-specific medium demand [91]. Another solution to reach higher productivity could be continuous harvesting avoiding virus degradation. The ATF system only partially allows continuous harvesting and virus accumulation as well as virus deactivating components inside of the bioreactor. An alternative might be the use of an AS, which has already been shown for influenza virus production in perfusion mode using HEK293 cells for concentrations up to 18 x 10^6 cells/mL [107].

4.3.3 Process-related impurities and glycosylation of HA

It is believed that the glycosylation has an influence on the vaccine efficacy, which is why site-specific glycopeptide analysis of IAV antigen HA propagated in the new porcine cell line (described on section 4.2.5) was performed. Although glycosylation sites located at the head region of HA have been shown to influence virulence, studies suggest there is no clear specific glycosylation site which has a crucial effect on immunogenicity as HA glycosylation can modulate humoral responses focused on different HA regions [191].

Compared to the glycosylation pattern of HA expressed in other host cell systems (i.e., chicken eggs, MDCK or Vero cells), IAV propagated in PBG.PK2.1 cells seems not to have complex-type *N*-glycosylations [153, 154, 192-194]. The high mannose glycosylation pattern identified resembles more the glycosylation of recombinant HA produced in *Spodoptera frugiperda* 9 (Sf9) cells [191, 194]. It is an unexpected finding as porcine cells are normally distinguished by highly complex *N*- and *O*- linked glycans. This finding could indicate different properties in terms of virulence and immunogenicity that need to be further elucidated by performing glycoimmunological experiments including animal trials.

Regarding the process-related impurities, for batch or perfusion mode, similar DNA and protein contents in influenza virus harvests have been reported in the past and were tackled by different purification techniques, most recently by single-use SXC [82] and pseudo affinity chromatography with sulfated cellulose membrane adsorbers [195]. Overall, this indicates that perfusion processes with their higher productivity do not necessarily put an additional burden to subsequent DSP compared to batch modes. It is evident that analysis of additional parameters (such as the viscosity of virus harvests and virion size distributions) and a proper assessment on purification performance are needed, but were out of scope here.

4.3.4 Suitability of the PBG.PK2.1 cell line for vaccine manufacturing

In summary, an ideal host cell line for influenza vaccine production should display: Robust growth in suspension with high viability, easy scale-up, fast virus production to high titers, permissivity to many influenza virus strains, suitability for cGMP manufacturing and low total protein and DNA concentrations in virus harvest broths to facilitate purification [44]. The produced influenza viruses should be highly effective as a vaccine. Insights about the vaccine efficacy could be given by analyzing the glycosylation of the HA.

PBG.PK2.1 cells showed average cell growth with high viability. A maximum cell density of 10^7 cells/mL was reached in bioreactor (batch mode). Scaling-up from SF to bioreactor scale was shown to be efficient, as similar t_d values and substrate consumption rates were observed. High virus titers were obtained in less than 48 hpi. Similar or higher CSVYs were obtained in batch mode, compared to other processes using suspension cells such as CAP, PER.C6 or HEK293 cells. However, CSVY (5375 virions/cell) was found to be lower compared to the highest CSVY reported in literature (up to 40000 virions/cell in MDCK cells [47]). PBG.PK2.1 cells showed to be a good candidate for cell culture in perfusion mode, since cell growth to high VCCs maintaining high viability was achieved. Most importantly, CSVY was maintained high, which allowed reaching HA titers of 3.93 $\log_{10}$(HAU/100 µL). Such a titer using a suspension cell line at bioreactor scale is, to the knowledge of the author, among the highest reported in literature. Furthermore, high infectious virus titers were obtained in batch (4.4×10^8 $TCID_{50}$/mL) and in perfusion mode (3.2×10^9 $TCID_{50}$/mL), which could be of interest for life-attenuated influenza virus production. PBG.PK2.1 cells have shown to be permissive for at least three influenza virus strains. Regular process-related impurities levels were observed, which are reported to be handled successfully in chromatography-based purification regimes including SXC [82].

Exclusively high-mannose-type *N*-glycans were detected on different HA sites, which is very different compared to the HA glycan structure found for IAV strains produced in MDCK or Vero cells. Whether this is related to differences in immunogenicity and/or virulence should be further investigated in follow-up studies.

Taking into account the high maximum VCCs obtained in batch mode, the cell growth in a chemically-defined medium, the suitability of the cell line for scale-up and process

intensification, and the obtained high influenza virus titers, the PBG.PK2.1 cell line is a promising candidate for next-generation influenza vaccine manufacturing.

However, although the cell line uses cGMP validated cell culture medium, the cell bank is not ideal for cGMP application. And at the present time, this cell line is not approved for cGMP manufacturing. The German Central Committee on Biological Safety (*Zentrale Kommision für die Biologische Sicherheit*; ZKBS) has recently re-evaluated and re-classified in 2018 the PBG.PK2.1 cell line from safety level 1 to safety level 2 [196] as mentioned in section 3.1.1. PBG.PK2.1 contains in its genome 62 copies encoding for porcine endogenous retrovirus (PERV). However, those produced particles were considered to be defective and non-infectious, leading on a first time to safety level 1 classification. Still, it was recently observed through PCR that the subtypes PERV-A and PERV-B (from a PBG.PK2.1 cell culture) are still able to infect and to be reproduced in human cells, which can be potentially dangerous [196]. In the conducted study, PBG.PK2.1 is used for inactive influenza virus production, so PERV particles would be also inactivated. However, for the manufacturing of IAV, the seed train would need to be performed in a safety level 2 production plant, which increases the complexity and costs. For a typical cell culture-based influenza virus manufacturing process, only the virus production phase should be under safety level 2. For this reason, the PBG.PK2.1 cell line could be considered as less attractive for human vaccine production, compared to AGE1.CR.pIX or MDCK cells.

However, the PBG.PK2.1 cell line might be still of very high interest for veterinary use as regulations are less stringent, and as a porcine cell line growing in suspension is not available on the market. This cell line has shown to produce a high porcine influenza virus titer (3.37 $\log_{10}$(HA units/100 µL)). The rest of the thesis will use only AGE1.CR.pIX cell line which is a cell line commercially available and used for human vaccine production (cGMP conform).

4.4 Author contributions

All the experiments were performed by Gwendal Gränicher, except for the glyco-analysis, performed by Alexander Pralow. Juliana Coronel helped to perform cell culture runs. The data from glyco-analysis were analyzed by Gwendal Gränicher and Alexander Pralow. The data from the DSP were analyzed by Gwendal Gränicher and Pavel Marichal-Gallardo. The chapter

was reviewed by the co-authors of the paper: *Efficient influenza A virus production in high cell density using the novel porcine suspension cell line PBG.PK2.1* [115].

Chapter 5

Performance of an acoustic settler versus a hollow fiber-based ATF technology for influenza A virus production in perfusion mode

---

This chapter was based on the following publication:

Gränicher, G., Coronel, J., Trampler, F., Jordan, I., *et al.*, Performance of an acoustic settler versus a hollow fiber-based ATF technology for influenza virus production in perfusion. *Appl Microbiol Biotechnol*, 2020.

5.1 Introduction

As described in the theoretical background (chapter 2), perfusion processes allow to intensify production and to quickly produce high amounts of vaccines in case of a pandemics (section 2.6). Different perfusion systems are available: membrane-based or non-membrane-based. The following is needed for an ideal cell retention technology: i) A cell retention device should be robust, ii) have a high cell retention efficiency while not damaging cells, iii) allow high-yield production, iv) be scalable to a perfusion flow rate of at least 1000 L/day, v) enable low running costs, vi) be commercially available (eventually in single-use) and, vii) depending on process requirements allow continuous harvesting.

Membrane-based ATF is to date the most commonly used cell retention technology for recombinant protein production such as mAbs [98]. For virus production, however, membrane surface properties and virus properties such as: i) enveloped/non-enveloped, ii) lytic/non-lytic, iii) intracellular/extracellular virus production, iv) virus particle size, v) half-life of infectious virions have to be considered. Therefore, the most suitable cell retention technology cannot be directly derived from the previous work with recombinant proteins.

Due to the lytic nature of many viruses and the large size of virus particles, the use of membrane-based perfusion systems for cell retention has been shown to be challenging. Membrane clogging [162] as well as unwanted virus accumulation inside the bioreactor [90, 91, 103, 110] have been reported.

Continuous harvesting of recombinant proteins has been shown to improve cell-specific productivity and product quality due to a shorter residence time inside the bioreactor [112]. Additionally, total process time could be further reduced if perfusion cultures were integrated with continuous DSP, potentially resulting in substantial financial benefits [98, 100]. The same benefits of continuous harvesting for recombinant protein followed by continuous DSP could be also beneficial for virus production.

Non-membrane-based cell retention devices such as the AS and the IS could potentially allow continuous virus harvesting. Promising results were obtained with an AS for production of IAV using HEK293 cells with maximum VCCs up to 18×10^6 cells/mL [107]. Overall, not many studies are available on perfusion to produce viruses and those that are available describe one virus system and process for one retention device (section 2.6). A direct comparison of a

membrane-based cell retention device with a non-membrane-based cell retention device with the same biological system: virus, cell line, medium and bioreactor has not been looked at so far.

The comparison performed here, focused on having as many as possible similarities (such as process parameters and infection conditions) between an AS and an ATF system using an AGE1.CR.pIX avian suspension cell line for IAV production in perfusion mode. This allowed to compare directly the performance of the retention devices. For this, overall process performance, virus titers, CSVY, scalability, impurity levels for further DSP were considered. To better assess the performance of a process, USP and DSP aspects should be considered together [197, 198]. Furthermore, product attributes, such as infectivity and virus aggregation, were also looked at.

The setup of the AS was specifically optimized for virus production and required evaluation of the cell recirculation strategy and selection of an appropriate flow rate inside the acoustic chamber (called recirculation flow rate). Two cell recirculation strategies were tested, which are: Pump-based recirculation and valve-based recirculation (sections 2.6.2 and 3.6.2). In contrast to traditional recombinant protein production [126, 199], the optimization of the acoustic recirculation strategy was shown to be crucial to increase influenza virus yields. The choice of a recirculation strategy and the recirculation flow rate have an impact on the temperature elevation inside of the acoustic chamber, the cell shear stress, eventual oxygen limitation of the cells inside the acoustic chamber and virus degradation.

5.2 Results

In order to assess the impact of the cell retention device and the recirculation strategy on the influenza virus production, perfusion cell cultures using similar infection conditions, but with different recirculation strategies and recirculation flow rates were carried out.

First, the cell growth before the infection phase was evaluated. Then the virus production performance in function of the perfusion parameters were evaluated (Table 14). Based on Table 14, linear regressions were generated for runs AS1-AS8 between different AS process parameters (such as temperature in the acoustic chamber, recirculation flow rate) and the total amount of virions produced to identify eventual correlations (the total amount of virions produced per run; Figure A.7–A.12). Analytics included VCCs, virus titers, retention efficiencies, harvest volumes, impurity levels, and the size distribution of large-sized virus and other aggregates from raw material harvested in the bioreactor cell culture supernatant.

Table 14: Process conditions, cell retention efficiency and product yields for influenza A/PR/8/34 virus using AGE1.CR.pIX cells in perfusion mode coupled with either an acoustic settler (different operation modes) or an ATF system.

	ATF		Acoustic settler							
Run	IAV_ATF1	IAV_ATF2 [a]	IAV_AS1	IAV_AS2	IAV_AS3	IAV_AS4	IAV_AS5	IAV_AS6	IAV_AS7	IAV_AS8
Bioreactor working volume [mL] [b]	750 [c]	800	600	670	600	600	680	600	1380	670
Recirculation strategy	-	-	Valve	Valve	Pump	Pump	Pump	Pump	Pump	Pump
Recirculation rate [day^{-1}] [b]	-	-	4.1	3.4	3.7	5.0	7.9	5.0	3.8	4.9
Recirculation flow rate [mL/day]	-	-	2460	2278	2220	3000	5372	3000	5244	3283
Max. back-flushing flow rate [mL/min]	-	-	53.4	11.2	2.8	3.2	4.8	3.0	5.5	3.6
Shear rate γ [s^{-1}]	2451	3395	336	70	17	20	30	19	34	23
Net perfusion rate [day^{-1}] [b]	2.1	-	1.8	2.0	2.1	1.9	1.9	1.5	1.5	2.1
Net perfusion flow rate [mL/day]	-	-	1080	1340	1260	1140	1292	900	2070	1407
Ratio Recirculation rate / perfusion rate [-]	-	-	2.28	1.70	1.76	2.63	4.16	3.33	2.53	2.33
τ in acoustic wave field [min] [b]	-	-	14	11	9	13	11	16	7	10
T range inlet line [°C] [d]	-	-	31–37	32–38	31–34	32–35	31–35	33–36	30–33	31–35 [e]
T range outlet line [°C] [d]	-	-	38–40	37–40	39–40	40–41	39–40	42–43	37–38	39–40 [e]
VCC at TOI [10^6 cells/mL]	25.4	23.8	24.8	24.7	26.7	25.0	25.1	24.8	26.8	49.3
Max. VCC p.i. [10^6 cells/mL]	37.7	23.8	35.1	30.3	36.7	34.6	32.5	27.2	32.6	69.4
Viable cell retention efficiency p.i. [%]	100.0	100.0	98.9	98.7	96.7	91.6	86.6	91.6	86.4	94.4
Dead cell retention efficiency p.i. [%]	100.0	100.0	97.7	98.6	96.1	83.2	88.8	92.5	81.0	84.3
Total number of virions produced [10^{13} virions] [f]	1.89	0.52	1.47	1.01	2.69 *	3.09 *	1.48	2.06	3.61 *	7.51 *
CSVY [virions/cell]	723	340	643	520	1124 *	1371 *	704	1163	1701 *	1665 *
P_v [10^{11} virions/L/day] [g]	5.49	1.81	5.38	2.79	7.11	9.28 *	3.59	6.98 [h]	16.49 [h]*	13.90 *

ATF, alternating tangential flow; IAV, influenza A virus; AS, acoustic settler; Valve, valve-based recirculation mode; Pump, pump-based recirculation mode; Max., maximum; τ, mean residence time; T, temperature; VCC, viable cell concentration; TOI, time of infection; p.i., post infection; *, higher value compared to control ATF1, with a difference higher than the error of the assay (sections 3.8.1 and 3.13.3); CSVY, cell-specific virus yield; P_v, volumetric virus productivity.

[a] From previous study [90];

[b] Constant for the virus production phase;

[c] The bioreactor was sampled once with a 50 mL sampling volume p.i. The working volume was then corrected to avoid a dilution with fresh medium, and started with 800 mL to 750 mL.

[d] Determined in a separate experiment as described in section 3.6.2;

[e] Determined from AS5 conditions (similar perfusion rate);

[f] Total number of produced virions, normalized to a bioreactor working volume of 650 mL;

[g] Process time (from calculated P_v) is from a starting VCC of 1.2 x 10^6 cells/mL until time point of maximum HA titer reached.

[h] Volumetric virus productivity calculated with a perfusion rate (1.5 day^{-1}) lower than for the control ATF1 (2.1 day^{-1}) resulted in an overestimation of the P_v value.

5.2.1 Cell growth behavior

Efficient perfusion cultures using AGE1.CR.pIX cells, which are characterized by short doubling times (t_d), high viabilities and high VCCs (up to 50 x 10^6 cells/mL), were described previously for cultivations with bioreactors coupled to an ATF device [90, 103, 110, 114]. Before evaluating virus yields and productivity, the growth performance of AGE1.CR.pIX cells was assessed for VCCs between 25 and 55 x 10^6 cells/mL using an AS.

A cell viability above 98% for VCCs between 10 and 55 x 10^6 cells/mL was obtained using the AS in either pump- or valve-based recirculation mode (Figure 26A). Small variations of t_d were observed for the different perfusion setups (Figure 26B), but differences were statistically not significant (t-test). All AS runs showed cell retention efficiencies before infection above 98% (data not shown).

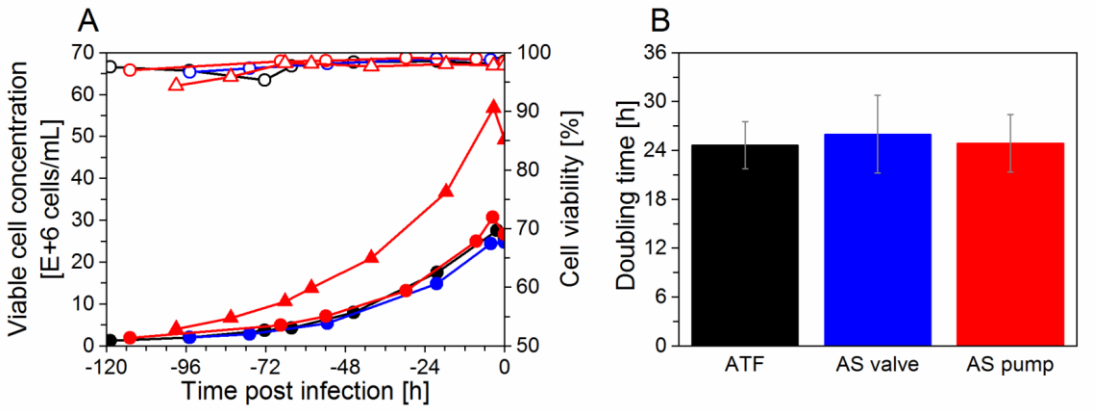

Figure 26: Growth of AGE1.CR.pIX cells cultivated in a 1 L STR in perfusion mode using different cell retention technologies and recirculation strategies. (A) Viable cell concentration (filled symbols) and cell viability (empty symbols) of one representative ATF run (ATF1) (●), one representative run for the acoustic settler with valve-based recirculation (AS2) (●) and two representative runs for the acoustic settler with pump-based recirculation (AS3 (●), and AS8 (▲)). (B) Cell population doubling time (t_d) calculated during the cell growth phase in perfusion mode (average between each sampling time point for each run ± standard deviation; section 3.13.1). The values correspond to ATF1 for ATF (black), AS1 and AS2 for the acoustic settler with valve-based recirculation (blue) and AS3-AS8 for the acoustic settler with pump-based recirculation (red). A CSPR of 60 pL/cell/day was applied for every perfusion run. Detailed operation conditions in Table 14.

5.2.2 Process performance

Two recirculation strategies and various recirculation rates were tested for AS operation. Following the cell growth phase, the cells were infected with influenza virus at a VCC of at least 25 x 10^6 cells/mL. Different product yields were obtained for the cultivations, namely CSVY and P_v (Table 14). For all runs (except run ATF2 from a previous study), the same MOI,

trypsin activity, perfusion rate and VCC at TOI were used. AS8 differed as a higher VCC at TOI was tested. The main differences were therefore related to the recirculation strategy and recirculation rate of the AS.

CSVYs and P_vs over 1124 virions/cell and 7.11 x 10^{11} virions/L/day were obtained, respectively, for cultivations using an AS with a pump-based recirculation rate between 3.7 and 5.0 day^{-1} (AS3, AS4, and AS7). Under these conditions, higher yields (about 1.5-fold higher) were obtained with the AS compared to the ATF system (ATF1; CSVY = 723 virions/cell, P_v = 5.49 x 10^{11} virions/L/day). For higher pump-based recirculation rates (7.9 day^{-1}, AS5), a lower CSVY (704 virions/cell) and a lower P_v (3.59 x 10^{11} virions/L/day) were observed, compared to the aforementioned cultivations with lower recirculation rates. In addition, AS perfusion runs using the valve-based recirculation mode (AS1 and AS2) resulted in lower yields compared to AS3 using a similar recirculation rate (but in pump-based recirculation mode). The valve-based recirculation strategy achieved the highest cell retention efficiency (over 98%, AS1 and AS2) whereas a slightly reduced cell retention efficiency after infection was observed with increased pump-based recirculation rate (from 3.7 to 7.9 day^{-1}). Virus accumulation inside of the bioreactor was observed for the ATF run as only 7.5% of Vir_{tot} was harvested through the membrane. For all AS runs, no virus accumulation was observed.

Based on the perfusion parameters of AS3 and AS4, a VCC of 49.3 x 10^6 cells/mL (at TOI) was achieved in virus production (AS8, Table 14). The CSVY of AS8 was not decreased compared to other runs using the same recirculation mode and same perfusion rate but infected at lower VCCs (AS3 and AS4). A P_v increase of 2.5 was obtained when comparing AS8 to the ATF1 run.

Following a correlation study between the AS process parameters and Vir_{tot}, the process parameter having the largest impact was found to be the temperature elevation at the lower part of the acoustic chamber (Figure A.7–A.12). The temperature at the chamber inlet was equal to 31–38°C for the valve-based strategy, which was the highest temperature variation compared to the other AS runs with pump-based recirculation, presenting as well the lowest Vir_{tot} (for AS1 and AS2). The AS parameter influencing mostly the temperature in the AS was found to be the perfusion flow rate (Figure A.13–A.14).

The virus production phase was evaluated as before by VCC and cell viability. In addition, as an indicator for cell metabolism and cell stress, lactate release and $Y_{lac/glc}$ yield of perfusion ATF1 and AS1–6 (Table 14) were monitored.

Similar viable cell growth and cell viability profiles were observed for runs ATF1 and AS1–AS5 (Figure 27A-B). In all cultivations, a VCC of at least 30 x 10^6 cells/mL was reached and cell viability was maintained above 95% during the first 24 hpi. A higher $Y_{lac/glc}$ and lactate concentration was observed with perfusion in a pump-based recirculation mode (AS3-5) compared to the AS1 and AS2 using a valve-based recirculation mode (Figure 27C-D) during at least the first 24 hpi. During the first 36 hpi, the ATF1 run showed similar $Y_{lac/glc}$ yields and lactate concentration compared to the runs with pump-based recirculation (using the AS).

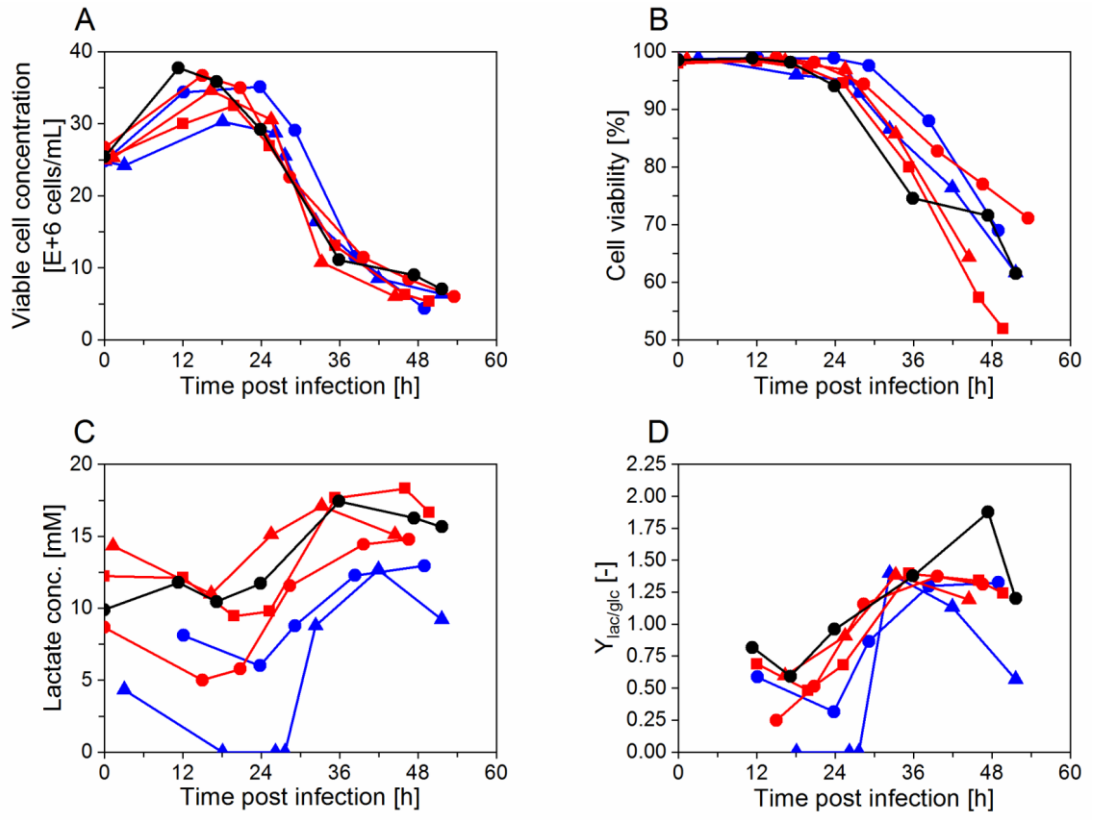

Figure 27: Influence of acoustic settler operation on viable cell concentration, viability and lactate metabolism during the influenza A/PR/8/34 virus production phase with AGE1.CR.pIX cells. (A) Viable cell concentration (B) cell viability (C) lactate concentration in the bioreactor supernatant. (D) $Y_{lac/glc}$ yield. ATF1 (●): performed with the ATF system. AS1 (●) and AS2 (▲): performed with the valve-based recirculation mode of the acoustic settler. AS3 (●), AS4 (▲) and AS5 (■): performed with the pump-based recirculation mode of the acoustic settler. Detailed operation conditions in Table 14.

5.2.3 Process-related impurities

As previously mentioned in sections 3.6 and 5.2.2, the choice of the cell retention device is expected to have an impact on influenza virus production in perfusion mode. While the AS allows continuous harvesting, the membrane-based cell retention technology tends to lead to accumulation of the virus inside the bioreactor. To assess which cell retention device would

facilitate DSP, the two main process-related impurities, namely host cell dsDNA and total protein concentrations were measured during the virus production phase.

In the bioreactor, higher host cell dsDNA and total protein concentrations were measured in comparison to the permeate for the ATF system (Figure 28A). In addition, a decline in the total number of accumulated virions was observed at 36 hpi (Figure 28B). In contrast, a higher accumulation of total protein and a higher total number of produced virions were observed for the cultivation using an AS (Figure 28B). Finally, host cell dsDNA as well as the total protein impurity levels per virion were similar at the respective optimum time of harvest (Figure 28C).

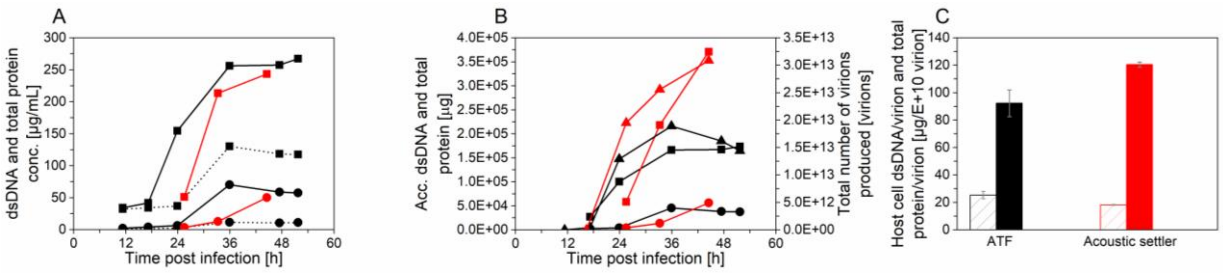

Figure 28: Host cell dsDNA and total protein impurity levels in the cell culture broth during influenza A/PR/8/34 virus production phase in AGE1.CR.pIX cells in perfusion mode using an ATF system (ATF1, black) or an acoustic settler with pump-based recirculation (one representative optimized run, AS4, red). (A) Host cell dsDNA concentration (●) and total protein concentration (■). Dashed lines represent additional data from the ATF permeate line. (B) Accumulated dsDNA (●), accumulated total protein (■) and total number of virions produced over time (▲). (C) Host cell dsDNA per virion (striped columns) and total protein per virion (filled columns) at optimum harvest time point (average ± standard deviation of technical duplicates). For the ATF cultivation, the bioreactor content was harvested at 36 hpi. When using the acoustic settler, virions from the bioreactor were also collected at the optimum harvest time point which corresponded to 45 hpi. For graph B, values were normalized to a working volume of 650 mL. Detailed operation conditions in Table 14.

5.2.4 Impact of the cell retention device on infectious virus titers and virus aggregation

Infectious titers and the extent of aggregation of virus particles can be important product quality attributes in the design of a vaccine production process. Infectivity is of particular interest in case of live-attenuated influenza vaccine manufacturing. Virus aggregation also influences infectivity and, even more important, may negatively affect virus recovery in subsequent purification.

A similar total number of infectious virions (sum of virions in the vessel and in the harvest) were obtained for both the ATF system and the AS (Figure 29A, difference within the error range of the $TCID_{50}$ assay). For both cell retention devices, the number of infectious virions decreased after maximum values were reached. Over time an increase in aggregation of

viruses and other large molecules was observed between 24 and 48 hpi, for both systems in either the bioreactor (ATF1, Figure 29B) or the harvest collected via continuous harvesting (AS4, Figure 29C). When using the AS, a higher amount of small debris (under 0.08 µm) and a lower amount of large-size debris (above 0.60 µm) were observed between 24 and 48 hpi compared to operation with the ATF system (Figure 29B-C).

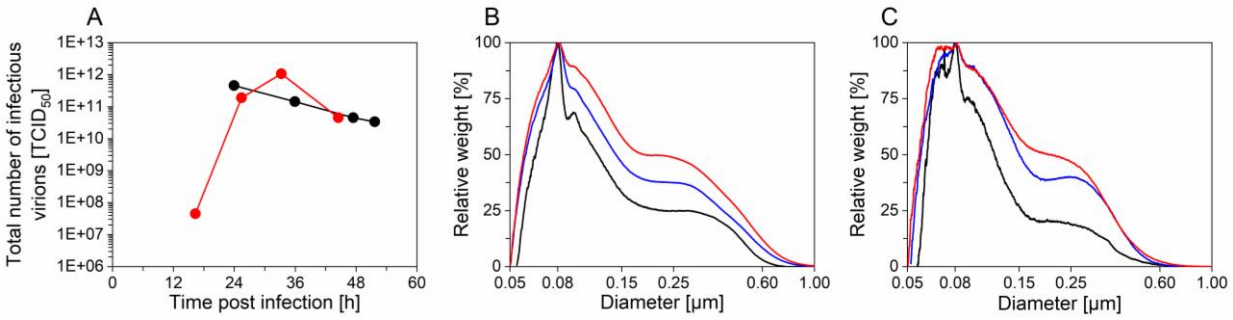

Figure 29: Infectious titer of influenza A/PR/8/34 virus and size distributions during influenza A/PR/8/34 virus production phase in AGE1.CR.pIX cells in perfusion mode using either an ATF system or an acoustic settler with pump-based recirculation. (A) Total number of infectious influenza virus particles produced using an ATF system (ATF1, ●) or an acoustic settler (one representative optimized run, AS4, ●). Size distributions of ATF1 (B) and AS4 (C). All samples were measured from the crude bioreactor supernatant. For graph B: black, blue and red lines correspond to 24, 36 and 47 hpi respectively. For graph C: black, blue and red lines correspond to 25, 33 and 45 hpi respectively. Detailed operation conditions in Table 14.

5.3 Discussion

HCD cultivation in perfusion mode has advantages for efficient production of viruses, viral vectors or recombinant proteins. While various options exist, the use of ASs has already been reported to be efficient for many virus production processes [40]. However, they can be set-up in different modes of operation and no results were available regarding the design and optimization of virus production processes performed at concentrations as high as 70 x 10^6 viable cells/mL (maximum VCC reached during virus production phase).

Compared to recombinant protein production, cell metabolism, cell viability, level of impurities and overall culture viscosity (due to cell lysis and death) change drastically after infection, which can have a significant impact on cell retention and virus harvesting. Previous studies using mammalian cell cultures for recombinant protein production have shown that the recirculation mode [126] and the recirculation rate (between 2 to 15 day^{-1}) [123, 128, 146, 199] influence the cell retention efficiency, but do not impact cell viability or productivity. Similar doubling times and high viabilities before infection were also observed for the cell

growth phase in the present study comparing an AS with different recirculation strategies and an ATF system. Furthermore, the t_d values obtained with the AS in this study were in agreement with values reported previously for AGE1.CR.pIX cells cultivated in perfusion mode with an ATF system operated at higher exchange rates (between 28 and 41 h) [90, 114].

Regarding the virus infection phase, however, the recirculation strategy of the AS turned out to have an impact on productivity, even for a process time as short as 48 h. Indeed, with recirculation rates above 7 day^{-1}, the CSVY decreased by a factor of 1.7 compared to recirculation rates between 3.7 and 5.0 day^{-1} (Table 14). One reason could be an increase in mechanical stress on cells from the peristaltic pump. As reported for other cell lines, peristaltic pumps can impact cell viability [200] or cell-specific productivity even at recirculation rates as low as 1.4 day^{-1} [201]. Furthermore, higher influenza virus yields have already been shown for low hydrodynamic stress conditions in an OSB without gas sparging and impeller agitation for AGE1.CR.pIX cells [114]. A cell line may be more sensitive to mechanical stress after infection due to metabolic changes and the addition of the protease trypsin that activates influenza virus infectivity but can also interfere with plasma membrane integrity. For example, Cortin et al. (2004) reported a higher sensitivity to hydrodynamic stress for human 293S cells infected with adenovirus that were cultivated at concentrations of only 8×10^6 cells/mL using a membrane-based perfusion system [162]. The use of recirculation rates between 3.7 and 5.0 day^{-1} with perfusion rates of 1.5–2.0 day^{-1} should also be feasible in large scale production. For example, Gorenflo et al. (2002) reported a 96% cell retention efficiency for CHO cells and production of recombinant proteins at a perfusion flow rate of 200 L/day and a volumetric recirculation flow rate of 600 L/day [128]. In this case, a ratio of 3 (600/200) was used similarly to the presented study (Table 14).

Regarding the AS, lower CSVY and P_v were observed for the valve-based recirculation strategy (AS1 and AS2) compared to the pump-based recirculation strategy (AS3), although a similar recirculation rate was used (Table 14). This was an unexpected result as the valve-based recirculation strategy avoids the use of a recirculation pump, which should reduce the mechanical stress on cells. However, for perfusion operation using the valve-based recirculation, lower $Y_{lac/glc}$ and lactate levels consistent with lower stress levels in the culture were also observed (Figure 27). Furthermore, oscillations in process conditions can influence (positively or negatively) the productivity of mammalian cell cultures [202, 203]. Cells in the

AS are exposed to fluctuations of the DO level and temperature [199, 204]. A higher maximum temperature was observed for the operation in valve-mode with a similar recirculation rate and perfusion rate compared to pump-based operation (AS1 and AS4 vs AS3 and AS4, Table 14). These physical observations may explain the negative impact on productivity of the recirculation strategy. Drouin et al. (2007) reported a decrease in the productivity for the investigated recombinant protein when the temperature in the upper part of the AS was oscillating up to 38.5°C [204]. Temperatures as high as 40°C were reached in the upper part of the tested acoustic chamber during the virus production phase independent of the recirculation strategy. However, temperatures of 35°C and 37°C were measured in the lower part of the acoustic chamber for the pump-based and valve-based recirculation strategy, respectively (Table 14). A higher temperature on the lower part of the AS (containing the aggregated cells) could have negatively influenced the virus production when recirculating the cells in the AS with the valve-based mode. Temperatures above 37°C might be detrimental for cell metabolism and virus stability. In addition to the impact of temperature, Dalm et al. (2005) reported DO levels dropping to zero in the AS for recirculation rates of up to 6 day^{-1} [199]. This might be detrimental for the cell-based virus production as well. Higher P_v and CSVY observed in AS7 (Table 14) with temperatures limited to 38°C on the upper part of the acoustic chamber suggest that virus production using ASs could be further improved (by more than a factor 1.5) compared to the ATF system. Possible options would be either the use of a smaller acoustic chamber and a more efficient cooling system or operation at a higher perfusion flow rate (> 1.2 L/day). The influence of the temperature elevation of the lower part of the acoustic chamber on Vir_{tot} was also shown in Figures A.7-A.12, as this parameter was the one influencing the most Vir_{tot}. It seems in general that the temperature at the lower part of the chamber should ideally not exceed 34°C to ensure high Vir_{tot}. Figures A.13-A.14 might indicate that temperature elevation is mainly influenced by the perfusion rate, which should be above 1600 mL/day for the 10 L AS model.

An increase by a factor of at least 1.5 for P_v and CSVY was observed in the most successful perfusion runs with the AS compared to cultivations performed with the ATF system (Table 14). This increase could be explained by several factors. Most likely, the continuous removal of virions resulted in lower infectivity losses due to a shorter exposition to proteases released from lysed cells. In addition, reduced levels of accumulated host cell proteins that can potentially inhibit virus production may also play a role. Moreover, ASs also allow for the

selective removal of dead cells over viable cells, which might be beneficial for virus production as it reduces the risk of virus degradation by protease activity and the accumulation of signaling molecules and unspecific inhibitors of virus replication. The positive influence on Vir_{tot} with selective removal of dead cells over viable cells was also for the experiments performed with the AS and IAV in this study (Figure A.8). For example, various studies have shown an increased product yield when increasing the cell viability [205, 206]. Lower shear rates during infection may also contribute to better yields. With a calculated $\gamma < 340\ s^{-1}$, the conditions in the AS seem to be superior to the ATF system ($\gamma = 2451\ s^{-1}$, Table 14). Although various mammalian and insect cell lines were shown to survive hydrodynamic stress up to $\gamma = 3000\ s^{-1}$ [163] or $\gamma = 4000\ s^{-1}$ [207], values as low as $\gamma=620\ s^{-1}$ were shown to be harmful for HEK cells after adenovirus infection [162].

The use of AS for influenza virus production when cells were infected at concentrations up to 50×10^6 cells/mL (AS8) was also possible. Finally, a maximum VCC of approximately 70×10^6 cells/mL was reached post infection. In this run, a high CSVY of 1665 virions/cell was obtained. For infections at 25×10^6 cells/mL (for example AS3 and AS4) CSVYs of 1124 to 1371 virions/cell were reached. The total amount of produced virions and P_v were, by consequence, also increased in AS8. This suggests that the P_v and the total amount of produced virions per bioreactor run can be even further increased if higher VCCs can be achieved after the growth phase.

Similar process-related impurity levels (host cell dsDNA and total protein per virion) were observed in the harvest of the ATF and the AS perfusion cultures (Figure 28C). For the ATF run, higher impurity concentrations were detected inside the bioreactor compared to the permeate line (Figure 28A). As expected from chapter 4, in addition to enrichment of viruses, dsDNA and proteins also accumulate inside the bioreactor in membrane-based perfusion cultures. In contrast to the AS, the harvest from ATF cultures needs to be taken directly from the bioreactor, which requires an additional clarification step for subsequent virus purification. Furthermore, an AS has a higher flexibility in terms of the optimum harvest time point. In addition, as the virus is harvested continuously through the acoustic chamber, there is a lower risk of virus degradation (as seen in Figure 28B for the ATF).

Continuous harvesting is, in particular, attractive due to the inherent instability of some viruses. For example, a loss of IAV infectivity by four orders of magnitude was observed after

an incubation time of 48 h at 37°C [107]. In the present study, perfusion rates of 1.5 to 2.0 day^{-1} were used with the AS that correspond to relatively short residence times of virions in the bioreactor. A higher total amount of infectious virions was obtained ($TCID_{50}$ assay) for the cultivation with the AS (4.6×10^{11} for the ATF vs 10.8×10^{11} for the AS, Figure 29A). However, this difference might be negligible as it is close to the assay error (about ± 0.3 $\log_{10}(TCID_{50}/mL)$ [151]). Therefore, operation at a perfusion rate of 2 day^{-1} seems not sufficient to avoid infectious virion losses. To a certain extend a partial reduction of virus infectivity for cultivations using an AS might also be expected due to the temperature increase in the acoustic chamber. Finally, in the case of influenza virus production with the vast majority of licensed vaccines using killed virus, the titer calculated from the HA assay (the total number of all virus particles) is of higher importance. For live vaccines using attenuated polio, yellow fever or measles virus, losses in the infectious titer would be more critical.

Virus aggregation and formation of other large-sized aggregates was observed for later time points of infection for cultivations with the ATF system and the AS. While profiles look similar, a lower amount of aggregates larger than 0.6 µm was observed for cultivations performed with the AS (Figure 29B-C). Perfusion rates higher than 2 day^{-1} might be considered to limit the formation of aggregates in the bioreactor and to facilitate subsequent purification steps. A further reduction of aggregates is desirable because virus aggregation typically results in lower process yields and high levels of protein aggregates can result in a strong but unwanted induction of immune responses [208-210].

Disadvantages regarding the use of ATF systems in viral vaccine production due to an accumulation and eventual degradation of virions inside of the bioreactor may be alleviated by selection of membranes that are better suited for this type of application or specifically designed for virus production processes. Similarly to what was tested for membrane-based perfusion culture in recombinant protein production [78, 211, 212], different membrane chemistries, pore sizes, and properties such as hydrophobicity and surface charge should be tested regarding product sieving and membrane fouling for a perfusion process, as performed later in chapter 8. Lately, Nikolay et al. (2020) studied product sieving and membrane fouling for yellow fever production, but not directly for perfusion cultures [80].

In conclusion, a scalable perfusion process based on an AS with concentrations above 50×10^6 cells/mL was developed for continuous harvesting of influenza viruses. For ASs, the

recirculation strategy, recirculation rates and temperature elevation in the inner acoustic chamber were found to have a large influence on the CSVY and the P_V. Ideally, the temperature in the lower part of the acoustic chamber should not exceed 34°C, which can be mainly controlled through the perfusion rate. Virus yields were 1.5 to 3.0-folds higher for the AS compared to ATF. ASs have been shown to be scalable to perfusion flow rates of at least 200 L/day [128] and one manufacturer (Applikon Biotechnology) commercializes ASs for perfusion flow rates of up to 1000 L/day. The results suggest that the acoustic cell retention technology could be applicable for production of viral vaccines even at large scale. Continuous harvesting may be especially beneficial for the production of live vaccines or viral vectors for gene therapy where prevention of infectivity losses due to degradation of particles is crucial for product quality. Furthermore, the establishment of continuous harvesting schemes using ASs might help to establish fully integrated vaccine production processes.

5.4 Author contributions

All the experiments were performed by Gwendal Gränicher. Juliana Coronel helped to perform a part of the cell culture runs. The chapter was reviewed by the co-authors of the paper: *Performance of an acoustic settler versus a hollow fiber-based ATF technology for influenza virus production in perfusion* [213].

Chapter 6

Application of an inclined settler for cell culture-based influenza A virus production in perfusion mode

---

This chapter was based on the following publication:

Coronel, J.*, **Gränicher, G.***, Sandig, V., Noll, T., *et al.*, Application of an inclined settler for cell culture-based influenza A virus production in perfusion mode. *Frontiers in Bioeng and Biotech*, 2020.

*Both authors contributed equally

6.1 Introduction

In the previous chapter (chapter 5), the AS perfusion system was established and optimized for IAV production. Several process parameters were then compared to a membrane-based ATF system. Continuous virus harvesting has been shown to increase virus production yields and decrease the amount of product aggregates. However, it has been observed that a temperature elevation in the acoustic chamber might decrease the productivity. For this reason, and in order to further push the productivity, another cell retention device, namely an IS, which does not need acoustic waves leading to temperature elevation has been subsequently tested and optimized for the production of IAV in perfusion mode.

As described in the theoretical background, section 2.6.3, the IS holds several advantages, making it interesting for the manufacturing of cell culture-based vaccine or gene therapies. The advantages are: i) Already successfully used for biologicals manufacturing [120, 132], ii) scalable and robust device (perfusion can last up to five months [135], at scales up to 3000 L/day [134]), iii) preferential removal of non-viable cells and debris, iv) available as single-use [136]. However, some of the disadvantages are: i) Limited to maximum VCC of 30 x 10^6 cells/mL for large-scale continuous recombinant protein production, ii) relatively long residence time of cells in the IS (up to 1.5 h, non-controlled environment) [111, 130], iii) need of a heat exchanger to minimize cell shear stress and the side effect of a long residence time in the IS, and to avoid temperature convection which increases cell separation efficiency [111, 118, 130, 137], iv) complex and time-consuming optimization of the IS process parameters such as the cooling temperature, the recirculation flow rate, the optimal settler geometry and size, and the intermittent vibration frequency, v) large footprint [111].

The use of such an IS in small scale for continuous harvesting of IAV is presented in this chapter. Therefore, AGE1.CR.pIX cells were cultivated to high VCCs (> 50 x 10^6 cells/mL) in a STR (1 L V_w) in perfusion mode. As a control, and similar to chapter 5, a perfusion cultivation was carried out at a VCC of 25 x 10^6 cells/mL using an ATF2 system. Additionally, imaging flow cytometry was used to monitor the viral infection dynamics in the bioreactor. Again the temperature within the perfusion device, here the heat exchanger (required for IS operation), was shown to be a crucial parameter in this case to obtain low cell population doubling times (t_d) before infection. The effect of “cooling cells” (in the recirculation loop) on cell growth and

virus production was studied in more detail in a cultivation using the same heat exchanger, but with an AS as a control.

On the last part of the chapter, a comparison between the ATF, AS and IS is shown regarding IAV production.

6.2 Results

To allow an efficient IAV production in perfusion mode using an IS, investigations started with the characterization of cell growth before infection. Once a short t_d was reached for AGE1.CR.pIX cells, IAV production was evaluated by calculating Vir_{tot}, CSVY and P_v. Results were compared to a virus production process also operated in perfusion mode, but coupled to an ATF system (see sections 6.2.2 and 6.2.3). Two VCCs at TOI and different trypsin addition strategies were tested with the IS. Furthermore, the temperature setting of the heat exchanger seemed to have an impact on cell growth and virus production. Therefore, this was further studied by using another cell retention device, an AS, equally enabling continuous virus harvesting. In contrast to an IS, a setting with and without heat exchanger was possible for the AS.

6.2.1 Conditions for efficient cell growth in perfusion mode using an inclined settler

The t_d in perfusion was evaluated for different recirculation water temperatures of the heat exchanger of the IS device (illustrated in Figure 14, section 3.6.3).

Initial cultivations were done using a thermostatic bath to cool the water in the heat exchanger, that is commonly used during IS operation in biopharmaceutical production using other cell lines (e.g. CHO cells) [134, 147, 214]. In the conducted study, AGE1.CR.pIX cells did not grow efficiently (t_d > 48 h) with set-points varying between 20–22°C (IS1, Figure 30A-B), so higher set-points were used during the cell growth phase for run IS2 (25–27°C) (Figure 30A-B). A temperature of 27°C was also reached in a process with simple water recirculation without cooling. This enabled successful cell growth at high viabilities (> 92%) for four bioreactor experiments (IS3-6, Figure 30A-B), which were used for infection studies with IAV (section 6.2.2). The temperature ranges tested with the heat exchanger are listed in Table 15.

Table 15: Temperature of the heat exchanger, concentration of AGE1.CR.pIX cells and influenza A virus yields for perfusion runs using the inclined settler (IS), the ATF system or the acoustic settler (AS).

Run	T recirc. [a] [°C]	X_v, viab. [b] [cell/mL, %]	$Vir_{tot, max}$ [c] [10^{13} virions]	CSVY [d] [virions/cell]	P_v [d] [x 10^{12} virions/L/d]
IAV_IS1	20–22	-	-	-	-
IAV_IS2	25–27	-	-	-	-
IAV_IS3	27	24 x 10^6, 92	5.7	3259	1.18
IAV_IS4	27	27 x 10^6, 95	6.5	3474	1.23
IAV_ATF1	No heat exchanger	25 x 10^6, 99	1.9	723	0.55
IAV_AS4	No heat exchanger	25	1.5	704	0.36
IAV_AS9	27	25	4.0	2439	0.66
IAV_IS5	27	52 x 10^6, 97	6.5	1953	0.83
IAV_IS6	27	48 x 10^6, 96	5.4	1753	0.66

T, Temperature; X_v, viable cell concentration; viab., cell viability; $Vir_{tot, max}$, Maximum total number of virions produced; CSVY, cell-specific virus yield; P_v, volumetric virus productivity.

[a] Temperature of the cooling water recirculated in the heat exchanger.

[b] X_v and cell viability at time of infection

[c] $Vir_{tot, max}$, normalized to a bioreactor volume of 650 mL (section 3.13.3).

[d] CSVY and P_v calculated according to section 3.13.3.

Growth up to 25 x 10^6 cells/mL (IS3, IS4) or 50 x 10^6 cells/mL (IS5, IS6) before addition of the virus seed was obtained. In the cultivation IS3 with settler operation at RT, t_d was improved (37 h) compared to IS1–2. In the cultivations IS1, IS2 and IS3, recirculation was started 48 h after inoculation, corresponding to the middle of the exponential cell growth phase. In the following cultivations (IS4–6), recirculation was started at time of inoculation. This resulted in a further improvement of t_d to a range of 26–32 h. The results indicated that both the temperature of the heat exchanger of the IS, and the time point of starting the recirculation have an impact on cell growth. In a cultivation using an ATF system performed as a control, infecting at a concentration of about 25 x 10^6 cells/mL, resulted in a slightly lower t_d of 25 h (Figure 30A and B).

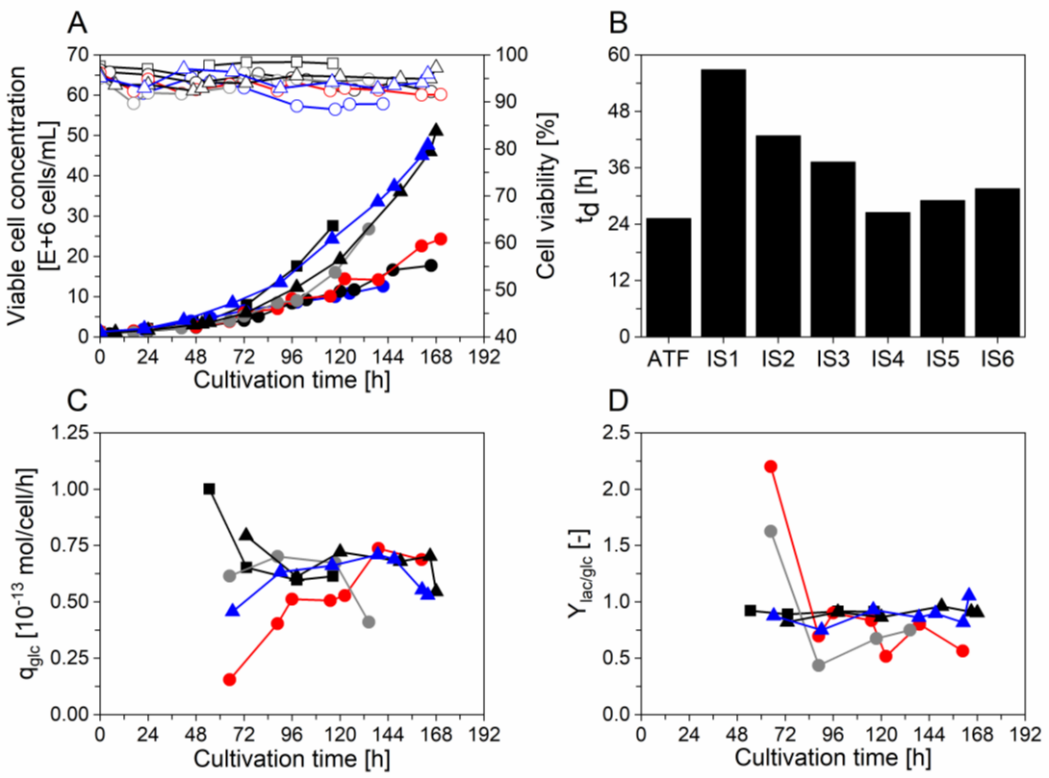

Figure 30: Growth and metabolism of AGE1.CR.pIX cells in perfusion mode using a stirred-tank bioreactor coupled to an inclined settler or an ATF system. Cultivations with an inclined settler (IS): IS1 (●), IS2 (●), IS3 (●), IS4 (●), IS5 (▲) and IS6 (▲). Cultivation with the ATF system (■). (A) Viable cell concentration (filled symbols) and cell viability (empty symbols). (B) Doubling time (t_d) during the cell growth phase. (C) Cell-specific glucose consumption rate (q_{glc}) during perfusion (after 48 h). (D) Lactate yield based on glucose consumption ($Y_{lac/glc}$) during perfusion (after 48 h).

For all the perfusion runs, the perfusion flow rate was adjusted daily to maintain the desired CSPR during the cell growth phase as described in section 3.7.1. Under these conditions, the glucose concentration always exceeded 2 g/L (data not shown). In addition, q_{glc} and $Y_{lac/glc}$ were analyzed for the successful runs (IS3-6 and ATF) to assess if the use of a recirculating loop coupled to a heat exchanger has an influence on cellular metabolism. As before, a cultivation with ATF-based perfusion served as a control. Similar q_{glc} and $Y_{lac/glc}$ were observed for both systems (Figure 30C-D). For IS3, a lower q_{glc} was observed between 48 h and 120 h, which was likely associated with the start of recirculation on day 2 leading to a slowdown of cell growth and metabolism. For IS4, a lower $Y_{lac/glc}$ was observed between 72 h and 96 h.

6.2.2 Influenza A virus production in perfusion cultures

After infection, the bioreactor was operated at a constant perfusion rate of 2 day^{-1}, except for IS3, which was operated CSPR-based during the entire cultivation period (Figure 31B). When

cells are infected with IAV at low MOIs (10^{-3}–10^{-5}), they can typically continue to grow for 12–24 hpi, until the majority of the cells is infected and the virus titer starts to increase strongly. To avoid substrate limitations, the CSPR was maintained during the initial virus production phase for cultivation IS5 infected at a VCC of 50 x 10^6 cells/mL and was only reduced 12 hpi (Figure 31D). No glucose depletion was observed in a control experiment (IS6) infected at the same VCC running for the complete virus production phase with the reduced perfusion rate of IS5 (see Figure 31D; data not shown).

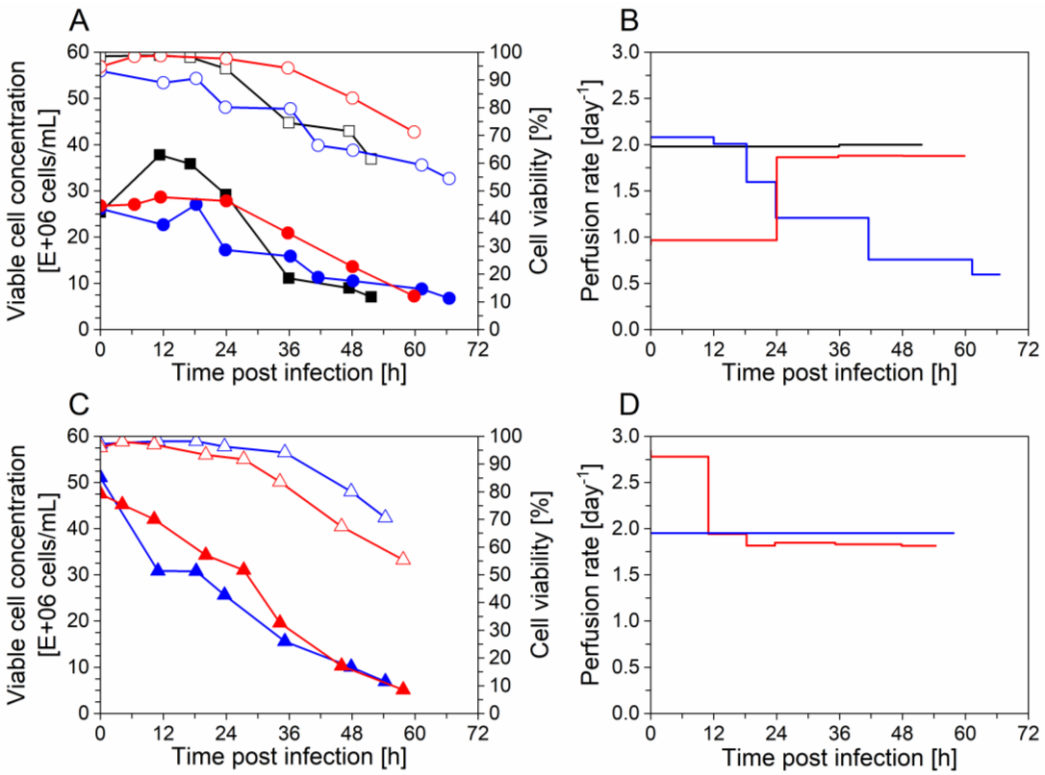

Figure 31. Production of influenza A virus in perfusion mode using an inclined settler (time of infection t = 0 h). Cultivations of AGE1.CR.pIX cells in 1 L stirred-tank bioreactor with an inclined settler (IS) IS3 (●), IS4 (●), IS5 (▲) and IS6 (▲) plus one control run with an ATF system (■) were carried out. (A, B) Cells were infected at 25 x 10^6 cells/mL (IS3, IS4, ATF) or (C, D) 50 x 10^6 cells/mL (IS5, IS6). (A, C) Viable cell concentration (filled symbols) and cell viability (empty symbols) shown as average of analytical duplicates. (B, D) Perfusion rate in bioreactor working volume per day (day^{-1}).

After infection with IAV, VCCs varied according to infection conditions and the perfusion system used (described in sections 3.6 and 3.10.1). For the cultivations infected at 25 x 10^6 cells/mL (Figure 31A), the VCC was maintained after infection in the IS cultivations whereas cell growth continued for about 12 hpi in the ATF culture. A comparison between IS3 (infected with 38 trypsin U/mL) and IS4 (13 trypsin U/mL) (Table 7) suggests that a lower trypsin activity (IS4) allowed for a better cell growth after infection. Nevertheless, even though the same

trypsin activity was used in experiments IS4 and ATF (13 U/mL) (Table 7), different cell growth profiles were obtained (Figure 31A). The VCC reached 38 x 10^6 cells/mL for the ATF culture after infection, while the VCC did not exceed 30 x 10^6 cells/mL for the runs using the IS. These results may suggest that infected cells in medium containing trypsin are less robust and more affected by ISs than ATF systems due to higher shear forces in the former (also see t_d and VCCs, Figure 30A-B; section 2.6.3). Higher shear forces is obtained due to the use of the peristaltic pump in the recirculation loop. In addition, cooling to 27°C might play a role in IS cultivations.

For infection at 50 x 10^6 cells/mL (Figure 31C), trypsin activities between 13 and 25 U/mL were employed (Table 7). In addition, one of the runs (IS6) was operated with trypsin supplementation in the feed medium (2 U/mL) instead of adding a second dose. Interestingly, a rapid decrease in VCC occurred soon after infection in the cultivations IS5 and IS6. This was in clear contrast to the behavior obtained in those infected at 25 x 10^6 cells/mL (IS3, IS4) (Figure 31A). The effect was more pronounced for IS5 (25 U/mL) compared to IS6 (13 U/mL). This behavior was also observed in pseudo-perfusion experiments in spin tubes previously carried out to select the best infection conditions using 13–25 U/mL of trypsin (data not shown).

Maximum $C_{vir,\,br}$ and $C_{vir,\,h}$ values in the range of 3.4–5.9 x 10^{10} virions/mL were obtained for cultures with the IS (IS3-IS6), whereas the highest titer with the ATF system was slightly lower with 2.8 x 10^{10} virions/mL (Figure 32A and C). Nevertheless, the increase of $C_{vir,\,tot}$ was in the range of the error of the titration assay (section 3.8.1). The virus titers measured in the harvest line of the IS followed a profile very similar to that measured in the bioreactor, demonstrating efficient continuous harvesting with this retention device. The small delay in achieving the maximum titer in the harvest compared to the bioreactor could be related to the dead volume of the IS unit (275 mL, section 3.6.3). In the experiment with the ATF system, very low virus titers were measured in the harvest, corroborating previous findings regarding membrane blocking [90, 115].

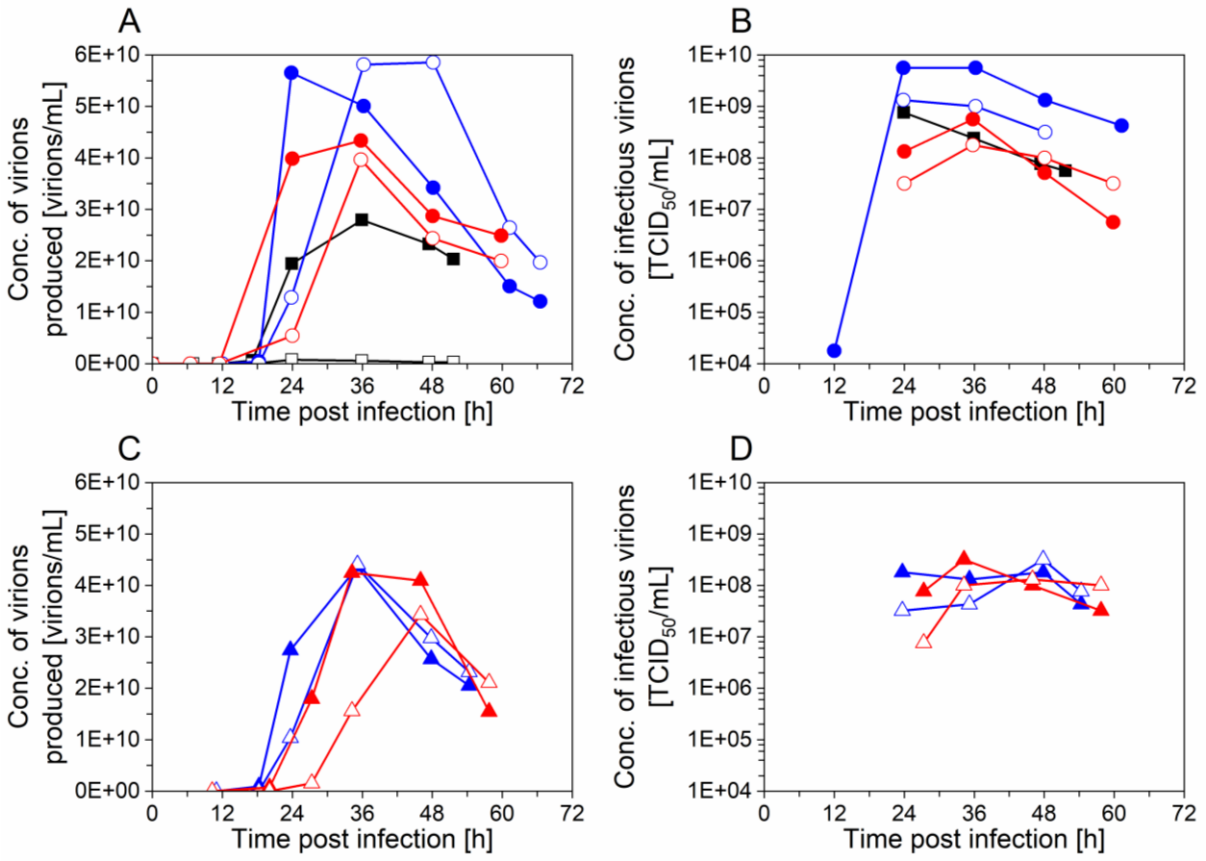

Figure 32: Influenza A virus production in perfusion cultivations of AGE1.CR.pIX cells with inclined settler (IS) IS3 (●), IS4 (●), IS5 (▲) IS6 (▲) and ATF system (■). Concentration of virions in the bioreactor and in the harvest, based on HA titer (A, C); concentration of infectious virions, based on $TCID_{50}$ (B, D). The samples were taken from the bioreactor (filled symbols) and the harvest (empty symbols).

Maximum infectious virus titers achieved 36–48 hpi were in the range 1.0–5.6 x 10^8 $TCID_{50}$/mL in IS cultivations and 7.6 x 10^8 $TCID_{50}$/mL with ATF system at 24 hpi (Figure 32B and D). For the ATF-based cultivation, maximum $TCID_{50}$ values were achieved earlier, which was most likely due to faster virus accumulation in the bioreactor after membrane blocking and, eventually, also due to the absence of a cooling system. For the IS experiments, viruses produced in the bioreactor were constantly harvested via the permeate. However, highest infectious titers for the IS cultivations were almost always measured for samples taken from the bioreactor but not from the harvest. This finding suggests that the infectivity of virions decreased during the passage through the heat exchanger and the settler device. Nevertheless, overall, a total of 2.5–6.1 x 10^{11} $TCID_{50}$ was produced, similarly to the ATF culture (5.0 x 10^{11} $TCID_{50}$).

The $Vir_{tot, max}$ for IS3–6 was in the range of 5.4–6.5 x 10^{13} virions, which represents a 3.2-fold increase compared to the ATF culture (Table 15). Very high CSVYs were obtained with the IS,

providing a 4.7-fold (IS3, IS4) or 2.6-fold (IS5, IS6) increase compared to the ATF culture (control). Since the cell growth phase was usually extended with the IS, the increase in P_v was of 2.2-fold (IS3, IS4) and 1.4-fold (IS5, IS6) compared to the ATF culture (Table 15). Except for the P_v of IS5 and IS6, the increase of the $Vir_{tot, max}$, CSVY and P_v between the ATF and IS3–6 exceeded the error of the titration assay (section 3.12.3).

The progression of virus infection in the cultivations was determined by flow cytometry as the fraction of infected cells (Figure 33A). The highest trypsin activity (1.5 x 10^{-6} U/cell or 38 U/mL) in the IS3 run led to a complete infection of the cell population at 24 hpi. For the runs IS4, IS5 and ATF that were infected using a lower dose of trypsin (0.5 x 10^{-6} U/cell or 13–25 U/mL), only 80-85% of cells were infected at 24 hpi and the peak infectivity was delayed to 36–48 hpi, corresponding to 90–95% of infected cells. Finally, when trypsin activity at TOI was further reduced in the cultivation IS6 (0.25 x 10^{-6} U/cell or 13 U/mL) and trypsin was fed in the medium during virus production phase, the percentage of infected cells at 24 hpi was considerably lower (60%, Figure 33A). A maximum of 80% was obtained at 48 hpi. However, at this time point, the virus production phase was nearly completed. Therefore, the concentration of infected cells was low (Figure 33B). Clearly, for maximum virus production, the majority of the cells should be infected within 24 h after addition of the virus seed when viability is also highest, showing room for process improvement at 50 x 10^6 cells/mL.

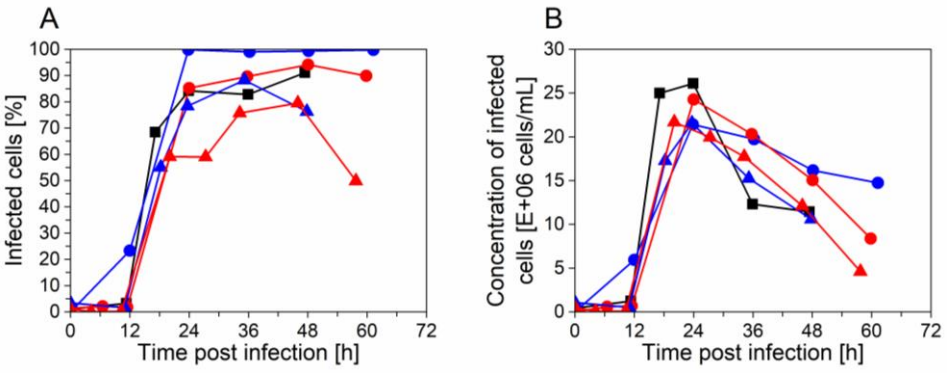

Figure 33: Progression of infection of cells with influenza A virus in perfusion cultivations determined by imaging flow cytometry. (A) Fraction of infected cells positive for virus nucleoprotein and (B) concentration of infected cells in the bioreactor, calculated from the measured total cell concentration and the fraction of infected cells. Runs: IS3 (●), IS4 (●), IS5 (▲), IS6 (▲) and ATF (■).

Although runs IS5 and IS6 were infected at 50 x 10^6 cells/mL, the actual number of infected cells at 24 hpi was approximately the same compared to the cultures infected at 25 x 10^6 cells/mL (IS3, IS4, and ATF) (Figure 33B). Therefore, a significant fraction of the cells present at TOI in IS5 and IS6 was not infected and/or a fraction of infected cells likely died before replicating and releasing progeny virions (which usually starts at about 6–8 hpi). Accordingly, virus production was similar in the four experiments with the IS (Figure 32A and C). Since the CSVY calculation considers the maximum VCC from TOI onwards, lower CSVYs were obtained in the case of experiments IS5 and IS6 (Table 15).

6.2.3 Influence of the heat exchanger on virus production

In order to evaluate the impact of the heat exchanger and cooling during perfusion and continuous virus harvesting, an AS was used in a setting similar to chapter 5. This cell retention device also enables continuous virus harvesting, but does not require the use of a heat exchanger.

Under the same infection conditions and same perfusion strategy (sections 3.7.1 and 3.10.1), two perfusion runs were performed using the AS either without (AS4, from chapter 5) or with (AS9) heat exchanger, and compared to cultures with an IS (IS3-4) and the ATF system (Figure 34). The temperature of the heat exchanger for each run is listed in Table 15.

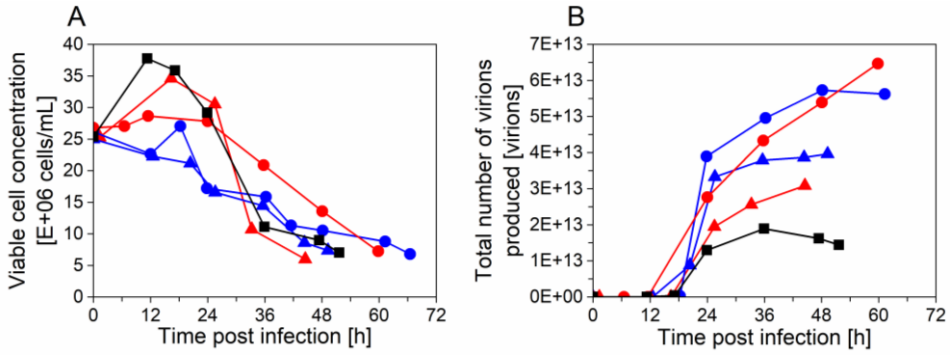

Figure 34: Evaluation of the influence of the temperature/use of heat exchanger during influenza A virus production using different perfusion systems. Cell growth (A) and total number of virions produced (Vir_{tot}, based on HA titer) after infection (B) using an acoustic settler with heat exchanger (AS9, ▲) or without heat exchanger (AS4, ▲), compared to runs IS3 (●), IS4 (●) and ATF (■). The total number of virions produced was normalized to a bioreactor working volume of 650 mL (see section 3.13.3).

As observed previously (section 6.2.2), the maximum VCC after infection decreased from 35 x 10^6 cells/mL (AS4) to 25 x 10^6 cells/mL (AS9) for perfusion systems using a heat exchanger (Figure 34A). Similar cell growth and virus release profiles were observed for the cultivations

with a heat exchanger, either with the AS (AS9) or the IS (IS3, IS4) (Figure 34A and B). Based on HA titers, a higher total number of virions were produced in these runs (AS9, IS3 and IS4) compared to cultures using an AS without heat exchanger (AS4) and the ATF system. The difference in virus release was detected at the limit of the titration error. Yet, the maximum total number of virions produced was only slightly higher for IS3 and IS4 (5.7–6.5 x 10^{13} virions) compared to cultures using an AS with heat exchanger (AS9, 4.0 x 10^{13} virions) (Figure 34B).

6.3 Discussion

The perfusion cultivations performed in a STR coupled to the IS yielded VCCs up to 50 x 10^6 cells/mL, with viabilities above 92% (Figure 30). The experimental set-up involved cell recirculation with a peristaltic pump operated at 27°C. Cell doubling times between 26–32 h (IS4, IS5 and IS6) were obtained, when recirculation was started directly after inoculation. This is at the lower range of results previously reported for perfusion cultivations using AGE1.CR cells (t_d 30–44 h) [103] and AGE1.CR.pIX cells (t_d 29–40 h) [90] in STR with ATF systems, or cultivations with AGE1.CR.pIX cells (t_d 26–43 h) in an OSB with ATF and TFF systems [114].

Although other cell lines such as CHO cells were reported to grow efficiently when cooling the IS to temperatures lower than 22°C [134, 147, 214], AGE1.CR.pIX cells seemed to be sensitive to low temperatures in the recirculation loop. A previous case study showed through orthogonal PLS multivariate analysis that the temperature in the IS is one of the most important factors for the productivity variability [215]. Here, it seems that the temperature also needs to be selected carefully to increase process performance.

Cooling of the IS is necessary as it enables to slow down cell metabolism, to maintain high cell viabilities and a high cell retention efficiency. In the present study, cell separation efficiency (SE) was maintained between 96% and 99% during the cell growth phase for IS3-6, showing no further need to cool the cells in the recirculation loop. As reviewed by Castilho and Medronho [122], SE is determined by the terminal settling velocity of particles in a laminar flow (Stokes' law). Among other factors, it is related to the cell diameter (section 2.6.3). With the onset of apoptosis and cell death after infection, the average diameter of the cell population typically decreases over the course of the virus production phase. Hence, a gradual drop in SE can occur, especially at late stages of infection. For the IS cultivations with infection

at low MOI (IS3-IS6), the optimum harvest time regarding maximum total virus production was around 60 hpi. SE remained reasonable high (> 85%) until the processes were ended. Minimum cell separation efficiency values measured at 54–60 hpi were 93% (IS3), 96% (IS4), 94% (IS5) and 85% (IS6). Therefore, the reduction of the SE during virus production was not critical for the current application.

In one scouting experiment maintained for a longer period after infection of AGE1.CR.pIX cells with IAV (data not shown), SE dropped to 86–50% at 67–92 hpi. At a later stage of infection (116 hpi), nearly the same VCC was measured in the bioreactor and in the harvest (SE ≈ 0). In this example, the average cell diameter was 14.0 µm during the cell growth phase and 10.8 µm at the end of the run. The SE is influenced by the settling velocity, which is reduced for smaller diameters of settling particles (section 2.6.3). For processes with lytic viruses, drastic cell diameter decrease and a fast decrease in SE, continuous virus harvesting might be problematic using ISs.

Another factor with a high impact on SE for operation with an IS is the harvest flow rate [137]. Therefore, equipment with a suitable capacity should be selected. The model CS-10 used in this work, which has a total area of 0.046 m^2, was designed for operation at flow rates up to 8 L/day. Here, the cultivations were carried out using recirculation rates of 2–3 day^{-1} (1.30–1.95 L/day), thus enabling high retention efficiencies, as previously mentioned. At large scale, 99% efficiency was reported for a biopharmaceutical process using perfusion rates over 2000 L/day for steady state at 20 x 10^6 cells/mL or higher [132], demonstrating that this perfusion device can be successfully scaled up with high SE.

For comparable t_d values, the cell-specific glucose uptake rate q_{glc} and the lactate yield based on glucose consumption $Y_{lac/glc}$ were in a similar range for cultivations with the IS compared to the ATF culture (IS4-6 and ATF, Figure 30C-D). Therefore, cell recirculation in the IS at 35 mL/min at 27°C seems not to influence significantly AGE1.CR.pIX cell growth and metabolism compared to an ATF cultivation. The conserved q_{glc} further suggests that the cell-specific perfusion rate adjusted to 60 pL/cell/day (based on glucose consumption as previously described [90, 110]) was equally suitable for IS cultivations.

To the knowledge of the author, the described process using an IS is the first report on the use of this technology in virus vaccine production. High volumetric productivities and cell-specific virus yields were obtained.

Infections at 25 x 10^6 cells/mL enabled very high CSVYs and P_vs in perfusion mode with the IS (4.7-fold and 2.2-fold increase compared to the ATF control run) (Table 15). For infections at 50 x 10^6 cells/mL, the CSVY was increased by a factor of 2.6. Cultivations using AGE1.CR.pIX cells for the production of human influenza A/PR/8/34 H1N1 virus in batch mode in STR led to a CSVY of 1344 virions/cells [90]. Cultivations in perfusion mode with ATF systems or hybrid fed-batch/perfusion processes for the production of the same IAV strain using the same cell line yielded 340–1300 virions/cell [90]. Other ATF perfusion cultivations using the parental AGE1.CR cells resulted in yields of 518–1708 virions/cell [103]. The CSVY obtained in the present work for IS cultivations infected at 25 x 10^6 cells/mL (3259–3474 virions/cells for IS3–4) clearly exceed those reported for batch or perfusion cultivations carried out in STRs. In terms of P_v, virus production using an IS allowed a 1.9-fold increase compared to a batch process using the same cell line and virus strain [90], showing the potential of IAV production in perfusion mode using an IS. The obtained CSVY (1753-1953 virions/mL) with the IS at a VCC of 50 x 10^6 cells/mL were also higher than in previous studies for cultivations performed in perfusion mode [103] using an ATF system producing the same virus strain with a very similar cell line (AGE1.CR cell line; 50 x 10^6 cells/mL at TOI; CSVY 1266 virions/cell). Further comparisons with other processes reported in literature would be difficult as host cells, media, virus strain and virus titration assays differ [115].

The high values obtained for CSVY in perfusion mode using an IS were to a certain degree related to the continuous virus harvesting strategy. In addition, high virus titers and yields were also mediated by variation in culture temperature between the bioreactor and IS. Even though the temperature in the bioreactor was maintained constant at 37°C, the cell suspension was cooled in the heat exchanger but the IS was kept at RT. Therefore, the cells were subjected to a temperature gradient of about 10°C. Petiot et al. (2011) investigated the stability and yield of IAV produced in HEK293 cells at different temperatures (37°C and 35°C) [107]. In this study, virus degradation was less pronounced for processes operated at 35°C with storage of the supernatant at 2–8°C. Consequently, virus titers and final yields were higher under these conditions. Lower temperatures of 32–35°C were also reported for production of IAV in various cell lines including MDCK and Vero [44], suggesting that production may benefit from lower temperatures. The use of the heat exchanger induced a very different cell growth profile after infection not only for the IS but also the AS. In particular, for cultivations performed with a heat exchanger, the maximum VCC obtained after infection

was reduced (compared to cultivations without heat exchanger, AS4 and ATF). This could be an advantage as virus production instead of cell growth seemed to be promoted under these conditions, in addition to reduced virus degradation. This is also supported by the results obtained for the cultivations with the AS with or without heat exchanger (section 6.2.3).

Concerning infectious titers, no major differences were observed between ATF and IS cultivations. Maximum titers of 1.8–7.6 x 10^8 $TCID_{50}$/mL were obtained. In addition, virus degradation was observed in the perfusion cultivations towards the end of the virus production phase regardless of the experimental conditions evaluated (Figure 32). One option for future studies with the focus to achieve higher concentrations of infectious particles (for life-attenuated vaccines) using an IS is to increase the perfusion rate. This way, the residence time of virions in the system is decreased, potentially reducing the degradation. Indeed, an increased residence time of the virions inside the bioreactor may lead to degradation not only due to higher temperature but also due to the release of cellular proteases at later stages of the infection phase [39].

Recently, a single-use OSB was evaluated by the Bioprocess Engineering group for human influenza A/PR/8/34 H1N1 virus production with AGE1.CR.pIX cells up to 10 L V_w. Yields of 1055–3487 virions/cell were obtained in perfusion mode with the OSB-ATF or OSB-TFF systems [114]. ISs are traditionally made of stainless steel [134], however novel single-use models of compact settlers are being produced [136] (section 2.6.3). Due to the many advantages of single-use technology [216], it could be interesting to evaluate single-use ISs combined to single-use bioreactor systems, such as OSB, for virus production in future studies. Process parameters such as recirculation flow rate and the effect of the heat exchanger on cell retention efficiency and process productivity should then be re-evaluated.

Influence of trypsin activity on IAV production and cell metabolism after infection was observed in the conducted experiments. Trypsin activates influenza virus through cleavage of hemagglutinin (HA) [217] involved with attachment to cells and consequently with virus entry [218]. The absence of this enzyme can lead to delayed virus propagation and reduced influenza virus yields [219]. In the present study, initial experiments were performed with infection at 25 x 10^6 cells/mL using 0.5–1.5 x 10^{-6} U/cell (13–38.0 U/mL) of trypsin (IS3, IS4 and ATF) (Table 7). Although different cell growth profiles post-infection were observed, similar virus production was achieved in IS3 and IS4 cultivations, which was significantly higher

compared to the ATF cultivation (Table 15). Subsequently, an infection at 50 x 10^6 cells/mL (IS5) was carried out using the lower limit previously tested in terms of trypsin activity per cell, that is 0.5 x 10^{-6} U/cell (25 U/mL). This corresponded to an activity two times higher in terms of unit per volume compared to IS4 and ATF (13 U/mL). Interestingly, a drop in VCC was observed (Figure 31C). One hypothesis to explain this finding was that the trypsin activity may have a negative impact on cultures at high VCCs in perfusion mode with an IS. In the subsequent perfusion cultivation (IS6), a lower trypsin activity was used at TOI, i.e. 0.25 x 10^{-6} U/cell (13 U/mL) and a feed medium with a low volumetric trypsin activity (2 U/mL) provided. Similarly to cultivation IS5, the VCC started to decrease for IS6 directly after infection (although this effect was less pronounced), leading to equivalent virus yields in the perfusion experiments for IS5 and IS6 (Table 15). Analysis of the progression of infection over time showed a lower percentage of infected cells in the cultivations infected at 50 x 10^6 cells/mL compared to those at 25 x 10^6 cells/mL (Figure 33).

Although cells are usually less robust after virus infection, previous perfusion cultivations with the ATF system using the same cell line and virus did not indicate a significant decrease in cell growth during early stages of infection [90, 220]. In these studies, infection with IAV H1N1 took place at high concentrations at TOI (up to 50 x 10^6 cells/mL), using an MOI 10^{-3} in the presence of 1 x 10^{-6} U/cell trypsin. Therefore, similar trypsin activities seem to have different effects on process performance for cultivations with an ATF system or an IS.

One difference between both systems is that the bottom part of an IS is filled with a large number of cells, which have settled and are returned to the bioreactor in the underflow. In this region, limitations in the supply of oxygen or nutrients may occur. According to Shimoni et al. (2018), the VCC can be 3–5 x higher compared to that of the cell suspension in the upper part of the bioreactor [215]. For infection studies with IAV, an increased oxygen demand after trypsin addition is usually observed [114]. Accordingly, for the IS5-6 cultivation performed at a high VCC at TOI, oxygen depletion might have played a role in reducing virus titers. In addition, cells subjected to trypsin at high VCCs (50 x 10^6 cells/mL), may also be more sensitive to the shear stress induced by the recirculation pump operated at 35 mL/min. Perfusion cultivations performed at 50 x 10^6 cells/mL using a low shear recirculating pump (e.g. a Levitronix MagLev pump) with variation in trypsin activities and recirculation flow rates, could help to clarify this detail in a future study.

6.3.1 Selecting the most adapted cell retention device for influenza virus production in perfusion mode

For VCCs in the range of 24–27 x 10^6 cells/mL, STR-IS systems seem to be a good choice to achieve high CSVYs and P_vs. Compared to the use of an STR-ATF system (run ATF1), a 3.2-fold (Vir_{tot}) increase, a 4.7-fold (CSVY) increase and a 2.2-fold (P_v) increase for IS3–4 were obtained (Table 15). Compared to the use of a STR-AS system (optimized run AS4), a 2.0-fold (Vir_{tot}) increase, a 2.5-fold (CSVY) increase and a 1.3-fold (P_v) increase for IS3–4 were obtained (Table 12 and Table 15). In part, this increase was related to a continuous virus harvesting regime and the use of a heat exchanger operated at 27°C promoting virus production while decreasing the risk of virus degradation. Especially for temperature labile viruses or for live vaccines that require optimization of infectious titers, the option to continuously harvest without the risk of membrane blockage could make the difference in process intensification, and render cell culture-based virus production a viable alternative to traditional manufacturing.

However, for VCCs at TOI ≥ 50 x 10^6 cells/mL, the AS cell retention device indicated to be the one performing the best, as a 1.3-fold (Vir_{tot}) increase and a 1.9-fold (P_v) increase were obtained compared to the STR-IS system (Table 12 and Table 15). The CSVY was similar for both cases.

Other aspects such as the scalability, process robustness, footprint reduction and the need of manual work should be considered as well when selecting the most adapted cell retention device. In this regard, the three different mentioned perfusion systems are evaluated in chapter 7.

6.4 Author contributions

All experiments and data analysis were performed by both Juliana Coronel and Gwendal Gränicher. The chapter was reviewed by the co-authors of the paper: *Application of an inclined settler for cell culture-based influenza A virus production in perfusion mode* [221].

Chapter 7

Production of Modified Vaccinia virus Ankara by intensified cell cultures: a comparison of platform technologies for viral vector production

---

This chapter was based on the following publication:

Gränicher, G., Jordan, I., Tapia, F., Behrendt, I., *et al.*, Production of Modified Vaccinia Ankara virus by intensified cell cultures: a comparison of platform technologies for viral vector production. *Biotechnology Journal*, 2020.

7.1 Introduction

Up to now, the main focus was on IAV production for influenza vaccination. Another fast growing field using cell culture-based virus is gene therapy. More viral vector carrying genes of therapeutic interest or for vaccination are needed. Here, the focus was on MVA, which is a promising viral vector for use against various infectious pathogens such as coronavirus [36], or for immunotherapy and the treatment of some types of cancers. MVA production needs to be again carefully optimized as it is different than IVA production. Some highly relevant differences are: i) the virus size (MVA is larger), ii) the different replication dynamics, iii) DNA versus RNA virus and iv) the need of MVA to be produced as infectious particles.

MVA has been generated by adaptation to CEF [37]. This adaptation made MVA replication competent only in avian cells. In human cells, viral entry and protein presentation is still active, but no replication to new infectious particles is possible. For large viral vaccine programs, the necessary yields are difficult to obtain with the conventional production substrate (using CEF; section 2.2.1). To circumvent this concern for production of MVA, an avian suspension cell line (AGE1.CR.pIX) has been developed previously [55], that together with a new MVA strain (adapted to the present cell line) [59, 60], facilitate process intensification and enable continuous virus harvesting. The virus strain, MVA-CR19, has a reduced dependency on direct cell-to-cell contacts, and allows the product harvesting directly from the supernatant without the need of cell lysis [59, 60].

Based on these developments, new options for process intensification were available. In this chapter, the focus was on cell cultures at HCD using batch or perfusion strategies (above 25×10^6 cells/mL) [99, 100], and on continuous cultivations at low VCCs (chemostat mode; 2–5×10^6 cells/mL) [104] for MVA production.

The use of the STR-ATF system led to successful production of the MVA-CR19 virus strain as well [110]. In addition, it was shown that pseudo perfusion in SFs was possible and that virus yields were comparable to the production in the ATF system. With this scale-down model, screening and optimization of different feeding strategies improved P_v [110, 145]. A follow-up study showed that this optimized strategy could successfully be transferred into a bioreactor set-up leading to a hybrid process combining a perfusion strategy at HCD (> 25×10^6 cells/mL)

during the whole run with V_w expansion after virus infection (STR-ATF hybrid perfusion system) [90].

Although a successful membrane-based perfusion system for MVA production was established, various other aspects needed to be addressed to further improve productivity. The first aspect was the possibility to harvest continuously the virions released. As already studied in chapters 5–6, a continuous virus harvesting during the perfusion process should reduce virus inactivation. To test this hypothesis on MVA, the STR-AS and STR-IS systems were tested as well. Both systems were operated under optimized process parameters determined previously for IAV production in chapters 5–6.

The second aspect concerned the option of MVA production in perfusion mode using exclusively single-use material. Considering production of MVA vectors for timely vaccine development against emerging diseases or pandemics such as COVID-19, it would be very important to quickly set-up high-yield production facilities at the place of highest need. In addition, single-use disposable components could easily be installed in laboratory containers or within hospital settings. The performance of two different perfusion systems that are commercially available in single-use was evaluated in a few, non-optimized scouting runs. The first system involved a single-use OSB coupled to a single-use ATF system (OSB-ATF system). Process conditions were adapted for MVA propagation in AGE1.CR.pIX cells following a previous study for IAV production [114]. The second system involved a small-scale HFBR, again operated with process parameters based on a previous study for IAV production [144] allowing here, as well, MVA production in perfusion mode. As both studies were designed only as scouting experiments without further optimization a fair comparison of productivities is difficult. Nevertheless, these platforms are available and show a high potential for success after further optimization.

Finally, the various options for intensification of MVA production are compared. For reasons of comparability, the focus was on AGE1.CR.pIX cell-based processes to identify the most promising cultivation strategy. To allow for a fair comparison, the CSVY, Vir_{tot} and P_v were calculated following the same method. Overall, a whole set of process options is now available, not all fully optimized, but all with high potential to establish a large-scale manufacturing platform for intensified MVA production. Together with the results on IAV this

can even be seen as a very comprehensive overview for process options to produce enveloped lytic viruses with a diameter of 100–400 nm.

7.2 Results

Over the last years, a considerable amount of work was already dedicated on the USP intensification of cell culture-based MVA production. However, so far, all approaches focused on STR-ATF systems only [90, 110]. Here, analogous to the presented IAV perfusion experiments, the two different cell retention devices for continuous virus harvesting (AS and IS) were tested, and options for fully single-use perfusion operation were also evaluated. Based on the newly generated data and recently published data [90, 110, 167], virus yields were calculated and compared to different intensified MVA production modes (Figure 35) to determine the option showing the highest virus yields.

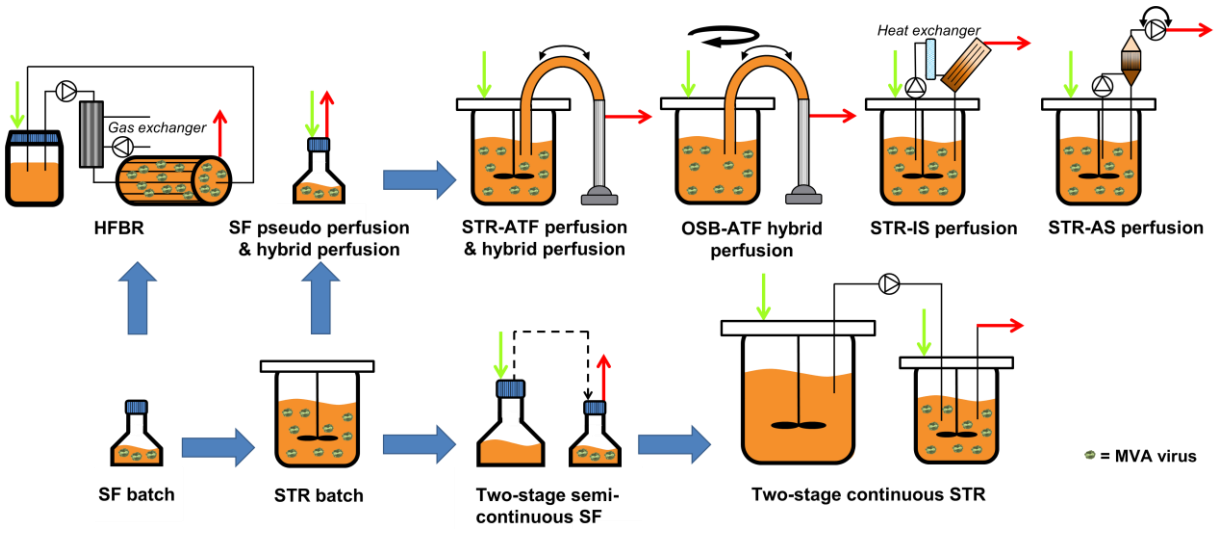

Figure 35: Simplified scheme of process options considered for yield comparisons towards establishment of a platform technology for MVA production. Green arrows indicate the continuous or semi-continuous addition of fresh medium during cultivation. Red arrows indicate continuous or semi-continuous removal of cell culture broth containing either only medium, medium with cell debris, medium with cells or – during virus production phase – medium with MVA or medium with cells, cell debris and MVA. Thick blue arrows indicate stepwise process development performed in the Bioprocess Engineering group.

7.2.1 Cell growth and virus production in perfusion cultures using different cell retention devices

Cells were cultivated in a STR coupled to either an ATF system, an AS or an IS. To allow for a better comparison, the same cell line (AGE1.CR.pIX) with the same virus seed (MVA-CR19.GFP) were used, and cultures were always infected at a VCC between 20 × 10^6 and 30 × 10^6 cells/mL for run 1 (STR-ATF), run 2 and 3 (STR-AS) and run 4 (STR-IS). After infection, the perfusion rate was kept constant at an average of 1.65 day^{-1} for runs 1–4. The selected process parameters corresponded to optimized parameters for the specific cell retention device reported earlier for production in perfusion mode of MVA [90, 115, 213, 221], and of IAV (chapters 5–6).

For all three perfusion set-ups, cell growth dynamics, cell viabilities and cell metabolites levels before and after infection were compared as illustrated in Figure 36. Similar cell growth dynamics and cell viabilities (> 90%) were observed for all systems during the cell growth phase (Figure 36A-B). After MVA infection, the highest maximum VCC was observed for the STR-ATF system, compared to the STR-AS and the STR-IS (STR-ATF: 51 × 10^6 cells/mL; STR-AS: 36 and STR-IS: 33 × 10^6 cells/mL). A decrease of VCCs and cell viabilities was observed about 36 hpi for all three cell retention devices (Figure 36A-B). Furthermore, no significant differences in lactate (5–20 mM) and ammonium levels (< 2 mM), which are the two main by-products of cellular metabolism, were observed. Equally, no limitation in glucose concentration (> 10 mM) was observed for runs 1, 2 and 4 (Figure 36C).

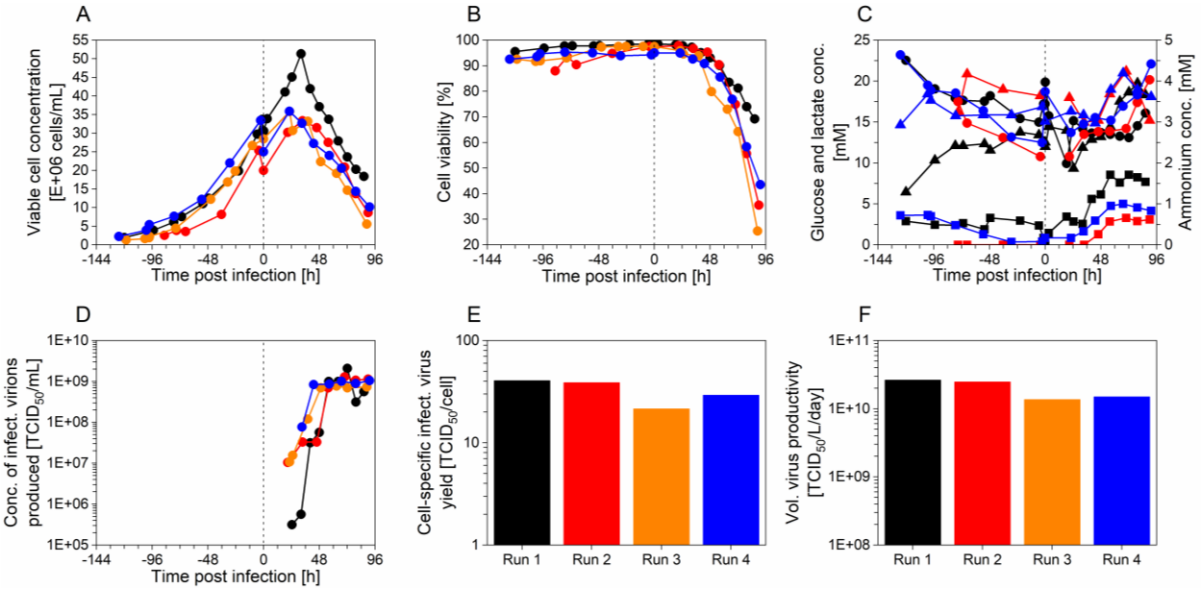

Figure 36: Perfusion mode cultivations in stirred-tank bioreactor for MVA-CR19.GFP production of AGE1.CR.pIX cells at high cell density. (A) Viable cell concentration (●), (B) cell viability (●), (C) cell metabolites (glucose (●), lactate (▲) and ammonium (■)), (D) concentration of infectious virions produced (●) (E) cell-specific infectious virus yield and (F) volumetric virus productivity with AGE1.CR.pIX cells for run 1 (ATF, black), run 2 (acoustic settler, red), run 3 (acoustic settler, orange) and run 4 (inclined settler, blue). Process parameters as described in sections 3.4 and 3.6. No data available for run 3, graph C. The vertical dotted lines correspond to the time of infection.

To assess the performance of the different perfusion set-ups, $C_{vir,\,tot}$, CSVY and P_v were determined (D-F). Similar dynamics of $C_{vir,\,tot}$ were found for runs 1–4. As expected, during the first 48 hpi, low amounts of infectious virions ($< 1 \times 10^8$ $TCID_{50}$/mL) were detected. The maximum $C_{vir,\,tot}$ was observed for all runs between 48 and 72 hpi (Figure 36D). A similar CSVY of 20–40 $TCID_{50}$/cell was calculated for all four runs. Taking into account the error of $TCID_{50}$ assays ($\pm$ 0.3 $\log_{10}$ ($TCID_{50}$/mL)), the differences are not significant. The same trend was observed for the P_v, where a yield of 2.6×10^{10} $TCID_{50}$/L/day was obtained for the ATF, again with a variation in yield for the other cell retention devices within the error of the assay (Figure 36E-F).

One concern regarding MVA production in STR-ATF systems with virus accumulation inside the bioreactor is the loss of infectivity due to temperature influences, degradation due to proteases released from lysed cells, and other unspecific mechanism. Therefore, as a control, the infectious virus titer was monitored by incubating a defined amount of $TCID_{50}$ in cell culture supernatant at 37°C (section 3.8.2). No decrease of MVA infectivity was observed for a time window of 24 h (Figure 37), which corresponded to the time between the start of virus release into the supernatant and the maximum $C_{vir,\,tot}$ (Figure 36D).

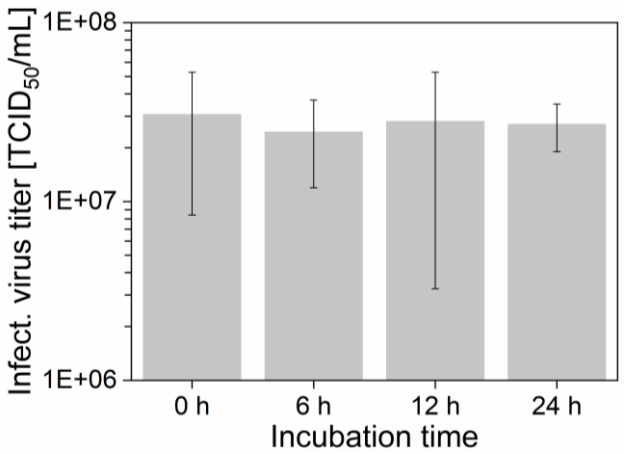

Figure 37: Stability of the MVA infectivity ($TCID_{50}$ titer) over time (0, 6, 12 and 24 h) when incubated at 37°C and pH over 7.2 in cell culture supernatant, as described in section 3.8.2. Error bars correspond to the standard deviation of biological triplicates.

7.2.2 MVA production in single-use perfusion systems – OSB-ATF and HFBR

Single-use equipment allows for rapid and flexible virus manufacturing. In the context of process intensification, a scouting study was performed that used process knowledge from intensified IAV production with single-use equipment [114, 144] as a proof-of-concept. Two different available systems were tested: the OSB (Adolf Kühner AG system) coupled to an ATF system (run 5), and the HFBR (PRIMER system from Biovest Intern. Inc.) (runs 6–7). The single-use OSB was connected to an ATF system as no advantage regarding a virus yield, CSVY or P_v was observed with other cell retention devices as shown above (Figure 36D-F). Cell growth, virus titers and yields were then compared to the two control runs reported by Vazquez et al. (2019) [90] using the same cell line (AGE1.CR.pIX) and same virus strain (MVA-CR19) (Figure 38). The control runs correspond to run 8 and 9. For all cultivations, the virus was always accumulated inside of the bioreactor as the used cell retention devices are membrane-based.

Suspension cells were infected at a VCC between 17×10^6 and 25×10^6 cells/mL for runs 5 and 8–9. Run 5 (OSB-ATF system) reached a VCC after infection above 40×10^6 cells/mL while a lower VCC was obtained for the STR-ATF system ($< 30 \times 10^6$ cells/mL, runs 8–9). However, a low maximum $C_{vir, tot}$ of 6.0×10^7 $TCID_{50}$/mL was achieved for the OSB-ATF compared to the STR-ATF control runs 8–9 ($5.6–8.0 \times 10^9$ $TCID_{50}$/mL) (Figure 38A-B). This led to very poor CSVY and P_v yields for run 5 compared to the control runs 8–9, which had a CSVY of 158–281 $TCID_{50}$/cell and a P_v of $7.4–22.8 \times 10^{10}$ $TCID_{50}$/L/h (Figure 38C-D).

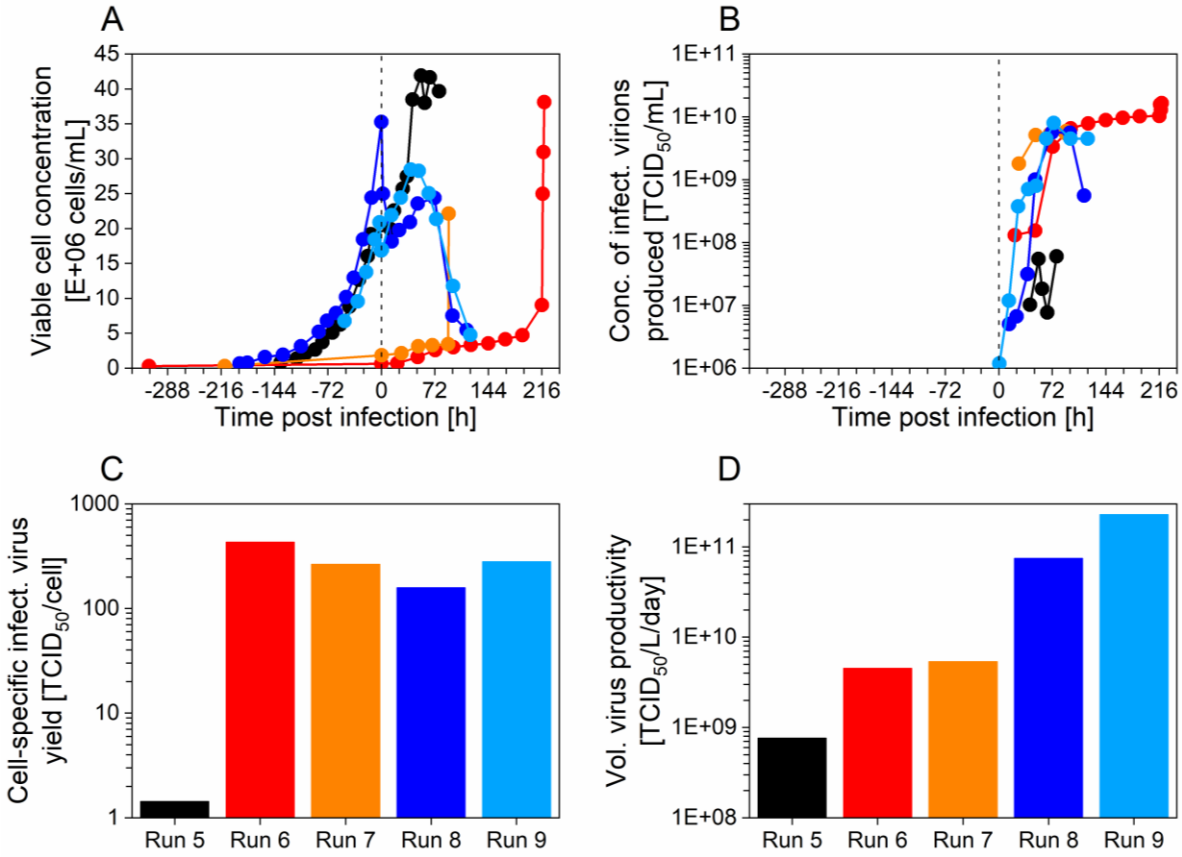

Figure 38: Perfusion mode cultivations in single-use orbital-shaken bioreactor with ATF (OSB-ATF) and hollow-fiber bioreactor (HFBR) for MVA-CR19 production in AGE1.CR.pIX cells at high cell density. (A) Viable cell concentration (●), (B) concentration of infectious virions produced (●) (C) cell-specific virus yield and (D) volumetric virus productivity for the production of MVA-CR19 for run 5 (black, OSB-ATF in hybrid perfusion mode), run 6 (red, HFBR in perfusion mode), run 7 (orange, HFBR in perfusion mode), run 8 (dark blue, stirred-tank bioreactor with ATF in hybrid perfusion mode, control experiment, run hybrid 1 from Vazquez et al. (2019) [90]) and run 9 (light blue, stirred-tank bioreactor with ATF in hybrid perfusion mode, control experiment, run hybrid 2 from Vazquez et al. (2019) [90]). For run 6 and 7, cell concentrations given are from samples taken from the extra-capillary space when medium was exchanged; however, as many cells were attached to the hollow-fiber the overall cell concentrations might be higher. For the three last sampling points of run 6 and the last sampling point of run 7, the HFBR was flushed thoroughly to detach all cells. The vertical dotted lines correspond to the time of infection.

Regarding the HFBR system (runs 6–7), cell growth dynamics differed clearly compared to the control runs 8–9. The VCC remained constant after infection up to 5×10^6 cells/mL except at the end of the run where VCCs in the range $22–38 \times 10^6$ cells/mL were reached due to thorough flushing of the HFBR system, detaching a large quantity of the cells adherently growing on the hollow-fiber membrane (Figure 38A). Therefore, maximum $C_{vir,\,tot}$ values of $5.9–16.5 \times 10^9$ $TCID_{50}$/mL were obtained for runs 6–7, which were higher than for the control runs (Figure 38B). Similar CSVYs were obtained for runs 6–7 compared to controls (Figure 38C). As the overall process time was longer compared to the control runs and, due to the high

consumption of perfused medium (data not shown), the P_v yields were about 25 times lower (Figure 38D).

7.2.3 Comparison between different options for MVA production in batch, perfusion, hybrid perfusion or continuous mode

Figure 39 shows data of this study together with results of the Bioprocess Engineering group [90, 110, 167] obtained for other production platforms and production modes (Figure 35) to compare $C_{vir,\,tot}$, Vir_{tot} and the total number of cells present during the virus infection phase.

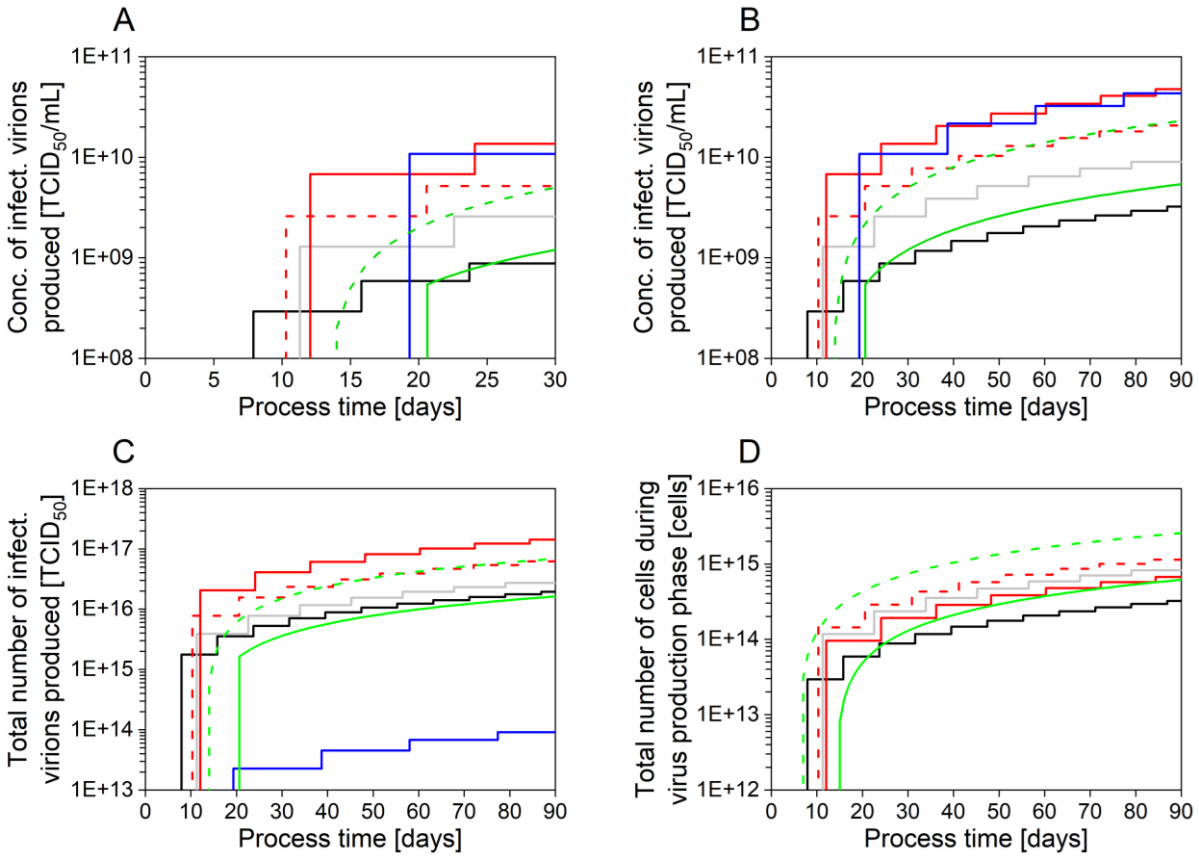

Figure 39: MVA production in batch, perfusion, hybrid perfusion or continuous mode. (A) Maximum concentration of infectious virions produced over a period of 30 days and (B) over a period of 90 days. (C) Total number of infectious virions produced considering the maximum production scale for single-use operation. (D) Total number of cells present during the virus production phase considering the maximum production scale for single-use operation. For graph D, the hollow-fiber bioreactor (HFBR) based process was not taken into account, as the monitoring of cell concentrations was difficult (section 3.4.4). Each step corresponds to one independent run. Batch (black, average of four runs, data not shown), perfusion (grey, average of runs 1–4), pseudo hybrid perfusion (dotted red, average of three runs, data not shown), hybrid perfusion (red, average of runs 8–9), HFBR (blue, average of runs 6–7), two-stage semi-continuous shake flask cultivation system (dotted green, average of runs SM25-A and SM25-B [167]) and two-stage continuous stirred-tank cultivation system (green, run T25 [167]). For a more accurate estimation, the process time includes one day for system set-up before the start of a cell culture run and one day for system clean-up/disassembly at the end of the run. For graphs C and D, the maximum single-use production scales assumed were: batch, 6000 L [222]; perfusion and hybrid perfusion, 3000 L (www.samsungbiologics.com); continuous, 6000 L (cell growth bioreactor) and 3000 L (virus production bioreactor) [222]; HFBR, 2.1 L [223, 224].

As expected, the lowest $C_{vir, tot}$ was achieved for MVA production in batch culture, although virus concentrations already increased after eight days (process time; Figure 39A-B). Over 90 days of process time, the highest $C_{vir, tot}$ value was found for the STR-ATF hybrid perfusion system and the HFBR (Figure 39B). Assuming that the CSVY is the same when all processes are optimized (not achieved here for continuous production), the focus would not only be on the virus production, but also on the cell production capacity. What is also compared among these systems is therefore how fast and easily cells that are readily infected and deliver a product (virus) could be produced, as illustrated in Figure 39D. Here, the highest theoretical amount of produced cells after infection would be obtained for the two-stage semi-continuous SF cultivation system (Figure 39D).

Due to a limited scalability, the lowest theoretical Vir_{tot} would be obtained for the HFBR after 90 days of process time (Figure 39C). When producing MVA in a HFBR or in a two-stage continuous STR cultivation system 19 and 21 days, respectively, were necessary before virus production started, which was the longest period compared to all other process options (Figure 39A-C).

Compared to batch culture, a higher $C_{vir, tot}$ was achieved after about 25 days for the two-stage continuous STR cultivation system (Figure 39A-B). More cells could be obtained during the virus production phase with the two-stage semi-continuous SF system compared to a non-continuous system after 11 days of process time (Figure 39D). Virus production in hybrid perfusion mode allowed to produce over four times more virus after 90 days of process time compared to the perfusion mode (Figure 39C). Interestingly, the small-scale experiments (pseudo hybrid perfusion and two-stage semi-continuous SF cultivation) did not follow the same trends as the respective large-scale experiments (hybrid perfusion and two-stage continuous STR cultivation). The increase in $C_{vir, tot}$ was 2-fold (after 90 day of process time) for the large-scale hybrid perfusion system compared to the pseudo hybrid perfusion system in SFs. A 4-fold decrease in $C_{vir, tot}$ was observed when scaling-up from the two-stage semi-continuous SF cultivation system to the two-stage continuous STR cultivation system, also after 90 days of process time (Figure 39B). Furthermore, fewer cells were produced when using the two-stage STR cultivation system compared to the semi-continuous SF cultivation system (Figure 39D).

7.3 Discussion

In the following, the different options for operation of perfusion system characterized in this study are compared based on virus production yields. In a next step, published results for other available cell culture platforms for MVA-CR19 production [90, 110, 167] are taken into account using the same approach.

Surprisingly, no increase in virus productivity (based on CSVY and P_v) was observed for the use of AS or IS cell retention devices allowing continuous harvesting (Figure 36E-F). This is in contrast to other studies conducted by other groups or described in chapters 5–6, on IAV, lentivirus and adenovirus production, which demonstrated advantages regarding continuous virus harvesting in perfusion cultures [40, 107-109, 213, 221]. Regarding the cell growth phase, a similar growth dynamics and a high cell viability (> 90%) was achieved. Non-toxic levels of released metabolites (< 20 mM lactate and < 3 mM ammonium) were observed regardless of the cell retention device, demonstrating a healthy state of the cells allowing high productivity after infection as already observed in previous studies [42-45] (Figure 36A-C). The period for virus release into the supernatant was observed to last 24 h, between 48–72 hpi (Figure 36D). The conducted study also showed a high stability of the infectious MVA when incubated in cell culture supernatant at 37°C for 24 h (Figure 37, method described in section 3.8.2). By consequence, for the ATF runs without an option for continuous harvesting, virus accumulation inside of the bioreactor should not have any negative impact, as long as the cell culture is harvested about 24 h after the virus titers start to increase. This could also explain that process yields were more or less the same for processes operated with different cell retention devices. The fact that $C_{vir,\,tot}$ decreased about 6.6-fold after 72 hpi for the ATF run, still hints to a certain risk of MVA degradation when incubated for more extended periods (run 1, Figure 36D). As the residence time in the bioreactor was lower than 24 h due to the high perfusion rate (1.65 day^{-1}), no decrease in $C_{vir,\,tot}$ was observed 72 hpi for the AS or the IS based processes, which might offer a larger flexibility regarding the time of harvest compared to the ATF run (Figure 36D). In case other hollow-fiber membranes will become available for use in ATF mode that allow for a continuous virus harvesting, then clearly this should be reevaluated (new prototype hollow-fiber membrane later tested, and reported in the Appendix, section 10.5).

The establishment of single-use virus production systems in perfusion mode presents many advantages over traditional batch processes in stainless steel bioreactors, i.e. reduced operating and validation costs coupled with the avoidance of clean-in-place and steam-in-place methods [216, 225]. Furthermore, single-use concepts offer high flexibility for the change of production campaigns and installation of manufacturing facilities at the place of need in case of pandemics. So far, however, only few studies have explored options for virus production in fully single-use perfusion systems [114, 144]. Similarly to Coronel et al. (2019), the specific growth rate of AGE1.CR.pIX cells in OSB-ATF was equal to that in conventional STRs coupled to an ATF system [114]. However, for the scouting experiment performed here with the OSB-ATF system, only low titers were obtained. Furthermore, the VCC increased strongly after infection when using the OSB (42 vs 28 × 10^6 cells/mL). This might indicate that only a small percentage of cells was infected by the MVA – probably due to the non-optimal MOI caused by the lack of seed virus for the chosen V_w of the OSB (Figure 38). This is in contrast with previous AGE1.CR.pIX cell cultivations in perfusion mode for the production of IAV using the OSB where very high yields were obtained with all cells being infected [114]. Nevertheless, this first scouting experiment showed that MVA production is possible at high VCCs (above 40 × 10^6 cells/mL) in single-use systems, but that further optimization would be needed to achieve titers comparable to STR-ATF system.

The CSVYs obtained with the HFBR seemed comparable to control runs (Figure 38C) although this value might be overestimated due to problems with cell counting. Tapia et al. (2014) estimated a theoretical MDCK VCC of 40 × 10^6 cells/mL based on the known cell concentration per cm^2 of confluent T-flasks, and measured a VCC of 28 × 10^6 cells/mL in the same HFBR system (in the same range as here: 22–38 × 10^6 cells/mL) [144]. A similar comparison could be performed for AGE1.CR.pIX cells. An increase of the CSVY was, however, expected in this study as adherent cells tend to allow for higher CSVY in general [144].

One major difference between recombinant protein production [99, 138, 226] and virus production in perfusion mode is that the virus cannot be produced over extended periods as virus infection involves apoptosis and cell lysis [39, 104]. For the establishment of a truly continuous system, two interconnected bioreactors are needed, one for cell growth and one for virus production [167]. This raises the question if the footprint of a plant can also be reduced when production requires several consecutive runs in perfusion mode to harvest an

equal number of virions (compared to a run in continuous mode or consecutive runs in batch). In order to evaluate the various options for virus production, not only the increase in $C_{vir, tot}$ and Vir_{tot} over time should be considered, but also many other aspects such as process complexity or robustness, as listed in Table 16.

Table 16: Advantages and disadvantages of MVA production in different cultivation systems. Each important aspect to be considered for virus production was rated from + (minimum) to ++++ (maximum).

	Batch	Pseudo perf.	STR-ATF [a]	STR-AS	STR-IS	OSB-ATF	HFBR	Semi-conti.	Conti.
Low complexity	++++	++	++	++	++	++	+++	+	++
Single-use	++++	++++	++++	+	++++	++++	++++	++++	++++
High P_v	+++	+++	++++	+++	+++	+	+	++	++
Process robustness [b]	++++	++	+++	++	+++	+++	++	+	++
Small footprint [c]	+	+++	++++	++++	+++	+	++++	+++	++++
Low manual work	++++	+	+++	+++	+++	+++	++	+	++
Scalable	++++	+	++++	+++	+++	++++	++	+	++++

Pseudo perf.; pseudo perfusion in shake flask, STR; stirred-tank bioreactor, AS; acoustic settler, IS; inclined settler, OSB; single-use orbital-shaken bioreactor, semi-conti.; two-stage semi-continuous shake flask cultivation system, conti.; two-stage continuous stirred-tank bioreactor cultivation system.

[a)] Includes the virus production in perfusion mode and in hybrid perfusion mode.

[b)] Estimated risk of failure during the run.

[c)] Takes into account the working volume of the bioreactor plus the volume of the cell retention device coupled to the bioreactor to produce MVA in perfusion mode (corresponds to the $C_{vir, tot}$ data presented in Figure 39A-B).

Batch cultures and cultivations in the STR-ATF system show most advantages regarding MVA production as illustrated in Table 16. The biggest advantages of the batch production over the other manufacturing platforms are the low complexity of the process, high process robustness and the low demand for manual work (Table 16). However, one major drawback is the relatively large footprint needed to produce an equal number of virions compared to any other process, as also shown in Figure 39C.

Cultivations in HFBR could be an interesting option for process intensification. Higher $C_{vir, tot}$ compared to the batch, perfusion and continuous systems were obtained with the HFBR, making this production platform one of the best options in terms of $C_{vir, tot}$ after 19 days (Figure 39A-B). However in contrast to the STR-ATF system, it is not easily scalable due to challenges regarding uniform cell seeding for large surfaces (unpublished results). HFBRs with up to 10 times the membrane area (2.1 m^2, AcuSyst-Xcellerator, Cell Culture Company) are available [223, 224]. This is, however, only a scale-up factor 42 compared to the tested HFBR (Figure 39C), and limits MVA production to laboratory scale use and production of material for first clinical trials. Furthermore, the HFBR cultivation resulted in low P_v values (Table 16 and Figure

38D), which could be explained by the high consumption of medium to produce large amounts of virions. However, this could be taken into account if media consumption would be the limiting cost factor.

A major drawback of two-stage continuous STR cultivation systems, as shown in Table 16, is their low robustness due to relatively high equipment requirements and complex handling. Furthermore, extended process times bear a certain risk of unwanted virus mutations, although this was not reported for MVA [167]. Overall, the process time has to exceed 25 days before this option outperforms batch processes (Figure 39A-B). However, continuous mode operation also has the potential for significant scale-up in volume. In addition, small-scale semi-continuous experiments showed not only high Vir_{tot} but also the highest increase in cell number during the infection phase (Figure 39C-D). Accordingly, it has the potential to reach the highest virus yields after 11 days in case that the CSVY would be in a similar range as for the other optimized processes. However, it has to be taken into account that $C_{vir,\ tot}$ of the two-stage continuous STR cultivation system was reduced 3-fold because of the large V_w needed for the cell growth plus the virus propagation phase. As batch cultures in SFs are the performance benchmark for optimizing larger batch processes in bioreactors, two-stage semi-continuous SF cultivation should function as a performance benchmark for optimizing a two-stage continuous STR cultivation.

A difference was observed after scale-up from SFs to STRs for pseudo perfusion and semi-continuous experiments. Cultivations in SFs show several significant differences compared to STRs, i.e. the ratio between the maximum local energy dissipation and the mean power input is smaller. Optimization of these process options in parallel (mini)bioreactors could circumvent scale-up issues [227-230].

Cultivations using the OSB-ATF system resulted in rather low production yields (Figure 38C-D). Furthermore, this set-up required a relatively large footprint (Table 16) which makes this option less attractive. Eventually, the use of an IS or an AS device would also be an interesting option compared to the ATF system; however, AS devices are at the moment not available in single-use and the IS has a rather large footprint (Table 16).

A limitation of the current approach is the limited number of cultivations performed for each set-up. As it is often the case for complex biotechnological processes, reproducibility can be an issue. In addition, due to the rather large error of infectivity assays used for virus

quantification (section 3.12.4), differences in P_v, Vir_{tot} or CSVY have to be rather large to be considered significant. Accordingly, the conducted investigation (and other similar studies on virus production) can only serve as a first orientation regarding the set-up of process platforms for large-scale manufacturing. The pros and cons of a large number of process options could be identified, which provide a solid basis for a more detailed process intensification approach.

A cost-effectiveness analysis when evaluating the different process options would be further beneficial. Various studies have used static or dynamic models to compare costs of fed-batch and perfusion strategies in recombinant protein production [120, 231-233]. However, to the knowledge of the author, no such study was performed for virus production in perfusion mode, so far. Software like SuperPro Designer® (Intelligen Inc., USA) could support this and allow to identify key factors limiting the use of particular production systems. Finally, for a complete analysis, DSP should also be integrated, which would further increase the level of complexity. The study described in chapter 8 contains an economic analysis for an end-to-end MVA production in batch and perfusion mode.

Intensified USP with increased MVA titers can have a significant impact on the DSP. Depending on unit operations established for conventional MVA-based processes, it might be required to modify DSP, i.e. cell clarification and product concentration steps before chromatography-based operations are used. In fact, DSP efficiency might be the criterion for the selection of the appropriate USP platform for an end-to-end virus production process. A recent study evaluating different production platforms for AAVs estimated DSP costs to be equal to about 40% of the overall cost of good per dose for a 1000 L suspension cell culture in batch [234]. However, in this case, neither the DSP technique and DSP yield nor DSP costs per dose were influenced by the intensification of the USP. Thus, the overall impact of DSP on the economic modelling was considered to be negligible [234]. Integration of the MVA production in perfusion with DSP, or MVA production in batch mode integrated to DSP would be studied more in detail in chapter 8. As observed in chapter 5, it was indicated possible issues with IAV production in a STR-ATF system where higher titers and product accumulation in the bioreactor resulted in the formation of large virus aggregates, in contrast to a STR-AS perfusion system allowing continuous harvesting. In particular, the presence of such large-sized aggregates might impair clarification and subsequent chromatography steps developed for normal batch USP conditions. As dilution by continuous harvesting decreases proteins,

host cell DNA and the virus concentration in the medium, STR-AS perfusion and STR-IS perfusion might facilitate DSP in general, which is the reason why the STR-AS perfusion system was chosen for process integration in chapter 8. For the two-stage continuous STR, the purification yield is expected to be similar to batch STR as similar virus titers are obtained in the harvest [167]. Regarding the amount of process-related impurities per produced dose, it was observed for IAV production in chapters 5–6 that the amount of host cell DNA and total protein per virions was not changed when producing the virus with a STR batch, a STR-ATF perfusion or a STR-AS perfusion.

In conclusion, various options for MVA production in batch and in perfusion mode using three different cell retention devices were compared. Virus yields did not depend on continuous harvesting due to the high stability of infectious MVA titers at 37°C. However, continuous harvesting may offer more flexibility regarding the time of harvest. Scouting experiments with a HFBR or an OSB-ATF system indicate that establishment of a fully single-use perfusion process should also be considered. However, regarding the OSB-ATF system, further optimization would be needed to increase productivity. Finally, a broad comparison between all available process options indicated an advantage of hybrid perfusion strategy in a STR-ATF system over standard perfusion and continuous cultivation regarding footprint reduction, P_v, scalability, process robustness, and options for single-use manufacturing. Once optimized, however, a two-stage continuous STR cultivation system might offer the highest potential for production of large volumes as it allowed to achieve the highest number of cells during the infection phase, which is necessary for obtaining maximum virus yields. Batch processes have still various advantages compared to cultivations performed in STR-ATF systems (Table 16). However, there is a higher potential for the hybrid perfusion strategy in an STR-ATF to outperform batch processes if advantageous aspects of batch processes (such as lower complexity, higher robustness and lower demand for routine tasks and supervision) can also be improved for perfusion processes. Process automation could for example make the hybrid perfusion strategy more attractive. With the presented process options, several high-yield platforms are now available to choose for efficient and economic viral vector manufacturing for future needs.

7.4 Author contributions

The experiments with the STR-ATF, STR-AS and STR-IS were performed by Gwendal Gränicher. The experiments with the HFBR were performed by Felipe Tapia. The experiment with the OSB-ATF was performed by Ilona Behrendt. Gwendal Gränicher performed all data analysis, except for the data obtained with the HFBR, analyzed jointly with Felipe Tapia. The chapter was reviewed by the co-authors of the paper: *Production of Modified Vaccinia Ankara Virus by Intensified Cell Cultures: A Comparison of Platform Technologies for Viral Vector Production* [235].

Chapter 8

An integrated end-to-end MVA production in perfusion mode

This chapter was based on the following publication:

Gränicher, G., Babakhani, M., Göbel, S., Jordan, I., et al., A high cell density perfusion process for Modified Vaccinia virus Ankara production: Process integration with inline DNA digestion and cost analysis. *Biotechnol Bioeng*, 2021.

8.1 Introduction

To date, the implementation of an integrated perfusion process is one option to decrease manufacturing costs and to potentially increase the quality of a product [98, 100, 138, 139]. A considerable amount of research has been conducted on integrated continuous production of recombinant proteins such as mAbs [78, 86, 106, 140-142]. There, the capability to offer improvements in biopharmaceutical product quality has been shown [143]. However, to the knowledge of the author, an integrated viral vector production system in perfusion mode has not been reported in the literature.

Similar to recombinant protein manufacturing, process intensification for viral vectors could be a solution to lower production costs and space requirements for culture vessels (section 2.6). Process intensification may also help to satisfy the increasing demand for viral vectors at high concentrations for R&D, clinical trials, and commercialization [7, 97]. Intensification can be achieved with bioreactors coupled to devices for harvesting of infectious viral particles with subsequent continuous purification. A techno-economic analysis would provide insights about cost differences between a batch and a perfusion process [234-236]. Similarly to recombinant protein production [120, 231-233], a model to compare costs of batch and perfusion strategies could allow to identify key factors and bottlenecks allowing to improve cost-effectiveness even more. Only a few studies in bioprocess economics related to viral vector manufacturing for gene therapy were performed, so far [165, 234]. Up to now, no studies evaluated the costs of virus production using a perfusion system linked to a suspension cell culture.

As mentioned in chapter 7, the establishment of integrated perfusion processes requires the use of cell retention systems that allow high process robustness, scalability, and continuous virus harvesting. In addition to cell retention as a preemptive processing step, continuous virus harvesting could also result in higher production yields and better product quality [107, 109, 213]. Based on chapter 7, an AS was chosen here as a cell retention device for process integration.

The use of an online probe measuring the electric capacitance allows to monitor VCC, cell size, metabolic state, apoptosis and viral infection [88-91]. In addition, it was shown that capacitance sensors can be used to determine other key process parameters, i.e. the optimal time of virus harvest [92, 93].

Here, for the first time a fully integrated cell culture-based perfusion system that allows an end-to-end viral vector production at HCD is presented. The avian suspension cell line AGE1.CR.pIX was used to produce MVA. A capacitance sensor was used to monitor cell growth, control the perfusion rate, and decide on the time of virus harvesting. For viral vector purification, a semi-continuous method using membrane-based SXC was directly linked to the continuous virus harvest stream. The collected data allowed then for an academic techno-economic analysis between batch and perfusion.

8.2 Results

8.2.1 Intensified cell culture for MVA production.

The two perfusion experiments using the AS (runs 10–11) were compared to a control batch process, operated in triplicate (runs A-C). Achieving maximum VCCs of 36.9–38.0 x 10^6 cells/mL (Figure 40A), an average recovery of 107 ± 18% was observed for the virus material collected after the settler (volume = 2.8–2.9 L; Figure 40B). The Vir_{tot} produced in the harvest and in the bioreactor vessel was 20.4 x 10^{11} and 9.1 x 10^{11} $TCID_{50}$ for run 10 and 11, respectively (Figure 40B). For the batch runs, an average Vir_{tot} of 2.4 ± 0.6 x 10^{11} $TCID_{50}$ was measured. For the perfusion runs, the CSVY was 24.0 and 55.4 $TCID_{50}$/cell, and the P_v 1.43 and 2.53 x 10^{10} $TCID_{50}$/L/day for run 10 and 11, respectively. As a comparison, an average CSVY of 46.9 ± 13.2 $TCID_{50}$/cell and an average P_v of 3.82 ± 0.93 x 10^{10} $TCID_{50}$/L/day were obtained for the batch runs A-C (Figure 40C-D).

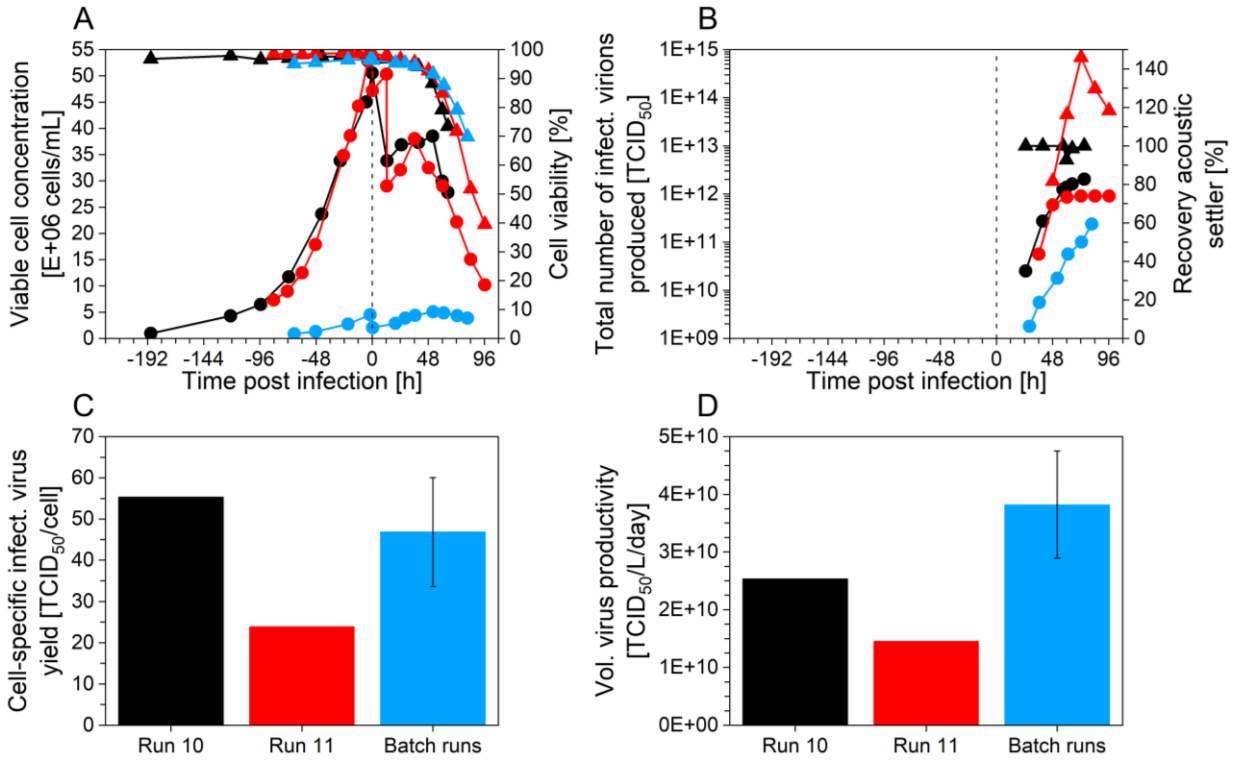

Figure 40: MVA production in AGE1.CR.pIX cells in perfusion and in batch mode (stirred-tank bioreactor, CD-U5 medium). (A) Viable cell concentration (●) and cell viability (▲), (B) total number of infectious virions produced (●) and recovery coefficient (from the acoustic settler filtration step) (▲), (C) cell-specific infectious virus yield and (D) volumetric virus productivity (for infectious virions). The black, red and blue colors correspond to run 10, run 11 (one replicate) and the batch runs (average from runs A-C, in triplicate), respectively. The error bars on graphs C and D correspond to the standard deviation of the batch runs performed in triplicate.

8.2.2 Process integration for viral vector production

Compared to the batch processes A-C, similar MVA recovery and impurity levels were obtained during purification (Figure 41; DSP as in section 3.11). Total recovery for batch (runs A to C) and perfusion (run 10) was equal to 54.7% and 50.5%, respectively (Figure 41A). Recovery for depth filtration was 59.8–81.6%. The DNA digestion step allowed for the perfusion and batch process an about 3 $\log_{10}$ depletion of host cell DNA per dose, reaching <10 ng host cell DNA/dose (assuming a MVA dose input of 1.43 x 10^8 $TCID_{50}$; section 3.13.4). Compared to the raw material in the bioreactor, the total protein amount per dose decreased by a factor of 18.3 for the perfusion and 2.2 for the batch system after purification by SXC (final value: 11–37 µg total protein/dose; Figure 41C). When performing a two-sample t-test, the decrease of host cell DNA per dose and the decrease of total protein per dose was found to be statistically significant (p value <0.05) for the perfusion and batch systems, respectively.

The large error observed for host cell DNA per dose (perfusion mode) after the depth filtration step (Figure 41B) was probably due to partial host cell DNA digestion as endonuclease was added in bottle B2 (Figure 19) and sampling times were different. Considering only the bioreactor volume for the volumetric virus yield calculation, a STY of 10.5×10^{10} $TCID_{50}/L_{bioreactor}$/day for the perfusion and $1.7 \pm 0.3 \times 10^{10}$ $TCID_{50}/L_{bioreactor}$/day for the batch processes were obtained. This comparison is relevant in order to assess the impact on the footprint and the potential of perfusion considering all the aspects from USP to DSP.

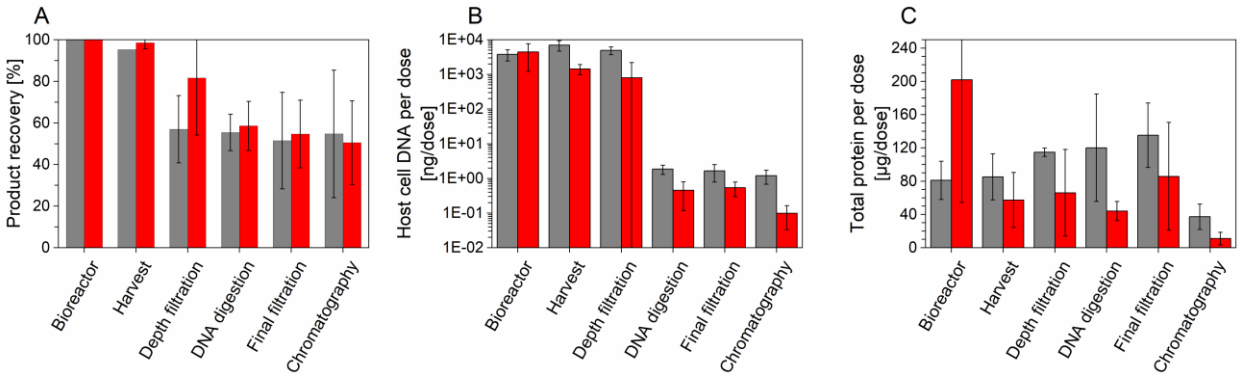

Figure 41: Product recovery and impurity removal of the different purification steps for the integrated batch or perfusion processes. (A) Percentage recovery of the total number of infectious virions of individual process steps, (B) level of host cell DNA per dose, and (C) level of total protein per dose of the integrated batch processes (grey) and the integrated perfusion run 10 (red). To estimate contamination levels, a MVA dose input of 1.43×10^8 $TCID_{50}$ was assumed (see section 3.13.4). The MVA raw material for steric exclusion chromatography was purified in semi-continuous mode, as described in section 3.11.3. Error bars of the batch process correspond to the standard deviation of triplicate runs, as described in section 3.9.2. Error bars of run 10 correspond to the standard deviation of the yields for continuous harvesting between 36 and 87 hpi (time intervals between samples < 14 h), as described in section 3.13.3.

8.2.3 Control of perfusion rate and MVA harvesting time based on online capacitance probe measurements

The perfusion rate during the cell growth phase could be successfully controlled using a capacitance probe for run 10. No offset between the offline VCC and online VCC was observed (Figure 42). A CSPR of 48.0 pL/cell/day was kept constant during at least three days before virus infection. The first CSPR value obtained 96 h before infection was estimated too high due to a pump calibration error. No limitation in glucose concentration was observed during the whole run (data not shown).

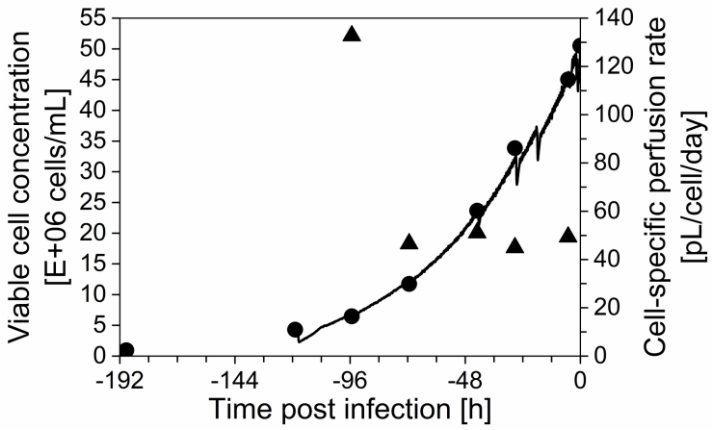

Figure 42: Online monitoring of cell concentrations using a capacitance probe for process automation and control during the growth phase of run 10 (AGE1.CR.pIX cells grown in perfusion mode using an acoustic filter). Offline (●) and online (black line) viable cell concentration, cell-specific perfusion rate (▲). The cell factor (described in section 3.7.2) converting the permittivity signal to a viable cell concentration was equal to 0.57.

During the virus production phase, the trends of the offline VCC followed the same dynamics as for the $\Delta\varepsilon_{max}$ signal (Figure 43A and Figure 43C), except that the values were given every 8 to 14 h for the offline VCC and every 0.2 h for the online permittivity signal. A correlation between the VCC or the $\Delta\varepsilon_{max}$ signal was observed with the time of MVA release (defined as in section 3.11). For all runs including the batch run, the expected time of MVA release in the supernatant (based on the permittivity signal decrease time point plus 10.6 h; corresponding to the time when about 8 to 10% of Vir_{tot} was released from the infected cells) seemed to correlate with the increase of the virus titer in the bioreactor supernatant, reaching a titer in the range of 0.5–1.0 x 10^8 $TCID_{50}$/mL at that time point (Figure 43). By harvesting the perfusion bioreactor 10.6 h after the maximum $\Delta\varepsilon_{max}$ signal or maximum offline VCC (illustrated by the vertical line in Figure 43), 81–95% of the produced infectious virions could be harvested (see Appendix, section 10.9). Note: This time interval is an average from run 10, run 11, the control run (data from run *4*, chapter 7) and a batch run (run C) (see section 10.9, illustrated in Figure 43). For batch run C, a delay of the virus release and cell death was observed. Overall, the maximum permittivity signal was determined between 24–48 hpi (Figure 43). It is therefore suggested that the permittivity signal could help to decide on harvesting time.

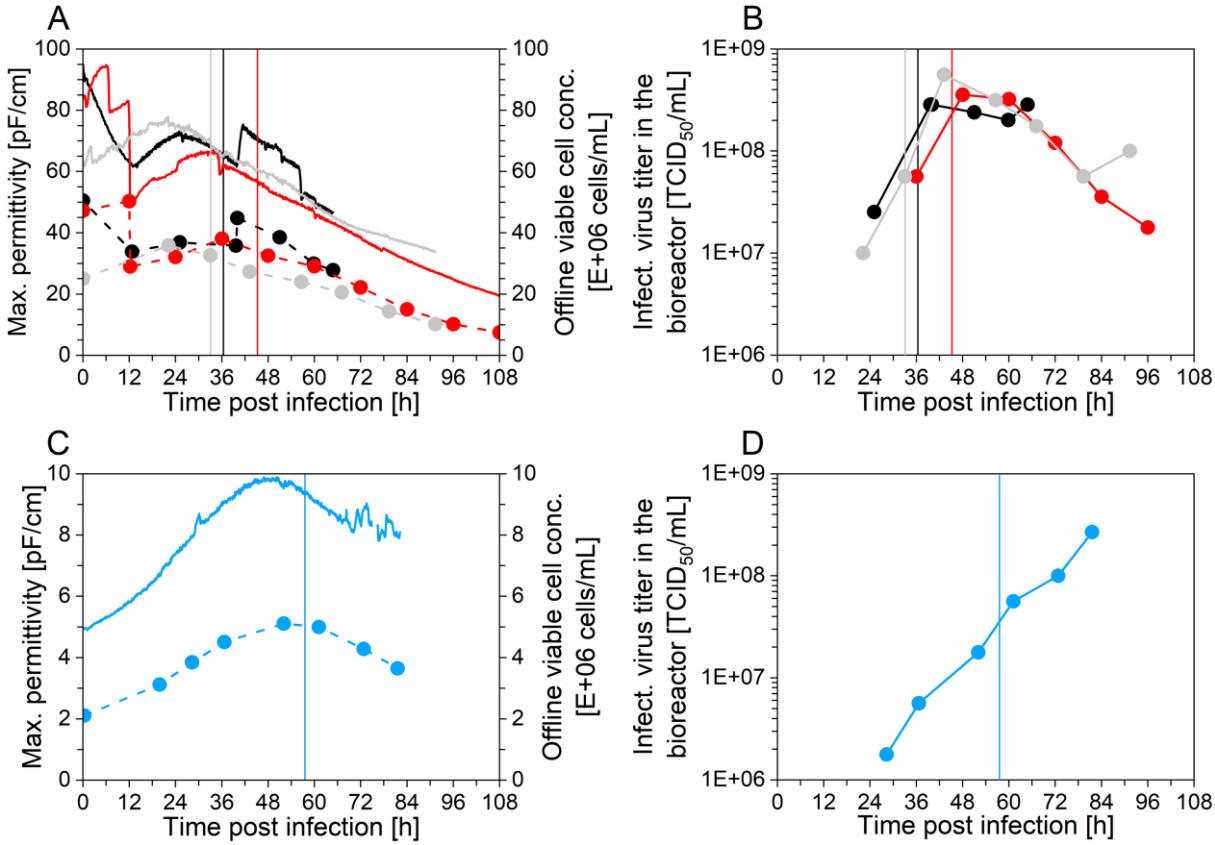

Figure 43: Online monitoring of a capacitance probe for process automation and control during MVA production using AGE1.CR.pIX cells. (A) Maximum permittivity signal ($\Delta\varepsilon_{max}$; solid line) and offline viable cell concentration (●) for 3 cultivations in perfusion mode (run 10 = black, run 11 = red, data from run *4*, chapter 7, = grey). (B) Infectious virus titer in the bioreactor supernatant for 3 cultivations in perfusion mode (run 10 = black, run 11 = red, data from run *4*, chapter 7 = grey). (C) Maximum permittivity signal ($\Delta\varepsilon_{max}$; solid line) and offline viable cell concentration (●) for 1 cultivation in batch (run C). (D) Infectious virus titer in the bioreactor supernatant for one cultivation in batch mode (run C). The vertical lines (for each run in the respective color) correspond to the expected time of MVA release in the supernatant, which is on average 10.6 h after the maximum permittivity signal (between 12 and 36 h post infection for perfusion and between 24 and 48 h post infection for batch). This time interval of 10.6 h was determined based on the optimal time of virus harvesting for a perfusion process (which is the time of MVA release, corresponding to the time when about 8 to 10% of the total number of infectious virions was released from the infected cells), as described in section 3.11. The cell factor (described in section 3.7.2) used to convert the permittivity signal to an online viable cell concentration was equal to 0.57, 0.65 and 0.44 for run 10, run 11 and the perfusion control run, respectively.

8.2.4 Economic analysis: Batch versus perfusion mode

To allow for an economic analysis, data for cost of goods from end-to-end MVA production in batch (average values for runs A, B and C) were compared to an end-to-end MVA production in perfusion mode. Data from the perfusion cultivations 10 and 11 were used to estimate the average Vir_{tot}, and the process time for the USP part (referred to as “Seed train” and “Cell culture” in Figure 44C). The data from run 10 was used to estimate the costs regarding the

DSP part (referred to as “Filtration and DNA digestion” and “Chromatography” in Figure 44C), as only run 10 was integrating USP with DSP.

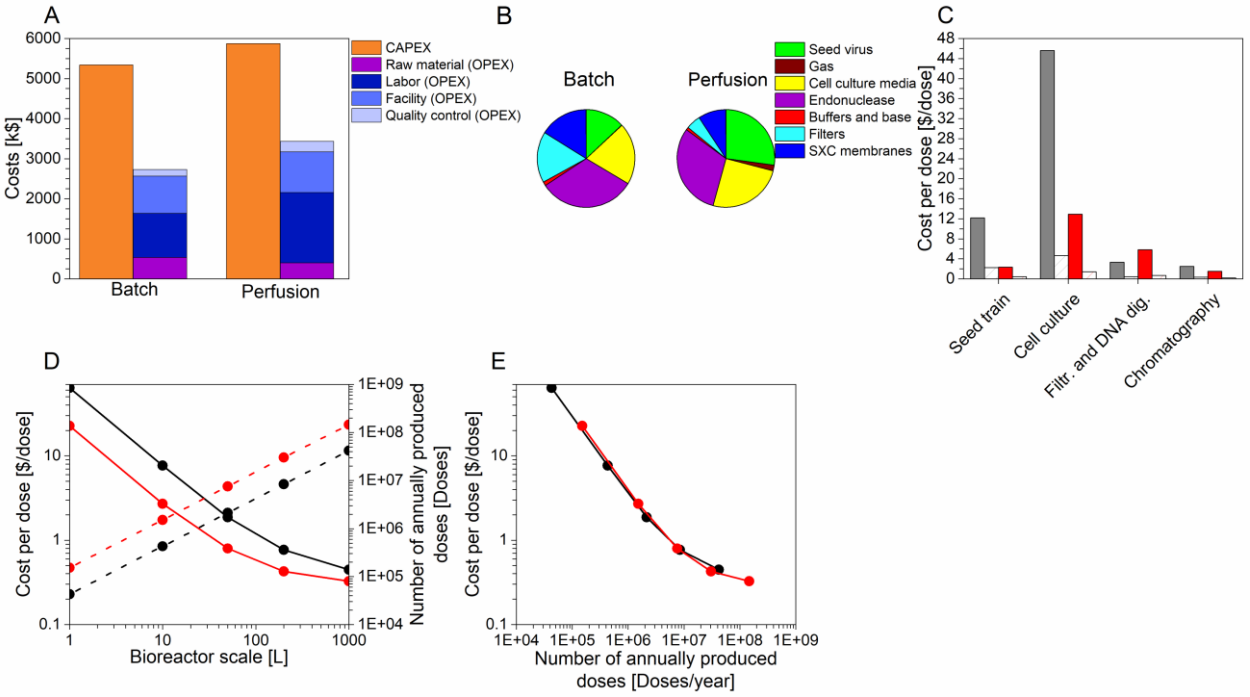

Figure 44: Economic analysis for an end-to-end production of MVA using AGE1.CR.pIX cells cultivated either in batch or in perfusion mode. (A) CAPEX and OPEX of a batch or a perfusion process at the 1 L scale operated over 47 weeks per year. (B) Raw material and consumables costs in batch and perfusion at the 1 L bioreactor scale. (C) Contribution of the seed train, cell culture, filtration plus DNA digestion and chromatography (SXC) steps on the cost per dose for batch (grey) or perfusion (red), at the 1 L scale (full) or at the 10 L scale (dashed). (D) Cost per dose (solid line) and number of annually produced doses (dotted line) as a function of the bioreactor scale (1, 10, 50, 200 and 1000 L working volume) for the batch (black) or the perfusion process (red). (E) Cost per dose as a function of the number of annually produced doses. A MVA dose input of 1.43 x 10^8 $TCID_{50}$ was considered for graphs C, D and E. For the economic analysis, the SuperPro designer software was used (section 3.14). Average data from runs A-C were used to estimate the costs for an integrated batch process. Average data from runs 10–11 were used to estimate the costs regarding the “Seed train” and the “Cell culture” (C) for the perfusion process. Finally, the data from run 10 were used to estimate the costs of DSP, i.e. “Filtration and DNA digestion” and “Chromatography” (C), as only run 10 was integrating USP with DSP for the perfusion mode.

The capital expenditures (CAPEX), was 10% higher for the perfusion than for the batch process for the 1 L bioreactor scale (Figure 44A). Concerning the operating expenditures (OPEX), the value for the perfusion process was overall 26% higher than for the batch process, which can be attributed to higher labor costs required for operation of the perfusion system (Figure 44A). More specifically, for both batch and perfusion systems, the highest costs came from the endonuclease used for DNA digestion (30–32%), followed by costs for cell culture medium (21–25%) and seed virus (13–27%) (Figure 44B). Costs for filters and SXC membranes were between 5–17%. Overall, for the different production steps from the seed train to the SXC,

the batch and perfusion systems had similar cost per dose at the 1 L bioreactor scale, except for the seed train and cell culture step: here, costs for the batch system were about 5.2 and 3.5-fold higher, respectively (Figure 44C). At the 1 L bioreactor scale, the perfusion process allowed to produce about 3.5-fold more doses per year than to the batch system (Figure 44D). This resulted in a 2.8-fold decrease of cost per dose. At the 1000 L scale, 42 and 147 millions of doses are projected yearly in the batch and perfusion systems, respectively. Targeting a defined number of doses per year, the perfusion system and the batch system showed similar costs per dose (Figure 44E). Nevertheless, for the same bioreactor scale, the operation of a perfusion system is always advantageous in terms of cost per dose (Figure 44D). At the 200 L scale, the cost per dose for a perfusion system is still 1.8-fold lower than for a batch process. More details about the economic analysis are available in the Appendix, section 10.10.

8.3 Discussion

8.3.1 Process integration using an acoustic settler

Cell growth, CSVY and P_v (Figure 40) of the presented perfusion system were in the same range as in previous experiments [235], with maximum values of 50 x 10^6 cells/mL, 55.4 $TCID_{50}$/cell, and 2.53 x 10^{10} $TCID_{50}$/L/day.

The total recovery for the perfusion and batch systems were similar (50.5% and 54.7%, respectively; Figure 41A), showing that the intensified perfusion process did not have a negative impact on cell clarification, host cell DNA removal and SXC. A total recovery of about 50–55% is in accordance with results reported from other groups using other DSP processes. Recoveries of 61–63% for adenovirus [66, 67], 41% for MVA [61], 52% for influenza virus [68] and 20–60% for AAV production [67, 69] were reported. Successful application of membrane-based SXC for influenza virus, yellow fever virus, AAV, baculovirus, hepatitis C virus, and Orf virus purifications have been reported [83, 237-240]. This suggests that the integrated process established here may also be transferrable to other virus manufacturing processes. The short purification cycles of the SXC method (of about 40 min) allowed to greatly simplify the semi-continuous purification process. In addition, the less complex bind-elute steps in single-

column SXC requires fewer optimizations than conventional multi-column chromatography trains [112, 241].

Clarification steps are particularly challenging due to the large size of MVA virions (250–350 nm). Here, a depth filtration efficiency of 59.8–81.6% (Figure 40) was observed for batch and perfusion systems, and depth filtration was the main cause for the reduction of process yields. Similar findings were reported for large scale manufacturing of vaccinia viruses with depth filters with < 5 µm pore size [61, 242]. Other publications reported recoveries of 85–90% when using polypropylene depth filters with pore sizes of 0.45–0.60 µm after a centrifugation step, or from the supernatant of an adherent cell culture for smaller viruses such as adenovirus [66], hepatitis C VLPs [243] or influenza virus [244]. Recoveries up to 74% for clarification of vaccinia virus raw material (centrifuged cell lysate and 1:5 diluted in 0.5 M ammonium sulfate and 3 M NaCl) with 0.8 µm cellulose acetate filter were also reported [245]. The polypropylene material used here for depth filtration, and also for the Artemis ATF column (section 10.5), seems well suited for clarification of virus-containing supernatants and is relatively inert [246, 247] with a surface tension energy lower than other common material such as polyethylene, polyethylene sulfone or polystyrene membranes [248, 249]. In addition, this material largely prevents electrostatic interaction with virus particles (MVA carries a high negative charge at neutral pH [250]) in contrast to diatomaceous earth, which is a standard material used for depth filtration (lower recovery observed, Appendix, section 10.6.2) [246, 247]. In addition, the adjustment of appropriate salt concentrations also improved yields in depth filtration (Appendix, section 10.6.1). This corresponds to previous findings that demonstrated that salt addition reduced the interaction of virus particles with cell debris and DNA [251, 252] and suppressed the aggregation of viral vectors [253].

Host cell DNA is one of the most critical and persistent contamination in virus particle purification. An inline endonuclease treatment step efficiently reduced host cell DNA levels before subsequent SXC purification. The use of chaotropes for efficient DNA digestion was also essential, as helped to separate DNA from the surface of virus particles [251]. A host cell DNA reduction of around 500-fold was needed for the perfusion process established here (Figure 41B) in order to meet the requirements typically set by regulatory authorities (<10 ng/dose). The establishment of this novel continuous inline DNA digestion step was inspired from the use of plug flow reactors with immobilized enzymes [254], and resulted in an over

10’000-fold reduction of DNA (Figure 41B). Unlike chemostats, plug flow reactors allow a narrow distribution of the residence time.

8.3.2 Process automation using a capacitance probe

The perfusion rate was controlled via estimation of the VCC by an online capacitance probe (Figure 42). Similar findings were reported by Nikolay et al. (2018) for a different avian cell line. It thus seems that this technique is a versatile method [145, 255] as long as the diameter of the cells remains constant during the time course of cultivations. There are several options to correlate the permittivity signal with the VCC [95]. Here, a simple linear regression between the permittivity signal and the offline VCC was precise enough to determine the VCC during the cell growth phase. During the virus production process, the time of MVA release (term defined in section 3.11) could be determined with $\Delta\varepsilon_{max}$ or offline VCC with a precision of about ± 4 h, over four different runs in perfusion or batch mode (Figure 43). The use of $\Delta\varepsilon_{max}$ was more accurate than offline VCC due its higher measurement frequency. Previous publications already used the permittivity signal to correlate with the optimal time of harvest of measles virus [93] and AAV in a baculovirus expression system [92]. Petiot et al. (2017) used $\Delta\varepsilon_{max}$ and critical frequency (Fc) values to determine changes in C_m and σ_i values over the virus infection for different enveloped (e.g. lentivirus, influenza virus) and non-enveloped viruses (reovirus) to monitor the status of the virus infection phase. In the conducted study, monitoring of Fc, C_m and σ_i did not lead to clear results (Appendix, section 10.9). More cultivations should be performed to infer about a correlation between the permittivity signal and MVA release for perfusion and batch systems (Figure 43 and Table A.12). This is in particular important for perfusion processes, were the time of significant virus accumulation needs to be identified for initiation of subsequent process steps, i.e. chromatographic purification. Furthermore, it would support the establishment of robust processes following the guidelines of the PAT initiative [84].

8.3.3 Economic analysis

In order to assess the benefit of integrated perfusion processes, an economic analysis was performed using SuperPro designer software. Based on the results shown in Figure 44, the cost per MVA dose could be reduced by a factor of 2.8 for production of MVA in perfusion mode at the 1 L scale, compared to the batch system. Advantages of perfusion systems were

already shown for USP in MVA production, although without cost evaluation (chapter 7). Although operation of the perfusion system is more labor intensive, the cost per dose was lower as the production capacity increased by a factor of 3.5 (1 L scale). Furthermore, the seed train costs were decreased as fewer bioreactor runs per year need to be performed (Figure 44). Costs were mainly reduced for the seed train and USP (Figure 44C), similarly to what was observed for AAV [234] and lentivirus manufacturing [165]. Higher costs for seed virus for perfusion over batch processes were estimated (Figure 44B), as cultures are infected at a higher VCC and, to keep the MOI, more virus is needed (> 10-fold). Nevertheless, process time was not drastically prolonged (Appendix, section 10.10). The cell culture medium cost was not higher for the perfusion system (Figure 44B) because the CSPR was kept to a minimum and, although the perfusion cultivations need higher medium volumes, more virus can be produced than in batch. As also observed in AAV manufacturing, the establishment of intensified USP systems has little impact on the DSP cost per dose [234], although the chromatography method used was different for the both cases. Concerning raw materials and consumables costs, the significant costs for DNA digestion could be further reduced by optimizing the endonuclease treatment step in the future. Finally, the low costs of the SXC purification step lead to a very low contribution to the overall consumable stocks, in contrast to other DSP techniques that required expensive resins or coated surfaces [165].

So far, few studies have addressed bioprocess economics for production of viral vectors [165, 234] or VLPs [256]. For all of them, using suspension cell culture in batch mode appeared to be the most cost-effective option. Here, suspension cell culture in perfusion mode is presented as an additional option to further reduce costs. Although for a fixed amount of MVA doses per year the perfusion system would not decrease the costs per dose compared to batch, the CAPEX is not the same across scales for batch and perfusion systems. For example, a 200 L batch bioreactor is predicted to produce as much as a 50 L perfusion bioreactor (7.6–8.4 x 10^6 doses per year). While the cost per dose is not reduced for the perfusion system, the CAPEX is about 1.2-fold lower resulting in a faster return of investments (Appendix, section 10.10). In addition, the use of perfusion systems is always advantageous for the same bioreactor scale (Figure 44), which might be of interest for modification of existing virus manufacturing plants towards an increase of product output.

As an outlook, the recovery of the integrated process could be further increased by optimizing the first depth filtration step, as this resulted in the most significant drop in virus titers (Figure 41A). For instance, depth filters with larger pore sizes could be added before the used depth filter, in order to remove more efficiently large cell debris without product retention. The concentration of the salt used as a chaotropic agent could also be re-evaluated. Indeed, an increase in the ionic strength might decrease the zeta potential of the membrane below a critical value. As a result, the electrostatic repulsion between the feed and the membrane could be decreased resulting in membrane fouling, unspecific product adsorption or aggregation of flocs that may also contain virus particles [257, 258]. The choice of the salt also has to be carefully analyzed as for example trivalent cations have been shown to better promote virus adsorption than monovalent ones, at similar concentration [258].

In conclusion, an integrated perfusion process for MVA production has been established with a minimum of clarification and purification steps. An overall product recovery of 50.5% was achieved, allowing to increase the STY by 600% compared to a batch system operated at the same scale. This was mainly due to the fact, that the virus production phase could be kept constant for both processes. Furthermore, the observed purification performance of membrane-based SXC was not hampered due to cell culture process intensification. The use of an online capacitance probe allowed the control of the perfusion rate during the cell growth phase and indicated the time of MVA release to initiate subsequent processing steps. Finally, a detailed cost analysis, based on several runs performed in batch and perfusion mode, indicated that the cost per dose in MVA production would be decreased by a factor of 2.8 if the system would be operated in perfusion mode at the 1 L scale.

8.4 Author contributions

All the experiments were performed by Gwendal Gränicher, except run 11 which was performed by Sven Göbel and Gwendal Gränicher. The economic model was built by Gwendal Gränicher and Masoud Babakhani. The chapter was reviewed by the co-authors of the manuscript: *A high cell density perfusion process for MVA virus production: process integration with inline DNA digestion, and cost analysis* (submitted to Biotech Bioeng) [259].

Chapter 9

Conclusion and Outlook

To efficiently produce high amounts of viral vaccines (such as inactivated influenza virus vaccines) and viral vectors (such as MVA), several aspects regarding cell culture-based virus production process were discussed in the presented thesis. First, two different lines, namely PBG.PK2.1 and AGE1.CR.pIX were evaluated and compared for virus production in order to increase virus production yields. Second, the production yields, process-related impurities and product quality of different perfusion cell culture platforms for intensified virus production were compared. Other cell culture modes, such as two-stage continuous cell culture, were considered as well. Third, to increase process robustness through automation or a better process monitoring, an online probe measuring the bio volume (and the VCC) was used during the cell growth phase and the virus production phase. Finally, a perfusion cell culture-based MVA production was integrated to semi-continuous DSP.

9.1 Cell lines

In case of pandemics in particular, influenza pandemics, having a cell substrate for fast and efficient influenza virus production would be crucial. The production yield can strongly differ depending on the respective influenza virus strain, thus having a large choice of cell substrates suitable for cGMP manufacturing would be ideal. In chapters 4–6, PBG.PK2.1 and AGE1.CR.pIX cells were used for IAV production. From the actual work and the perfusion cell cultures reported in the literature, the highest IAV titer in a bioreactor was obtained (in 2019, at its time of publication, later overcome by MDCK cells [255]) when using PBG.PK2.1 cell line for A/PR/8/34 virus production (4.0 $\log_{10}$(HAU/100 µL). Such titer made the cell line attractive for intensified inactivated influenza A vaccine production. However, the PBG.PK2.1 cell line was later found to have active PERV particles able to replicate in human cells [196], decreasing its safety of use. For this reason, the AGE1.CR.pIX cell was chosen later as it is cGMP compliant and permissive to many virus types such as IAV and MVA.

Possible outlooks would be the engineering of the cell substrate to allow for even higher virus production, or the use of alternative cell substrates more commonly accepted for virus production (but for more advanced bioprocesses).

9.2 Platforms for intensified virus production

In chapters 5–6, as two-stage continuous IAV production is not efficient [168], perfusion processes were performed and optimized in order to intensify IAV production and to determine, which perfusion platform was the most suitable. ATF, AS and IS technologies were selected here as promising cell retention technologies for intensified virus production. For the membrane-based ATF system, continuous influenza virus harvesting was previously shown to be challenging [90, 103, 114]. In chapter 5, it was shown that a cell retention device allowing continuous harvesting decreases the amount of large-sized aggregates, potentially improving the DSP. However, process-related impurities such as host cell DNA or host cell proteins were not decreased by continuous harvesting. For similar processes and compared to the ATF, the P_v was increased by a factor of 1.7 and 2.2 for the AS and the IS, respectively (6.3.1). The AS and IS are therefore interesting alternatives to the ATF system. However, for both systems, their process parameters have to be carefully optimized. For the AS, the temperature elevation in the acoustic chamber was found to be critical in order to obtain high P_v. The temperature could be controlled mainly by setting a high perfusion rate (> 1600 mL/day). For the IS, the cooling in the heat exchanger was found to have a critical effect on the AGE1.CR.pIX cell growth (ideally set at 27°C in the conducted study).

In chapter 7, a broad comparison for MVA production strategies between all available process options indicated an advantage of hybrid perfusion in a STR-ATF system over standard perfusion and continuous cultivation. The criteria for comparison included footprint reduction, P_v, scalability, process robustness, and options for single-use manufacturing. Once optimized, a two-stage continuous STR cultivation system might offer the highest potential for production of large amount of virus as it allowed to achieve the highest number of cells over time during the infection phase (it could be prolonged over months). It was as well shown to be possible to produce viral vectors with suspension cells in fully single-use intensified cell culture systems (HFBR and OSB-ATF).

In the future, the individual bioprocess steps should be better optimized within the virus production workflow using DoE approaches with automatized and parallelized down-scales models such as Sartorius' Ambr15®, Sartorius' Ambr250® or Tecan's Freedom EVO®. Parameters such as the medium composition, eventual additives during virus production phase, cell retention temperature, osmolality, and aeration rate could be considered. Once

the cell culture is fully optimized, an economic analysis could be ideally again performed for each cell culture platform to better visualize the bottlenecks and potential for scale-up. In addition, an optimized DSP should be integrated to it, as soon as possible, as the DSP is sometimes the decisive step regarding the choice of the most cost-effective manufacturing platform.

9.3 Process integration

In chapter 8, an integrated perfusion process for MVA production was successfully established, and compared to an integrated batch system. To decrease the host cell DNA level prior to semi-continuous SXC, a plug flow reactor was designed for continuous DNA digestion using endonuclease. Overall, the total recovery for the perfusion and batch systems were similar (50.5% and 54.7%). The STY of the integrated perfusion system was about 600% higher. The use of a capacitance probe allowed the successful control of the perfusion rate and the determination of the optimal time of harvesting for the integrated perfusion system. Finally, the implementation of the techno-economic model, comparing both integrated perfusion and integrated batch systems showed that the cost per dose is not lower for the perfusion system when targeting a pre-defined amount of yearly doses. However, the CAPEX is lower for perfusion cell cultures, allowing a faster return on investment. In addition, for a same bioreactor scale, the cost per dose is always lower for perfusion cultures.

As an outlook, the process should be tested at larger scale. Using data from industry, the presented economic model could be improved. In addition, other viral vectors suitable for gene therapy such as lentivirus or AAV should be tested using the same setup. The filtration material and filtration conditions should be further optimized for depth filtration as this was shown to be the factor decreasing the most the overall product recovery. Continuous harvesting with the ATF system, followed by its integration with (semi-)continuous purification should be further tested as well.

To improve process robustness and automation of the system, a supervising and control data acquisition (SCADA) system could be implemented. A SCADA system would allow making real-time decisions from USP to DSP in order to optimize the process. Data from the USP such as oxygen uptake rate, pH, permittivity signal, and perfusion flow rate combined with data from

the DSP such as trans membrane pressure elevation of depth filters, UV signal from the SXC and system pressure increase from the SXC could be collected. Based on this comprehensive information, the process could be further optimized through machine learning approaches to improve virus titers, recovery of individual process steps yield and product purity.

On a more general point of view, and from what could be learnt from the current COVID-19 pandemic, the choice of the platform technology for therapeutics and vaccines should be considered as well. The time to have commercially-available new vaccine product might be the crucial point to consider when selecting a platform technology. In this regard, mRNA technology outpaces viral-based vaccines. In the personal view of the author, cell culture-based vaccine production might still be of high importance due to its cost-effectiveness and usual high stability, allowing storage at 4°C or even at room temperature. Another field of high importance concerning virus manufacturing is gene therapy. There, considering the high doses and multiple clinical trials using viral vectors such as AAV, process intensification and integration might be highly relevant.

References

[1] Ozawa S, Clark S, Portnoy A, Grewal S, Brenzel L, Walker DG. Return On Investment From Childhood Immunization In Low- And Middle-Income Countries, 2011–20. Health Affairs. 2016;35:199-207.
[2] Mehand MS, Al-Shorbaji F, Millett P, Murgue B. The WHO R&D Blueprint: 2018 review of emerging infectious diseases requiring urgent research and development efforts. Antiviral Research. 2018;159:63-7.
[3] Bernasconi V, Kristiansen PA, Whelan M, Román RG, Bettis A, Yimer SA, et al. Developing vaccines against epidemic-prone emerging infectious diseases. Bundesgesundheitsblatt - Gesundheitsforschung - Gesundheitsschutz. 2020;63:65-73.
[4] FDA FaDA. Long Term Follow-Up After Administration of Human Gene therapy Products Guidance for Industry. In: Services UDoHah, editor. Silver Spring, MD, USA: Food and Drug Administration, center for biologics Evaluation and Research; 2020. p. 1-35.
[5] Anguela XM, High KA. Entering the Modern Era of Gene Therapy. Annual Review of Medicine. 2019;70:273-88.
[6] Bulcha JT, Wang Y, Ma H, Tai PWL, Gao G. Viral vector platforms within the gene therapy landscape. Signal Transduction and Targeted Therapy. 2021;6:53.
[7] Kaemmerer WF. How will the field of gene therapy survive its success? Bioeng Transl Med. 2018;3:166-77.
[8] Clément N. Large-Scale Clinical Manufacturing of AAV Vectors for Systemic Muscle Gene Therapy. In: Duan D, Mendell JR, editors. Muscle Gene Therapy. Cham: Springer International Publishing; 2019. p. 253-73.
[9] Shukla V, Seoane-Vazquez E, Fawaz S, Brown L, Rodriguez-Monguio R. The Landscape of Cellular and Gene Therapy Products: Authorization, Discontinuations, and Cost. Human Gene Therapy Clinical Development. 2019;30:102-13.
[10] van Overbeeke E, Michelsen S, Toumi M, Stevens H, Trusheim M, Huys I, et al. Market access of gene therapies across Europe, USA, and Canada: challenges, trends, and solutions. Drug Discovery Today. 2020;26:399-415.
[11] Xie F. Highly Priced Gene Therapies: A Wake-Up Call for Early Price Regulation. PharmacoEconomics. 2018;36:883-8.
[12] Brennan TA, Wilson JM. The special case of gene therapy pricing. Nature Biotechnology. 2014;32:874-6.
[13] Orkin SH, Reilly P. Paying for future success in gene therapy. Science. 2016;352:1059.
[14] Rappuoli R, Hanon E. Sustainable vaccine development: a vaccine manufacturer's perspective. Curr Opin Immunol. 2018;53:111-8.
[15] Rappuoli R, Pizza M, Del Giudice G, De Gregorio E. Vaccines, new opportunities for a new society. Proceedings of the National Academy of Sciences. 2014;111:12288-93.
[16] Plotkin SA. Introduction. In: Plotkin SA, editor. History of Vaccine Development. New York, NY: Springer New York; 2011. p. 1-4.
[17] Plotkin SA. Vaccines: the fourth century. Clin Vaccine Immunol. 2009;16:1709-19.
[18] WHO. Global vaccine Action plan 2011-2020. 2020.
[19] Plotkin SA. Vaccines: Past, present and future. Nature Medicine. 2005;11:S5-S11.
[20] Yamayoshi S, Kawaoka Y. Current and future influenza vaccines. Nature Medicine. 2019;25:212-20.
[21] Krammer F, Palese P. Advances in the development of influenza virus vaccines. Nat Rev Drug Discov. 2015;14:167-82.

[22] Harding AT, Heaton NS. Efforts to Improve the Seasonal Influenza Vaccine. Vaccines (Basel). 2018;6:1.
[23] WHO. Vaccines against influenza WHO position paper. Weekly epidemiological record. 2012;87:461-76.
[24] Milian E, Kamen AA. Current and emerging cell culture manufacturing technologies for influenza vaccines. Biomed Res Int. 2015;2015:1-11.
[25] Ulmer JB, Valley U, Rappuoli R. Vaccine manufacturing: challenges and solutions. Nat Biotechnol. 2006;24:1377-83.
[26] Barr IG, Donis RO, Katz JM, McCauley JW, Odagiri T, Trusheim H, et al. Cell culture-derived influenza vaccines in the severe 2017-2018 epidemic season: a step towards improved influenza vaccine effectiveness. NPJ Vaccines. 2018;3:1-5.
[27] FDA. What is Gene Therapy? 2018.
[28] Nóbrega C, Mendonça L, Matos CA. Gene and Cell Therapy. A Handbook of Gene and Cell Therapy. Cham: Springer International Publishing; 2020. p. 1-22.
[29] Nóbrega C, Mendonça L, Matos CA. Viral Vectors for Gene Therapy. A Handbook of Gene and Cell Therapy. Cham: Springer International Publishing; 2020. p. 39-90.
[30] Mitragotri S, Burke PA, Langer R. Overcoming the challenges in administering biopharmaceuticals: formulation and delivery strategies. Nature Reviews Drug Discovery. 2014;13:655-72.
[31] Rosenblum D, Joshi N, Tao W, Karp JM, Peer D. Progress and challenges towards targeted delivery of cancer therapeutics. Nature Communications. 2018;9:1410.
[32] Mu X, Greenwald E, Ahmad S, Hur S. An origin of the immunogenicity of in vitro transcribed RNA. Nucleic Acids Research. 2018;46:5239-49.
[33] Beissert T, Koste L, Perkovic M, Walzer KC, Erbar S, Selmi A, et al. Improvement of In Vivo Expression of Genes Delivered by Self-Amplifying RNA Using Vaccinia Virus Immune Evasion Proteins. Human Gene Therapy. 2017;28:1138-46.
[34] Volz A, Sutter G. Chapter Five - Modified Vaccinia Virus Ankara: History, Value in Basic Research, and Current Perspectives for Vaccine Development. In: Kielian M, Mettenleiter TC, Roossinck MJ, editors. Advances in Virus Research: Academic Press; 2017. p. 187-243.
[35] Condit RC, Moussatche N, Traktman P. In A Nutshell: Structure and Assembly of the Vaccinia Virion. Advances in Virus Research: Academic Press; 2006. p. 31-124.
[36] Koch T, Dahlke C, Fathi A, Kupke A, Krähling V, Okba NMA, et al. Safety and immunogenicity of a modified vaccinia virus Ankara vector vaccine candidate for Middle East respiratory syndrome: an open-label, phase 1 trial. The Lancet Infectious Diseases. 2020;20:827-38.
[37] Mayr A, Hochstein-Mintzel V, Stickl H. Abstammung, Eigenschaften und Verwendung des attenuierten Vaccinia-Stammes MVA. Infection. 1975;3:6-14.
[38] Wyatt LS, Earl PL, Eller LA, Moss B. Highly attenuated smallpox vaccine protects mice with and without immune deficiencies against pathogenic vaccinia virus challenge. Proceedings of the National Academy of Sciences. 2004;101:4590-5.
[39] Gallo-Ramirez LE, Nikolay A, Genzel Y, Reichl U. Bioreactor concepts for cell culture-based viral vaccine production. Expert Rev Vaccines. 2015;14:1181-95.
[40] Gutiérrez-Granados S, Gòdia F, Cervera L. Continuous manufacturing of viral particles. Current Opinion in Chemical Engineering. 2018;22:107-14.
[41] Dormitzer PR. Cell Culture-Derived Influenza Vaccines. In: Rappuoli R, Del Giudice G, editors. Influenza Vaccines for the Future. Basel: Springer Basel; 2011. p. 293-312.
[42] Millipore E. Application note: Generic process of cell culture based influenza vaccine. EMD Millipore; 2014.

[43] Lohr V. Characterization of the avian designer cells AGE1.CR and AGE1.CR.pIX considering growth, metabolism and production of influenza virus and Modified Vaccinia Virus Ankara (MVA), Dissertation. Magdeburg: Otto-von-Guericke Universität; 2014.
[44] Genzel Y, Reichl U. Continuous cell lines as a production system for influenza vaccines. Expert Rev Vaccines. 2009;8:1681–92.
[45] Aubrit F, Perugi F, Leon A, Guehenneux F, Champion-Arnaud P, Lahmar M, et al. Cell substrates for the production of viral vaccines. Vaccine. 2015;33:5905-12.
[46] Petiot E, Proust A, Traversier A, Durous L, Dappozze F, Gras M, et al. Influenza viruses production: Evaluation of a novel avian cell line DuckCelt(R)-T17. Vaccine. 2018;36:3101-11.
[47] Huang D, Peng WJ, Ye Q, Liu XP, Zhao L, Fan L, et al. Serum-Free Suspension Culture of MDCK Cells for Production of Influenza H1N1 Vaccines. PLoS One. 2015;10:e0141686.
[48] Lee M-S, Hu AY-C. A cell-based backup to speed up pandemic influenza vaccine production. Trends in Microbiology. 2012;20:103-5.
[49] Gaush CR, Smith TF. Replication and Plaque Assay of Influenza Virus in an Established Line of Canine Kidney Cells. Applied Microbiology. 1968;16:588.
[50] Genzel Y, Dietzsch C, Rapp E, Schwarzer J, Reichl U. MDCK and Vero cells for influenza virus vaccine production: a one-to-one comparison up to lab-scale bioreactor cultivation. Appl Microbiol Biotechnol. 2010;88:461-75.
[51] Audsley JM, Tannock GA. The growth of attenuated influenza vaccine donor strains in continuous cell lines. Journal of Virological Methods. 2005;123:187-93.
[52] Gröner A, Vorlop J. Animal cells and processes for the replication of influenza viruses. In: patent I, editor.1997.
[53] Doroshenko A, Halperin SA. Trivalent MDCK cell culture-derived influenza vaccine Optaflu® (Novartis Vaccines). Expert Review of Vaccines. 2009;8:679-88.
[54] Kiesslich S, Kamen AA. Vero cell upstream bioprocess development for the production of viral vectors and vaccines. Biotechnology Advances. 2020;44:107608.
[55] Jordan I, Vos A, Beilfuss S, Neubert A, Breul S, Sandig V. An avian cell line designed for production of highly attenuated viruses. Vaccine. 2009;27:748-56.
[56] Jordan I, Northoff S, Thiele M, Hartmann S, Horn D, Höwing K, et al. A chemically defined production process for highly attenuated poxviruses. Biologicals. 2011;39:50-8.
[57] Folegatti PM, Bellamy D, Flaxman A, Mair C, Ellis C, Ramon RL, et al. Safety and Immunogenicity of the Heterosubtypic Influenza A Vaccine MVA-NP+M1 Manufactured on the AGE1.CR.pIX Avian Cell Line. Vaccines. 2019;7:33.
[58] Venkatraman N, Ndiaye BP, Bowyer G, Wade D, Sridhar S, Wright D, et al. Safety and Immunogenicity of a Heterologous Prime-Boost Ebola Virus Vaccine Regimen in Healthy Adults in the United Kingdom and Senegal. J Infect Dis. 2019;219:1187-97.
[59] Jordan I, Horn D, John K, Sandig V. A genotype of modified vaccinia Ankara (MVA) that facilitates replication in suspension cultures in chemically defined medium. Viruses. 2013;5:321-39.
[60] Jordan I, Horn D, Thiele K, Haag L, Fiddeke K, Sandig V. A Deleted Deletion Site in a New Vector Strain and Exceptional Genomic Stability of Plaque-Purified Modified Vaccinia Ankara (MVA). Virol Sin. 2020;35:212-26.
[61] Leon A, David AL, Madeline B, Guianvarc'h L, Dureau E, Champion-Arnaud P, et al. The EB66(R) cell line as a valuable cell substrate for MVA-based vaccines production. Vaccine. 2016;34:5878-85.
[62] Brown SW, Mehtali M. The Avian EB66® Cell Line, Application to Vaccines, and Therapeutic Protein Production. PDA Journal of Pharmaceutical Science and Technology. 2010;64:419.

[63] Kalbfuss B, Reichl U. Viral Vaccines Purification. In: Wen E, Ellis R, Pujar N, editors. Vaccine Development and Manufacturing: John Wiley & Sons, Inc.; 2014. p. 97-180.
[64] Wolf MW, Reichl U. Downstream processing of cell culture-derived virus particles. Expert Review of Vaccines. 2011;10:1451-75.
[65] Nestola P, Peixoto C, Silva RRJS, Alves PM, Mota JPB, Carrondo MJT. Improved virus purification processes for vaccines and gene therapy. Biotechnology and Bioengineering. 2015;112:843-57.
[66] Fernandes P, Peixoto C, Santiago VM, Kremer EJ, Coroadinha AS, Alves PM. Bioprocess development for canine adenovirus type 2 vectors. Gene Therapy. 2013;20:353-60.
[67] Moleirinho MG, Silva RJS, Alves PM, Carrondo MJT, Peixoto C. Current challenges in biotherapeutic particles manufacturing. Expert Opinion on Biological Therapy. 2020;20:451-65.
[68] Kalbfuss B, Wolff M, Morenweiser R, Reichl U. Purification of cell culture-derived human influenza A virus by size-exclusion and anion-exchange chromatography. Biotechnol Bioeng. 2007;96:932-44.
[69] Terova O, Soltys S, Hermans P, De Rooij J, Detmers F. Overcoming downstream purification challenges for viral vector manufacturing: enabling advancement of gene therapies in the clinic. Cell Gen Therapy Insights. 2018;4:101-11.
[70] Wang S, Godfrey S, Ravikrishnan J, Lin H, Vogel J, Coffman J. Shear contributions to cell culture performance and product recovery in ATF and TFF perfusion systems. J Biotechnol. 2017;246:52-60.
[71] Walther J, McLarty J, Johnson T. The effects of alternating tangential flow (ATF) residence time, hydrodynamic stress, and filtration flux on high-density perfusion cell culture. Biotechnology and Bioengineering. 2019;116:320-32.
[72] Choi H, Zhang K, Dionysiou DD, Oerther DB, Sorial GA. Influence of cross-flow velocity on membrane performance during filtration of biological suspension. Journal of Membrane Science. 2005;248:189-99.
[73] Stressmann M, Moresoli C. Effect of pore size, shear rate, and harvest time during the constant permeate flux microfiltration of CHO cell culture supernatant. Biotechnology Progress. 2008;24:890-7.
[74] Hadpe SR, Sharma AK, Mohite VV, Rathore AS. ATF for cell culture harvest clarification: mechanistic modelling and comparison with TFF. Journal of Chemical Technology & Biotechnology. 2017;92:732-40.
[75] Bolton GR, Apostolidis AJ. Mechanistic modeling of the loss of protein sieving due to internal and external fouling of microfilters. Biotechnology Progress. 2017;33:1323-33.
[76] Kelly W, Scully J, Zhang D, Feng G, Lavengood M, Condon J, et al. Understanding and modeling alternating tangential flow filtration for perfusion cell culture. Biotechnology Progress. 2014;30:1291-300.
[77] Karst DJ, Ramer K, Hughes EH, Jiang C, Jacobs PJ, Mitchelson FG. Modulation of transmembrane pressure in manufacturing scale tangential flow filtration N-1 perfusion seed culture. Biotechnology Progress. 2020;n/a:e3040.
[78] Pinto NDS, Napoli WN, Brower M. Impact of micro and macroporous TFF membranes on product sieving and chromatography loading for perfusion cell culture. Biotechnol Bioeng. 2019.
[79] Wang SB, Godfrey S, Radoniqi F, Lin H, Coffman J. Larger Pore Size Hollow Fiber Membranes as a Solution to the Product Retention Issue in Filtration-Based Perfusion Bioreactors. Biotechnology Journal. 2019;14:1800137.

[80] Nikolay A, de Grooth J, Genzel Y, Wood JA, Reichl U. Virus harvesting in perfusion culture: Choosing the right type of hollow fiber membrane. Biotechnology and Bioengineering. 2020;117:3040-52.
[81] Lee J, Gan HT, Latiff SMA, Chuah C, Lee WY, Yang Y-S, et al. Principles and applications of steric exclusion chromatography. Journal of Chromatography A. 2012;1270:162-70.
[82] Marichal-Gallardo P, Pieler MM, Wolff MW, Reichl U. Steric exclusion chromatography for purification of cell culture-derived influenza A virus using regenerated cellulose membranes and polyethylene glycol. Journal of Chromatography A. 2017;1483:110-9.
[83] Marichal-Gallardo P. Chromatographic purification of biological macromolecules by their capture on hydrophilic surfaces with the aid of non-ionic polymers. Magdeburg: Otto-von-Guericke-Universität; 2019.
[84] FDA. Guidance for industry PAT - a framework for innovative pharmaceutical development, manufacturing and quality assurance. In: U.S. Department of Health and Human Services FDA, Center for Biologics Evaluation and Research, editor. Rockville2004.
[85] Jenzsch M, Bell C, Buziol S, Kepert F, Wegele H, Hakemeyer C. Trends in Process Analytical Technology: Present State in Bioprocessing. In: Kiss B, Gottschalk U, Pohlscheidt M, editors. New Bioprocessing Strategies: Development and Manufacturing of Recombinant Antibodies and Proteins. Cham: Springer International Publishing; 2018. p. 211-52.
[86] Karst DJ, Steinebach F, Morbidelli M. Continuous integrated manufacturing of therapeutic proteins. Curr Opin Biotechnol. 2018;53:76-84.
[87] Yee JC, Rehmann MS, Yao G, Sowa SW, Aron KL, Tian J, et al. Advances in process control strategies for mammalian fed-batch cultures. Current Opinion in Chemical Engineering. 2018;22:34-41.
[88] Justice C, Brix A, Freimark D, Kraume M, Pfromm P, Eichenmueller B, et al. Process control in cell culture technology using dielectric spectroscopy. Biotechnology Advances. 2011;29:391-401.
[89] Petiot E, Ansorge S, Rosa-Calatrava M, Kamen A. Critical phases of viral production processes monitored by capacitance. J Biotechnol. 2017;242:19-29.
[90] Vazquez-Ramirez D, Jordan I, Sandig V, Genzel Y, Reichl U. High titer MVA and influenza A virus production using a hybrid fed-batch/perfusion strategy with an ATF system. Appl Microbiol Biotechnol. 2019;103:3025-35.
[91] Nikolay A, Leon A, Schwamborn K, Genzel Y, Reichl U. Process intensification of EB66(R) cell cultivations leads to high-yield yellow fever and Zika virus production. Appl Microbiol Biotechnol. 2018;102:8725-37.
[92] Negrete A, Esteban G, Kotin RM. Process optimization of large-scale production of recombinant adeno-associated vectors using dielectric spectroscopy. Applied Microbiology and Biotechnology. 2007;76:761-72.
[93] Grein TA, Loewe D, Dieken H, Salzig D, Weidner T, Czermak P. High titer oncolytic measles virus production process by integration of dielectric spectroscopy as online monitoring system. Biotechnology and Bioengineering. 2018;115:1186-94.
[94] Harris CM, Todd RW, Bungard SJ, Lovitt RW, Morris JG, Kell DB. Dielectric permittivity of microbial suspensions at radio frequencies: a novel method for the real-time estimation of microbial biomass. Enzyme and Microbial Technology. 1987;9:181-6.
[95] Cannizzaro C, Gügerli R, Marison I, von Stockar U. On-line biomass monitoring of CHO perfusion culture with scanning dielectric spectroscopy. Biotechnology and Bioengineering. 2003;84:597-610.

[96] Downey BJ, Graham LJ, Breit JF, Glutting NK. A novel approach for using dielectric spectroscopy to predict viable cell volume (VCV) in early process development. Biotechnology Progress. 2014;30:479-87.
[97] van der Loo JCM, Wright JF. Progress and challenges in viral vector manufacturing. Human Molecular Genetics. 2015;25:R42-R52.
[98] Bielser JM, Wolf M, Souquet J, Broly H, Morbidelli M. Perfusion mammalian cell culture for recombinant protein manufacturing - A critical review. Biotechnol Adv. 2018;36:1328-40.
[99] Chen C, Wong HE, Goudar CT. Upstream process intensification and continuous manufacturing. Current Opinion in Chemical Engineering. 2018;22:191-8.
[100] Walther J, Godawat R, Hwang C, Abe Y, Sinclair A, Konstantinov K. The business impact of an integrated continuous biomanufacturing platform for recombinant protein production. J Biotechnol. 2015;213:3-12.
[101] Hegde NR. Cell culture-based influenza vaccines: A necessary and indispensable investment for the future. Hum Vaccin Immunother. 2015;11:1223-34.
[102] Clincke M-F, Mölleryd C, Zhang Y, Lindskog E, Walsh K, Chotteau V. Very high density of CHO cells in perfusion by ATF or TFF in WAVE bioreactor™. Part I. Effect of the cell density on the process. Biotechnology Progress. 2013;29:754-67.
[103] Genzel Y, Vogel T, Buck J, Behrendt I, Ramirez DV, Schiedner G, et al. High cell density cultivations by alternating tangential flow (ATF) perfusion for influenza A virus production using suspension cells. Vaccine. 2014;32:2770-81.
[104] Tapia F, Vazquez-Ramirez D, Genzel Y, Reichl U. Bioreactors for high cell density and continuous multi-stage cultivations: options for process intensification in cell culture-based viral vaccine production. Appl Microbiol Biotechnol. 2016;100:2121-32.
[105] Woodside SM, Bowen BD, Piret JM. Mammalian cell retention devices for stirred perfusion bioreactors. Cytotechnology. 1998;28:163-75.
[106] Konstantinov KB, Cooney CL. White Paper on Continuous Bioprocessing May 20–21 2014 Continuous Manufacturing Symposium. Journal of Pharmaceutical Sciences. 2015;104:813-20.
[107] Petiot E, Jacob D, Lanthier S, Lohr V, Ansorge S, Kamen AA. Metabolic and Kinetic analyses of influenza production in perfusion HEK293 cell culture. BMC Biotechnology. 2011;11:1-12.
[108] Henry O, Dormond E, Perrier M, Kamen A. Insights into adenoviral vector production kinetics in acoustic filter-based perfusion cultures. Biotechnol Bioeng. 2004;86:765-74.
[109] Manceur AP, Kim H, Misic V, Andreev N, Dorion-Thibaudeau J, Lanthier S, et al. Scalable Lentiviral Vector Production Using Stable HEK293SF Producer Cell Lines. Hum Gene Ther Methods. 2017;28:330-9.
[110] Vazquez-Ramirez D, Genzel Y, Jordan I, Sandig V, Reichl U. High-cell-density cultivations to increase MVA virus production. Vaccine. 2018;36:3124-33.
[111] Voisard D, Meuwly F, Ruffieux PA, Baer G, Kadouri A. Potential of cell retention techniques for large-scale high-density perfusion culture of suspended mammalian cells. Biotechnol Bioeng. 2003;82:751-65.
[112] Patil R, Walther J. Continuous Manufacturing of Recombinant Therapeutic Proteins: Upstream and Downstream Technologies. In: Kiss B, Gottschalk U, Pohlscheidt M, editors. New Bioprocessing Strategies: Development and Manufacturing of Recombinant Antibodies and Proteins. Cham: Springer International Publishing; 2018. p. 277-322.
[113] Perrin P, Madhusudana S, Gontier-Jallet C, Petres S, Tordo N, Merten O-W. An experimental rabies vaccine produced with a new BHK-21 suspension cell culture process: use of serum-free medium and perfusion-reactor system. Vaccine. 1995;13:1244-50.

[114] Coronel J, Behrendt I, Burgin T, Anderlei T, Sandig V, Reichl U, et al. Influenza A virus production in a single-use orbital shaken bioreactor with ATF or TFF perfusion systems. Vaccine. 2019;37:7011-8.
[115] Gränicher G, Coronel J, Pralow A, Marichal-Gallardo P, Wolff M, Rapp E, et al. Efficient influenza A virus production in high cell density using the novel porcine suspension cell line PBG.PK2.1. Vaccine. 2019;37:7019-28.
[116] Elsayed EA, Medronho RA, Wagner R, Deckwer W-D. Use of Hydrocyclones for Mammalian Cell Retention: Separation Efficiency and Cell Viability (Part 1). Engineering in Life Sciences. 2006;6:347-54.
[117] Castilho LR. Continuous Animal Cell Perfusion Processes: The First Step Toward Integrated Continuous Biomanufacturing. In: Subramanian G, editor. Continuous Processing in Pharmaceutical Manufacturing. Weinheim: Wiley-VCH; 2014. p. 115-54.
[118] Chotteau V. Perfusion Processes. In: Al-Rubeai M, editor. Animal Cell Culture. Cham: Springer International Publishing; 2015. p. 407-43.
[119] Karst DJ, Serra E, Villiger TK, Soos M, Morbidelli M. Characterization and comparison of ATF and TFF in stirred bioreactors for continuous mammalian cell culture processes. Biochemical Engineering Journal. 2016;110:17-26.
[120] Pollock J, Ho SV, Farid SS. Fed-batch and perfusion culture processes: Economic, environmental, and operational feasibility under uncertainty. Biotechnology and Bioengineering. 2013;110:206-19.
[121] Radoniqi F, Zhang H, Bardliving CL, Shamlou P, Coffman J. Computational fluid dynamic modeling of alternating tangential flow filtration for perfusion cell culture. Biotechnology and Bioengineering. 2018;115:2751-9.
[122] Castilho LR, Medronho RA. Cell Retention Devices for Suspended-Cell Perfusion Cultures. In: Schügerl K, Zeng AP, Aunins JG, Bader A, Bell W, Biebl H, et al., editors. Tools and Applications of Biochemical Engineering Science. Berlin: Springer; 2002. p. 129-69.
[123] Shirgaonkar IZ, Lanthier S, Kamen A. Acoustic cell filter: a proven cell retention technology for perfusion of animal cell cultures. Biotechnol Adv. 2004;22:433-44.
[124] Chitale KC, Lipkens B, Jr. WP, Desjardins O. Understanding the fluid dynamics associated with macro scale ultrasonic separators. Proceedings of Meetings on Acoustics. 2015;23:045004.
[125] Trampler F, Sonderhoff SA, Pui PWS, Kilburn DG, Piret JM. Acoustic Cell Filter for High Density Perfusion Culture of Hybridoma Cells. Bio/Technology. 1994;12:281-4.
[126] Gorenflo VM, Angepat S, Bowen BD, Piret JM. Optimization of an Acoustic Cell Filter with a Novel Air-Backflush System. Biotechnol Prog. 2003;19:30-6.
[127] Dalm MC, Cuijten SM, van Grunsven WM, Tramper J, Martens DE. Effect of feed and bleed rate on hybridoma cells in an acoustic perfusion bioreactor: part I. Cell density, viability, and cell-cycle distribution. Biotechnol Bioeng. 2004;88:547-57.
[128] Gorenflo VM, Smith L, Dedinsky B, Persson B, Piret JM. Scale-up and optimization of an acoustic filter for 200 L/day perfusion of a CHO cell culture. Biotechnol Bioeng. 2002;80:438-44.
[129] Boycott AE. Sedimentation of Blood Corpuscles. Nature. 1920;104:532-.
[130] Searles JA, Todd P, Kompala DS. PERFUSION CULTURE OF SUSPENDED CHO CELLS EMPLOYING INCLINED SEDIMENTATION. In: Spier RE, Griffiths JB, Berthold W, editors. Animal Cell Technology: Butterworth-Heinemann; 1994. p. 240-2.
[131] Batt BC, Davis RH, Kompala DS. Inclined Sedimentation for Selective Retention of Viable Hybridomas in a Continuous Suspension Bioreactor. Biotechnology Progress. 1990;6:458-64.

[132] Vogel JH, Nguyen H, Giovannini R, Ignowski J, Garger S, Salgotra A, et al. A new large-scale manufacturing platform for complex biopharmaceuticals. Biotechnology and Bioengineering. 2012;109:3049-58.
[133] Berrios J, Altamirano C, Osses N, Gonzalez R. Continuous CHO cell cultures with improved recombinant protein productivity by using mannose as carbon source: Metabolic analysis and scale-up simulation. Chemical Engineering Science. 2011;66:2431-9.
[134] Pohlscheidt M, Jacobs M, Wolf S, Thiele J, Jockwer A, Gabelsberger J, et al. Optimizing capacity utilization by large scale 3000 L perfusion in seed train bioreactors. Biotechnology Progress. 2013;29:222-9.
[135] Henzler H-J. Kontinuierliche Fermentation mit tierischen Zellen. Teil 2. Chemie Ingenieur Technik. 2012;84:1469-81.
[136] Kompala D, Harris M, Glascock C, Samuel P. Single use plastic settlers for clarifying cell culture broth, selective removal of dead cells and affinity capture of antibodies on protein A beads. In: Ding W, Micheletti M, Repetto R, editors. Single-Use Technologies III: Scientific and Technological Advancements. Snowbird, Utah: ECI Symposium Series; 2018.
[137] Shen Y, Yanagimachi K. CFD-aided cell settler design optimization and scale-up: Effect of geometric design and operational variables on separation performance. Biotechnology Progress. 2011;27:1282-96.
[138] Walther J, Lu J, Hollenbach M, Yu M, Hwang C, McLarty J, et al. Perfusion Cell Culture Decreases Process and Product Heterogeneity in a Head-to-Head Comparison With Fed-Batch. Biotechnology Journal. 2019;14:1-10.
[139] Xu S, Chen H. High-density mammalian cell cultures in stirred-tank bioreactor without external pH control. Journal of Biotechnology. 2016;231:149-59.
[140] Karst DJ, Steinebach F, Soos M, Morbidelli M. Process performance and product quality in an integrated continuous antibody production process. Biotechnol Bioeng. 2017;114:298-307.
[141] Warikoo V, Godawat R, Brower K, Jain S, Cummings D, Simons E, et al. Integrated continuous production of recombinant therapeutic proteins. Biotechnology and Bioengineering. 2012;109:3018-29.
[142] Godawat R, Konstantinov K, Rohani M, Warikoo V. End-to-end integrated fully continuous production of recombinant monoclonal antibodies. Journal of Biotechnology. 2015;213:13-9.
[143] Allison G, Cain YT, Cooney C, Garcia T, Bizjak TG, Holte O, et al. Regulatory and Quality Considerations for Continuous Manufacturing May 20–21, 2014 Continuous Manufacturing Symposium. Journal of Pharmaceutical Sciences. 2015;104:803-12.
[144] Tapia F, Vogel T, Genzel Y, Behrendt I, Hirschel M, Gangemi JD, et al. Production of high-titer human influenza A virus with adherent and suspension MDCK cells cultured in a single-use hollow fiber bioreactor. Vaccine. 2014;32:1003-11.
[145] Nikolay A, Bissinger T, Gränicher G, Wu Y, Genzel Y, Reichl U. Perfusion control for high cell density cultivation and viral vaccine production. In: Pörtner R, editor. Animal cell biotechnology: Humana Press, New York, NY; 2020. p. 141-68.
[146] Gorenflo VM, Ritter JB, Aeschliman DS, Drouin H, Bowen BD, Piret JM. Characterization and optimization of acoustic filter performance by experimental design methodology. Biotechnol Bioeng. 2005;90:746-53.
[147] Coronel J, Heinrich C, Klausing S, Noll T, Figueredo-Cardero A, Castilho LR. Perfusion process combining low temperature and valeric acid for enhanced recombinant factor VIII production. Biotechnol Prog. 2020;36:1-11.

[148] Jordan I, John K, Howing K, Lohr V, Penzes Z, Gubucz-Sombor E, et al. Continuous cell lines from the Muscovy duck as potential replacement for primary cells in the production of avian vaccines. Avian Pathol. 2016;45:137-55.
[149] Lohr V, Rath A, Genzel Y, Jordan I, Sandig V, Reichl U. New avian suspension cell lines provide production of influenza virus and MVA in serum-free media: studies on growth, metabolism and virus propagation. Vaccine. 2009;27:4975-82.
[150] Kalbfuss B, Knöchlein A, Kröber T, Reichl U. Monitoring influenza virus content in vaccine production: Precise assays for the quantitation of hemagglutination and neuraminidase activity. Biologicals. 2008;36:145-61.
[151] Genzel Y, Reichl U. Vaccine Production. In: Poertner R, editor. Animal Cell Biotechnology: Methods and Protocols. Totowa, NJ: Humana Press; 2007. p. 457-73.
[152] Frensing T, Kupke SY, Bachmann M, Fritzsche S, Gallo-Ramirez LE, Reichl U. Influenza virus intracellular replication dynamics, release kinetics, and particle morphology during propagation in MDCK cells. Appl Microbiol Biotechnol. 2016;100:7181-92.
[153] Hennig R, Rapp E, Kottler R, Cajic S, Borowiak M, Reichl U. N-Glycosylation Fingerprinting of Viral Glycoproteins by xCGE-LIF. In: Lepenies B, editor. Carbohydrate-Based Vaccines: Methods and Protocols. New York, NY: Springer New York; 2015. p. 123-43.
[154] Schwarzer J, Rapp E, Reichl U. N-glycan analysis by CGE–LIF: Profiling influenza A virus hemagglutinin N-glycosylation during vaccine production. Electrophoresis. 2008;29:4203-14.
[155] Pralow A, Hoffmann M, Nguyen-Khuong T, Rapp E, Reichl U. Improvement of the glycoproteomic toolbox with the discovery of a unique C-terminal cleavage specificity of flavastacin for N-glycosylated asparagine. Scientific Reports. 2017;7:11419.
[156] Hoffmann M, Pioch M, Pralow A, Hennig R, Kottler R, Reichl U, et al. The Fine Art of Destruction: A Guide to In-Depth Glycoproteomic Analyses–Exploiting the Diagnostic Potential of Fragment Ions. Proteomics. 2018.
[157] Wisniewski JR, Zougman A, Nagaraj N, Mann M. Universal sample preparation method for proteome analysis. Nature methods. 2009;6:359-62.
[158] Selman MH, Hemayatkar M, Deelder AM, Wuhrer M. Cotton HILIC SPE microtips for microscale purification and enrichment of glycans and glycopeptides. Analytical chemistry. 2011;83:2492-9.
[159] Pioch M, Hoffmann M, Pralow A, Reichl U, Rapp E. glyXtoolMS: An Open-Source Pipeline for Semiautomated Analysis of Glycopeptide Mass Spectrometry Data. Analytical Chemistry. 2018.
[160] Pieler MM, Heyse A, Wolff MW, Reichl U. Specific ion effects on the particle size distributions of cell culture-derived influenza A virus particles within the Hofmeister series. Engineering in Life Sciences. 2017;17:470-8.
[161] Hu W-S. Cell Culture Bioprocess Engineering (2nd ed.). Boca Raton, USA: CRC Press; 2020.
[162] Cortin V, Thibault J, Jacob D, Garnier A. High-titer adenovirus vector production in 293S cell perfusion culture. Biotechnol Prog. 2004;20:858-63.
[163] Maiorella B, Dorin G, Carion A, Harano D. Crossflow microfiltration of animal cells. Biotechnol Bioeng. 1991;37:121-6.
[164] ATCC. FAQ's: Converting TCID[50] to plaque forming units (PFU): Is it possible to determine from the TCID[50] how many plaque forming units to expect? 2012.
[165] Comisel R-M, Kara B, Fiesser FH, Farid SS. Lentiviral vector bioprocess economics for cell and gene therapy commercialisation. Biochemical Engineering Journal. 2020:107868.
[166] Pohlscheidt M, Langer U, Minuth T, Bodeker B, Apeler H, Horlein HD, et al. Development and optimisation of a procedure for the production of Parapoxvirus ovis by

large-scale microcarrier cell culture in a non-animal, non-human and non-plant-derived medium. Vaccine. 2008;26:1552-65.
[167] Tapia F, Jordan I, Genzel Y, Reichl U. Efficient and stable production of Modified Vaccinia Ankara virus in two-stage semi-continuous and in continuous stirred tank cultivation systems. PLoS One. 2017;12:1-17.
[168] Frensing T, Heldt FS, Pflugmacher A, Behrendt I, Jordan I, Flockerzi D, et al. Continuous Influenza Virus Production in Cell Culture Shows a Periodic Accumulation of Defective Interfering Particles. PLOS ONE. 2013;8:e72288.
[169] Bissinger T, Fritsch J, Mihut A, Wu Y, Liu X, Genzel Y, et al. Semi-perfusion cultures of suspension MDCK cells enable high cell concentrations and efficient influenza A virus production. Vaccine. 2019;37:7003-10.
[170] Reperant LA, Moesker FM, Osterhaus ADME. Influenza: from zoonosis to pandemic. ERJ Open Research. 2016;2:00013-2016.
[171] Le Ru A, Jacob D, Transfiguracion J, Ansorge S, Henry O, Kamen AA. Scalable production of influenza virus in HEK-293 cells for efficient vaccine manufacturing. Vaccine. 2010;28:3661-71.
[172] Pau MG, Ophorst C, Koldijk MH, Schouten G, Mehtali M, F. U. The human cell line PER.C6 provides a new manufacturing system for the production of influenza vaccines. Vaccine. 2001;19:2716–21.
[173] Eagle H. Amino acid metabolism in mammalian cell cultures. Science. 1959;130:432-7.
[174] Ferreira TB, Ferreira AL, Carrondo MJ, Alves PM. Effect of re-feed strategies and non-ammoniagenic medium on adenovirus production at high cell densities. Journal of Biotechnology. 2005;119:272-80.
[175] Lindsay DA, Betenbaugh MJ. Quantification of Cell Culture Factors Affecting Recombinant Protein Yields in Baculovirus-Infected Insect Cells. Biotechnology and Bioengineering. 1992;39:614-8.
[176] EMA - Guideline on development, production, characterisation and specifications for monoclonal antibodies and related products - draft (2009). 2013.
[177] EMA - Guideline on Influenza Vaccines - Quality module (2017). 2017.
[178] Hutter J, Rodig JV, Hoper D, Seeberger PH, Reichl U, Rapp E, et al. Toward animal cell culture-based influenza vaccine design: viral hemagglutinin N-glycosylation markedly impacts immunogenicity. J Immunol. 2013;190:220-30.
[179] de Vries RP, Smit CH, de Bruin E, Rigter A, de Vries E, Cornelissen LA, et al. Glycan-dependent immunogenicity of recombinant soluble trimeric hemagglutinin. Journal of virology. 2012:JVI. 01084-12.
[180] Lohr V, Genzel Y, Behrendt I, Scharfenberg K, Reichl U. A new MDCK suspension line cultivated in a fully defined medium in stirred-tank and wave bioreactor. Vaccine. 2010;28:6256-64.
[181] Marks DM. Equipment design considerations for large scale cell culture. Cytotechnology. 2003;42:21-33.
[182] King JA, Miller WM. Bioreactor development for stem cell expansion and controlled differentiation. Curr Opin Chem Biol. 2007;11:394-8.
[183] Hassel T, Gleave S, Butler M. Growth Inhibition in Animal Cell Culture. The Effect of Lactate and Ammonia. Applied Biochemistry and Biotechnology. 1991;30:29-41.
[184] Ozturk SS, Riley MR, Palsson BO. Effects of Ammonia and Lactate on Hybridoma Growth, Metabolism, and Antibody Production. Biotechnology and Bioengineering. 1992;39:418-31.

[185] Cruz HJ, Freitas CM, Alves PM, Moreira JL, Carrondo MJT. Effects of ammonia and lactate on growth, metabolism, and productivity of BHK cells. Enzyme and Microbial Technology. 2000;27:43-52.
[186] Schneider M, Marison IW, von Stockar U. The importance of ammonia in mammalian cell culture. Journal of Biotechnology. 1996;46:161-85.
[187] Lohr V, Hädicke O, Genzel Y, Jordan I, Büntemeyer H, Klamt S, et al. The avian cell line AGE1.CR.pIX characterized by metabolic flux analysis. BMC Biotechnology. 2014;14:72.
[188] Genzel Y, Behrendt I, Rodig J, Rapp E, Kueppers C, Kochanek S, et al. CAP, a new human suspension cell line for influenza virus production. Appl Microbiol Biotechnol. 2013;97:111-22.
[189] Huang D, Xia-Hou K, Liu XP, Zhao L, Fan L, Ye Z, et al. Rational design of medium supplementation strategy for improved influenza viruses production based on analyzing nutritional requirements of MDCK Cells. Vaccine. 2014;32:7091-7.
[190] Konstantinov K, Goudar C, Ng M, Meneses R, Thrift J, Chuppa S, et al. The "Push-to-Low" Approach for Optimization of High-Density Perfusion Cultures of Animal Cells. In: Hu W-S, editor. Cell Culture Engineering. Berlin, Heidelberg: Springer Berlin Heidelberg; 2006. p. 75-98.
[191] Tate M, Job E, Deng Y-M, Gunalan V, Maurer-Stroh S, Reading P. Playing Hide and Seek: How Glycosylation of the Influenza Virus Hemagglutinin Can Modulate the Immune Response to Infection. Viruses. 2014;6:1294.
[192] Harvey DJ. Mass spectrometric analysis of glycosylated viral proteins. Expert Review of Proteomics. 2018;15:391-412.
[193] Schwarzer J, Rapp E, Hennig R, Genzel Y, Jordan I, Sandig V, et al. Glycan analysis in cell culture-based influenza vaccine production: Influence of host cell line and virus strain on the glycosylation pattern of viral hemagglutinin. Vaccine. 2009;27:4325-36.
[194] Yanming A, Parsons LM, Jankowska E, Melnyk D, Joshi M, Cipollo JF. N-Glycosylation of Seasonal Influenza Vaccine Hemagglutinins: Implication for Potency Testing and Immune Processing. J Virol. 2019;93:e01693-18.
[195] Fortuna AR, Taft F, Villain L, Wolff MW, Reichl U. Optimization of cell culture-derived influenza A virus particles purification using sulfated cellulose membrane adsorbers. Engineering in Life Sciences. 2018;18:29-39.
[196] ZKBS. Stellungnahme der ZKBS zur Neueinstufung der Zelllinie PK(15) als Spender- oder Empfängerorganismus gemäß § 5 Absatz 1 GenTSV. In: Safety FOoCPaF, editor. Berlin2018.
[197] Agarabi CD, Chavez BK, Lute SC, Read EK, Rogstad S, Awotwe-Otoo D, et al. Exploring the linkage between cell culture process parameters and downstream processing utilizing a plackett-burman design for a model monoclonal antibody. Biotechnol Prog. 2017;33:163-70.
[198] Wilson LJ, Lewis W, Kucia-Tran R, Bracewell DG. Identification of upstream culture conditions and harvest time parameters that affect host cell protein clearance. Biotechnol Prog. 2019;35:e2805.
[199] Dalm MC, Jansen M, Keijzer TM, van Grunsven WM, Oudshoorn A, Tramper J, et al. Stable hybridoma cultivation in a pilot-scale acoustic perfusion system: long-term process performance and effect of recirculation rate. Biotechnol Bioeng. 2005;91:894-900.
[200] Blaschczok K, Kaiser SC, Löffelholz C, Imseng N, Burkart J, Bösch P, et al. Investigations on Mechanical Stress Caused to CHO Suspension Cells by Standard and Single-Use Pumps. Chemie Ingenieur Technik. 2013;85:144-52.
[201] Merten O-W. Constructive improvement of the ultrasonic separation device ADI 1015. Cytotechnology. 2000;34:175-9.

[202] Lara AR, Galindo E, Ramírez OT, Palomares LA. Living With Heterogeneities in Bioreactors. Molecular Biotechnology. 2006;34:355-81.
[203] Spadiut O, Rittmann S, Dietzsch C, Herwig C. Dynamic process conditions in bioprocess development. Engineering in Life Sciences. 2013;13:88-101.
[204] Drouin H, Ritter JB, Gorenflo VM, Bowen BD, Piret JM. Cell Separator Operation within Temperature Ranges To Minimize Effects on Chinese Hamster Ovary Cell Perfusion Culture. Biotechnol Prog. 2007;23:1473-84.
[205] Antoni BA, Sabbatini P, Rabson AB, White E. Inhibition of apoptosis in human immunodeficiency virus-infected cells enhances virus production and facilitates persistent infection. Journal of Virology. 1995;69:2384-92.
[206] Palomares LA, Gonzalez M, Ramirez OT. Evidence of Pluronic F-68 direct interaction with insect cells: impact on shear protection, recombinant protein, and baculovirus production. Enzyme and Microbial Technology. 2000;26:324-31.
[207] van Reis R, Leonard LC, Hsu CC, Builder SE. Industrial scale harvest of proteins from mammalian cell culture by tangential flow filtration. Biotechnol Bioeng. 1991;38:413-22.
[208] Ratanji KD, Derrick JP, Dearman RJ, Kimber I. Immunogenicity of therapeutic proteins: influence of aggregation. J Immunotoxicol. 2014;11:99-109.
[209] Rosenberg AS. Effect of Protein Aggregates: An Immunologic perspective. The AAPS Journal. 2006;8:501-7.
[210] Wang W, Singh SK, Li N, Toler MR, King KR, Nema S. Immunogenicity of protein aggregates--concerns and realities. Int J Pharm. 2012;431:1-11.
[211] Esclade LRJ, Carrel S, Péringer P. Influence of the screen material on the fouling of spin filters. Biotechnol Bioeng. 1991;38:159-68.
[212] Mercille S, Johnson M, Lemieux R, Massie B. Filtration-Based Perfusion of Hybridoma Cultures in Protein-Free Medium: Reduction of Membrane Fouling by Medium Supplementation with DNase I. Biotechnol Bioeng. 1994;43:833-46.
[213] Gränicher G, Coronel J, Trampler F, Jordan I, Genzel Y, Reichl U. Performance of an acoustic settler versus a hollow fiber-based ATF technology for influenza virus production in perfusion. Appl Microbiol Biotechnol. 2020;104:4877–88.
[214] Choo C-Y, Tian Y, Kim W-S, Blatter E, Conary J, Brady CP. High-Level Production of a Monoclonal Antibody in Murine Myeloma Cells by Perfusion Culture Using a Gravity Settler. Biotechnology Progress. 2007;23:225-31.
[215] Shimoni Y, Forsyth T, Srinivasan V, Szeto R. Reducing Variability in Cell-Specific Productivity in Perfusion Culture. BioProcess International. 2018;16:22-31.
[216] Galliher PM. Single Use Technology and Equipment. In: Jagschies G, Lindskog E, Łącki K, Galliher PM, editors. Development, Design, and Implementation of Manufacturing Processes. Cambridge: Elsevier; 2017. p. 557-77.
[217] Lazarowitz SG, Choppin PW. Enhancement of the infectivity of influenza A and B viruses by proteolytic cleavage of the hemagglutinin polypeptide. Virology. 1975;68:440-54.
[218] Dou D, Revol R, Östbye H, Wang H, Daniels R. Influenza A Virus Cell Entry, Replication, Virion Assembly and Movement. Frontiers in Immunology. 2018;9:1-17.
[219] Seitz C, Isken B, Heynisch B, Rettkowski M, Frensing T, Reichl U. Trypsin promotes efficient influenza vaccine production in MDCK cells by interfering with the antiviral host response. Appl Microbiol Biotechnol. 2012;93:601-11.
[220] Genzel Y. Designing cell lines for viral vaccine production: Where do we stand? Biotechnol J. 2015;10:728-40.

[221] Coronel J, Gränicher G, Sandig V, Noll T, Y. G, U. R. Use of an inclined settler for cell culture-based influenza A virus production in perfusion mode. Frontiers in Bioeng and Biotech. 2020.
[222] Schirmer C, Müller J, Steffen N, Werner S, Eibl R, Eibl D. How to Produce mAbs in a Cube-Shaped Stirred Single-Use Bioreactor at 200 L Scale. In: Pörtner R, editor. Animal Cell Biotechnology: Methods and Protocols. New York, NY: Springer US; 2020. p. 169-86.
[223] Gramer MJ, Maas J, Lieberman MM. Use of hollow fiber systems for rapid and direct scale up of antibody production from hybridoma cell lines cultured in CL-1000 flasks using BD Cell MAb medium. Cytotechnology. 2003;42:155-62.
[224] Whitford WG, Cadwell JJS. Interest in Hollow-Fiber Perfusion Bioreactors Is Growing. BioProcess International. 2009;1:54-63.
[225] Eibl D, Eibl R. Single-Use Equipment in Biopharmaceutical Manufacture. In: Eibl D, Eibl R, editors. Single-Use Technology in Biopharmaceutical Manufacture. Wiley ed. online version: Wiley; 2019. p. 1-11.
[226] Dorceus M, Willard SS, Suttle A, Han K, Chen P-J, Sha M. Comparing Culture Methods in Monoclonal Antibody Production: Batch, Fed-Batch, and Perfusion. BioProcess International. 2017;15:38-46.
[227] Weuster-Botz D. Parallel Reactor Systems for Bioprocess Development. In: Kragl U, editor. Technology Transfer in Biotechnology: From lab to Industry to Production. Berlin, Heidelberg: Springer Berlin Heidelberg; 2005. p. 125-43.
[228] Betts JI, Baganz F. Miniature bioreactors: current practices and future opportunities. Microbial Cell Factories. 2006;5:21.
[229] Kumar S, Wittmann C, Heinzle E. Minibioreactors. Biotechnology Letters. 2004;26:1-10.
[230] Amanullah A, Otero JM, Mikola M, Hsu A, Zhang J, Aunins J, et al. Novel micro-bioreactor high throughput technology for cell culture process development: Reproducibility and scalability assessment of fed-batch CHO cultures. Biotechnology and Bioengineering. 2010;106:57-67.
[231] Lim AC, Washbrook J, Titchener-Hooker NJ, Farid SS. A computer-aided approach to compare the production economics of fed-batch and perfusion culture under uncertainty. Biotechnology and Bioengineering. 2006;93:687-97.
[232] Pleitt K, Somasundaram B, Johnson B, Shave E, Lua LHL. Evaluation of process simulation as a decisional tool for biopharmaceutical contract development and manufacturing organizations. Biochemical Engineering Journal. 2019;150:107252.
[233] Klutz S, Holtmann L, Lobedann M, Schembecker G. Cost evaluation of antibody production processes in different operation modes. Chemical Engineering Science. 2016;141:63-74.
[234] Cameau E, Pedregal A, Glover C. Cost modelling comparison of adherent multi-trays with suspension and fixed-bed bioreactors for the manufacturing of gene therapy products. Cell and Gene Therapy Insights. 2019;5:1663-74.
[235] Gränicher G, Tapia F, Behrendt I, Jordan I, Genzel Y, Reichl U. Production of Modified Vaccinia Ankara Virus by Intensified Cell Cultures: A Comparison of Platform Technologies for Viral Vector Production. Biotechnology Journal. 2020:2000024.
[236] Pearson S. Process Intensification of Viral-Based Vaccines. Where Are the Bottlenecks? BioProcess International. 2020;18:68-70.
[237] Lothert K, Sprick G, Beyer F, Lauria G, Czermak P, Wolff MW. Membrane-based steric exclusion chromatography for the purification of a recombinant baculovirus and its application for cell therapy. Journal of Virological Methods. 2020;275:113756.

[238] Lothert K, Pagallies F, Feger T, Amann R, Wolff MW. Selection of chromatographic methods for the purification of cell culture-derived Orf virus for its application as a vaccine or viral vector. Journal of Biotechnology. 2020;323:62-72.
[239] Lothert K, Offersgaard AF, Pihl AF, Mathiesen CK, Jensen TB, Alzua GP, et al. Development of a downstream process for the production of an inactivated whole hepatitis C virus vaccine. Scientific Reports. 2020;10:16261.
[240] Marichal-Gallardo P, Börner K, Pieler MM, Sonntag-Buck V, Obr M, Bejarano D, et al. Single-use capture purification of adeno-associated viral gene transfer vectors by membrane-based steric exclusion chromatography. Human Gene Therapy. 2021.
[241] Gerstweiler L, Bi J, Middelberg APJ. Continuous downstream bioprocessing for intensified manufacture of biopharmaceuticals and antibodies. Chemical Engineering Science. 2021;231:116272.
[242] Ungerechts G, Bossow S, Leuchs B, Holm PS, Rommelaere J, Coffey M, et al. Moving oncolytic viruses into the clinic: clinical-grade production, purification, and characterization of diverse oncolytic viruses. Molecular Therapy - Methods & Clinical Development. 2016;3:16018.
[243] Xenopoulos A. Production and Purification of Hepatitis C Virus-like Particles [Webinar]. In: Millipore E, editor. EMD Millipore Webinar Series2015.
[244] Kalbfuss B, Genzel Y, Wolff M, Zimmermann A, Morenweiser R, Reichl U. Harvesting and concentration of human influenza A virus produced in serum-free mammalian cell culture for the production of vaccines. Biotechnology and Bioengineering. 2007;97:73-85.
[245] Vincent DIW. Purification of Recombinant Vaccinia Virus for Oncolytic and Immunotherapeutic Applications using Monolithic Column Technology. London: University College London; 2017.
[246] Besnard L, Fabre V, Fettig M, Gousseinov E, Kawakami Y, Laroudie N, et al. Clarification of vaccines: An overview of filter based technology trends and best practices. Biotechnology Advances. 2016;34:1-13.
[247] Cherradi Y, Le Merdy S, Sim L-J, Ito T, Pattanaik P, Haas J, et al. Filter-Based Clarification of Viral Vaccines and Vectors. BioProcess International. 2018;16:48-53.
[248] Fenouillot F, Cassagnau P, Majesté JC. Uneven distribution of nanoparticles in immiscible fluids: Morphology development in polymer blends. Polymer. 2009;50:1333-50.
[249] Kim Y, Rana D, Matsuura T, Chung W-J, Khulbe KC. Relationship between surface structure and separation performance of poly(ether sulfone) ultra-filtration membranes blended with surface modifying macromolecules. Separation and Purification Technology. 2010;72:123-32.
[250] Michen B, Graule T. Isoelectric points of viruses. Journal of Applied Microbiology. 2010;109:388-97.
[251] Jordan I, Weimer D, Iarusso S, Bernhardt H, Lohr V, Sandig V. Purification of modified vaccinia virus Ankara from suspension cell culture. BMC Proc. 2015;9:O13-O.
[252] Hughes K, Zachertowska A, Wan S, Li L, Klimaszewski D, Euloth M, et al. Yield increases in intact influenza vaccine virus from chicken allantoic fluid through isolation from insoluble allantoic debris. Vaccine. 2007;25:4456-63.
[253] Wright JF, Le T, Prado J, Bahr-Davidson J, Smith PH, Zhen Z, et al. Identification of factors that contribute to recombinant AAV2 particle aggregation and methods to prevent its occurrence during vector purification and formulation. Molecular Therapy. 2005;12:171-8.
[254] Pitcher WH. Design and operation of immobilized enzyme reactors. Berlin, Heidelberg: Springer Berlin Heidelberg; 1978. p. 1-26.

[255] Wu Y, Bissinger T, Genzel Y, Liu X, Reichl U, Tan W-S. High cell density perfusion process for high yield of influenza A virus production using MDCK suspension cells. Applied Microbiology and Biotechnology. 2021;105:1421-34.
[256] Chuan YP, Wibowo N, Lua LHL, Middelberg APJ. The economics of virus-like particle and capsomere vaccines. Biochemical Engineering Journal. 2014;90:255-63.
[257] Breite D, Went M, Prager A, Schulze A. The critical zeta potential of polymer membranes: how electrolytes impact membrane fouling. RSC Advances. 2016;6:98180-9.
[258] Lukasik J, Scott TM, Andryshak D, Farrah SR. Influence of Salts on Virus Adsorption to Microporous Filters. Applied and Environmental Microbiology. 2000;66:2914-20.
[259] Gränicher G, Babakhani M, Göbel S, Jordan I, Marichal-Gallardo P, Y. G, et al. A high cell density perfusion process for Modified Vaccinia virus Ankara production: Process integration with inline DNA digestion and cost analysis. Biotechnol Bioeng. 2021;118:4720-34.
[260] Repligen. ATF System Engineering Scale-Up. 2021.
[261] Khanal O, Singh N, Traylor SJ, Xu X, Ghose S, Li ZJ, et al. Contributions of depth filter components to protein adsorption in bioprocessing. Biotechnology and Bioengineering. 2018;115:1938-48.
[262] Afshar S, Salimi E, Fazelkhah A, Braasch K, Mishra N, Butler M, et al. Progression of change in membrane capacitance and cytoplasm conductivity of cells during controlled starvation using dual-frequency DEP cytometry. Analytica Chimica Acta. 2019;1059:59-67.
[263] Labeed FH, Coley HM, Hughes MP. Differences in the biophysical properties of membrane and cytoplasm of apoptotic cells revealed using dielectrophoresis. Biochimica et Biophysica Acta (BBA) - General Subjects. 2006;1760:922-9.
[264] Zimmermann D, Zhou A, Kiesel M, Feldbauer K, Terpitz U, Haase W, et al. Effects on capacitance by overexpression of membrane proteins. Biochemical and Biophysical Research Communications. 2008;369:1022-6.
[265] Johnson L, Gupta AK, Ghafoor A, Akin D, Bashir R. Characterization of vaccinia virus particles using microscale silicon cantilever resonators and atomic force microscopy. Sensors and Actuators B: Chemical. 2006;115:189-97.
[266] Niklas J, Schräder E, Sandig V, Noll T, Heinzle E. Quantitative characterization of metabolism and metabolic shifts during growth of the new human cell line AGE1.HN using time resolved metabolic flux analysis. Bioprocess Biosyst Eng. 2011;34:533-45.

Chapter 10

Appendix

10.1 Scale-up and scale-down considerations for an ATF system

When designing an ATF system, several aspects need to be considered for a smooth scale-up or scale-down model [260]. It is important to keep the factor of dip-tube length / dip-tube diameter constant. The connections should have the same diameter as the dip-tube to ensure a laminar flow.

The perfusion flow rate per hollow-fiber membrane filtration surface (in LMH, $L/m^2_{filter\ from\ ATF}/h$) should be kept constant when scaling-up a process. The exchange flow rate should be carefully selected as well. In general, the ATF exchange flow rate / perfusion flow rate ratio should be adjusted to 100, in order to obtain backflush (known as the Starling effect, section 2.6.1). In addition, the pump displacement volume / dead volume in the ATF system ratio should be kept at 1.5. The dead volume includes the filter, the dip-tube and the silicon tubing connecting the ATF to the bioreactor. For the ATF2 system, the pump displacement volume is equal to 115 mL. The dead volume can be variable due to changes of the hollow-fiber geometry. The linear fluid velocity inside the fiber (m/s) should be kept constant (it is a function of the ATF exchange flow rate) so that the effective shear is maintained across scales (for hollow-fibers with conserved internal diameter; see Equation 20, section 3.13.2).

The residence time inside the ATF column should be ideally kept constant when scaling-up. Supposing that the pump displacement volume / dead volume in the ATF system ratio is 1.5, it is estimated that 66% of the dead volume is recirculated in the bioreactor with one exchange cycle. After the second exchange cycle, only 11% of the dead volume before the first cycle is remaining. Four cycles should be considered to calculate the residence time in the ATF system. Depending on the exchange flow rate, the recirculation cycle time of the ATF2 is between 5 and 23 s, meaning that the residence time is estimated to be between 20 and 92 s. When scaling-up, the residence time should be calculated with the new system, knowing the recirculation cycle time length, the pump displacement volume, and the dead volume.

As an additional note, due to membrane clogging and membrane fouling (during a scale-up), the perfusion flow rate might decrease although the peristaltic pump rpm is kept the same. Therefore, it is recommended to place a balance under the harvested volume to better monitor the perfusion flow rate. If needed, the peristaltic pump rpm has to be increased to keep the same perfusion rate.

10.2 Materials and Methods

10.2.1 SOP list

The SOPs listed in Table A.1 are available upon request from the Bioprocess Engineering group of the Max Planck Institute for Dynamics of Complex Technical Systems (Magdeburg, Germany), headed by Prof. Dr.-Ing. Udo Reichl, except for SOPs indicated as confidential.

Table A.1: List of SOPs and method documents used in the thesis. The SOPs indicated in bold are (co-)authored by the PhD Thesis Author.

Method / assay	Document title(s)	Author(s)
Amino acid quantification with the HPLC	Aminosäure Analytik (AAA) mit dem ACCQ-TAG Ultra von Waters, Nr. G/27, V 24.02.2016	S. König
Autoclaving	Dampfsterilizator Laboklav	S. König
Bioreactor operation: BIOSTAT system	Inbetriebsnahme BIOSTAT, V 18.02.2016	K. Hermann, A. Bock
Bioreactor operation: DASGIP system	i) Dasgip fedbatch pro® System, Nr. G/1, V 16.06.2005 **ii) SOP: Dasgip System using DASware Control 5 software, V 05.10.2018**	i) L. Geisler **ii) G. Gränicher**
Bradford assay for total protein quantification	i) Inactivation with β-Propiolactone, V 1.6 ii) Protein Estimation in Microtiter Plates, V 2.2	B. Kalbfuss
Cell banking	Kryokonservierung von Zellen, Nr. Z/06, V 05.01.2007	A. Kiesel, S. König, C. Best
Cell counting with Vicell XR	Kurzanleitung Zellzählgerät ViCell XR, Nr. G/21, V 1.5	J. Schulze-Horsel
Cell culture basics	i) Allgemeines steriles Arbeiten, Nr. Z/07, V 08.09.2006 ii) Mycoplasmen test, Nr. Z/09, V 24.11.2008 iii) Zellkulturloesungen, Nr. Z/00, V 01.08.2012 iv) Passagieren von MDCK-Zellen in serumhaltigem Medium, Nr. Z/04, V 14.07.2015 v) Passagieren von MDCK-Zellen in serumfreien Medien, Nr. Z/05, V 11.09.2006	i) S. König, N. Schlawin ii) N. Wynserski, F. Weber iii) C. Best iv) A. Kiesel, I. Behrendt, S. König, N. Schlawin v) I. Gehrendt, S. König, N. Schlawin
Cell storage at -196°C	6.0 Lagerung, Kryokonservierung von Zellen, Nr. Z/06, V 05.01.2007	A. Kiesel, S. König, C. Best
Cell thawing	i) Auftauen von MDCK-Zellen, Nr. Z/02, V 25.06.2003 ii) Unfreezing and cultivation of MDCK suspension cells	i) I. Behrendt ii) N. Wynserski, F. Weber

Glycoanalysis for site-specific glycopeptide analysis	i) Arbeitsanweisung für die Ultrazentrifuge Optima LE-80K, Nr. G/19, V 05.04.2006 ii) CONFIDENTIAL: Gradient centrifugation (Sample concentration), glyXera Magdeburg, Nr. A1, V 1.0 iii) (for protein quantification only) Instruction for protein quantification using the QuantIT protein assay (Q33210) iv) CONFIDENTIAL: SOP Proteolytic Digest Using Filter-Aided Sample Preparation (FASP), V 1.5 v) CONFIDENTIAL: SOP Spin-Cotton-HILIC Purification for Glykopeptide Analysis, V 1.2	i) N. Schlawin, J. Schwarzer ii) R. Hennig, A. Bock iii) Life Technologies iv) M. Hoffman, A. Pralow v) M. Hoffmann, A. Pralow, T. Nguyen-Khuong
Hemagglutinin quantification for influenza virus	i) Hemagglutination assay (HA assay), Nr. V/05, V 2.2 ii) Herstellung einer Erythrocytenlösung mit definierter Zellzahl, Nr. V/07, V 06.11.2019	i) V. Lohr ii) C. Best
Metabolite quantification with the Bioprofile	i) Metabolitbestimmung aus Zellkultur, Nr. A/02 V 1.0 ii) Bedienungsanweisung Bioprofile 100Plus, Nr. G/22, V 13.03.2020	i) V. Lohr ii) S. König
MVA-CR19.GFP genome relative quantification with qPCR	**CONFIDENTIAL: Relative quantification of Modified Vaccinia virus Ankara viral genome via a qPCR method, Nr. V/XX, V 1.0**	**G. Gränicher**
Perfusion operation with bioreactor [a)]	**i) 3.7 Bioreactor with Manual CSPR Control** **ii) 3.8 Bioreactor with Automated CSPR control**	A. Nikolay, T. Bissinger, **G. Gränicher**, Y. Wu
Perfusion operation with shake flask [a)]	**3.6 Pseudo Perfusion**	A. Nikolay, T. Bissinger, **G. Gränicher**, Y. Wu
Picogreen assay for DNA quantification	i) Inactivation with β-Propiolactone, V 1.6 ii) dsDNA estimation in Microtiter Plates, V 2.3	A. Zimmermann, B. Kalbfuss
qPCR assay for host cell DNA quantification	**CONFIDENTIAL: Quantification of AGE1.CR.pIX host cell DNA concentration via a qPCR method, Nr. Z/XX, V 1.0**	**G. Gränicher**
Size distribution measurement of cell culture supernatant	Standard Operating Procedure - Measurement of influenza virus particle size distributions with the CPS Disc Centrifuge DC24000, V 2	M. Pieler
SRID	i) Inactivation with β-Propiolactone, V 1.6 ii) Single-Radial-Immunodiffusion (SRID)-Assay Influenza A virus (strain A/Puerto Rico/8/1934 H1N1), V 24.02.2016	i) B. Kalbfuss ii) A. Bastian, L. Fichtmüller
$TCID_{50}$ measurement for influenza virus	i) Bestimmung des $TCID_{50}$ (influenza virus), Nr. V/12, V 2.0 ii) Axio Observer, Nr. G/26, V 1	i) I. Behrendt, N. Wynserski, S. König ii) N. Wynserski
$TCID_{50}$ measurement for MVA-CR19	i) Bestimmung des $TCID_{50}$ für MVA (Modified Vaccinia Virus Ankara), Nr. V/09, V 1.1 ii) Axio Observer, Nr. G/26, V 1	i) V. Lohr, C. Best, S. König ii) N. Wynserski
$TCID_{50}$ measurements for MVA-CR19.GFP with 10x dilution steps	i) Bestimmung des TCID50 für MVA (Modified Vaccinia Virus Ankara) GFP gelabelt, Nr. V/09, V 1.1 ii) Axio Observer, Nr. G/26, V 1	i) V. Lohr, C. Best, S. König ii) N. Wynserski
$TCID_{50}$ measurements for MVA-CR19.GFP with 2x dilution steps	**Determination of the TCID50 for MVA (Modified Vaccinia Virus Ankara), GFP labelled, and with 2-fold dilution steps, Nr. V/XX, V 1.0**	**G. Gränicher**
Trypsin production	Trypsinherstellung für die Virusvermehrung, Nr. V/02, V 2	A. Kiesel, Y. Genzel, C. Best
Virus dynamics measurement with flow cytometry	Imaging flow cytometry: sample preparation, staining and data acquisition, Nr. BA077, V 12.06.2019	J. Coronel, S. Kupke

[a)] Published in a book including methods and protocols (Animal Cell Biotechnology): Nikolay et al. (2020) [145].

10.2.2 Viable cell and amino acid concentration assays

Table A.2: Vi-CELL XR cell properties settings for the different cell lines

	Adherent cells [a]	**PBR.PK2.1 cells**	**AGE1.CR.pIX cells**
Min. diameter [µm]	5	10	8
Max. diameter [µm]	28	30	30
Number of images	50	100	100
Aspirate cycle	3	3	3
Trypan blue mixing cycle	3	3	3
Cell brightness [%]	85	85	90
Cell sharpness	80	90	100
Viable cell spot brightness [%]	90	75	85
Viable cell spot area [%]	4	5	3
Min. circularity	0	0.5	0.5
Decluster degree	Medium	Medium	High

[a] The following setting was used for adherent MDCK and Vero cell cultures (needed for $TCID_{50}$ assays).

Table A.3: Validated metabolite measurement ranges and relative standard deviation

Device	Metabolite	Measurement range [mM]	Relative standard deviation [%]
Bioprofile 100 Plus	Glucose	2.8–41.1	11.0
	Glutamate	0.2–2.6	4.7
	Glutamine	0.2–2.6	3.4
	Lactate	2.2–333.0	1.6
	Ammonium	0.2–5.2	2.2
AccQ-TAG Ultra HPLC	Amino Acids	0.00125–0.150000	< 7

10.3 Ion spectra from PBG.PK2.1-based HA glycopeptide analysis

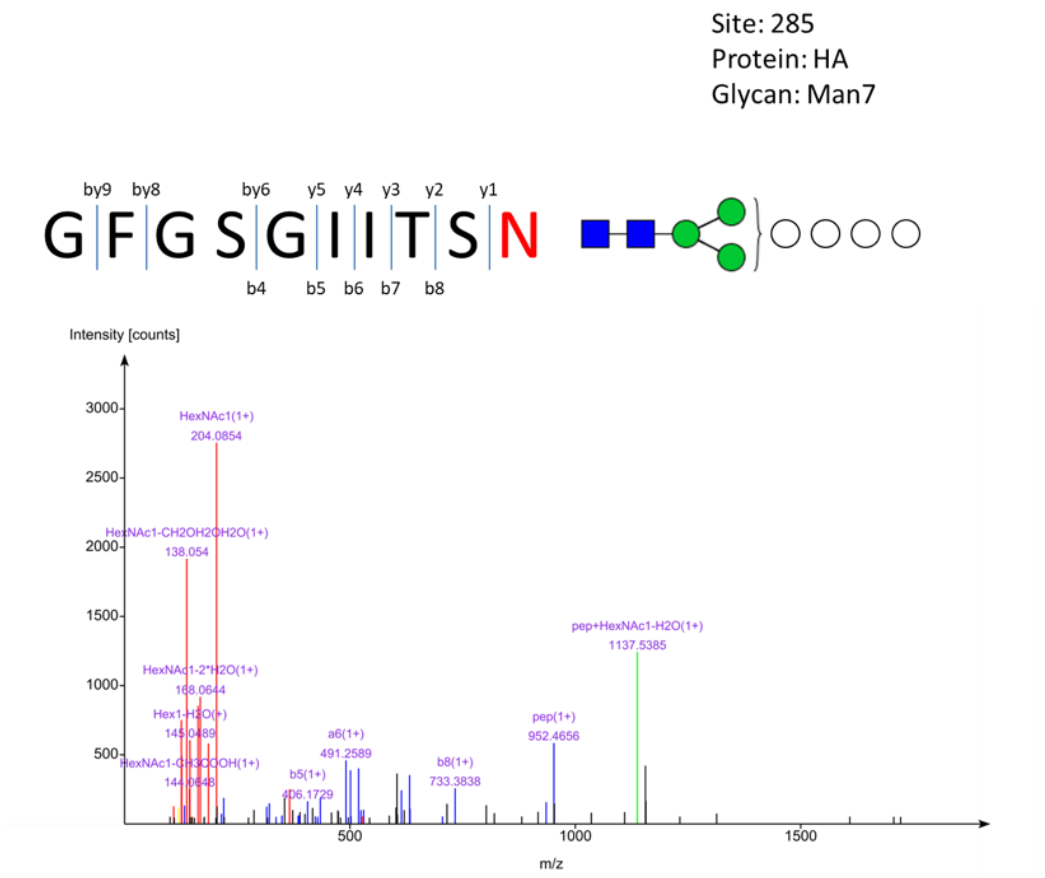

Figure A.1: Fragment ion spectra of the detected Man7 *N*-glycopeptide on site N285 from the hemagglutinin antigen produced with PBG.PK2.1 infected with influenza A/PR/8/34 virus.

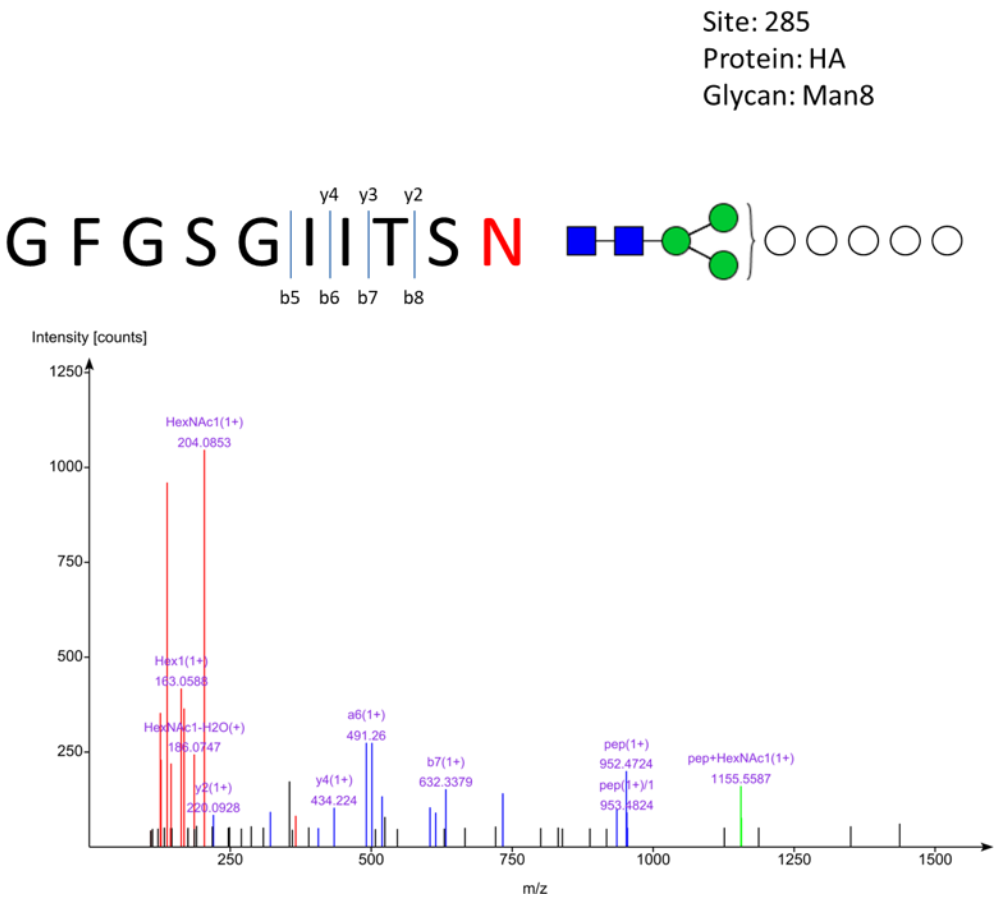

Figure A.2: Fragment ion spectra of the detected Man8 *N*-glycopeptide on site N285 from the hemagglutinin antigen produced with PBG.PK2.1 infected with influenza A/PR/8/34 virus.

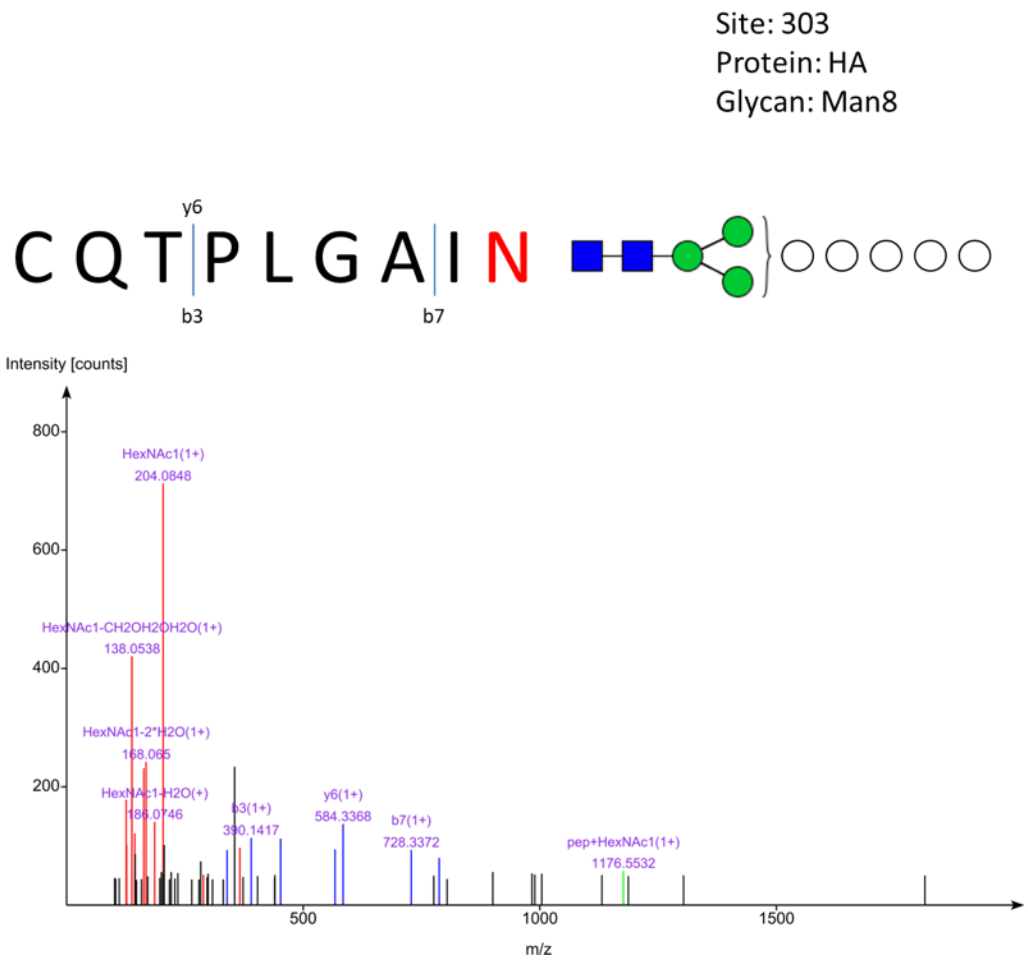

Figure A.3: Fragment ion spectra of the detected Man8 *N*-glycopeptide on site N303 from the hemagglutinin antigen produced with PBG.PK2.1 infected with influenza A/PR/8/34 virus.

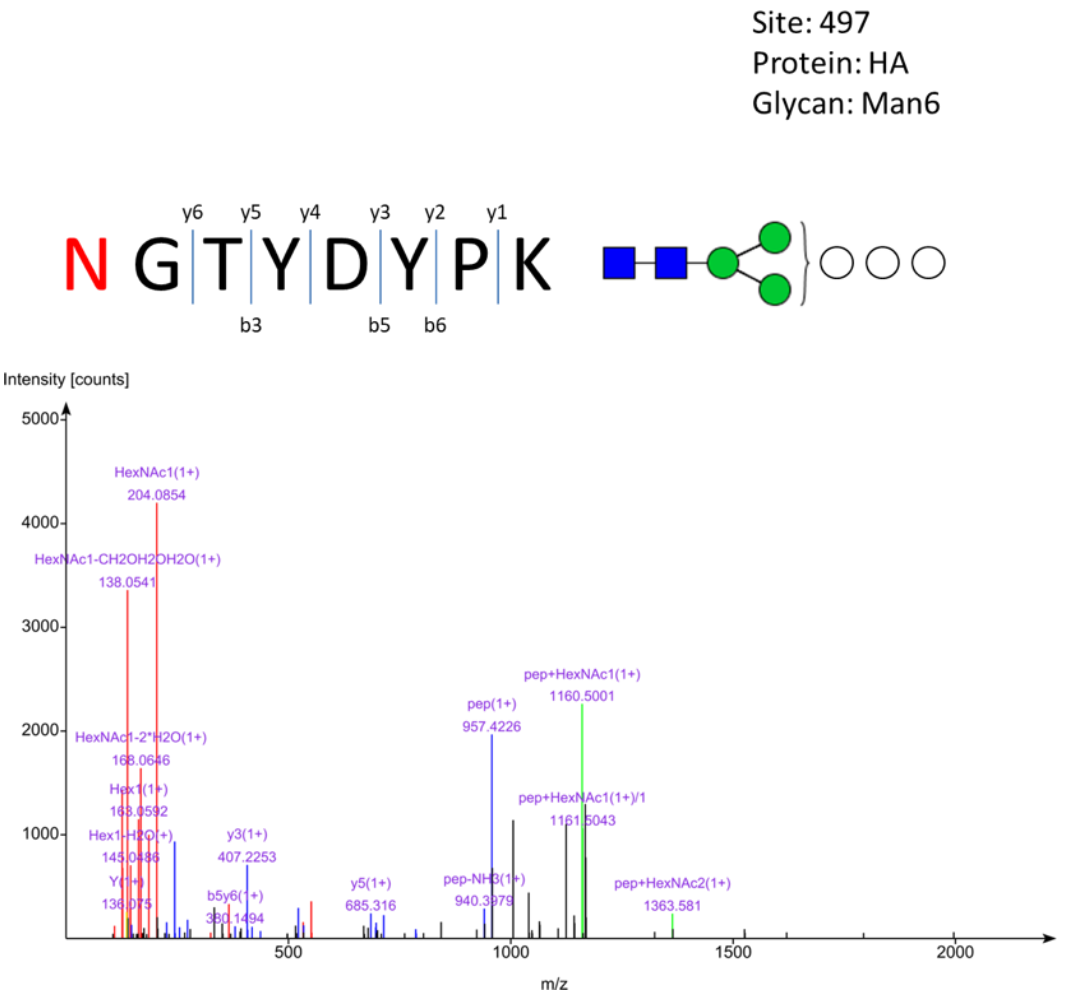

Figure A.4: Fragment ion spectra of the detected Man6 *N*-glycopeptide on site N497 from the hemagglutinin antigen produced with PBG.PK2.1 infected with influenza A/PR/8/34 virus.

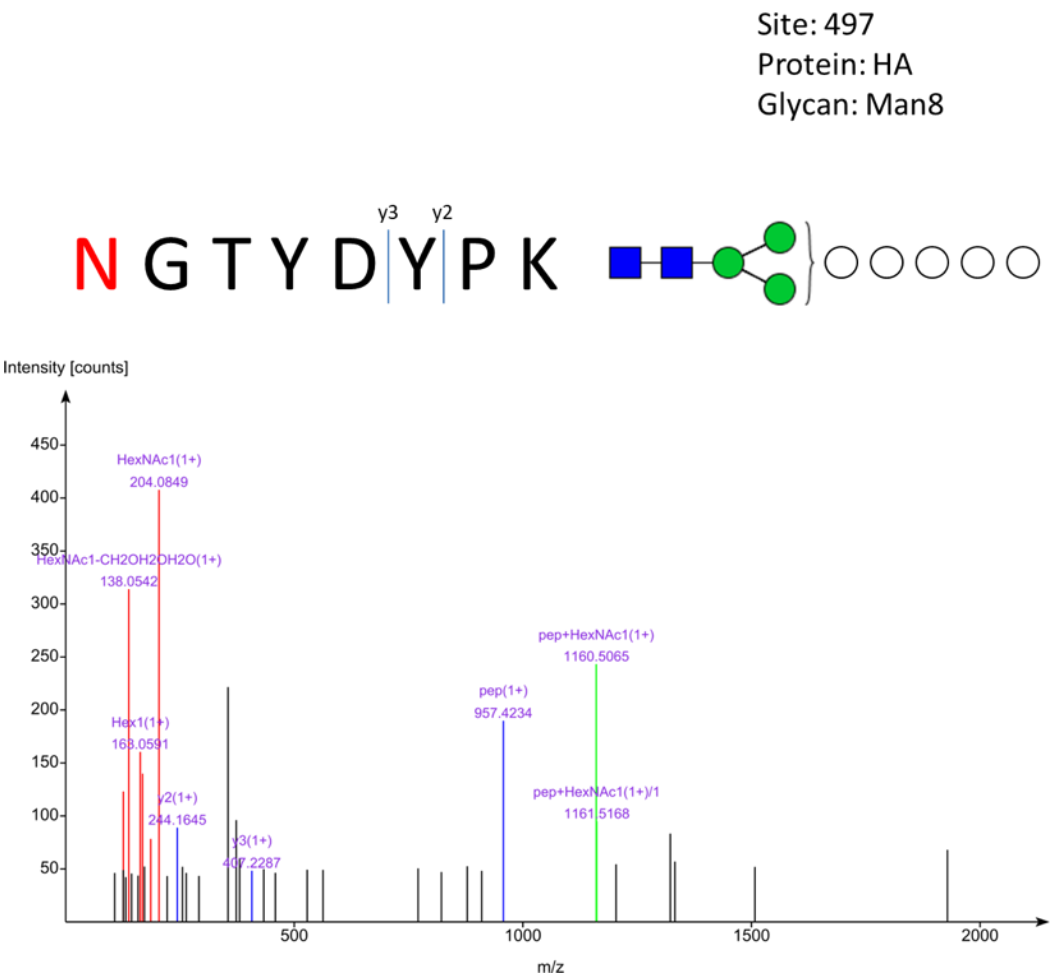

Figure A.5: Fragment ion spectra of the detected Man8 *N*-glycopeptide on site N497 from the hemagglutinin antigen produced with PBG.PK2.1 infected with influenza A/PR/8/34 virus.

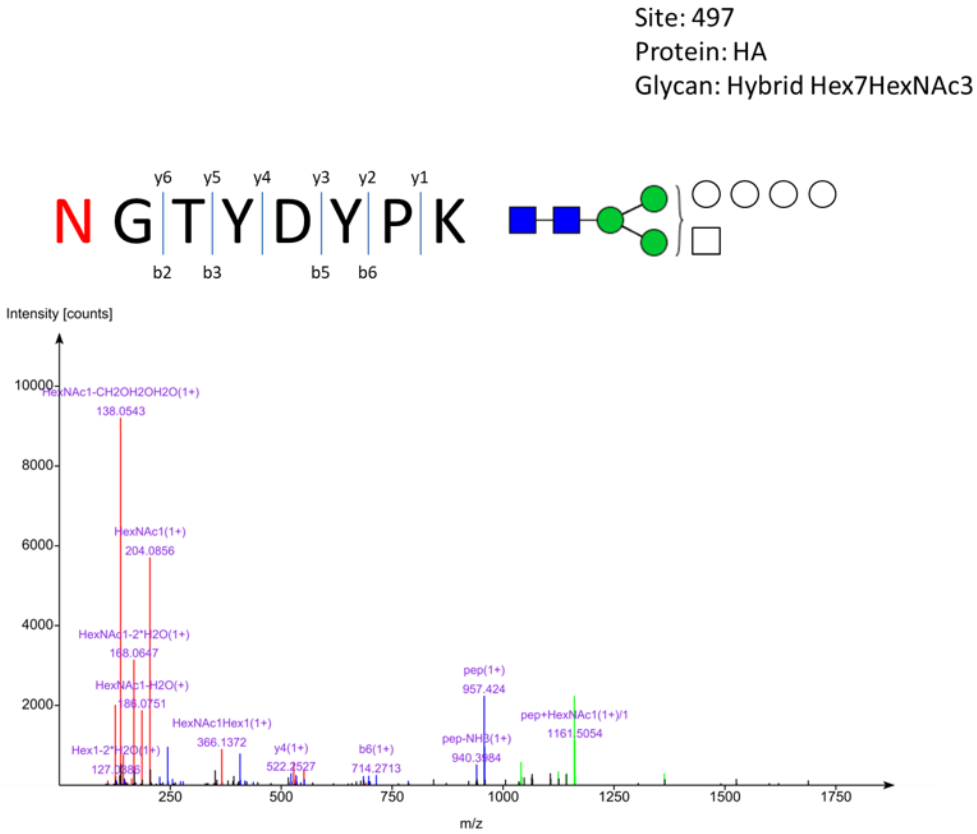

Figure A.6: Fragment ion spectra of the detected Hybrid Hex7HexNAc3 *N*-glycopeptide on site N497 from the hemagglutinin antigen produced with PBG.PK2.1 infected with influenza A/PR/8/34 virus.

10.4 Linear regression curves between different acoustic settler parameters for IAV production

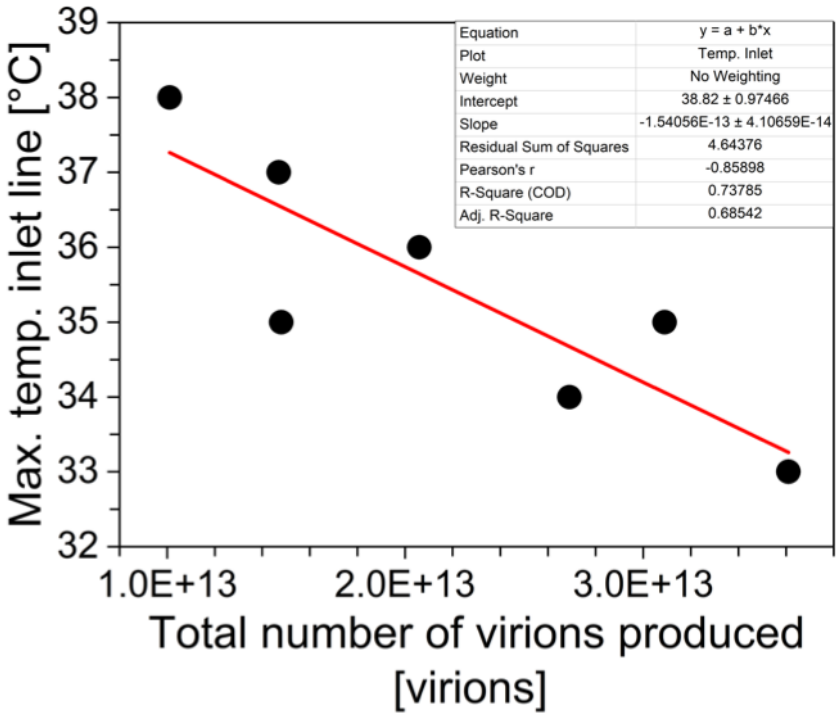

Figure A.7: Linear regression of the maximum temperature in the inlet line of the acoustic settler in function of the total number of virions produced (runs AS1–7).

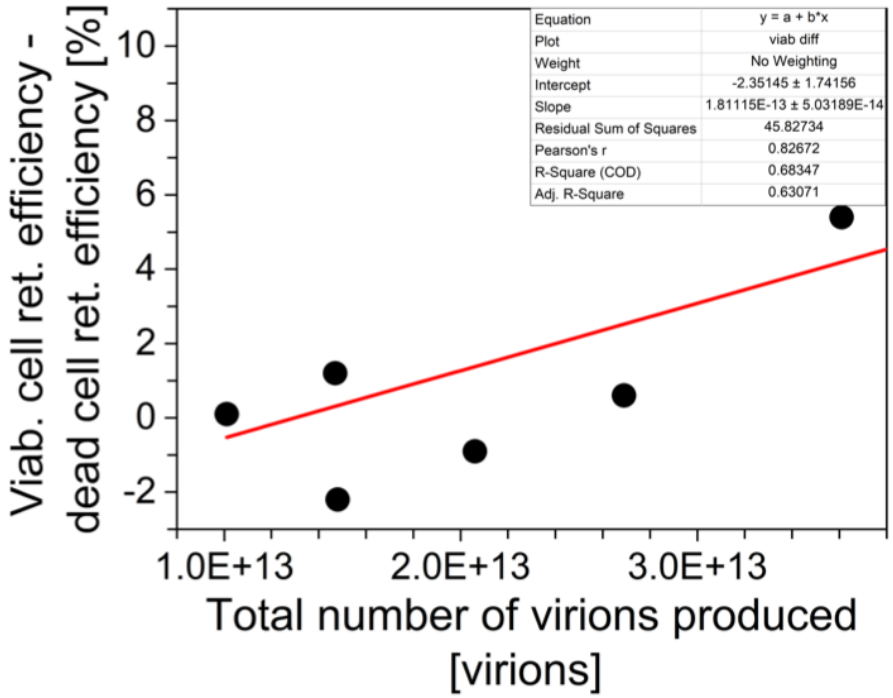

Figure A.8: Linear regression of the cell retention efficiency for viable cells minus the cell retention efficiency for dead cells in function of the total number of virions produced (runs AS3–8).

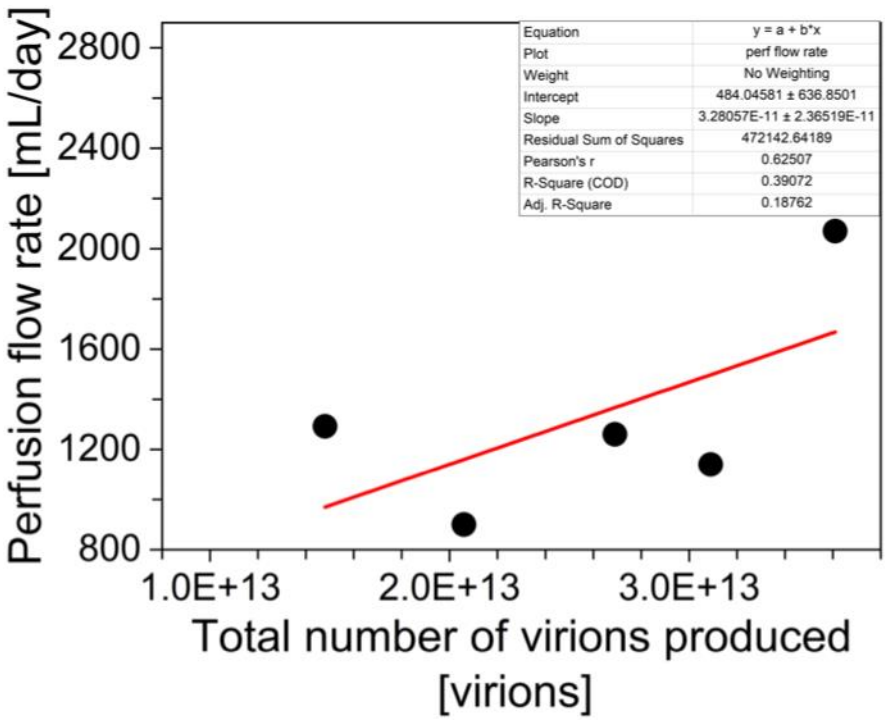

Figure A.9: Linear regression of the perfusion flow rate in function of the total number of virions produced (runs AS3–7).

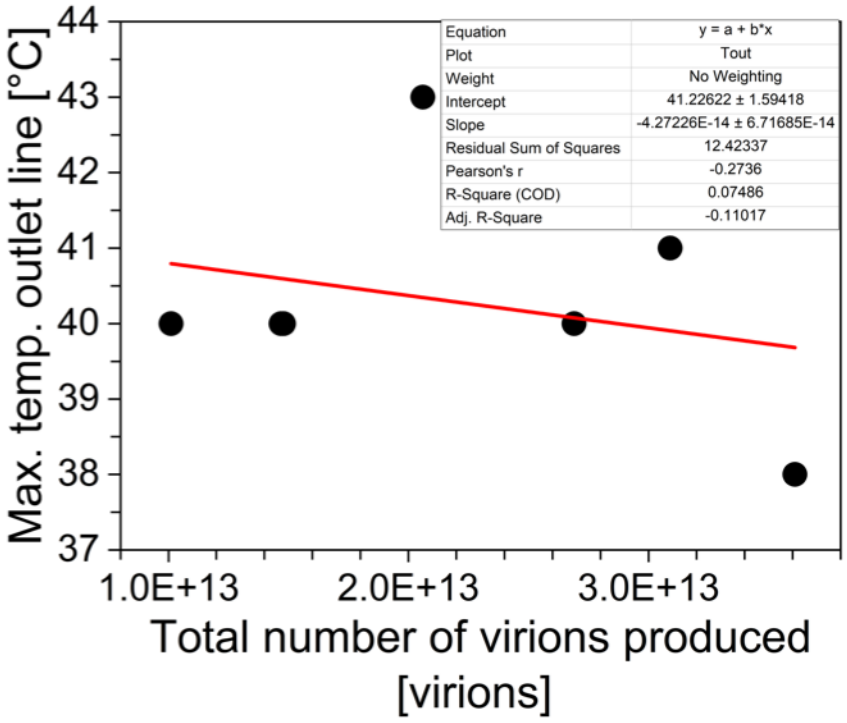

Figure A.10: Linear regression of the maximum temperature in the outlet line of the acoustic settler in function of the total number of virions produced (runs AS1–7).

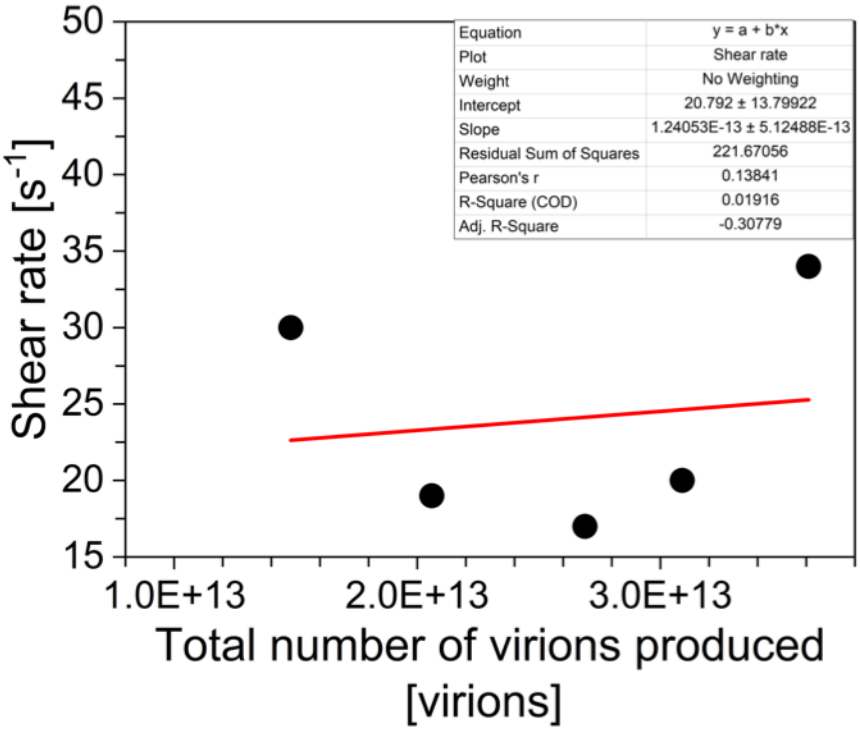

Figure A.11: Linear regression of the shear rate in function of the total number of virions produced (runs AS3–7).

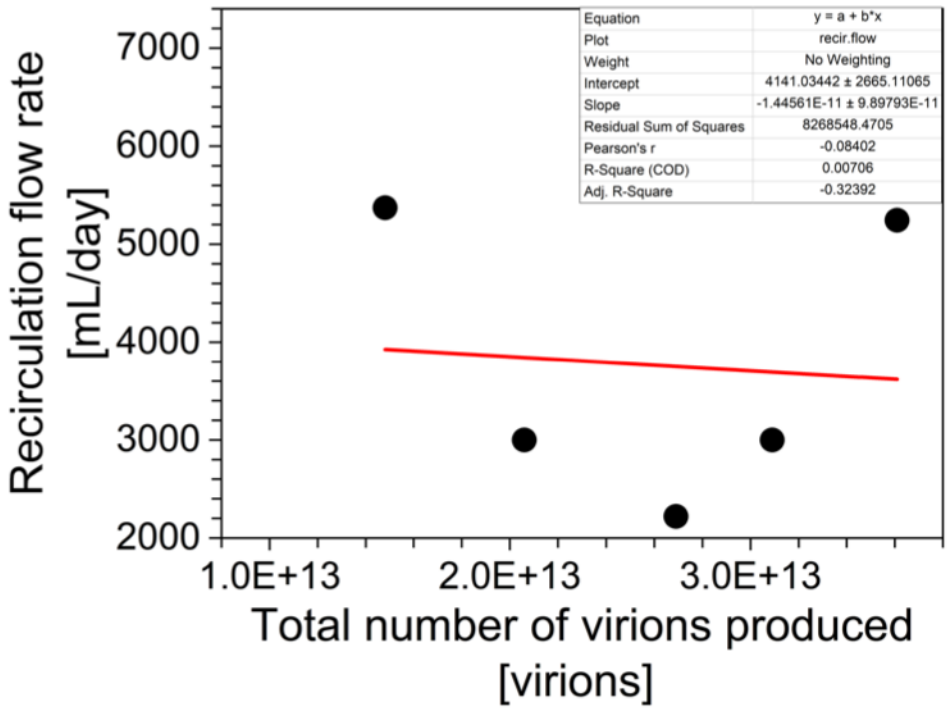

Figure A.12: Linear regression of the recirculation flow rate in function of the total number of virions produced (runs AS3–7).

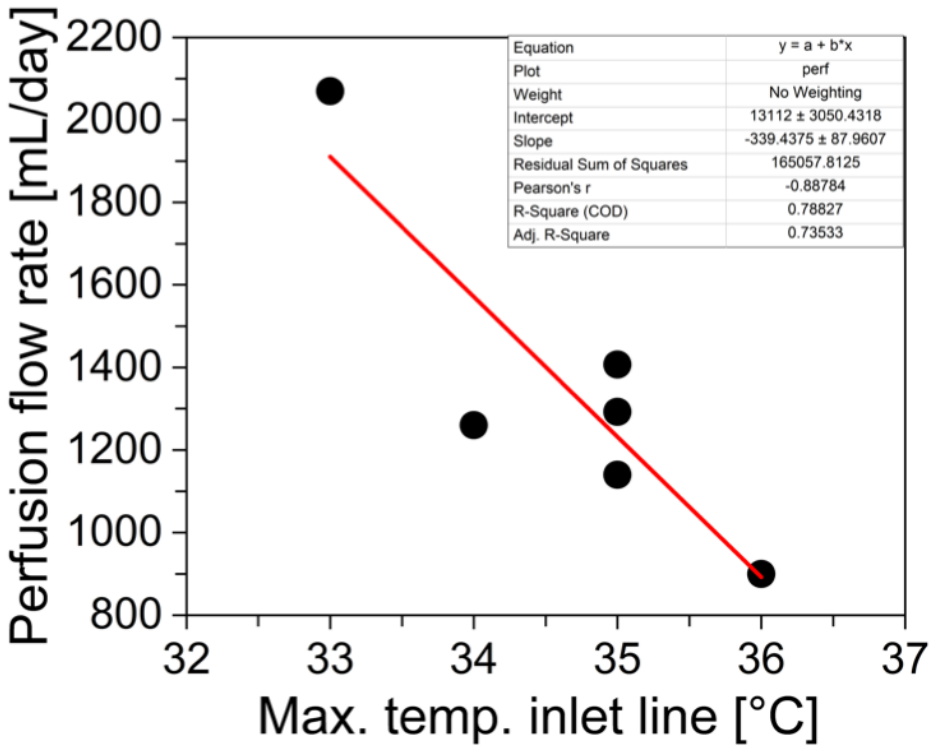

Figure A.13: Linear regression of the perfusion flow rate in function of the maximum temperature in the inlet line of the acoustic settler (runs AS3–8).

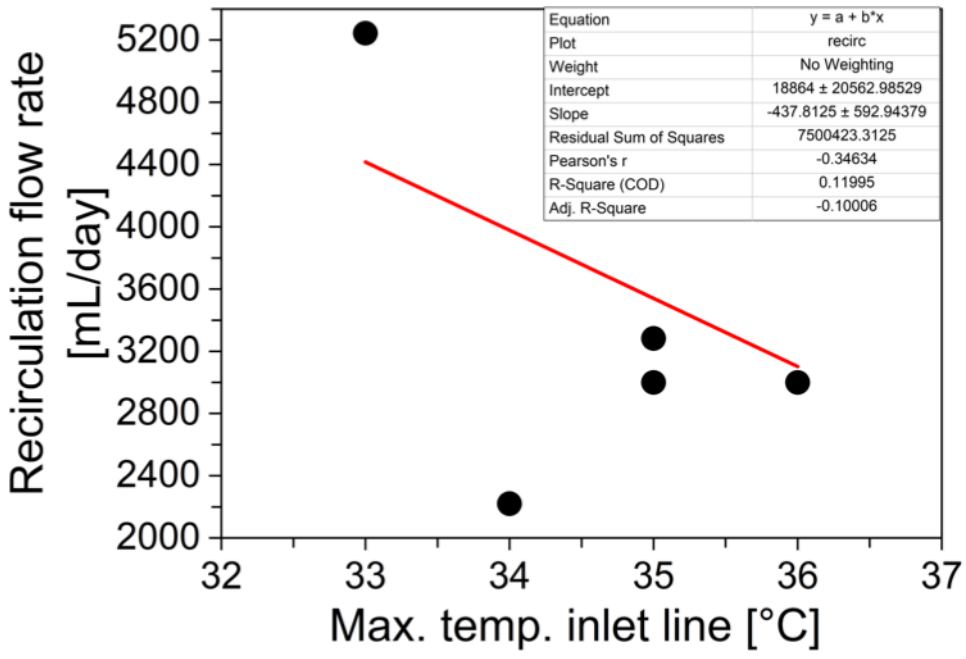

Figure A.14: Linear regression of the recirculation flow rate in function of the maximum temperature in the inlet line of the acoustic settler (runs AS3–8).

10.5 Continuous harvesting of MVA for a membrane-based ATF perfusion system

Based on the results and discussion presented in chapter 7, a major drawback from the ATF system was the non-ability to harvest MVA through the membrane. Therefore, a prototype hollow-fiber membrane (VHU2 membrane, Artemis) was later tested for continuous virus harvesting (run 12) and compared to the perfusion runs performed with the acoustic setter (run 10 and run 11), as described in section 3.6 (runs 10–12 all use CD-U5 medium). A higher maximum VCC (47.7 x 10^6 cells/mL versus 36.9–38.0 x 10^6 cells/mL) was observed when producing the virus in perfusion mode with the ATF system (Figure A.15A). On average, a recovery of 101 ± 12% was observed for run 12, corresponding to no virus accumulation in the bioreactor, as for run 10 and run 11 (Figure A.15C). A Vir_{tot} value of 5.7–20.4 x 10^{11} $TCID_{50}$ was measured for runs 10–12 (Figure A.15B). The CSVY was equal to 24–55 $TCID_{50}$/cell for the AS (runs 10–11) and to 11 $TCID_{50}$/cell for the ATF (run 12). The P_v was equal to 1.5–2.5 x 10^{10} $TCID_{50}$/L/day for the AS (runs 10–11) and to 0.6 x 10^{10} $TCID_{50}$/L/day for the ATF (run 12). Due to a contamination occurring 72 hpi, the bioreactor run 12 was stopped at that time point. A plateau for Vir_{tot} was not observed for run 12 (Figure A.15B).

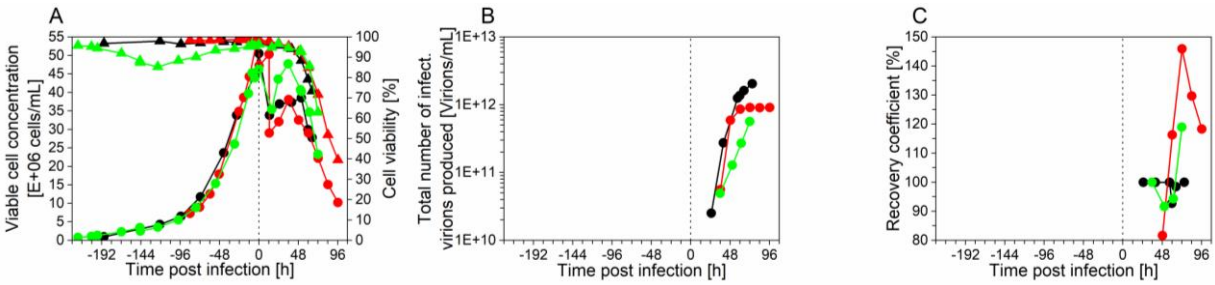

Figure A.15: Production performance and recovery for MVA production in perfusion mode using an acoustic settler (run 10, black and run 11, red) or an ATF (run 12, green). (A) Viable cell concentration (●) and cell viability (▲). (B) Total number of infectious virions produced (●) and (C) recovery (from the acoustic settler or ATF filtration step) (●).

Lower values for CSVY and P_v for the ATF run were obtained, however, this could be due to the premature stop of the run, due to an occurring contamination. The choice of the membrane for the membrane-based ATF perfusion showed to be crucial to efficiently continuously harvest MVA. For the first time, no product sieving has been observed (Figure A.15C) for a perfusion-based MVA production, when using a membrane [90, 235].

As already shown for filter pore sizes higher than 2 µm, but for recombinant protein production [78, 79], the VHU2 ATF membrane allowed continuous product harvesting. The membrane manufacturer (Artemis Biosystems) also claimed no virus retention, for lentivirus production, at VCCs above 5 x 10^6 cells/mL (https://artemisbiosystems.com/). Similarly to a previous study performed by the Bioprocess Engineering group [80], an in-depth study analyzing the physical properties of the Artemis VHU2 membrane such as the pore size distribution and the zeta-potential would be needed to precisely identify factors influencing the virus sieving of this specific membrane. In addition, further cooperation with Artemis Biosystems would be needed to discuss optimal handling of the ATF column, in order to avoid eventual contamination. For the presented result, the column was autoclaved, which is actually not recommended by the manufacturer. The ATF column already comes as gamma-irradiated sterilized.

10.6 Preliminary testing for MVA raw material depth filtration

A pressure sensor (KrosFlo Digital Pressure Monitor; Spectrum Labs, Waltham, USA) was used and connected upstream of the filtration device to monitor the TMP increase (measuring in psi). The used pressure sensor could measure values up to 36 psi, therefore, experiments with pressure exceeding 36 psi were systematically stopped. The filtration testing strategy was based on keeping a constant filtration rate, quantified in LMH (based on the manufacturers' recommendations).

10.6.1 Influence of salt content in MVA raw material on depth filtration

The raw material was either cell clarified using either an AS or an IS. The influence of salts level in the raw material on depth filtration recovery was tested using the Millistack+® depth filter (diatomaceous earth material, pore size range: about 0.2–2.0 µm, 23 cm^2, Millistack+® C0HC µPod format; Merck KGaA, Darmstadt, Germany), as shown below (Table A.4). The following depth filter model was tested here as it was reported internally (non-published results; shown at the American Chemical Society 255th National Meeting, New Orleans, LA, USA, 21.03.2018; DSP section from the Bioprocess Engineering group) that depth filtration with Millistack+®

C0HC of cell clarified MVA lysate allowed 100% recovery with a filtration capacity of 300 L/m^2, a filtration rate of 156 LMH, and a salt concentration of 900 mM.

Table A.4: Conditions and recovery for the depth filtration of cell clarified MVA perfusion harvest, with or without the use of salts.

Condition	NaCl/NaBr/ KCl salts [mM]	Tested filtration capacity [L/m2]	Filtration rate [L/m2/h]	Raw material origin [a]	Cell clarification method	Initial titer [$TCID_{50}$/mL]	Recovery [%]
1	0	340	150 [b]	Run 4 harvest	Inclined settler	1.84 x 10^8	11.2
2	300	320	150 [b]	Run 4 harvest	Inclined settler	1.74 x 10^8	31.1
3	700 [c]	230 [d]	150 [b]	Run 11 harvest	Acoustic settler	7.81 x 10^8	100 [e]
4	700 [c]	220 [d]	150 [b]	Run 4 harvest	Inclined settler	2.87 x 10^9	31.6
5	700 [c]	90 [d]	22 [f]	Run 4 harvest	Inclined settler	2.87 x 10^9	51.2

[a] Run number according to chapters 7–8.
[b] Filtration rate recommended by the manufacturer.
[c] Salt level and composition recommended by ProBioGen AG.
[d] Reduced volume due to limited raw material
[e] Possibility that the following result is an outlier (hypothesis: defective depth filter)
[f] Reduced filtration rate to mimic filtration rate in case the filter is connected to an integrated perfusion process (chapter 8).

According to the manufacturer, a pressure above 49 psi should not be exceeded. For all the experiments, the pressure never exceeded 5 psi, except during the flush. There, pressure until 7 psi was reached. For all the experiments, the depth filter was first filled with PBS at 150 LMH (by opening the vent caps). When filled, the filter was flushed with PBS by gradually increasing the flow rate to 600 LMH. The flow rate of 600 LMH was set for 1 min. The depth filter was then used to filter the raw material. At the end of the filtration, the filter was again flushed with PBS for 1 min at 600 LMH to collect MVA from the filter dead volume. The recovery was calculated based on the MVA $TCID_{50}$ assay, as described in section 3.13.3. The extra volume from the flush in the filtrate was included in the recovery calculation. All the samples were stored at -80°C.

There is no depth filter from the Millistack+® C0HC with a format smaller than the µPod format (23 cm^2 filter surface). By consequent a high volume of raw material was needed each time, reducing the amount of tested conditions and without duplicate/triplicate (207–800 mL tested each time; Table A.4).

An increased recovery was observed when increasing the salt concentration in the raw material (from 11.2% to an average of 60.9%, when adding 700 mM salts). However, a full recovery (previously internally reported) was not observed. A salt concentration of 900 mM was previously used. Here a maximum salt concentration of 700 mM was tested (recommended salt level from ProBioGen AG). The 200 mM different should not greatly influence recovery (internal communication from ProBioGen AG) and was not tested due to low availability of depth filters and raw material.

10.6.2 Depth filtration with different filters

For the depth filtration, previous publications showed recovery yields of 85–90% when using polypropylene depth filters with pore sizes of 0.45–0.60 µm, after a centrifugation step or from the supernatant of an adherent cell culture, for the cell clarification of adenovirus [66], Hepatitis C VLP [243] or influenza virus [244]. Polypropylene might be better suited than diatomaceous earth filter for virus product clarification as it is relatively inert [246, 247], with a surface tension energy lower than other common material such as polyethylene, polyethylene sulfone or polystyrene membranes [248, 249]. In addition, this material allows less electrostatic interaction with the virus product (MVA is highly negative at neutral pH, even compared to other viruses [250]), compared to diatomaceous earth. Diatomaceous earth is positively charged, and is a standard material for depth filtration of biopharmaceuticals [246, 247]. Its positive charge allows to retain charged content by adsorption such as host cell protein impurities or host cell DNA impurities (negatively charged) while filtering the raw material [247, 261]. In the present case, diatomaceous earth may adsorb as well MVA.

Therefore, depth filters with polypropylene were tested in the present section. Based on the result from section 10.6.1, 700 mM of salts were systematically added to the raw material. MVA raw material was produced from three batch cell cultures (as described in section 3.9.2; pooled material; final MVA titer: 2.4 x 10^8 $TCID_{50}$/mL).

Depth filtration of non cell clarified MVA raw material

For cell cultures in batch mode, there is no need to use an AS for cell clarification. Therefore, the following depth filters were tested as shown below (Table A.5) with non cell clarified material, in order to assess the necessity of an AS for an integrated batch production process. A filtration capacity of at least 200 L/m^2 was considered as satisfactory.

Table A.5: Tested depth filtration conditions of non cell-clarified MVA raw material (using the acoustic settler), from cell cultures in batch mode.

Condition	Depth filter	Manufacturer	Material	Pore size [µm]	Filter surface [cm²]	Filtration rate [L/m2/h]	Filtration capacity [L/m²] [a]
1	Millistack+® C0HC	Merck KGaA, Darmstadt, Germany	Diatomaceous earth	0.2–2.0	23.0	150 [b]	34
2	Sartoscale 25 Sartopure PP3 0.45	Sartorius AG, Göttingen, Germany	Polypropylene	≤ 0.45	4.5	600 [b]	30
3	Sartoscale 25 Sartopure PP3 1.2	Sartorius AG, Göttingen, Germany	Polypropylene	≤ 1.2	4.5	600 [b]	50
4	Sartoscale 25 Sartoguard NF	Sartorius AG, Göttingen, Germany	Polyethylene sulfone	≤ 0.65	4.5	600 [b]	20

[a] Resulting filtration before membrane blocking (exponential pressure increase, > 36 psi).

[b] Filtration rate recommended by the manufacturer.

The Millistack+® C0HC was flushed as described in section 10.6.1. The other depth filters (from Sartorius AG) were first flushed at 3000 LMH (filtration rate targeted gradually; recommended by the manufacturer) for 1 min with PBS to "wet" the membrane. At the end of the run the same flushing procedure was operated again for the Sartorius depth filters. The maximum pressure for the tested Sartorius depth filters (recommended by the manufacturer) was 29 psi.

For all the tested membranes, the membranes rapidly blocked, between 20 and 50 L/m^2 (Table A.5). To facilitate the process integration of batch cell cultures for MVA production, it was then chosen to first cell clarify the raw material with an AS, followed by a depth filtration step.

Depth filtration of cell clarified material (through an acoustic settler)

To facilitate depth filtration of cell cultures in batch mode (tested in section 10.6.2), the raw material (pooled cell cultures in batch mode) was cell clarified using an acoustic settler as described in section 3.11.1. To further increase the depth filtration yield using a Millistack+® C0HC, a depth filter using another material, polypropylene, was tested on cell clarified raw material. As the starting material was different than in section 10.6.1, the Millistack+® C0HC was tested again as a control. For a better comparability, the depth filters were compared for a same filtration capacity. The following tested conditions and results are shown below (Table A.6). Due to raw material limitation, no replicate could be performed.

Table A.6: Conditions and recovery for the depth filtration of cell clarified MVA raw material, with different depth filters, from cell cultures in batch mode.

Condition	Depth filter	Manufacturer	Material	Pore size [µm]	Filter surface [cm^2]	Filtration rate [$L/m^2/h$]	Filtration capacity [L/m^2]	Recovery [%]
1	Millistack+ N0HC	Merck KGaA, Darmstadt, Germany	Diatomaceous earth	0.2–2.0	23.0	150	220	23.7
2	Sartoscale 25 Sartopure PP3 0.45	Sartorius AG, Göttingen, Germany	Polypropylene	≤ 0.45	4.5	600	220	65.1

A higher recovery was observed for the depth filter using polypropylene. However, the following experiment was not performed in duplicate. The TMP did not exceed 15 and 8.5 psi during filtration for the polypropylene and the diatomaceous earth depth filters, respectively. Results shown in chapter 8 (using Sartopure PP3 depth filter, also with pore size ≤ 0.45 µm, but with a higher surface of 120 cm^2) confirm the same recovery (range of 59.8–81.6%).

Considering the recovery of the depth filtration with the Millistack+® C0HC when filtering cell clarified MVA raw material (also with 700 mM salts), a recovery of 23.7–51.2% was obtained (from the three filtration runs from sections 10.6.1–10.6.2, excluding the 100% recovery outlier from section 10.6.1). This suggests that polypropylene filter might better perform for cell clarified MVA depth filtration. The following depth filter (Sartopure PP3 0.45, in polypropylene) was chosen for process integration (section 3.11).

10.7 AGE1.CR.pIX host cell DNA digestion optimization

The influence of the chaotropes (here salts) on the host cell DNA depletion through endonuclease digestion was first tested. The starting raw material for host cell DNA digestion was cell culture supernatant (after the AS cell clarification) of the MVA production run 11 in perfusion mode (chapter 8). Briefly, taking each time > 0.8 mL, the following conditions were tested (Table A.7):

Table A.7: Tested conditions for host cell DNA digestion, with different salt levels in the raw material.

	DENARASE activity [U/mL]	NaCl/NaBr/KCl salts [mM]	$MgCl_2$ [mM]	NaN_3 [% v/v]	Mixing [rpm]
Condition 1 (in duplicate) [a]	100	0	4	0.05	700
Condition 2 (in duplicate) [a]	100	250	4	0.05	700
Condition 3 (in duplicate) [a]	100	250	4	0.05	700
Condition 4 (in duplicate) [a]	100	400	4	0.05	700
Condition 5 (in duplicate) [a]	0	0	4	0.05	700

[a] For each condition, duplicate were collected and stored at -80°C after 18 and 25 h incubation time.

A thermomixer block (Eppendorf AG, Hamburg, Germany) was used for incubation at 37°C, with mixing (Table A.7). The host cell DNA concentration in each sample was measured using a qPCR assay with primer templates specific to the host cell DNA, according to SOP *Quantification of AGE.CR.pIX host cell DNA concentration via a qPCR method* (see Appendix, Table A.1). Briefly, the samples were treated with 15 mM EDTA to stop the DNA digestion. The DNA was then digested at an endonuclease activity of 100 U/mL, with different salt levels. The qPCR mix was prepared and measured using the thermal cycler and fluorimeter (Rotor-Gene Q real-time PCR cycler; Qiagen, Hilden, Germany). The host cell DNA depletion over time is reported below (Figure A.16).

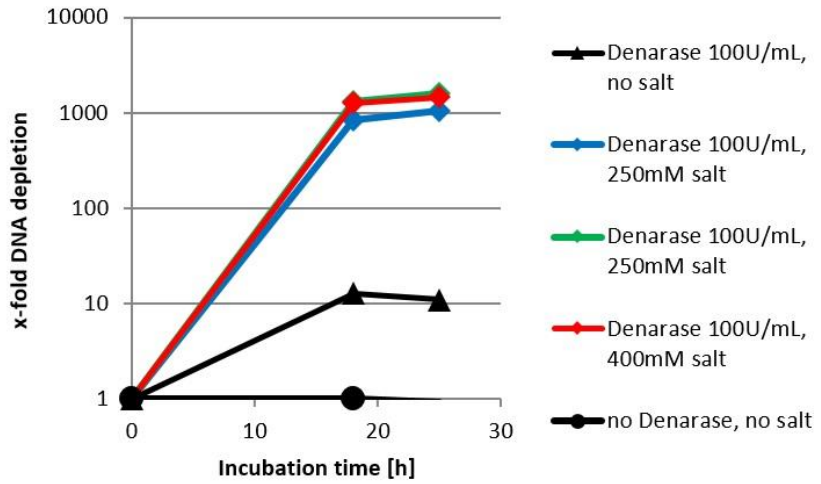

Figure A.16: AGE1.CR.pIX host cell DNA depletion over time, using different salt levels in the raw material, as described in Table A.7.

As observed in Figure A.16, the host cell DNA could be digested by the endonuclease only when using salts. The salts act as a chaotrope and separates the host cell DNA attached to the virus particle, as already reported [251].

The endonuclease activity was then optimized, using salts. The host cell DNA was digested according to SOP *Relative quantification of Modified Vaccinia virus Ankara viral genome via a qPCR method* (see Appendix, Table A.1), except that the DENARASE endonuclease activity was varied. The starting raw material for host cell DNA digestion was cell culture supernatant (after the AS cell clarification) of the MVA production run 11 in perfusion mode (chapter 8). Briefly, taking each time >0.8 mL of supernatant, the following conditions were tested (Table A.8):

Table A.8: Tested conditions for host cell DNA digestion, with different endonuclease activities.

	DENARASE activity [U/mL]	**NaCl/NaBr/KCl salts [mM]**	**$MgCl_2$ [mM]**	**NaN_3 [% v/v]**	**Mixing [rpm]**
Condition 1 (in duplicate) [a)]	10	700	4	0.05	700
Condition 2 (in duplicate) [a)]	20	700	4	0.05	700
Condition 3 (in duplicate) [a)]	32	700	4	0.05	700
Condition 4 (in duplicate) [a)]	55	700	4	0.05	700
Condition 5 (in duplicate) [a)]	77	700	4	0.05	700
Condition 6 (in duplicate) [a)]	32	700	4	0.05	0

[a)] For each condition, duplicate were collected and stored at -80°C after 1.00, 2.50, 4.25, 5.50 and 7.50 h incubation time.

A Thermomixer block (Eppendorf AG, Hamburg, Germany) was used for incubation at 37°C, with mixing (Table A.8). The tested range of endonuclease activity was between 10–77 U/mL, with a maximum incubation time of 7.5 h. The host cell DNA concentration in each sample was then measured using a qPCR assay with primer templates specific to the host cell DNA, according to SOP *Quantification of AGE.CR.pIX host cell DNA concentration via a qPCR method* (see Appendix, Table A.1). Briefly, the samples were treated with 15 mM EDTA to stop the DNA digestion with eventual endonuclease. The DNA was then extracted, the qPCR mix was prepared and measured using the thermal cycler and fluorimeter (Rotor-Gene Q real-time PCR cycler; Qiagen, Hilden, Germany). The ct-values of the samples were correlated to a host cell DNA concentration through a standard curve. The host cell DNA depletion over time is reported below (Figure A.17).

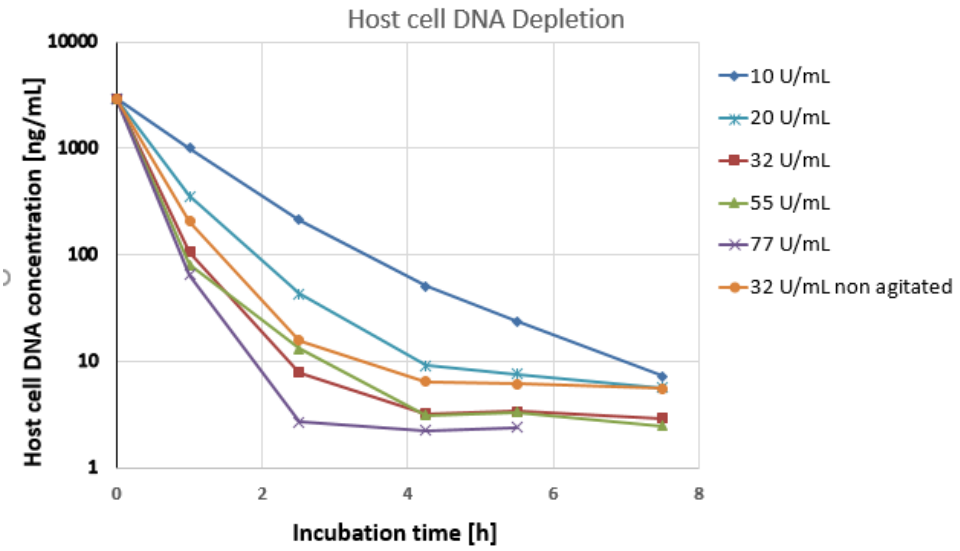

Figure A.17: AGE1.CR.pIX host cell DNA depletion over time, using different DENARASE endonuclease activity (from 10 U/mL to 77 U/mL9, as described in Table A.8.

After an incubation time of 4h with a DENARASE activity of 40 U/mL, almost all the host cell DNA in the supernatant was depleted. At least a 1000-fold depletion is observed after 4h incubation with 32 U/mL DENARASE, agitated or non-agitated (Figure A.17). For the experiment in the thesis, an endonuclease activity of 40 U/mL with an incubation time of 4 h was chosen (section 3.11.2).

The host cell DNA was as well efficiently digested when not agitated (Figure A.17). This shows the potential to use a plug-flow reactor (non-agitated system) for host cell DNA digestion, as described in section 3.11.2.

10.8 Preliminary testing for MVA purification using SXC

10.8.1 MVA raw material pre-treatment prior to SXC

Prior to MVA purification using the SXC, the material should be filtered. A filtration with a cutoff of maximum 0.45 µm should be performed, as described in section 3.11. Previous tests were performed without 0.45 µm cellulose acetate filtration, leading to almost instantaneous SXC column blockage. Blockage was observed as the system pressure increased up to 0.9 MPa.

There the AKTA system automatically reduces the system flow rate, in order to protect the online pH probe.

Endonuclease effectively allows to digest host cell DNA in the raw material. Host cell DNA is the main process-related impurity which has to be removed. The use of endonuclease is an expensive step. Ideally, a chromatography step should be able to separate the host cell DNA from the product of interest (here: MVA). In the present section, the influence of the MVA material pre-treatment on the SXC recovery and host cell DNA per MVA dose is presented (Table A.9). For all the tested conditions (in section 10.8.1), the PEG concentration and AKTA system flow rate were equal to 8% and 5 mL/min, respectively. For each purification cycle, 40 mL of raw material was used. The membrane material and surface are as in section 3.11.3. The starting material consisted of a pooled harvest of a perfusion run (*run 4* from chapter 7, which was centrifuged at 300g for 10 min plus filtered with a cellulose acetate filter (Minisart NML syringe filter, 6.2 cm^2 filtration area)). The titer of the starting material was equal to 5.68 x 10^8 $TCID_{50}$/mL. As this was only a SXC preliminary testing, no replicates were performed for conditions 1–2.

Table A.9: Tested conditions for MVA purification via steric exclusion chromatography, with different endonuclease activities in the starting material.

Condition	DENARASE treatment	NaCl/NaBr/KCl salts [mM] [a)]	Recovery [%]	Host cell DNA per dose [µg/dose] [b)]
1	No	0	8.6	3280
2	No	700	12.0	2060
3 (in triplicate)	Yes	700	30.9–74.9	< 1

[a)] The salt concentration is the final concentration in the column loading material (see section 3.11.3).

[b)] Calculated as in section 3.13.4.

The SXC method did not allow to separate the contaminating host cell DNA from the MVA in the eluate. In addition, a lower recovery was observed when not digesting the DNA before loading in the SXC column (Table A.9). Therefore, it was decided to digest host cell DNA from the MVA raw material prior the SXC.

10.8.2 SXC process parameters optimization

Based on the results from section 10.8.1, the optimization was performed using a DoE in the design space shown in Table A.10. Other SXC parameters are described in section 3.11.3.

Based on 10 randomized runs, a surface response was generated. For the DoE testing, the starting material consisted of a pooled harvest of a perfusion run (*run 4* from chapter 7; performed as described in section 3.10.2), and cell clarified and endonuclease treated as described in section 3.11. The MVA titer of the pooled harvest was equal to 4.05×10^8 $TCID_{50}$/mL. The endonuclease was needed, as preliminary results from section 10.8.1 showed a systematic co-elution of the host cell contaminating DNA with the virus and a decrease in product recovery. The PEG molecular weight, the membrane surface, the membrane material, and the salt concentration in the buffers and raw material were not modified (section 3.11.3).

Table A.10: Design space for the steric exclusion chromatography method optimization.

Parameter	Lower range	Middle range	Upper range
PEG concentration [% w/v]	6	8	10
System flow rate [mL/min]	2	5	8

To calculate the recovery, the MVA viral genome was quantified using a qPCR assay following the SOP *Relative quantification of Modified Vaccinia virus Ankara viral genome via a qPCR method* (see Appendix, Table A.1). The amount of virions in the eluate could be estimated and a response contour plot was designed (illustrated in Figure A.18; based on the design space in Table A.10), using the MODDE software (Sartorius AG, Göttingen, Germany).

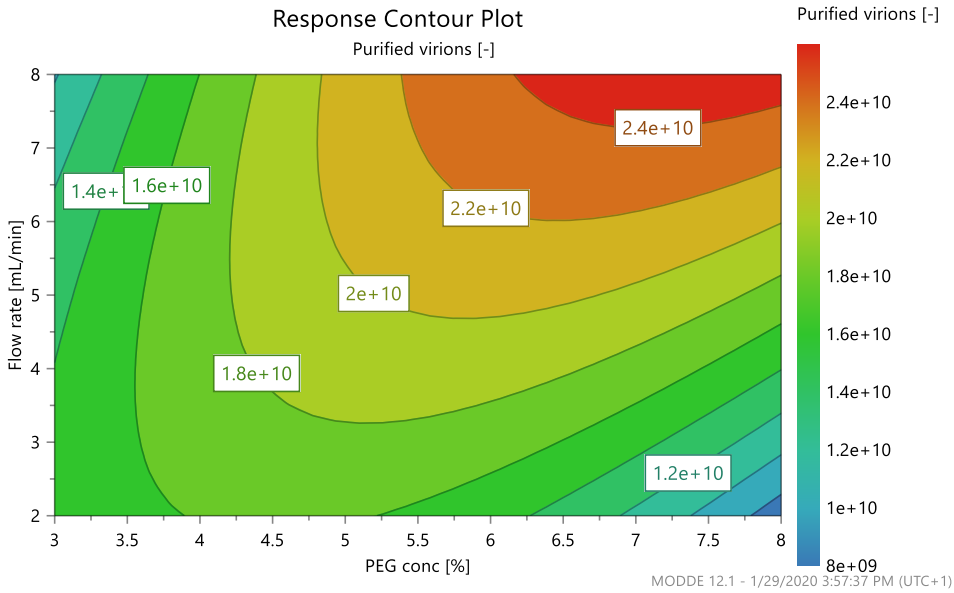

Figure A.18: Response contour plot generated by a DoE approach, for MVA purification via steric exclusion chromatography, set in the design space from Table A.10.

A maximum value of 2.4 x 10^{10} purified virions was obtained, which corresponds here to a 100% recovery in the eluate. The optimal SXC conditions resulted as follow: PEG concentration 7.2% w/v, system flow rate 8.2 mL/min.

10.8.3 SXC membrane testing

Based on the optimal raw material pre-treatment and optimal purification parameters (sections 10.8.1–10.8.2; material pre-treatment and purification parameters as described in section 3.11.3), different membrane chemistries of the SXC stationary phase (cellulose and cellulose acetate) were tested and compared with the regenerated cellulose membrane (standard membrane). No difference higher than the error of the calculated recovery (section 3.13.3) was observed between the different product recovery values (no replicates performed as it was only a preliminary SXC testing; Table A.11). The preliminary results show that other membrane chemistries could be potentially used. Further testing should be performed to confirm the reported results. The starting material was the same as described in section 10.8.2.

Table A.11: Tested conditions and recovery for MVA purification via steric exclusion chromatography, with different membrane materials in the stationary phase.

Conditions	Membrane material	Pore size [µm]	Membrane surface [cm^2] [a)]	Cat. no.	Manufacturer	Recovery [%]
1 [b)]	Regenerated cellulose	1	70 (14 x 5)	10410014	GE (now Cytiva), Uppsala, Sweden	100.0
2	Cellulose acetate	5	60 (12 x 5)	12342--25-K	Sartorius AG, Göttingen, Germany	100.0
3	Cellulose	2.7	40 (8 x 5)	1542-055	GE (now Cytiva), Uppsala, Sweden	69.7

[a)] The thickness of the tested membranes was larger compared to the standard regenerated cellulose membrane (section 3.11.3). Therefore, less membranes were packed in the SXC column in order to avoid leakage.
[b)] Result from section 10.8.2

10.9 Capacitance probe measurements during MVA production

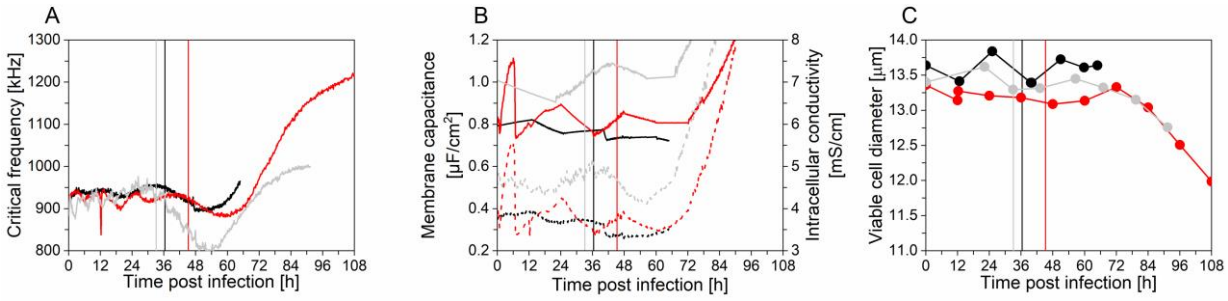

Figure A.19: Capacitance probe data for process automation and control during MVA production using AGE1.CR.pIX cells in perfusion mode. (A) Critical frequency (Fc), (B) membrane capacitance (C_m; solid line) and intracellular conductivity (σ_i; dotted line) and (C) viable cell diameter for three cultivations in perfusion mode (run 10= black, run 11= red, data from *run 4*, chapter 7, = grey). The vertical lines (for each run in the respective color) correspond to the expected time of MVA release in the supernatant, which is on average 10.6 h after the maximum permittivity signal (between 12 and 36 h post infection for perfusion). This time interval of 10.6 h was determined based on the optimal time of virus harvesting for a perfusion process (which is the time of MVA release, corresponding to the time when about 8 to 10% of the total number of infectious virions was released from the infected cells), as described in section 3.11. The cell factor (described in section 3.7.2) converting the permittivity signal to the viable cell concentration was equal to 0.57, 0.65 and 0.44 for run 10, run 11 and the perfusion control run, respectively.

A range of 0.8–1.8 µF/cm^2 for C_m and 3.5–11.0 mS/cm for σ_i were obtained (Figure A.19), which corresponds to the range of other reported C_m and σ_i values for human cell lines or CHO cells [89, 262-264]. Higher Fc values were observed for the batch system (Figure A.20) compared to the perfusion system (Figure A.19C), which could be eventually explained by a different geometry of the bioreactor, leading to a closer proximity of the capacitance probe with the metallic part of the bioreactor.

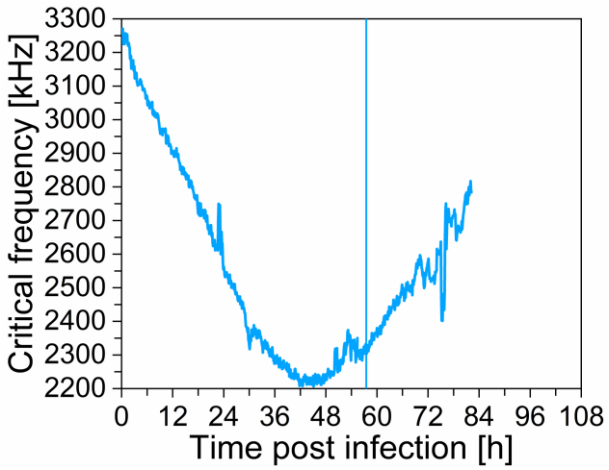

Figure A.20: Capacitance probe data for process automation and control during MVA production using AGE1.CR.pIX cells in batch mode. Critical frequency (Fc) for one cultivation in batch mode (run C). **).** The vertical line corresponds to the expected time of MVA release in the supernatant, which is on average 10.6 h after the maximum permittivity signal (between 24 and 48 h post infection for batch). This time interval of 10.6 h was determined based on the optimal time of virus harvesting for a perfusion process (which is the time of MVA release, corresponding to the time when about 8 to 10% of the total number of infectious virions was released from the infected cells), as described in section 3.11.

Table A.12: Critical time points used to predict the virus release using the capacitance probe.

Parameters	Run 10	Run 11	Control run, run 4	Batch run C
Time of maximum $\Delta\varepsilon_{max}$ [hpi] [a)]	25.4	34.2	22.1	46.9
Time of expected virus release [hpi] [b)]	36.0	44.8	32.7	57.5
Time of measured virus release [hpi] [c)]	40.0	41.0	35.5	54.5
Calculated percentage of harvested virions after the expected virus release [%]	93.4	81.1	94.8	84.8 [d)]

hpi: Hours post infection, $\Delta\varepsilon_{max}$: Maximum permittivity signal, Fc: Critical frequency.

[a)] Value considered between 12 and 36 hpi for runs 10–11 and the control run. Due to the major delay in term of virus release and cell death, the range was set between 24 and 48 hpi for the batch run C.

[b)] Value considering the maximum permittivity signal plus 10.6 h.

[c)] Considering the frequency of virus sampling (section 3.11), the time of virus release was rounded up to every 0.5 h.

[d)] For the batch run C, the totality of the batch was harvested at the end of the run (as there is no continuous harvest). The presented value indicates here the percentage of virus released in the supernatant after the expected virus time release.

10.10 Economic analysis for an integrated MVA production

The detailed economic report for MVA production is shown for each bioreactor scale (from 1 to 1000 L; Tables A.13–15) in batch or in perfusion mode. In addition, the economic report for the seed train generation is also shown here (Tables A.16–17).

Table A.13: Materials and consumables costs per unit.

Material or consumable	Unit	Price per unit [$]	Source
AGE1.CR.pIX cells: Seed cells for 1 L bioreactor [a)]	mg of dry weight	66.70	Table A.17
AGE1.CR.pIX cells: Seed cells for 10 L bioreactor [a)]	mg of dry weight	12.24	Table A.17
AGE1.CR.pIX cells: Seed cells for 50 L bioreactor [a)]	mg of dry weight	2.44	Table A.17
AGE1.CR.pIX cells: Seed cells for 200 L bioreactor [a)]	mg of dry weight	0.92	Table A.17
AGE1.CR.pIX cells: Seed cells for 1000 L bioreactor [a)]	mg of dry weight	0.30	Table A.17
NaOH 0.55 M (liquid)	kg	0.27	Molbase.com
Air	kg	0.01 [b)]	SuperPro Designer
Carbone dioxide	kg	2.00	Molbase.com
Oxygen	kg	0.01 [b)]	SuperPro Designer
CD-U5 medium (liquid)	kg	44.00	Biochrom-Merck KGaA
Seed virus (MVA.CR19-GFP)	mg of virus [c)]	35444.00	Model on SuperPro Designer
PBS (liquid)	kg	0.12	Molbase.com
KCl (solid salt)	kg	3.00	Molbase.com
NaBr (solid salt)	kg	3.00	Molbase.com
NaCl (solid salt)	kg	8.00	Molbase.com
NaOH (solid salt)	kg	1.26	Molbase.com
Sodium azide 6.2% (liquid)	kg	0.15	Molbase.com
$MgCl_2$ (solid salt)	kg	0.08	Molbase.com
DENARASE (endonuclease in liquid)	mg [d)]	499.50	c-Lecta
Water (liquid)	kg	0.10	SuperPro Designer
PEG 7.2% w/v in PBS (liquid)	kg	1.07	Sigma
Depth filter	cm^2	0.15	Sartorius AG
Microfilter	cm^2	0.45	Sartorius AG
Cellulose membrane for chromatography	cm^2	0.09	GE Healthcare
Shake flask (maximum 1000 mL working volume)	1 item	1.80	SuperPro Designer

[a)] These costs were included in the "Seed train" costs of Figure 44C, and reported according to Table A.16.

[b)] Negligible costs as air and oxygen gas supply already included in the plant (CAPEX costs).

[c)] One $TCID_{50}$ was considered as one infectious MVA particle, which has a mass of about 7.9 fg [265].

[d)] 1 mg approximated to a volume of 1 mL, with an activity of 250 endonuclease U/µL according to manufacturer (https://www.c-lecta.com/products-services/products/denarase/)

Table A.14: Economic analysis for MVA production at the 1, 10, 50, 200, and 1000 L bioreactor scale in batch mode.

Parameters	1 L	10 L	50 L	200 L	1000 L
Batches per year [Batch/year]	53	53	53	53	53
Yearly produced doses [10^4 Doses/year] [a]	4	43	215	842	4210
Cost per dose [$/dose] [a]	63.60	7.66	1.87	0.77	0.45
Operating time for one integrated run [h]	173	173	173	173	173
			Capital expenditure		
Bioreactor and gas system [k$] [b]	576	576	576	614	750
Acoustic settler [k$]	14	14	150	150	600
Filtration equipment [b]	50	50	50	50	59
Chromatography equipment [b]	186	208	337	698	2706
Other equipment such as intermediate tanks [b]	-	-	-	-	-
Direct fixed capital costs [k$] [b] [c]	4948	5043	6522	8366	21292
Capital expenditure (Total) [k$] [b]	**5341**	**5447**	**7035**	**9078**	**23232**
			Operating expenditure		
Seed train, dry weight AGE1.CR.pIX [k$/year]	523	961	957	1417	2310
NaOH 0.55 M (liquid) [$/year]	1	3	15	58	291
Air [$/year]	1	1	1	1	1
Carbone dioxide [$/year]	4	37	185	727	3635
Oxygen [$/year]	1	1	1	1	1
CD-U5 medium (liquid) [$/year]	2332	23320	116600	457600	2288000
Seed virus (MVA.CR19-GFP) [$/year]	1484	1480	74202	291208	1456040
PBS (liquid) [$/year]	18	177	885	3451	17244
KCl / NaBr / NaCl (solid salt) [$/year]	12	113	561	2203	11014
Sodium azide 6.2 % (liquid) [$/year]	0	0	0	0	0
NaOH (solid salt) [$/year]	58	581	2904	11282	56355
$MgCl_2$ (solid salt) [$/year]	1	2	10	40	197
DENARASE (endonuclease in liquid) [$/year]	3647	36474	182368	715709	3578546
Water (liquid) [$/year]	9	93	464	1802	9003
PEG 7.2% w/v in PBS (liquid) [$/year]	44	437	2185	8490	42408
Depth filter [$/year]	586	5863	29315	115046	575229
Microfilter [$/year]	1338	13376	66879	262470	1312352
Cellulose membrane for chromatography [$/year]	1836	18365	91823	356756	1781980
Labor costs [k$/year] [b] [d]	1098	1098	1101	1090	1139
Facility-dependent costs [k$/year] [b]	932	950	1228	1577	4017
Quality control / Quality assurance (QC/QA) costs [k$/year] [b]	165	165	165	163	171
Operating expenditure (Total) [k$/year]	**2729**	**3287**	**4021**	**6476**	**18779**

[a] One MVA dose is equal to 1.43×10^8 purified $TCID_{50}$.

[b] Calculated with SuperPro Designer.

[c] Includes: Total plant direct costs (Equipment purchase, installation, process piping, instrumentation, insulation, electrical, buildings, yard improvement, auxiliary facilities), Total plant indirect costs (Engineering, construction) and contractor's fee & contingency.

[d] Labor costs were determined with an average operator salary of 69$/h.

Table A.15: Economic analysis for MVA production at the 1, 10, 50, 200, and 1000 L bioreactor scale in perfusion mode.

Parameters	1 L	10 L	50 L	200 L	1000 L
Batches per year [Batch/year]	31	31	31	31	31
Yearly produced doses [10^4 Doses/year] [a]	15	152	758	3033	14674
Cost per dose [$/dose] [a]	22.63	2.72	0.80	0.43	0.33
Operating time for one integrated run [h]	274	274	274	274	274
			Capital expenditure		
Bioreactor and gas system [k$] [b]	576	576	576	613	748
Acoustic settler [k$] [b]	14	14	150	150	600
Filtration equipment [b]	50	50	50	50	88
Chromatography equipment [b]	182	203	332	698	2744
Other equipment such as intermediate tanks [b]	77	77	77	77	77
Direct fixed capital costs [k$] [b] [c]	5392	5487	6915	8773	21804
Capital expenditure (Total) [k$] [b]	**5874**	**6003**	**7639**	**10082**	**26384**
			Operating expenditure		
Seed train, dry weight AGE1.CR.pIX [k$/year]	354	649	647	976	1539
NaOH 0.55 M (liquid) [$/year]	0	0	0	0	0
Air [$/year]	1	1	1	1	1
Carbone dioxide [$/year]	786	7865	39324	157295	761104
Oxygen [$/year]	1	1	1	1	1
CD-U5 medium (liquid) [$/year]	10432	104318	521589	2086356	10095723
Seed virus (MVA.CR19-GFP) [$/year]	11295	112953	564765	2259059	10930930
PBS (liquid) [$/year]	23	221	1102	4407	21236
KCl / NaBr / NaCl (solid salt) [$/year]	29	293	1467	5866	28384
Sodium azide	1	2	10	41	197
NaOH (solid salt) [$/year]	122	1220	6099	24396	117575
$MgCl_2$ (solid salt) [$/year]	1	2	10	40	197
DENARASE (endonuclease in liquid) [$/year]	12759	127589	637943	2551770	12347275
Water (liquid) [$/year]	19	195	974	3898	18784
PEG 7.2% w/v in PBS (liquid) [$/year]	211	2107	10533	42130	203501
Depth filter [$/year]	558	5582	27908	111633	540162
Microfilter [$/year]	1418	14179	70895	283579	1372158
Cellulose membrane for chromatography [$/year]	3857	38572	192859	771435	3717819
Labor costs [k$/year] [b] [d]	1756	1756	1757	1758	1711
Facility-dependent costs [k$/year] [b]	1016	1034	1303	1654	4116
Quality control / Quality assurance (QC/QA) costs [k$/year] [b]	263	263	263	264	257
Operating expenditure (Total) [k$/year]	**3431**	**4117**	**6046**	**12957**	**47793**

[a] One MVA dose is equal to 1.43×10^8 purified $TCID_{50}$.

[b] Calculated with SuperPro Designer.

[c] Includes: Total plant direct costs (Equipment purchase, installation, process piping, instrumentation, insulation, electrical, buildings, yard improvement, auxiliary facilities), Total plant indirect costs (Engineering, construction) and contractor's fee & contingency.

[d] Labor costs were determined with an average operator salary of 69$/h.

Table A.16: Economic analysis for the AGE1.CR.pIX N-1 seed train generation across the scales.

Parameters	N-1 for 1 L bio. [a]	N-1 for 2 L bio. [a]	N-1 for 5 L bio. [a]	N-1 for 10 L bio.	N-1 for 20 L bio.	N-1 for 50 L bio.	N-1 for 100 L bio.	N-1 for 200 L bio.	N-1 for 1000 L bio.
Cell culture working volume [L]	0.1	0.2	0.5	1.0	2.0	5.0	10.0	20.0	100.0
Batches per year [Batch/year]	53	53	53	53	53	53	53	53	53
Yearly produced cells [kg of dry weight/year] [b]	15	30	74	148	296	741	1482	2964	14819
Cost per mg of cells [$/mg of dry weight]	66.70	33.36	13.36	5.57	2.79	1.33	0.68	0.36	0.11
Operating time for one run [h]	96	96	96	96	96	96	96	96	96
					Capital expenditure				
Bioreactor and gas system [k$]	100	100	100	100	100	233	241	283	666
Direct fixed capital costs [k$] [c] [d]	622	622	622	622	622	1407	1459	1703	3977
Capital expenditure (Total) [k$] [c]	**740**	**740**	**740**	**740**	**740**	**1566**	**1622**	**1882**	**4296**
					Operating expenditure [d]				
Air [$/year]	-	-	-	-	-	1	1	1	1
Carbone dioxide [$/year]	1	1	2	4	8	19	37	74	370
Oxygen [$/year]	-	-	-	-	-	-	-	-	-
CD-U5 medium (liquid) [$/year]	233	466	1166	2332	4664	11660	23320	46640	233200
Shake flasks [$/year]	10	10	10	10	20	-	-	-	-
Labor costs [k$/year] [c] [f]	614	614	614	614	614	614	615	615	616
Facility-dependent costs [k$/year] [c]	117	117	117	117	117	265	275	321	749
Quality control / Quality assurance (QC/QA) costs [k$/year] [c]	92	92	92	92	92	92	92	92	92
Operating expenditure (Total) [k$/year]	**989**	**989**	**990**	**826**	**828**	**983**	**1005**	**1074**	**1692**

[a] As the N-1 step for inoculation is at a low volume scale (100–500 mL), the costs before the N-1 were included in the OPEX by an increase of +20% of the actual calculated operational expenditure.

[b] Calculated following the measured cell volume (measured with a ViCell XR), converted to dry weight using the volumetric weight of 0.25 g dry weight / 1 mL cell volume. Value measured for a similar cell line, AGE1.HN [266].

[c] Calculated with SuperPro Designer.

[d] Includes: Total plant direct costs (Equipment purchase, installation, process piping, instrumentation, insulation, electrical, buildings, yard improvement, auxiliary facilities), Total plant indirect costs (Engineering, construction) and contractor's fee & contingency.

[e] For the calculation of the operating expenditure, the AGE1.CR.pIX cell culture seed train was here not taken into account, and will be calculated later on Table A.16 in order to consider the whole seed train from the shake flask to the final production bioreactor (at the final scale of 1, 10, 50, 200 or 1000 L).

[f] Labor costs were determined with an average operator salary of 69$/h.

Table A.17: Assumptions made for the generation of the full seed trains for AGE1.CR.pIX cells to inoculate the MVA production bioreactor at a 1, 10, 50, 200, or 1000 L scale.

Seed train step	Parameter	1 L	10 L	50 L	200 L	1000 L
N-4	Cell culture working volume at the N-4 step [L]	-	-	-	-	0.1
	mg of cell dry weight needed at N-4 to generate 1 mg at final scale [mg of dry weight]	-	-	-	-	0.001
	Costs at the N-4 step to generate 1 mg at final scale [$/mg of dry weight at final scale]	-	-	-	-	0.06
N-3	Cell culture working volume at the N-3 step [L]	-	-	-	0.2	1.0
	mg of cell dry weight needed at N-3 to generate 1 mg at final scale [mg of dry weight]	-	-	-	0.01	0.01
	Costs at the N-3 step to generate 1 mg at final scale [$/mg of dry weight at final scale]	-	-	-	0.28	0.06
N-2	Cell culture working volume at the N-2 step [L]	-	0.1	0.5	2.0	10.0
	mg of cell dry weight needed at N-2 to generate 1 mg at final scale [mg of dry weight]	-	0.1	0.1	0.1	0.1
	Costs at the N-2 step to generate 1 mg at final scale [$/mg of dry weight at final scale]	-	6.67	1.11	0.28	0.07
N-1	Cell culture working volume at the N-1 step [L]	0.1	1.0	5.0	20.0	100.0
	mg of cell dry weight needed at N-1 to generate 1 mg at final scale [mg of dry weight]	1	1	1	1	1
	Costs at the N-1 step to generate 1 mg at final scale [$/mg of dry weight at final scale]	66.70	5.57	1.33	0.36	0.11
From N-3 to N stage	**Total costs of the seed train [$/mg of dry weight at final scale]** [a)]	**66.70**	**12.24**	**2.44**	**0.92**	**0.30**

[a)] These costs were used in Table A.12.

List of publications

Peer-reviewed journal articles

Gränicher G, Babakhani M, Göbel S, Jordan I, Marichal-Gallardo P, Genzel Y, Reichl U. A high cell density perfusion process for Modified Vaccinia virus Ankara production: Process integration with inline DNA digestion and cost analysis*. Biotechnol Bioeng*. 2021;118:4720-34

Gränicher G, Tapia F, Behrendt I, Jordan I, Genzel Y, Reichl U. Production of Modified Vaccinia Ankara Virus by Intensified Cell Cultures: A Comparison of Platform Technologies for Viral Vector Production. *Biotechnology Journal*. 2020:2000024.

Coronel J*, **Gränicher G***, Sandig V, Noll T, Y. G, U. R. Application of an inclined settler for cell culture-based influenza A virus production in perfusion mode. *Frontiers in Bioeng and Biotech*. 2020;8:1-13.

Gränicher G, Coronel J, Trampler F, Jordan I, Genzel Y, Reichl U. Performance of an acoustic settler versus a hollow fiber-based ATF technology for influenza virus production in perfusion. *Appl Microbiol Biotechnol*. 2020;104:4877–88.

Gränicher G, Coronel J, Pralow A, Marichal-Gallardo P, Wolff M, Rapp E, Karlas, A, Sandig V, Genzel Y, Reichl U. Efficient influenza A virus production in high cell density using the novel porcine suspension cell line PBG.PK2.1. *Vaccine*. 2019;37:7019-28.

* Both authors contributed equally.

Book chapter

Nikolay A*, Bissinger T*, **Gränicher G**, Wu Y, Genzel Y, Reichl U. Perfusion control for high cell density cultivation and viral vaccine production. In: Pörtner R, editor. Animal cell biotechnology: Humana Press, New York, NY; 2020. p. 141-68.

* Both authors contributed equally.

Supervised projects

Babakhani M (2020). Techno-economic modeling of an integrated MVA production process, in batch and in perfusion mode. Internship (Master), Institut für Bioverfahrenstechnik, Otto-von-Guericke University Magdeburg.

Göbel S (2020). Process intensification for cell culture-based MVA production. Master Thesis, Institut für Bioverfahrenstechnik, Universität Stuttgart.

Conference and poster proceedings

Talks

Gränicher G, Marichal-Gallardo P, Göbel S, Babakhani M, Jordan I, Sandig V, Genzel Y, Reichl U. Integrated end-to-end MVA viral vector production: Perfusion culture shows economical advantage over batch culture. Advancing Manufacture of Cell and Gene Therapies VII, Coronado, CA, USA, 2022.

Gränicher G, Coronel J, Trampler F, Sandig V, Genzel Y, Reichl U. Process intensification for cell culture-based virus production. IVT Kolloquium OvGU, Magdeburg, Germany, 2019

Gränicher G, Pralow A, Rapp E, John K, Karlas A, Sandig V, Genzel, Y, Reichl U. Evaluation of a new porcine suspension cell line (PBG.PK-21) for influenza A virus production at high cell density. 2nd ESACT Frontiers Retreat, Zagreb, Croatia, 2018.

Posters

Gränicher G, Coronel J, Trampler F, Sandig V, Genzel Y, Reichl U. Challenging acoustic settler and ATF cell retention device for high cell density influenza and MVA virus production. 26th ESACT Meeting, Copenhagen, Denmark, 2019.

Gränicher G, Genzel Y, John K, Karlas A, Sandig V, Reichl U. A new porcine suspension cell line (PBG.PK-21) provides efficient production for influenza and yellow fever vaccine viruses. Vaccine Technology VII, Mont-Tremblant, Canada, 2018.

Due to the COVID-19 pandemic, several conferences during the 2020-2021 time period were cancelled or reported:

Gränicher G, Marichal-Gallardo P, Coronel J, Göbel S, Jordan I, Sandig V, Genzel Y, Reichl U. Integrated perfusion systems for production processes of viral vaccines and gene therapies. *Invited Speaker*. Value through intensified bioprocessing II, Oxford, UK, 2020.

Gränicher G, Marichal-Gallardo P, Göbel S, Jordan I, Sandig V, Genzel Y, Reichl U. An integrated end-to-end perfusion process for intensified production of a Modified Vaccinia virus Ankara vector. *Submitted for a talk*. Vaccine Technology VIII, Sitges, Spain, 2020.

Gränicher G, Marichal-Gallardo P, Göbel S, Jordan I, Sandig V, Genzel Y, Reichl U. Towards an integrated end-to-end Modified Vaccinia virus Ankara vector production in perfusion culture. *Accepted for poster presentation*. Cell culture Engineering XVII, Tucson, AZ, USA, 2020.

Curriculum Vitae

The Curriculum Vitae section is empty in the electronic PDF version of this dissertation according to paragraph 4.1.1. of the Regulations for the submission of depositary copies to the library of the Otto von Guericke University Magdeburg within the framework of doctoral and habilitation procedures as of 5th November 2019, which partially states that "[. . .]. The document does not include a CV, acknowledgments or further personal data. [. . .]".

More information:

https://www.ub.ovgu.de/ub_media/Service/Formulare/Pflichtexemplarrichtlinie_englisch-p-934.PDF.